Investigating the role of serine-ADP-ribosylation in human cells



Evgeniia Prokhorova

Lincoln College

Sir William Dunn School of Pathology

University of Oxford

A thesis submitted for the degree of

Doctor of Philosophy

Hilary Term 2022

Acknowledgements

First of all, I would like to thank my supervisor, Ivan Ahel, for constantly sharing with me his ideas, excitement and enthusiasm for science throughout my DPhil journey. I am incredibly grateful for his continuous support, encouragement and guidance, and for always staying positive and being there for me in times of need. I have learned so much from our numerous discussions, and I truly appreciate all his time and efforts to make this work happen.

My experience has been greatly enriched by many wonderful people that I have met during my time at Oxford. I have very much enjoyed working together with many of the past and present members of Ivan and Dragana Ahel labs. Thank you for all of your support and advice, and for all of the fun times that we have shared together.

I would like to thank all the colleagues and collaborators who have helped with progressing this work, especially Marcin, Florian and Thomas in our lab, with whom we worked together on the two main projects to which I contributed during my DPhil. I would also like to thank Josephine and Kira, who have joined the lab more recently for their DPhil studies, but have greatly helped us with finishing those projects. A special thanks goes to Nina, who has started a DPhil in the lab most recently, and to Josephine and Kira again, who have all taught me the most important lesson of my DPhil on how much it takes to be a good supervisor. I also thank Josephine, Kira and Nina for their helpful feedback and comments on this thesis.

Above all, I am thankful for my partner in life, Mikhail, who has supported me in every possible way during this journey. The words will never be enough, just like time. I am also grateful to Mikhail's parents for making me feel a part of the family from the first day we met. A special and enormous thank you to my closest friend, like a sister I never had, Polina, who has always been there for me throughout this time.

I would further like to acknowledge my previous supervisors, Boris Zhivotovsky, Inna Lavrik and Gelina Kopeina, Fabio Martinon and Aude de Gassart, whose enthusiasm for research has motivated me to pursue a DPhil in the first place. A special thank you to Svetlana Khoronenkova, without whom my application to this DPhil would not have been successful. I would also not have been able to pursue this DPhil without the financial support from the Clarendon Fund and the Dunn School.

Last but not least, I would like to thank my family for their unconditional love and support, and for always believing in me no matter how out of this world my goals may have seemed at the time.

Declaration

I declare that the work presented in this thesis is wholly my own, except if stated otherwise. A number of findings and figures in chapters 2, 3 and 4 were adapted as indicated in the text and corresponding figure legends from the following previously published articles to which I contributed during my DPhil. I confirm that the other co-authors of these publications gave me their permission to include these materials in my thesis.

Chapter 2:

Palazzo L*, Leidecker O*, **Prokhorova E***, Dauben H, Matic I#, Ahel I#. Serine is the major residue for ADP-ribosylation upon DNA damage. Elife. 2018; 26;7, pii: e34334;

Hendriks IA*, Buch-Larsen SC*, **Prokhorova E**, Elsborg JD, Rebak AKLFS, Zhu K, Ahel D, Lukas C, Ahel I, Nielsen ML. The regulatory landscape of the human HPF1- and ARH3-dependent ADP-ribosylome. Nat Commun. 2021; 12(1):5893;

Bartlett E*, Bonfiglio JJ*, **Prokhorova E**, Colby T, Zobel F, Ahel I#, Matic I#. Interplay of Histone Marks with Serine ADP-Ribosylation. Cell Rep. 2018; 24(13):3488-3502.

Chapter 3:

Prokhorova E*, Zobel F*, Smith R, Zentout S, Gibbs-Seymour I, Schützenhofer K, Peters A, Groslambert J, Zorzini V, Agnew T, Brognard J, Nielsen ML, Ahel D, Huet S, Suskiewicz MJ#, Ahel I#. Serine-linked PARP1 auto-modification controls PARP inhibitor response. Nat Commun. 2021; 12(1):4055.

Chapter 4:

Prokhorova E*, Agnew T*, Wondisford AR, Tellier M, Kaminski N, Beijer D, Holder J, Groslambert J, Suskiewicz MJ, Zhu K, Reber JM, Krassnig SC, Palazzo L, Murphy S, Nielsen ML, Mangerich A, Ahel D, Baets J, O'Sullivan RJ, Ahel I. Unrestrained poly-ADP-ribosylation provides insights into chromatin regulation and human disease. Mol Cell. 2021; 81(12):2640-2655.e8;

Hanzlikova H, **Prokhorova E**, Krejcikova K, Cihlarova Z, Kalasova I, Kubovciak J, Sachova J, Hailstone R, Brazina J, Ghosh S, Cirak S, Gleeson JG, Ahel I, Caldecott KW. Pathogenic ARH3 mutations result in ADP-ribose chromatin scars during DNA strand break repair. Nat Commun. 2020; 11(1):3391.

Abstract

ADP-ribosylation (ADPr) is a widespread post-translational modification that controls many cellular processes, in particular DNA repair. Poly(ADP-ribose) polymerase 1 (PARP1) is the main ADPr enzyme that performs about 85-90% of DNA damage-induced ADPr. In response to DNA damage, PARP1 rapidly binds to DNA ends at the sites of DNA damage and modifies itself, histones and other proteins, thus promoting and regulating DNA repair. However, despite the critical role of PARP1 in DNA repair, for over 50 years the amino acid specificity of PARP1 remained controversial. Recently, our group and others discovered that PARP1 in complex with HPF1 predominantly performs ADPr at serine residues, both in response to exogenous DNA damage and under physiological conditions, and ARH3 is the hydrolase responsible for its timely reversal.

Here, we assessed the abundance of serine-ADPr in human cells, and performed the validation of several serine-ADPr substrates, including histones. Our results established serine as the primary site of ADPr in DNA damage signalling and described serine-ADPr as an additional component of histone code.

Then, we investigated the relationship between the levels of physiological serine-ADPr and cell sensitivity to PARP inhibitors, which are currently approved or in clinical trials against various types of cancer. We demonstrated that serine-ADPr, in particular on PARP1 serines 499, 507 and 519, counteracts PARP inhibitor-induced DNA damage and cell death, contributing to PARP inhibitor resistance.

Furthermore, we discovered a synthetic lethal interaction between ARH3 and the main poly-ADPr hydrolase PARG. We showed that simultaneous suppression of the two hydrolases results in excessive accumulation of poly-ADPr on serine residues, which disrupts histone modification and transcription states, and eventually leads to PARP-dependent cell death.

Overall, our findings provide novel insights into the role of serine-ADPr in human cells and highlight serine-ADPr regulators HPF1 and ARH3 as novel biomarkers for cancer cell sensitivity to PARP and PARG inhibitors. Fundamentally, our results allow us to suggest the existence of minimum and maximum thresholds for serine-ADPr, crossing of which would be detrimental to cellular homeostasis.

Contents

Acknowledgements **2**

Declaration **3**

Abstract **4**

Contents **5**

List of commonly used abbreviations **7**

List of Figures **9**

List of Tables **13**

1. Introduction **14**

1.1. Protein ADP-ribosylation 14

1.1.1. ‘Writers’ and acceptors of protein ADP-ribosylation 14

1.1.2. ‘Erasers’ of protein ADP-ribosylation 16

1.1.3. PARP1/2-HPF1 complex as the ‘writer’ of serine-ADP-ribosylation 20

1.1.4. ‘Readers’ of protein ADP-ribosylation 23

1.2. Protein ADP-ribosylation and human disease 25

1.2.1. ‘Writers’ of ADP-ribosylation as therapeutic targets 26

1.2.1.1. Clinical use of PARP1/2 inhibitors 28

1.2.1.2. Mechanisms of resistance to PARP1/2 inhibitors 29

1.2.2. ‘Erasers’ of ADP-ribosylation as potential targets in cancer therapy 31

2. Serine is the major site of ADP-ribosylation in response to DNA damage 32

2.1. Introduction 32

2.2. Results 33

2.2.1. Global ADP-ribosylation is dependent on serine-ADP-ribosylation 'writer' PARP1-HPF1 and 'eraser' ARH3 33

2.2.2. Targets of DNA damage-induced serine-ADP-ribosylation 36

2.2.3. ‘KS’ and ‘RS’ motifs are preferred targets for serine-ADP-ribosylation on histone H3 42

2.2.4. Crosstalk between DNA damage-induced histone serine-ADP-ribosylation and canonical histone posttranslational modifications....43

2.3. Discussion....45

3. Serine-ADP-ribosylation controls cell response to PARP1/2 inhibition....48

3.1. Introduction....48

3.2. Results....49

3.2.1. HPF1 and ARH3 control serine-ADP-ribosylation levels and determine cellular response to PARP1/2 inhibitors....49

3.2.2. Serines 499, 507 and 519 are the major sites of PARP1 ADP-ribosylation .55

3.2.3. Loss of PARP1 ADP-ribosylation at serines 499, 507 and 519 leads to increased sensitivity to PARP1/2 inhibition....59

3.3. Discussion....61

4. Functional synergy and synthetic lethal interaction between the major ADP-ribosylation 'erasers' ARH3 and PARG....66

4.1. Introduction....66

4.2. Results....66

4.2.1. Loss of ARH3 activity results in the accumulation of chromatin-associated serine-linked mono-ADP-ribosylation throughout the cell cycle....66

4.2.2. Both ARH3 and PARG are required for timely reversal of endogenous and exogenous stress-induced poly-ADP-ribosylation....69

4.2.3. ARH3 loss sensitises cancer cells to PARG inhibition and renders cells more resistant to PARP1/2 inhibitors....75

4.2.4. Accumulation and persistence of chromatin-bound poly-ADP-ribosylation affects histone modification and transcription profiles....81

4.2.5. Loss of ARH3 function sensitises primary patient fibroblasts to the induction of poly-ADP-ribosylation....89

4.3. Discussion....93

5. General Discussion....100

6. Conclusions and Future Directions....105

7. Materials and Methods....107

7.1. Cell culture 107
7.2. Generation of cell lines 108
7.3. Western blotting 110
7.4. Plasmids and site-directed mutagenesis 111
7.5. siRNA transfection 111
7.6. Plasmid transfection and protein immunoprecipitation 112
7.7. Immunofluorescence and confocal microscopy 112
7.8. Live-cell imaging following laser micro-irradiation 113
7.9. Flow cytometry 114
7.10. Cell proliferation assays 114
7.11. *In vitro* ADP-ribosylation assays 114
7.12. RNA-sequencing data generation and analysis 115
7.13. Quantification and statistical analysis 116
References 117
Appendix 132

List of commonly used abbreviations

ADPr	ADP-ribosylation
ARH3	ADP-ribosylhydrolase 3
ART	ADP-ribosyltransferase
ATM	Ataxia telangiectasia mutated protein
ATR	Ataxia telangiectasia and RAD3-related protein
BER	Base excision repair
DDR	DNA damage response
DSB	Double-strand break

GFP	Green fluorescent protein
GSEA	Gene Set Enrichment Analysis
H_2O_2	Hydrogen peroxide
H3K9ac	Histone H3 lysine 9 acetylation
H3K9me3	Histone H3 lysine 9 tri-methylation
H3S10ADPr	Histone H3 serine 10 ADP-ribosylation
H3S10P	Histone H3 serine 10 phosphorylation
HPF1	Histone PARylation factor 1
HR	Homologous recombination
IP	Immunoprecipitation
KO	Knockout
MAR	Mono(ADP-ribose)
MEFs	Mouse embryonic fibroblasts
MMS	Methyl methanesulfonate
NAD^+	Nicotinamide adenine dinucleotide
OE	Overexpression
PAR	Poly(ADP-ribose)
PARG	Poly(ADP-Ribose) glycohydrolase
PARGi(s)	PARG inhibitor(s)
PARP	Poly(ADP-ribose) polymerase
PARPi(s)	PARP1/2 inhibitor(s)
PTM	Posttranslational modification

SSB	Single-strand break
TNBC	Triple-negative breast cancer
WT	Wild-type

List of Figures

Figure 1. Schematic representation of the substrate specificity of human ADPr hydrolases. 17

Figure 2. Model of ARH3 in complex with ADPr and two Mg^{2+} ions. 18

Figure 3. Schematic representation of serine-ADPr synthesis and reversal. 20

Figure 4. HPF1 and PARP1/2 form a composite active site. 21

Figure 5. Proposed catalytic mechanism of glutamate/aspartate- and serine-linked ADPr. 22

Figure 6. Schematic representation of ADPr recognition by ‘readers’ containing ADPr-binding domains. 23

Figure 7. Serine-ADPr is the main type of DNA damage-induced ADPr. 35

Figure 8. Serines 6 and 10 are the main ADPr sites on histone H2B and H3, respectively. 37

Figure 9. ADPr of high-mobility group and histone H1 proteins is HPF1-dependent. 39

Figure 10. Serines 188 and 27 are the main sites of ADPr on histone H1.2 and H1.4, respectively. 41

Figure 11. Serines 8, 181 and 25 are the main ADPr sites of HMGA1, HMGB1 and HMGN1, respectively. 42

Figure 12. The preceding lysine is important for histone H3 serine 10 ADPr. 43

Figure 13. DNA damage-induced histone H3 serine-ADPr interferes with proximal acetylation and phosphorylation, but not methylation. 45

Figure 14. Serine-ADPr as an additional component of the histone code. 47

Figure 15. Loss of HPF1 specifically sensitises cells to PARP1/2 inhibitors but not to inhibitors of other factors involved in the regulation of cellular ADPr. 50

Figure 16. Cytotoxic effects of PARP1/2 inhibition depend on cellular HPF1 and ARH3 protein levels. 52

Figure 17. HPF1-mediated serine-ADPr promotes PARP1 release from damaged DNA. 53

Figure 18. ARH3 overexpression renders cells more sensitive to PARP1/2 inhibition. 54

Figure 19. Loss of ARH3 confers resistance to PARP1/2 inhibitor treatment. 55

Figure 20. DNA damaging agents H_2O_2 and MMS induce similar patterns of cellular ADPr. 56

Figure 21. Model of PARP1 bound to a single-strand DNA break including mass spectrometry-identified sites in the auto-modification domain of PARP1. 57

Figure 22. Serines 499, 507 and 519 are the main sites of PARP1 ADPr. 58

Figure 23. Loss of the main PARP1 ADPr sites serine 499, 507 and 519 leads to increased cell sensitivity to PARP1/2 inhibition and DNA damage accumulation. 60

Figure 24. PARP1 ADPr at serines 499, 507 and 519 promotes PARP1 release from damaged DNA. 61

Figure 25. Proposed model of the effect of HPF1 loss and ARH3 overexpression on PARPi response. 64

Figure 26. The role of HPF1 and ARH3 in the regulation of PARP1 function. 65

Figure 27. Loss of ARH3 leads to accumulation of chromatin-bound mono-ADPr. 67

Figure 28. ARH3-deficient cells accumulate chromatin-bound mono-ADPr throughout different stages of the cell cycle. 68

Figure 29. PARG inhibition leads to greater accumulation and persistence of both ADPr in unstressed conditions and ADPr induced by exogenous DNA damage in ARH3-deficient cells. 70

Figure 30. Excessive accumulation of ADPr upon simultaneous PARG inhibition and ARH3 deficiency does not lead to increased γH2AX formation. 71

Figure 31. PARG inhibition leads to excessive accumulation of poly-ADPr in ARH3-deficient cells. 72

Figure 32. Excessive accumulation of ADPr is observed both upon PARG inhibition and siRNA-mediated PARG knockdown, and is a widespread phenomenon. 73

Figure 33. Distinct regulation of the initiation and elongation stages in the ADPr reaction *in vitro*. 74

Figure 34. ARH3 deficiency is synthetically lethal with PARG inhibition in a PARP1/2-dependent manner. 76

Figure 35. Complementation with ARH3 WT, but not catalytically inactive D77/78N mutant, rescues PARGi sensitivity and ADPr reversal in ARH3-deficient cells. 77

Figure 36. PARG inhibition disrupts cell cycle progression in ARH3-deficient cells in a PARP1/2-dependent manner. 79

Figure 37. ARH3 loss renders cancer cells resistant to PARP1/2 inhibition. 80

Figure 38. Excessive ADPr in PARGi-treated ARH3-deficient cells interferes with histone acetylation. 82

Figure 39. Accumulation of histone H3 ADPr interferes with neighbouring acetylation marks even in the absence of exogenous DNA damage. 83

Figure 40. ARH3 loss leads to reduced histone H3 lysine 9 acetylation in newly incorporated nucleosomes. 84

Figure 41. Excessive ADPr in PARGi-treated ARH3-deficient cells leads to a decrease in PARP1 and PARP2 protein levels. 86

Figure 42. PARG inhibition results in dysregulation of transcription in ARH3-deficient cells. 87

Figure 43. Overexpression of PARP1 further exacerbated PARGi-induced toxicity and ADPr accumulation. 88

Figure 44. Loss of ARH3 function in patient-derived primary human fibroblasts leads to the accumulation of endogenous chromatin ADPr throughout the cell cycle. 90

Figure 45. Loss of ARH3 activity in patient-derived primary human fibroblasts leads to the accumulation of ADPr, PARGi sensitivity and PARPi resistance. 91

Figure 46. Complementation with ARH3 WT, but not catalytically inactive D77/78N mutant, rescues the phenotype of ARH3-deficient patient-derived primary human fibroblasts. 92

Figure 47. ARH3 deficiency leads to the accumulation ADPr, PARGi sensitivity and PARPi resistance in glioblastoma cells. 93

Figure 48. Proposed model of two-step ADPr reaction and stress-induced pathogenesis in neurodegeneration patients with ARH3 deficiency. 96

Figure 49. Serine-ADPr reaction and its crosstalk with neighbouring acetylation modifications in human cells. 101

Figure 50. Proposed model of the relationship between serine-ADPr levels controlled by HPF1 and ARH3 and cellular response to PARP1/2 and PARG inhibition. 104

Figure S1. Total DNA damage-induced ADPr is dependent on HPF1. Related to Figure 7. 132

Figure S2. Reversal of H1.2 and H1.4 ADPr is ARH3-dependent. Related to Figure 9. 133

Figure S3. Olaparib-induced γH2AX formation depends on cellular HPF1 and ARH3 protein levels. Related to Figure 16. 134

Figure S4. Flow cytometry gating strategy for analysis of Olaparib-induced changes in cell cycle distribution and γH2AX formation. Related to Figure 16. 135

Figure S5. Comparison of control and ARH3 KO cell proliferation rates. Related to Section 4.2.1. 135

Figure S6. Complementation with ARH3 WT, but not catalytically inactive D77/78N mutant, rescues the reversal of DNA damage-induced ADPr. Related to Figure 35. 136

Figure S7. Representative scatterplots of cell cycle analysis by flow cytometry of EdU- and DAPI-stained cells. Related to Figure 36. 137

Figure S8. Long-term PARG inhibition perturbs cell proliferation in ARH3 KO cells. Related to Figure 36. 137

Figure S9. Assessment of ADPr and BRCA1/2 protein levels upon BRCA1/2 knockdown, and in BRCA1 WT and BRCA1 mutant TNBC cells. Related to Figure 37. 138

Figure S10. PARG inhibition does not lead to a significant reduction of NAD^+ levels in ARH3-deficient cells. Related to Section 4.2.4. 138

Figure S11. Long-term PARG inhibition leads to a decrease in H3K9ac levels in ARH3-deficient cells. Related to Figure 40. 139

Figure S12. Heat map of Pearson's correlation coefficients used to measure reproducibility of sample preparation and RNA-sequencing results. Related to Figure 42. 140

Figure S13. C26F mutation causes a substantial reduction in ARH3 protein levels. Related to Section 4.2.5. 140

List of Tables

Table 1. The mechanisms of PARPi resistance. 29

1. Introduction

1.1. Protein ADP-ribosylation

The first notion of ADP-ribosylation (ADPr) is going back as far as 1963 (Chambon et al., 1963). Once described biochemically as a transfer of ADP-ribose from NAD^+ onto an acceptor molecule with the simultaneous release of nicotinamide, ADPr historically was first characterised as the pathogenic mode of action of diphtheria toxin, inhibiting protein biosynthesis in mammalian cells by ADPr of the eukaryotic elongation factor 2 (eEF2) (Gill et al., 1969; Honjo et al., 1968). Thousands of proteins from different organisms were later found to be modified by ADPr, leading to its recognition as an evolutionarily conserved and highly widespread posttranslational modification (PTM). Now, with as much as one third of the human nuclear proteome being targeted by ADPr (Hendriks et al., 2019), it is widely acknowledged that protein ADPr is critical in the regulation of many key cellular processes, including DNA damage response (DDR), cell death, chromatin remodelling, transcription and translation (Gupte et al., 2017; Posavec Marjanović et al., 2017). In addition, while for a long time ADPr was only known to occur on proteins, recent reports have shown that other molecules, such as small chemical groups, DNA and RNA can also be ADP-ribosylated (Crawford et al., 2018; Groslambert et al., 2021). However, the physiological roles of these forms of ADPr remain largely unknown.

1.1.1. ‘Writers’ and acceptors of protein ADP-ribosylation

ADPr is catalysed by the ADP-ribosyltransferase (ART) superfamily defined by their structurally similar catalytic ART domain required for the binding and processing of NAD^+. The ART superfamily is comprised of three distinct families of enzymes, namely poly-ADP-ribose polymerases (PARPs), arginine-specific ectoenzymes (ARTCs), and sirtuins (Crawford et al., 2018). PARPs are the most thoroughly characterised ART family, which in humans consists of 17 members with a conserved catalytic ART domain, but distinct regulatory domains that dictate their biochemical and cellular functions (Azarm and Smith, 2020).

Although the proteins of the PARP family were named after its founding member, PARP1, which is able to elongate protein-linked mono(ADP-ribose) (MAR) to form long poly(ADP-ribose) (PAR) chains, only PARP1, PARP2 and PARP5a/PARP5b (TNKS1/TNKS2) have been characterised as PAR-synthesizing enzymes. PARP3, PARP4, PARP6, PARP9, PARP10, PARP14, PARP15 and PARP16 can catalyse

only the attachment of MAR onto their target proteins (Vyas et al., 2014; Yang et al., 2017), while PARP13 is thought to be catalytically inactive (Vyas et al., 2014).

PARP1 is the most studied member of the family, and is particularly known for its key role in the DDR, a network of cellular pathways that have evolved to detect, signal and repair DNA lesions that are constantly caused by endogenous and environmental factors, even in the course of normal cellular metabolism (Gupte et al., 2017). If unrepaired, or repaired incorrectly, DNA lesions lead to mutations, whose accumulation impairs normal cell homeostasis and often results in the development of various diseases, in particular cancer. To counter this threat, multiple sensors of DNA damage, including PARP1, as well as other PARP family members, PARP2 and PARP3, are swiftly recruited to signal the presence of damaged DNA and facilitate its repair (Liu et al., 2017).

ADPr is one of the earliest PTMs in response to DNA damage, and it is the first event at the sites of DNA damage induced by laser micro-irradiation (Liu et al., 2017). PARP1 is the main 'writer' of cellular ADPr, which accounts for around 85-90% of ADPr following DNA damage, while PARP2 performs around 10% of DNA damage-induced ADPr (Amé et al., 1999; Chen et al., 2018; Liu et al., 2017; Szántó et al., 2012). Accordingly, PARP1 or PARP2-deficient mice and mouse embryonic fibroblasts (MEFs), although viable, show various chromosomal aberrations and DNA repair defects, whereas the double knockout (KO) of PARP1 and PARP2 results in early embryonic lethality (Ménissier de Murcia et al., 2003). Both PARP1 and PARP2 rapidly detect DNA ends at the sites of damage, bind to them and modify themselves, histones and other neighbouring proteins, promoting recruitment of multiple DDR factors and facilitating DNA repair.

Despite the critical role of PARP1 and PARP2 in the DDR, until recently, the amino acid specificity of these enzymes remained controversial. Historically, the acidic residues glutamate and aspartate, the main ADPr sites in an *in vitro* reaction comprising PARP1 or PARP2, activated DNA and NAD^+, were considered to be the predominant cellular modification targets (Daniels et al., 2015). However, lysine, arginine and cysteine have also been suggested.

In 2016, the Ivan Matic and our groups discovered that serine residues can also serve as acceptors of ADP-ribose (Leidecker et al., 2016) and revealed the basic molecular mechanisms behind this modification, characterising Histone PARylation Factor 1 (HPF1/C4orf27) (Gibbs-Seymour et al., 2016) as a PARP1/2-interacting protein required for switching its specificity towards serine residues (Bonfiglio et al.,

2017). Around the same time, lysine residues were reported to be the dominant targets of ADPr in HeLa cells treated with H_2O_2 by an independent study (Martello et al., 2016). However, subsequent computational reanalysis of the respective mass spectrometry dataset (Martello et al., 2016), implementing an unbiased approach allowing ADPr detection on all reactive amino acids, suggested that about 250 ADPr sites annotated as lysine modifications could be instead the sites of serine-ADPr, which were found to be predominantly preceded by lysines (Bonfiglio et al., 2017). This suggested that serine-ADPr could be a widespread modification in DNA damage signalling.

By now, a number of recent works from our and other groups, have provided compelling evidence that serine-ADPr can be efficiently synthesized by PARP1/2 only in the complex with HPF1, forming a composite active site (Bilokapic et al., 2020; Bonfiglio et al., 2017; Gaullier et al., 2020; Gibbs-Seymour et al., 2016; Hendriks et al., 2021; Rudolph et al., 2021; Sun et al., 2021; Suskiewicz et al., 2020), and that serine residues are the main acceptors of both ADPr in unstressed conditions and ADPr induced by exogenous DNA damage in human cells (Bilan et al., 2017; Bonfiglio et al., 2017; Buch-Larsen et al., 2020, 2021; Hendriks et al., 2019, 2021; Larsen et al., 2018; Nowak et al., 2020; Palazzo et al., 2018). The recent works have also provided insights into the entire landscape of cellular ADPr, obtaining only weak evidence of trace ADPr at glutamate and aspartate residues, which were historically thought to be the main ADPr targets (Daniels et al., 2015). Instead, the next three most abundantly modified amino acids after serine were arginine, tyrosine and histidine following induction of ADPr using a DNA damaging agent hydrogen peroxide (H_2O_2), and arginine, histidine and cysteine under physiological conditions. While serine-ADPr was shown to predominantly modify nuclear proteins, arginine-ADPr was linked to the endoplasmic reticulum and the Golgi apparatus, histidine-ADPr to the mitochondrion and tyrosine-ADPr to the ribosome (Buch-Larsen et al., 2020; Hendriks et al., 2019). Cysteine ADPr did not show a particular trend for any of the annotated cellular compartments.

1.1.2. ‘Erasers’ of protein ADP-ribosylation

Similar to other PTMs, ADPr is a reversible modification, and several ‘eraser’ enzymes that possess ADP-ribosylglycohydrolase activity belonging to macrodomain and ADP-ribosylhydrolases (ARH) superfamilies have been identified in human cells.

The timely reversal of ADPr is essential for the precise regulation of many signalling pathways, as well as nucleotide recycling, and is especially needed in the event of

DNA damage to prevent the trapping of proteins recruited in an ADPr-dependent manner and allow access for the downstream DDR proteins (Liu et al., 2017). PAR glycohydrolase (PARG), a macrodomain superfamily member, and ADP-ribosyl hydrolase 3 (ARH3/ADPRHL2), ARH superfamily member, are the two vertebrate enzymes that are capable of cleaving the O-glycosidic bond between ADPr subunits within PAR *in vitro* (Lin et al., 1997; Oka et al., 2006) (Figure 1, top).

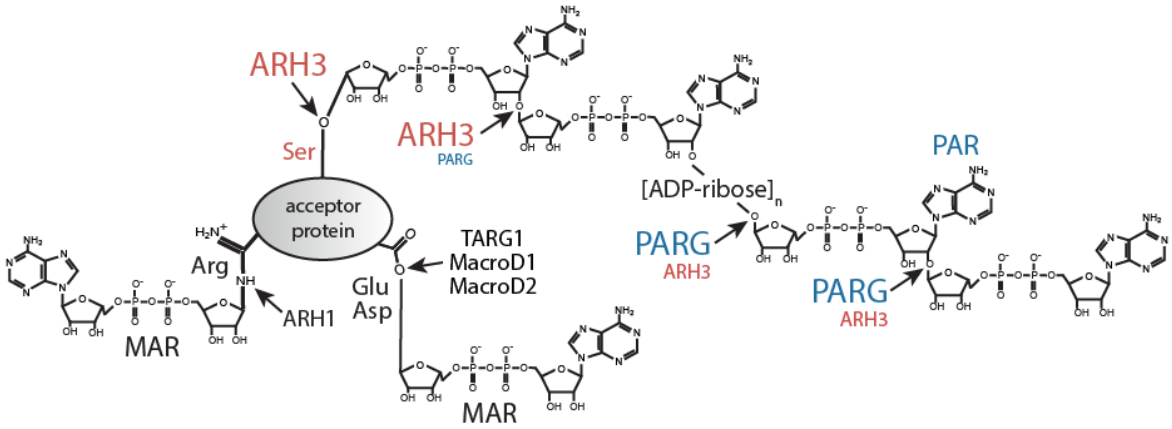


Figure 1. Schematic representation of the substrate specificity of human ADPr hydrolases.

All macrodomain proteins are unified by a conserved α/β/α sandwich structure with a conserved ADP-ribose binding site along the crest of the domain. However, the catalytic centre of these domains has diversified and thus five distinct mechanisms for ADPr hydrolysis have emerged, whilst some macrodomains have lost their catalytic ability and serve now as modification readers (Rack et al., 2020).

ARH superfamily members are mainly α-helical enzymes with a catalytic binuclear bivalent metal centre. In humans, ARH superfamily is comprised of two active (ARH3 and ARH1) and one inactive (ARH2) enzymes. Enzymatic activity of ARH3 requires the presence of two Mg^{2+} ions (Figure 2), whilst no detailed investigation for ARH1 has been carried out so far (Rack et al., 2020).

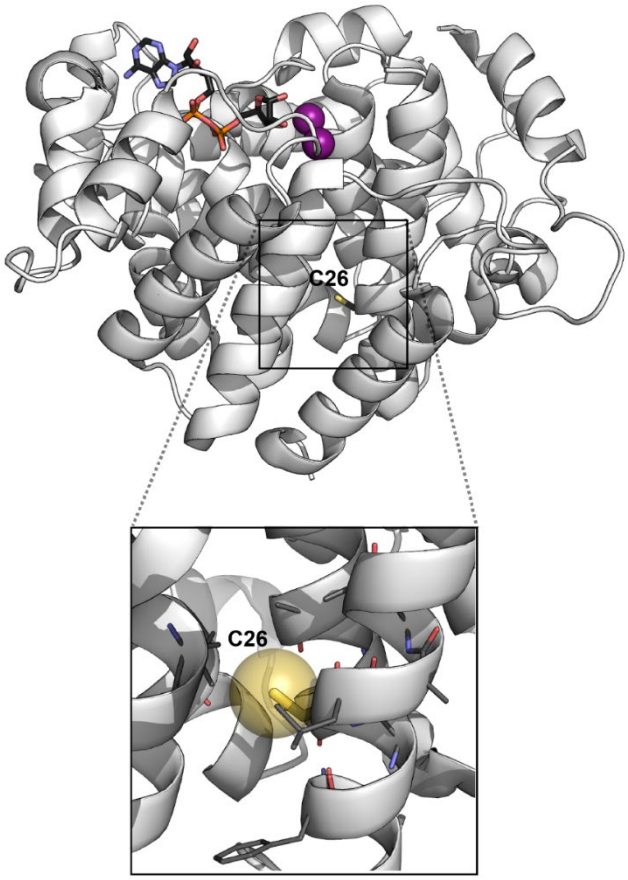


Figure 2. Model of ARH3 in complex with ADPr and two Mg^{2+} ions.

Ribbon representation of human ARH3 from PDB accession 6D36 in complex with ADPr (orange) and two $Mg2^{+}$ ions (purple). Cysteine 26 (C26) is the residue substitutes to phenylalanine as a result of a pathogenic missense mutation NM_017825: c.77G>T (p.Cys26Phe) described here in Section 4.2.5. Bottom panel, Van der Waals radius of C26 sulphur side chain sulphur atom is depicted as a transparent yellow sphere. C26 is located in the core of a conserved helical bundle. The figure was partially adapted from (Beijer et al., 2021).

PARG is the most active PAR hydrolase in human cells and is essential for mouse and *Drosophila* development (Hanai et al., 2004; Koh et al., 2004), with PARG KO resulting in only rarely surviving flies exhibiting increased poly-ADPr levels and progressive neurodegeneration (Hanai et al., 2004). Similar to the loss of PARP1 or PARP2, while mice lacking nuclear 110 kDa PARG isoform ($PARG_{110}$) are viable, $PARG_{110}$-deficient mice and mouse embryonic fibroblasts (MEFs) are hypersensitive to DNA damage (Cortes et al., 2004; Min et al., 2010). PARG activity is reduced with decreasing chain length down to low levels for oligomers comprised of 2-4 ADPr units (Barkauskaite et al., 2013), and PARG is unable to hydrolyse protein-linked MAR (Fontana et al., 2017; Slade et al., 2011).

ARH3 activity against long PAR chains is 1-2 orders of magnitude lower than that of PARG (Fontana et al., 2017; Oka et al., 2006). However, our group revealed that ARH3 is responsible for the specific reversal of serine-linked MAR (Fontana et al.,

2017), which has been confirmed later by (Abplanalp et al., 2017; Hendriks et al., 2021) and (Prokhorova et al., 2021a), with a part of the results from the latter study presented here in Section 4.2.1. In addition, ARH3 may still contribute to the degradation of poly-ADPr in certain cellular contexts (Mashimo et al., 2013). Although ARH3-deficient mice are viable with no obvious phenotypic defects without external challenges, ARH3-deficient mice and MEFs show increased sensitivity to high levels of H_2O_2, that can be rescued by PARP1/2 inhibition (Mashimo et al., 2013, 2019). Furthermore, loss-of-function mutations in ARH3, including a missense mutation NM_017825: c.77G>T (p.Cys26Phe), which is further described here in Section 4.2.5 and results in the substitution of cysteine 26 to phenylalanine (Figure 2), have been linked to the pathogenesis of several neurodegenerative phenotypes in human patients (Beijer et al., 2021; Danhauser et al., 2018; Ghosh et al., 2018; Mashimo et al., 2019), implying that similar to PARG, ARH3 may protect cells from the accumulation of poly-ADPr. Indeed, as we show here in Section 4.2.2, both ARH3 and PARG are essential for maintaining low levels of cellular poly-ADPr, although ARH3 mainly acts indirectly through removal of initial serine-linked MAR which then prevents its elongation into PAR products. Notably, simultaneous loss of ARH3 and PARG activity resulted not in an additive but in a markedly greater effect on cellular poly-ADPr levels, indicating the synergistic roles of the two hydrolases in human cells (Prokhorova et al., 2021a).

Other ‘erasers’ of ADPr that have been described to date are only capable of cleaving the bond between the ribose and the side chain of the acceptor amino acid. These include ARH superfamily member, ARH1, that is able to hydrolyse arginine-linked MAR, and macrodomain-type proteins, terminal ADP-ribosyl protein glycohydrolase (TARG1), MacroD1 and MacroD2, which were shown to reverse glutamate and aspartate-linked ADPr (Barkauskaite et al., 2015) (Figure 1, bottom). NUDT9 and NUDT16, and ENPP1, respectively belonging to the nucleoside diphosphate-linked moiety X (Nudix) and nucleotide pyrophosphatase/phosphodiesterases (NPP) families, are able to hydrolyse the phosphodiester bond within protein ADPr (Palazzo et al., 2015, 2016), although it remains an open question whether NUDT9, NUDT16 and ENPP1 can also process ADP-ribosylated substrates in human cells. Interestingly, the hydrolase activity of another Nudix enzyme, NUDT5, diverges from the other ADPr-processing family members. While NUDT5 cannot hydrolyse protein-conjugated ADP-ribose and thus cannot be classified as an ADP-ribose eraser per se, it generates ATP from free

ADP-ribose and pyrophosphate in a recycling-like process that replenishes nuclear ATP levels following ADPr catabolism (Wright et al., 2016).

1.1.3. PARP1/2-HPF1 complex as the 'writer' of serine-ADP-ribosylation

Since the discovery of serine-ADPr in 2016 (Leidecker et al., 2016), a number of studies by our and other groups have established HPF1 together with PARP1/2 and ARH3 as the key regulators of its cellular levels, performing the synthesis and reversal of the reaction, respectively (Figure 3).

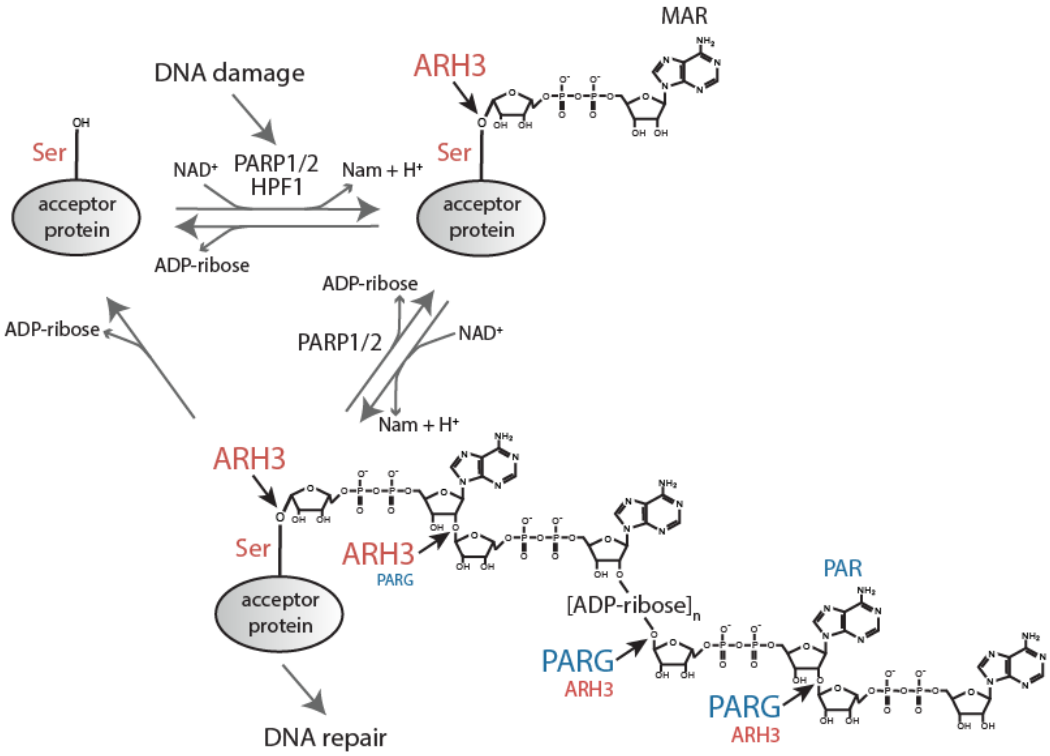


Figure 3. Schematic representation of serine-ADPr synthesis and reversal.

Indeed, PARP1 or PARP2 and HPF1 have been shown to form a composite active site (Figure 4), for which HPF1 provides critical substrate-binding and catalytic residues, changing the substrate specificity of PARP1/2 towards serine sites (Bilokapic et al., 2020; Gaullier et al., 2020; Rudolph et al., 2021; Sun et al., 2021; Suskiewicz et al., 2020). HPF1 specifically binds to the activated PARP1/2 bound to damaged DNA. Then, a substrate presumably binds to a putative peptide-binding site formed at the interface between HPF1 and PARP1/2 complex, which as shown by mapping electrostatic potential onto its surface, includes a strongly negatively charged surface provided by HPF1 (Figure 4C). This likely explains a strong preference of HPF1-PARP1/2 enzyme for positively charged lysine-serine 'KS' motifs as was noted by many studies (Bartlett et al., 2018; Bilan et al., 2017; Bonfiglio et al., 2017; Buch-Larsen et al., 2020, 2021; Hendriks et al., 2019, 2021; Larsen et al.,

2018; Leidecker et al., 2016) and briefly explored here on the example of histone H3 in Section 2.2.3.

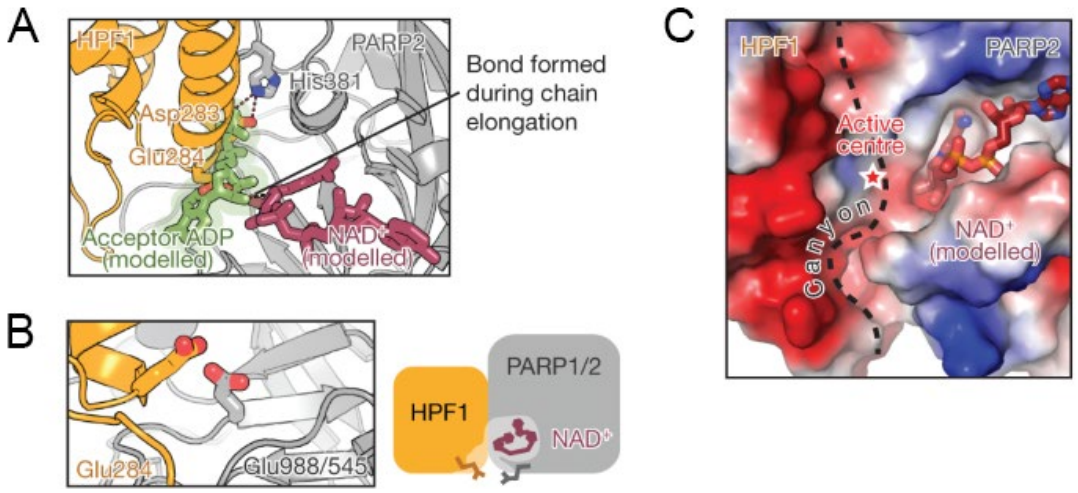


Figure 4. HPF1 and PARP1/2 form a composite active site.

(A, B) The active site of human HPF1 (orange) and PARP2 (grey) complex (PDB accession 6TX3). (A) HPF1 catalytic glutamate 284 is stabilized by the interaction between aspartate 283 of HPF1 and histidine 381 of PARP2 (equivalent to histidine 826 in PARP1). Modelled-in NAD^+ (red) and acceptor ADP fragment (green) were positioned by alignment with PDB accession 1A26. (B) HPF1 catalytic glutamate 284 is placed near the catalytic glutamate 988 of PARP1 (glutamate 545 in PARP2). (C) A putative peptide-binding canyon formed at the interface of HPF1 and PARP1/2 as indicated by a dashed line. Electrostatic surface potentials are coloured red and blue for negative and positive charges, respectively, and white colour represents neutral residues. The figure was adapted from (Suskiewicz et al., 2020).

In the joint active site, HPF1 catalytic glutamate 284 is placed near the catalytic glutamate 988 of PARP1 (glutamate 545 in PARP2) (Figure 4B) and the NAD^+ molecule, likely abstracting a proton from the acceptor serine in a substrate (Rudolph et al., 2021; Sun et al., 2021; Suskiewicz et al., 2020), similarly to conserved catalytic aspartate found in protein serine/threonine/tyrosine kinases (Endicott et al., 2012). Remarkably, this is the first reported instance of a composite active site in the field of PTMs, with a famous example from 25 years ago in the regulation of small GTPases by GTPase-activating proteins (GAPs), which contribute a missing catalytic arginine to complete the GTPase active site (Ahmadian et al., 1997). The deprotonation step performed by HPF1 glutamate 284 would also explain why HPF1, while required for serine modification, becomes dispensable when the acceptor is a glutamate or aspartate, which are deprotonated at neutral pH in contrast to serine residues (Figure 5). In addition to its role in determining the site specificity of PARP1/2-mediated ADPr, HPF1 also controls the length of the modification products, sterically interfering with the generation of poly-ADPr by PARP1/2 (Bacic et al., 2021; Gibbs-Seymour et

al., 2016; Langelier et al., 2021; Mohapatra et al., 2021; Rudolph et al., 2021; Suskiewicz et al., 2020).

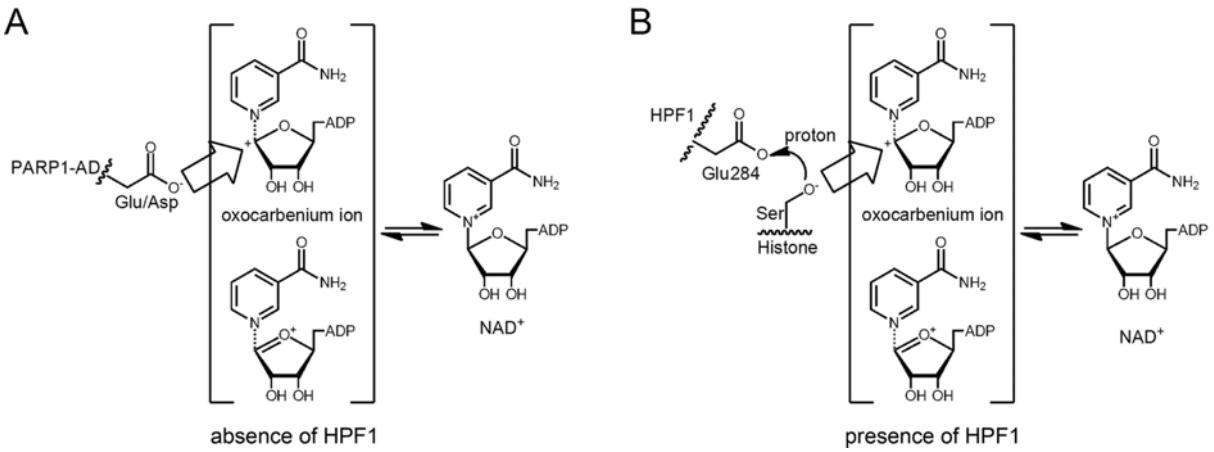


Figure 5. Proposed catalytic mechanism of glutamate/aspartate- and serine-linked ADPr.

(A) ADPr of glutamate or aspartate, which are deprotonated at neutral pH, does not require a catalytic base and can be performed by PARP1 auto-modification domain (AD) alone. (B) ADPr of serine requires its deprotonation by a catalytic base, which is provided by HPF1 glutamate 284. The figure was adapted from (Sun et al., 2021).

Given that the cellular protein concentration of PARP1 far exceeds that of HPF1, with PARP1 being about 20 times more abundant than HPF1 as assessed by proteomics in HeLa cells (Hein et al., 2015; Wang et al., 2012a), it has until very recently been unclear how HPF1 could efficiently direct PARP1 specificity. We have shown that while HPF1 is critical for the initiation of serine-ADPr, it is dispensable, and even unfavourable, during the extension of the initial modifications (Prokhorova et al., 2021a). Thus, we have suggested the existence of distinct initiation and elongation steps in the serine-ADPr reaction, that are mainly performed by HPF1-PARP1/2 and PARP1/2 alone, respectively, which is elaborated in our model in Section 4.2.2. A more recent biochemical study has supported the proposed model, demonstrating that HPF1 can work efficiently even at sub-stoichiometric ratios relative to PARP1 (with HPF1 to PARP1 ratios as low as 1:100 *in vitro*), rapidly associating and dissociating from PARP1, and notably stimulating the rate of serine-ADPr initiation compared to its elongation or initiation of glutamate- or aspartate-linked ADPr (Langelier et al., 2021). This regulation is aided by a dynamic ‘hit and run’ interaction between HPF1 and PARP1 with rapid association and dissociation as indicated by surface plasmon resonance (SPR) analysis. Thus, HPF1 not only interferes with poly-ADPr generation by PARP1/2 through sterically blocking its acceptor site, but also by markedly stimulating the rate of ADPr initiation at serine residues.

Then, given the 1:20 ratio of HPF1 and PARP1 concentrations in human cells, PARP1 is likely able to form multiple protein complexes. Indeed, in addition to PARP1-HPF1 protein complex, PARP1-Timeless (Xie et al., 2015; Young et al., 2015) and PARP1-NMNAT1 (Huang et al., 2020) complexes have been characterised. However, the extent and context of their cellular contribution remain unclear.

1.1.4. 'Readers' of protein ADP-ribosylation

PARP1/2-mediated ADPr performed at the sites of DNA damage plays an important role in the recruitment of a number of ADPr-binding DNA repair proteins. These 'readers' of ADPr contain ADPr-binding domains, including: 1) PAR-binding motif (PBM), 2) PAR-binding zinc-finger motif (PBZ), 3) macrodomain, 4) WWE domain or 5) Oligonucleotide/oligosaccharide-binding (OB) fold, which are characterized by certain structural features and interaction modes with ADPr (Figure 6).

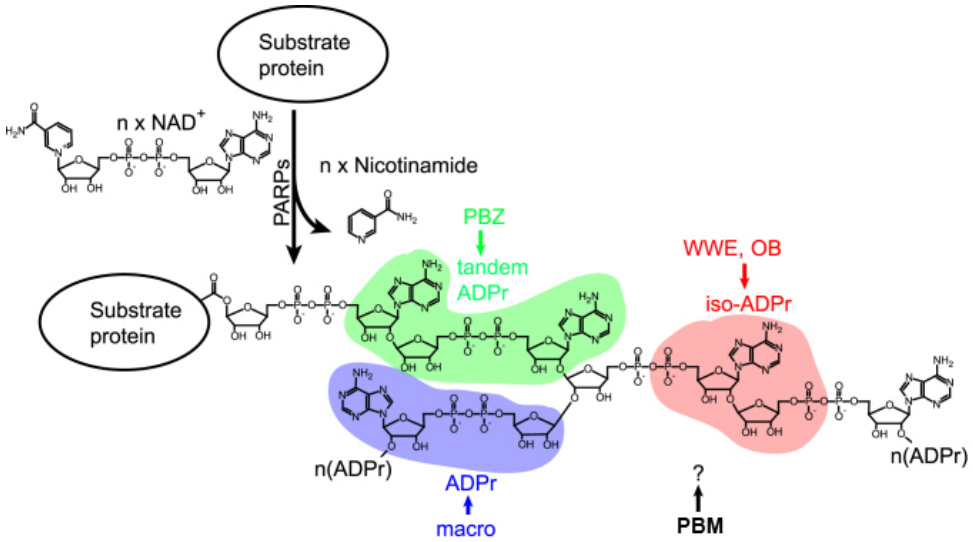


Figure 6. Schematic representation of ADPr recognition by 'readers' containing ADPr-binding domains.

The PBZ domain recognizes tandem ADP-ribose. The WWE and OB motifs recognize iso-ADP-ribose. The exact mode of the PBM domain interaction with ADP-ribose remains unclear and is likely due to electrostatic interactions between the positively charged residues present in the PBM consensus motif and the negatively charged ADPr. The figure was partially adapted from (Liu et al., 2017).

PBM, described as a weakly conserved consensus sequence of about 20 amino acid ($[HKR]_1$-X_2-X_3-$[AIQVY]_4$-$[KR]_5$-$[KR]_6$-$[AILV]_7$-$[FILPV]_8$), is a prevalent PAR interaction domain present in hundreds of proteins, including histones, p53, p21 and XRCC1 (X-ray repair cross-complementing protein 1) (Kliza et al., 2021; Pleschke et al., 2000; Teloni and Altmeyer, 2016), although recently PBM has also been suggested to interact with MAR in certain cases (Kliza et al., 2021). XRCC1 is a scaffolding protein

that together with PARP1/2 plays a key role in single-strand break (SSB) repair. XRCC1 is recruited to SSBs through direct interaction with PARP1/2-synsetised PAR and its central BRCT (BRCA1 C-terminus) domain, and in turn promotes the recruitment of the enzymes required for SSB repair, including PNKP (polynucleotide kinase/phosphatase), APTX (aprataxin), DNA polymerase β and DNA ligase 3 (Caldecott, 2014).

PBZ domains are short modules of about 30 amino acids with the consensus sequence [K/R]-X-X-C-X-[F/Y]-G-X-X-C-X-[K/R]-[K/R]-X-X-X-X-H-X-X-X-[F/Y]-X-H that bind to the junctions between two ADP-ribose units in PAR chains, whereas some PBZ domains can also recognize ADP-ribose monomers (Ahel et al., 2008). The proteins containing PBZ motifs include an E3 ubiquitin ligase CHFR and an XRCC1 binder APLF, both of which are recruited to the sites of DNA damage through its PBZ domains and participate in the DDR and checkpoint regulation.

Macrodomains are larger globular α/β/α sandwich domains consisting of about 130-190 amino acids that interact with an ADP-ribose monomer or the terminal ADP-ribose moiety in a PAR chain. In addition to the previously mentioned PARP family members PARP9, PARP14 and PARP15, and hydrolases PARG, TARG1, MacroD1 and MacroD2, macrodomain-containing proteins include chromatin remodelling factors histone variant macroH2A1.1 and ALC1 (Amplified in Liver Cancer 1), also known as CHD1L (chromodomain-helicase-DNA-binding protein 1-like) (Liu et al., 2017).

WWE and OB domains recognize the iso-ADPR linkages formed by two consecutive ADPr units, thus binding exclusively to oligo or poly-ADPr (Wang et al., 2012b; Zhang et al., 2014). WWE domains are about 80-100 amino acid long and contain conserved tryptophan (W) and glutamate (E) residues (Wang et al., 2012b). WWE domains are reported to be present in E3 ubiquitin-protein ligases such as RNF146, HUWE1, Deltex1, Deltex2 and Deltex4, and in PARP family members PARP11 and PARP14. OB-fold is about 70-150 amino acid long and contains antiparallel five-stranded beta-barrel with a terminating alpha-helix found in proteins that bind to single-stranded nucleic acids or oligosaccharides (Zhang et al., 2014). The proteins containing the OB-fold include DNA repair proteins SSB1 and BRCA2, with the OB-fold domains allowing their quick recruitment to DNA lesions (Zhang et al., 2015).

With the recent discovery of serine-ADPr, specific ‘readers’ of this ADPr type and whether HPF1 function affects the recruitment of XRCC1 and other PAR-binding factors remain to be characterised. However, one study has already shown the

importance of HPF1 at least for the recruitment of XRCC1 and DNA ligase 3 complex in alternative Okazaki fragment ligation when DNA ligase 1 is absent (Kumamoto et al., 2021). Notably, another recent study has described a chromatin remodelling protein ALC1, which is rapidly recruited to the sites of DNA damage by PAR chains of a minimum of three ADPr units (Ahel et al., 2009; Singh et al., 2017), as a binder of HPF1-dependent ADPr (Bacic et al., 2021). Excitingly, ALC1 has recently attracted a particular interest as a potential target in cancer therapy, as its loss has been shown to sensitise cells to PARP1/2 inhibition to an extent similar to that following the loss of HPF1 (Blessing et al., 2020; Hewitt et al., 2021; Juhász et al., 2020; Verma et al., 2021).

1.2. Protein ADP-ribosylation and human disease

Dysregulation of PARP1 and other enzymes involved in ADPr signalling has been linked to a number of inherited and acquired human diseases, most notably cancer and neurodegeneration.

PARP1 is involved in many cellular pathways, in particular the pathways of the DDR network, in which PARP1 plays a key role in the repair of SSBs, initiating the recruitment of SSB repair factors though a scaffolding protein, XRCC1 (Caldecott, 2014), as described in the section above. Identification of the critical role of PARP1 in the regulation of the DDR and maintenance of genome stability provided the rationale for inhibitor development in order to promote cancer cell death through supressing the repair of chemotherapy- and radiotherapy-inflicted DNA damage. In 2005, it was discovered that cells deficient in double strand break (DSB) repair by homologous recombination (HR) due to loss-of-function mutations in BRCA1 or BRCA2 (Moynahan et al., 1999, 2001) rely on PARP1 function in DNA repair and are hypersensitive to PARP1/2 inhibitors (PARPis) (Bryant et al., 2005; Farmer et al., 2005). This interaction between PARP1 and BRCA1/2 can be described as synthetic lethal. The phenomenon of synthetic lethality has its roots in genetic experiments mainly performed in model organisms with smaller genomes such as yeast or fruit flies, and occurs between two genes where individual loss of either gene is compatible with life, but simultaneous loss of both genes results in cell death. For a long time, it has been suggested that a synthetic lethal approach could be used in the treatment of cancer allowing for selective tumour targeting by inducing synthetic lethality between two genes (Hartwell et al., 1997). The prospect of achieving this selective tumour targeting by inducing synthetic lethality between PARP1 and BRCA1/2 has fuelled interest in developing clinically relevant PARP1/2 inhibitors

(PARPis) that still remains high. In 2014, building on numerous preclinical investigations, approval of a PARPi Olaparib as maintenance therapy for platinum-sensitive advanced ovarian cancer with BRCA1/2 germline mutations (Kim et al., 2015) became the first example of a successful synthetic lethal approach that has entered the clinic.

While normally endogenous DNA damage induces moderate activation of PARP1, excessive activation results in NAD^+/ATP depletion and/or release of PAR chains with subsequent induction of parthanatos, a mode of regulated necrotic cell death (Prokhorova et al., 2020). These events, together with some other findings, including impairment of PARP1 function in the regulation of gene expression (Curtin and Szabo, 2020), have been implicated in the development of neurodegeneration and other pathological conditions. This has made PARP1 an attractive target to protect cells from its overactivation in neurodegenerative and other non-oncological diseases, especially if increased levels of DNA damage constitute a part of the pathophysiological response.

Defective reversal of ADPr by PARG (Hanai et al., 2004), TARG1 (Sharifi et al., 2013) and ARH3 hydrolases (Beijer et al., 2021; Danhauser et al., 2018; Ghosh et al., 2018; Mashimo et al., 2019) has also been shown to lead to neurodegenerative phenotypes due to the resultant increase in ADPr levels.

Compared to PARPs that are able to catalyse poly-ADPr, the roles of ADP-ribosyltransferases remain poorly understood, although recent studies have highlighted their involvement in various cellular pathways, including the DDR, tumorigenesis, inflammatory and antiviral responses (Challa et al., 2021). We hope that further characterisation of their functions will be facilitated by the recent progress in the development of individual inhibitors, most notably by the efforts of Ribon Therapeutics, Michael Cohen and Herwig Schuler labs, including specific and potent cell-permeable inhibitors targeting PARP3, PARP4, PARP7, PARP10, PARP11 and PARP14. The outcomes of recent studies are very encouraging and suggest that these inhibitors could find applications in the treatment of cancer, inflammatory diseases and viral infections (Challa et al., 2021).

1.2.1. ‘Writers’ of ADP-ribosylation as therapeutic targets

With the first discovered PARP1 inhibitor being nicotinamide itself (Clark et al., 1971), all subsequently developed inhibitors of PARP1 contain a similar pharmacophore and compete with NAD^+ for the catalytic site (Slade et al., 2020). For many of the

developed PARPis, the inhibition of the ART catalytic domain of PARP1 causes its prolonged retention on DNA often referred to as trapping (Hopkins et al., 2015), indicating that production of ADPr by PARP1 is necessary for its electrostatic repulsion from damaged DNA. Moreover, PARPis have been suggested to induce PARP1 trapping as a result of their allosteric binding effect (Zandarashvili et al., 2020). Depending on the way that a particular PARPi engages in the NAD^+ binding site adjacent to the HD domain, PARPi molecules exhibit different allosteric binding to PARP1. Accordingly, PARPis be classified into three types: Type I, allosteric pro-retention on DNA, PARPis that destabilize the HD domain and increase PARP1 affinity for damaged DNA; Type II, non-allosteric, PARPis that have no effect on the HD domain; and Type III, allosteric pro-release from DNA, PARPis that stabilize the HD domain and decrease PARP-1 affinity for damaged DNA (Zandarashvili et al., 2020).

Prolonged retention, or trapping, of PARP1 on DNA increases the number of DNA damage lesions, including DSBs, which are thought to mainly arise after the trapped PARP1 is encountered by the transcription machinery or replication fork (Pommier et al., 2016). This additionally overwhelms cells with deficiencies in DNA repair genes, going beyond the initially discovered HR deficiency caused by BRCA1/2 mutations (Slade, 2020), and eventually leads to cell death. PARP1 is the predominant target for PARPi-induced trapping, as depletion of PARP1, but not PARP2, rescues PARPi toxicity (Murai et al., 2012). Among the established clinically relevant inhibitors, Talazoparib exhibits the highest trapping efficiency in human cells and, accordingly, demonstrates the highest cytotoxicity, while Veliparib is the weakest PARP1 trapper (Talazoparib >> Niraparib > Olaparib = Rucaparib >> Veliparib) (Murai et al., 2014). In the above-mentioned classification, Talazoparib and Olaparib are classified as non-allosteric, Type II inhibitors, whereas Niraparib, Rucaparib and Veliparib belong to the allosteric pro-release, Type III group (Zandarashvili et al., 2020).

While all of the developed clinically relevant PARPis induce substantial trapping of PARP1, even in the case of Veliparib with the weakest trapping activity, application of non-trapping PARPis would be the most desirable in the treatment of non-oncological diseases, including neurodegeneration. Indeed, genetic deletion of PARP1 showed a great promise in animal models of neurological disorders, including Parkinson's disease, amyotrophic lateral sclerosis, cerebellar ataxia and neuronal injury, and models of ischaemia-reperfusion injury, including stroke, cardiac infarction and ischemic renal injury (Kim et al., 2021). While CRISPR-Cas9 and RNA interference

technologies could be potentially applied to achieve this effect in patients, degrading protein targets, e.g., using PROTAC (proteolysis-targeting chimera) approach, presents another promising option with at least 15 targeted degraders expected to be soon used in the clinic (Mullard, 2021). Among several recently developed PARP1 PROTAC compounds, highly selective and potent iRucaparib-AP6, which, unlike a regular PARPi, does not cause PARP1 trapping, DNA damage or cell death, has shown a particular promise in preclinical studies (Kim et al., 2021). Whilst to our knowledge, no clinical trials are currently ongoing for the treatment of non-oncological diseases using PARPis, we hope that non-trapping PARP1 PROTAC degraders which would provide protection against PARP1 hyperactivation without inducing cytotoxicity caused by PARP1 trapping will present a viable therapeutic option.

In addition to PARP1/2, PARP5a/PARP5b are also capable of catalysing poly-ADPr. While several selective PARP5a/5b inhibitors have been developed (Kinosada et al., 2021; Thorsell et al., 2017), only E7449, a novel PARP1/2 and PARP5a/5b inhibitor has entered clinical trial (Plummer et al., 2020), and is expected to be particularly promising against advanced solid tumours with aberrant activation of the WNT/β-catenin signalling pathway which promotes tumour progression.

Compared to PARPs capable of poly-ADPr, the development of inhibitors against mono-ADPr PARPs is largely in its infancy. However and excitingly, a recently developed first-in-class PARP7 inhibitor RBN-2397 has already entered clinical trials for treatment of advanced solid tumours (Falchook et al., 2021).

1.2.1.1. Clinical use of PARP1/2 inhibitors

Building on numerous preclinical studies investigating the effects of PARPi treatment, Olaparib was first approved in 2014 as maintenance therapy for platinum-sensitive advanced ovarian cancer with BRCA1/2 germline mutations (Kim et al., 2015). To this day, four PARPis, namely Olaparib, Rucaparib (Balasubramaniam et al., 2017), Niraparib (Ison et al., 2018) and Talazoparib (Hoy, 2018), have been approved by U.S. Food and Drug Administration (FDA) and European Medicines Agency (EMA) for the treatment of breast, ovarian, pancreatic or prostate cancers. Approval of another PARPi, Veliparib, a Phase 3 monotherapy candidate, has not been achieved, although multiple clinical trials including Veliparib and other PARPis are still ongoing.

Despite the clinical success of the approved PARPis, all the four compounds have shown substantial haematological toxicities, suggesting that these side effects are

associated with their primary pharmacology (LaFargue et al., 2019; Pilié et al., 2019). Of note, these four compounds share a lack of selectivity for PARP1 over PARP2, and PARP2 was previously linked to haematological toxicity in a study using PARP2 KO mice (Farreś et al., 2013). Since the synthetic lethality between BRCA1/2 mutations and PARP1/2 inhibition was shown to be solely driven by PARP1 (Murai et al., 2012; Ronson et al., 2018), this suggested that an inhibitor selective for PARP1 over PARP2 could exhibit a similar potency, but at a substantially reduced toxicity.

While Olaparib and Niraparib are not selective for PARP1 over PARP2, as shown by a fluorescence polarization binding assay, Veliparib, Rucaparib and Talazoparib are modestly selective (18-, 25- and 51-fold, respectively), although Veliparib is also slightly active against PARP5a (Johannes et al., 2021). A recently developed potent PARP1 inhibitor AZD5305, in contrast to the clinically used PARPis, is highly selective over PARP2 (140-fold selectivity in a fluorescence polarization binding assay), PARP5a and other PARPs (Johannes et al., 2021), and therefore might exhibit a reduced haematological toxicity in the clinic. This inhibitor has already shown good pharmacokinetic and safety properties in preclinical studies (Johannes et al., 2021), and is currently undergoing Phase 1/2 clinical trials (NCT04644068) in patients with advanced solid breast, ovarian, pancreatic and prostate tumours.

1.2.1.2. Mechanisms of resistance to PARP1/2 inhibitors

Despite high response rate to PARPis seen among HR-deficient cancers, in particular those with mutations in the BRCA1/2 genes, innate and acquired resistance is frequent and leads to disease relapse. Multiple mechanisms have been identified to date, and the major types are presented, in brief, in Table 1.

Table 1. The mechanisms of PARPi resistance.

Effect	Resistance mechanism	References
HR restoration	Reversion mutations in mutant BRCA1/2 genes	(Edwards et al., 2008; Sakai et al., 2009)
	Enhanced end resection resulting from the loss of 53BP1 or its downstream REV7, RIF1 and Shieldin factors	(Bouwman et al., 2010; Callen et al., 2013; Chapman et al., 2013; Jaspers et al., 2013; Noordermeer et al., 2018; Xu et al., 2015)

Upregulation of drug efflux	Overexpression of the efflux transporter MDR1 or P-glycoprotein (P-gp)	(Christie et al., 2019; Rottenberg et al., 2008)
Restoration of replication fork stability via increased protection from fork degradation	Loss of PTIP expression resulting in impaired recruitment of MRE11 to stalled replication forks	(Chaudhuri et al., 2016; Guillemette et al., 2015)
	Loss of EZH2/MUS81 axis of fork degradation	(Rondinelli et al., 2017)
	Loss of the histone acetyltransferase PCAF	(Kim et al., 2020b)
	Loss of cell-cycle checkpoint arrest owing to the loss of SLFN11	(Murai et al., 2016)
Drug target alterations	Point mutation in PARP1	(Pettitt et al., 2018)
Restoration of PARP1 signalling	Loss of PARG or ARH3 hydrolases	(Gogola et al., 2018; Gomez et al., 2020; Prokhorova et al., 2021b, 2021a)
Removal of trapped PARP1	PARP1 SUMOylation by PIAS4, followed by RNF4-mediated ubiquitination and subsequent processing by p97 ATPase	(Baxter et al., 2022; Krastev et al., 2022)

With an improved understanding of the mechanisms underlying PARPi resistance, recent studies have suggested a number of potential strategies to either directly or indirectly counteract these pathways, and therefore overcome or even prevent PARPi resistance in the clinic (Andronikou and Rottenberg, 2021; Fugger et al., 2021; Prados-Carvajal et al., 2022). However, the vast majority of these strategies have been based only on preclinical data, while the clinical landscape of PARPi resistance has remained largely uncharacterised, with BRCA1/2 reversions so far being the only clinically validated mechanism of PARPi resistance.

1.2.2. ‘Erasers’ of ADP-ribosylation as potential targets in cancer therapy

Adding to the clinical success of PARPis, inhibition of PARG, the main ‘eraser’ of poly-ADPr, has recently emerged as a promising approach in cancer treatment, particularly in combination with DNA damaging agents or radiotherapy (Slade, 2020). Although PARGi PDD00017273 is unsuitable for clinical studies due to poor bioavailability (Gravells et al., 2017; James et al., 2016), recently developed PARGis, COH34 and JA2131, with improved potency and properties may prove good candidates for clinical application (Chen and Yu, 2019; Houl et al., 2019). A particularly promising PARGi developed by IDEAYA Biosciences, that already showed good efficacy and safety in HR-deficient and PARPi-resistant preclinical models, has been targeted to enter clinical trials at the end of 2022, subject to further preclinical trials that are currently ongoing (https://media.ideayabio.com/2022-01-10-IDEAYA-Biosciences-Announces-Corporate-and-Portfolio-Update-for-J-P-Morgan-40th-Annual-Healthcare-Conference).

Regarding ‘erasers’ of mono-ADPr, only initial attempts at the development of ARH3 (Liu et al., 2020) and MacroD1 inhibitors (Haikarainen et al., 2018) have been made, and no inhibitors for ARH1, TARG1 or MacroD2 have been reported. Taking into account our data in Section 3.2.1 and Section 4.2.3 that ARH3 deficiency leads to PARPi resistance, along with recently reported PARG loss (Gogola et al., 2018; Gomez et al., 2020), ARH3 downregulation could be another mechanism of PARPi resistance in cancers due to the resultant increase in ADPr (Prokhorova et al., 2021b, 2021a). Moreover, given our discovery of the synthetic lethal interaction between ARH3 and PARG caused by the accumulation of excessive poly-ADPr in Section 4.2.3, ARH3 inhibition could be a promising strategy for counteracting PARPi resistance in cancers with PARG downregulation. Then, similarly to PARG inhibition, single use of ARH3 inhibitors or combinations with either DNA damaging agents or radiotherapy and/or PARG inhibition could prove promising against a wider range of cancers. These observations particularly underscore the need for ARH3 inhibitor development, which we hope will be facilitated by previous structural and biochemical studies from our and other groups (Drown et al., 2018; Liu et al., 2020; Rack et al., 2018).

2. Serine is the major site of ADP-ribosylation in response to DNA damage

2.1. Introduction

Following the recent discovery of serine-ADPr (Leidecker et al., 2016) and characterisation of the basic molecular mechanisms behind this modification (Bonfiglio et al., 2017; Fontana et al., 2017; Gibbs-Seymour et al., 2016), we sought to assess the relevant abundance of serine-ADPr in human cells. The study of specific types of ADPr has been profoundly hampered by technical limitations, including multiple challenges in mass spectrometry-based detection and the lack of available biochemical and cell biology tools. Reanalysing a previously generated mass spectrometry dataset (Martello et al., 2016) using an unbiased approach, that considers ADPr on all reactive amino acids, allowed the identification of over 250 potential serine-ADPr sites in H_2O_2-treated HeLa cells (Bonfiglio et al., 2017). This suggested that serine-ADPr might be a widespread modification, in particular in response to DNA damage. Antibody detection of ADPr is also possible, however, until recently, only anti-poly-ADPr antibodies that bind PAR chains of more than 10-20 ADPr units (Fahrer et al., 2007; Kawamitsu et al., 1984) were available. Development of two additional antibodies, anti-pan-ADPr reagent, recognising ADPr of any length (Gibson et al., 2016), and anti-mono-ADPr reagent (Gibson et al., 2017) allowed for the detection of not only poly-, but also oligo- and mono-ADPr, in this work.

Therefore, in this chapter, we utilized the recently acquired knowledge of the molecular basis of serine-ADPr and the recently developed ADPr detection reagents to assess the relative abundance of serine-ADPr by Western blotting in human cells. Moreover, we attempted to validate a number of potential serine-ADPr sites from mass spectrometry studies (Bonfiglio et al., 2017; Leidecker et al., 2016), starting with two of the primary substrates of ADPr, histone H2B and H3. Finally, we provided initial insights into the cellular crosstalk between serine-ADPr and canonical modifications of histone H3.

2.2. Results

2.2.1. Global ADP-ribosylation is dependent on serine-ADP-ribosylation 'writer' PARP1-HPF1 and 'eraser' ARH3

To assess the relevant abundance of serine-ADPr in human cells, human osteosarcoma U2OS cell line, being one of the most widely used cell lines in the ADPr field, as well as in cell biology studies in general due to its convenience for the use in biochemical and imaging assays, was first selected as an experimental model system. I compared the total levels of ADPr in U2OS control, ARH3 KO, HPF1 KO and PARP1 KO cells by Western blotting using anti-pan-ADPr, anti-poly-ADPr and anti-mono-ADPr reagents. In control cells treated with H_2O_2, which is known to cause oxidative stress and subsequent DNA damage, the ADPr peak is detected after 10 min of DNA damage induction (Figure 7A). The most easily identifiable ADPr signals correspond to PARP1 and histone ADPr, and are detected by all three reagents (Figure 7A). 2 h after DNA damage induction, ADPr signals are normally reduced back to the basal levels. However, in ARH3 KO cells, ADPr signals still persisted at the 2 h time point, and the cells showed higher levels of ADPr under unstimulated conditions and 10 min after treatment, as previously observed in our lab (Fontana et al., 2017). This was the most evident with the anti-pan-ADPr and anti-mono-ADPr reagents, but less clear with anti-poly-ADPr antibody, suggesting that the turnover of long PAR chains is much less affected by the absence of ARH3. Strikingly, in HPF1 KO cells, I observed almost no increase in ADPr upon the induction of DNA damage. This was particularly clear with anti-pan-ADPr and anti-mono-ADPr reagents, producing ADPr patterns almost identical to those in cells deficient in PARP1, the enzyme that performs around 85-90% of ADPr in response to DNA damage (Amé et al., 1999; Chen et al., 2018). The only exception was poly-ADPr of PARP1, although its levels in HPF1 KO cells were noticeably lower than in control cells. To validate that total ADPr is truly dependent on HPF1, I compared two independent HPF1 KO clones, and obtained similar ADPr patterns (Figure S1). These results indicate that both PARP1 and HPF1 are required for ADPr induced in response to DNA damage in human cells, and that serine residues are the main acceptors of ADPr in DNA damage signalling.

To confirm that serine is the main site of ADPr following DNA damage, I used a different DNA damaging agent, an alkylating agent methyl methanesulfonate (MMS). U2OS control, ARH3 KO and HPF1 KO cells were treated with MMS for 1 h, and left to recover for 10, 40 or 120 min. PARP1 KO U2OS cell line was omitted to simplify

the experimental setup. Consistent with the observations for H_2O_2 treatment, the MMS-induced ADPr was HPF1-dependent, and was increased and prolonged in ARH3 KO cells (Figure 7B).

To further validate the above observations, I selected an additional cell line, human embryonic kidney (HEK) 293T due to its common use and convenience in biochemical studies. As in U2OS cells, the H_2O_2-induced ADPr was strictly dependent on HPF1 (Figure 7C). In ARH3 KO 293T cells, ADPr signals were notably increased in both untreated and treated cells, and persisted 2 h after the induction of DNA damage.

Therefore, HPF1-dependent serine-ADPr is the major form of ADPr in response to DNA damage, and ARH3 is important for the timely reversal of DNA damage-induced ADPr.

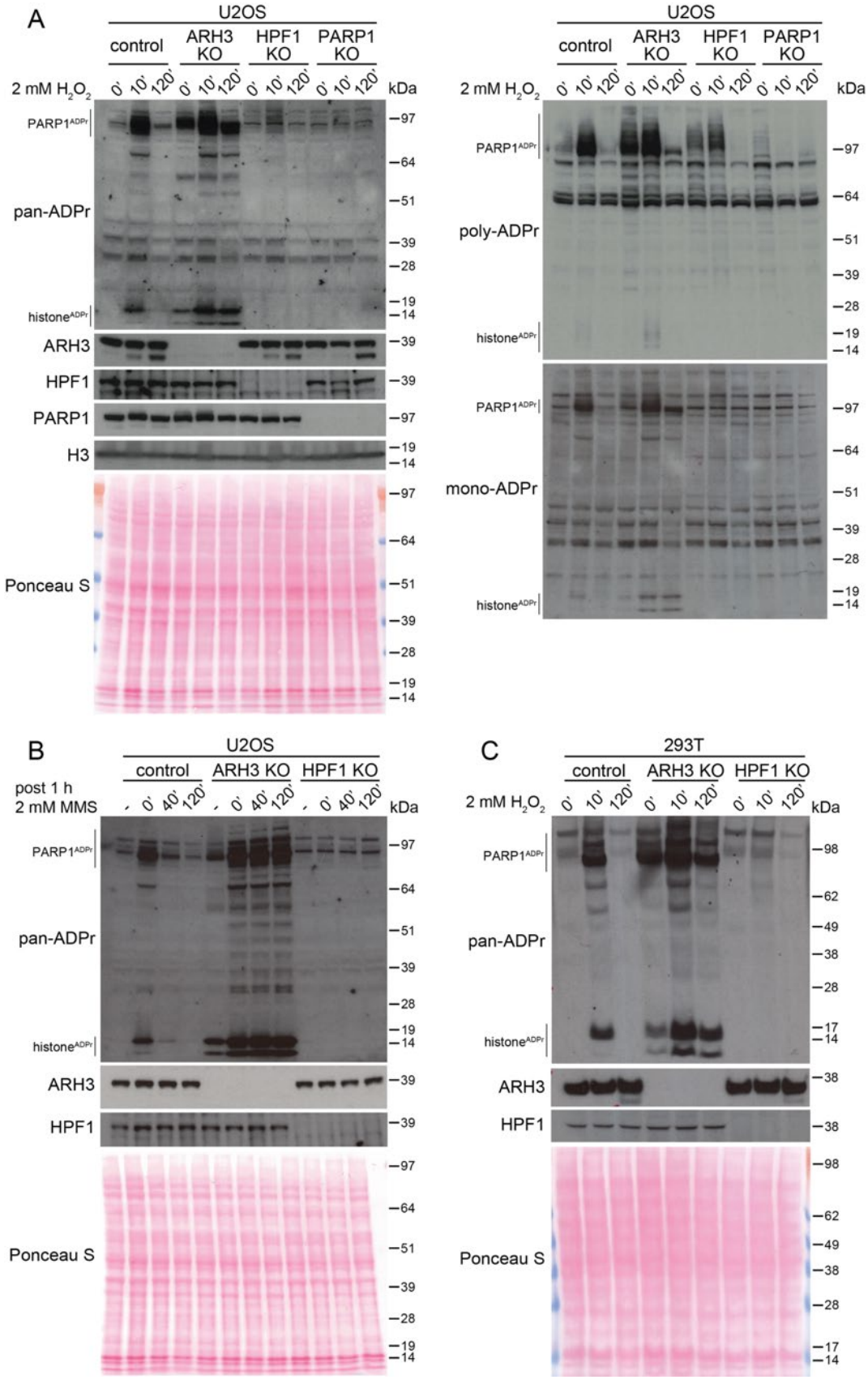


Figure 7. Serine-ADPr is the main type of DNA damage-induced ADPr.

(A) The levels of ADPr in control, ARH3 KO, HPF1 KO and PARP1 KO U2OS cells treated with H_2O_2 as indicated were compared by Western blotting. Anti-pan-ADPr reagent recognising all ADPr forms was used to assess total ADPr levels, anti-poly-ADPr antibody was used for the detection of long PAR chains only, and anti-mono-ADPr reagent was used to detect single ADPr units. Representative

Western blots from 4 independent experiments are shown. (B) Control, ARH3 KO and HPF1 KO U2OS cells were treated with MMS for 1 h and were left to recover from the damage for the indicated time. The total levels of ADPr were assessed by Western blotting. Representative Western blots from 3 independent experiments are shown. (C) Control, ARH3 KO and HPF1 KO 293T cells were treated with H_2O_2, and total ADPr levels were compared by Western blotting. Representative Western blots from 4 independent experiments are shown. Figures A and B were adapted from (Palazzo et al., 2018).

2.2.2. Targets of DNA damage-induced serine-ADP-ribosylation

More than 250 serine-ADPr sites were initially identified by mass spectrometry in H_2O_2-treated HeLa cells (Bonfiglio et al., 2017; Leidecker et al., 2016), however none of them have been confirmed by an independent approach in human cells. Here, we first set out to check whether the ADPr site on one of the primary ADPr substrates, histone H2B, was predicted correctly. We generated mammalian expression constructs of Flag-tagged H2B wild-type (WT) and S6A with the main candidate ADPr site serine 6 substituted with alanine by site-directed mutagenesis. We transiently expressed the constructs in control and HPF1 KO 293T cells, treated the cells with H_2O_2, performed Flag-immunoprecipitation of Flag-H2B, and analysed the efficiency of its ADPr by Western blotting using anti-pan-ADPr reagent. While the WT Flag-H2B was efficiently ADP-ribosylated in response to treatment in control cells, the ADPr of Flag-H2B was completely abolished in HPF1-deficient cells or when serine 6 was mutated to alanine (Figure 8A). This confirmed that serine 6 is the main ADPr site on H2B, and that H2B serine-ADPr is HPF1-dependent.

Next, I employed the same approach to validate the initially predicted ADPr sites on histone H3 (Bonfiglio et al., 2017; Leidecker et al., 2016). I prepared the constructs for the expression of Flag-H3 WT, S10A and S28A mutants, as well as the double mutant (S10/28A). While the substitution of serine 10 to alanine led to an almost complete loss of Flag-H3 ADPr, serine 28 to alanine mutation resulted in a noticeable, but much smaller, reduction of ADPr (Figure 8B). The substitution of both serine sites to alanine completely abolished the DNA damage-induced ADPr of Flag-H3.

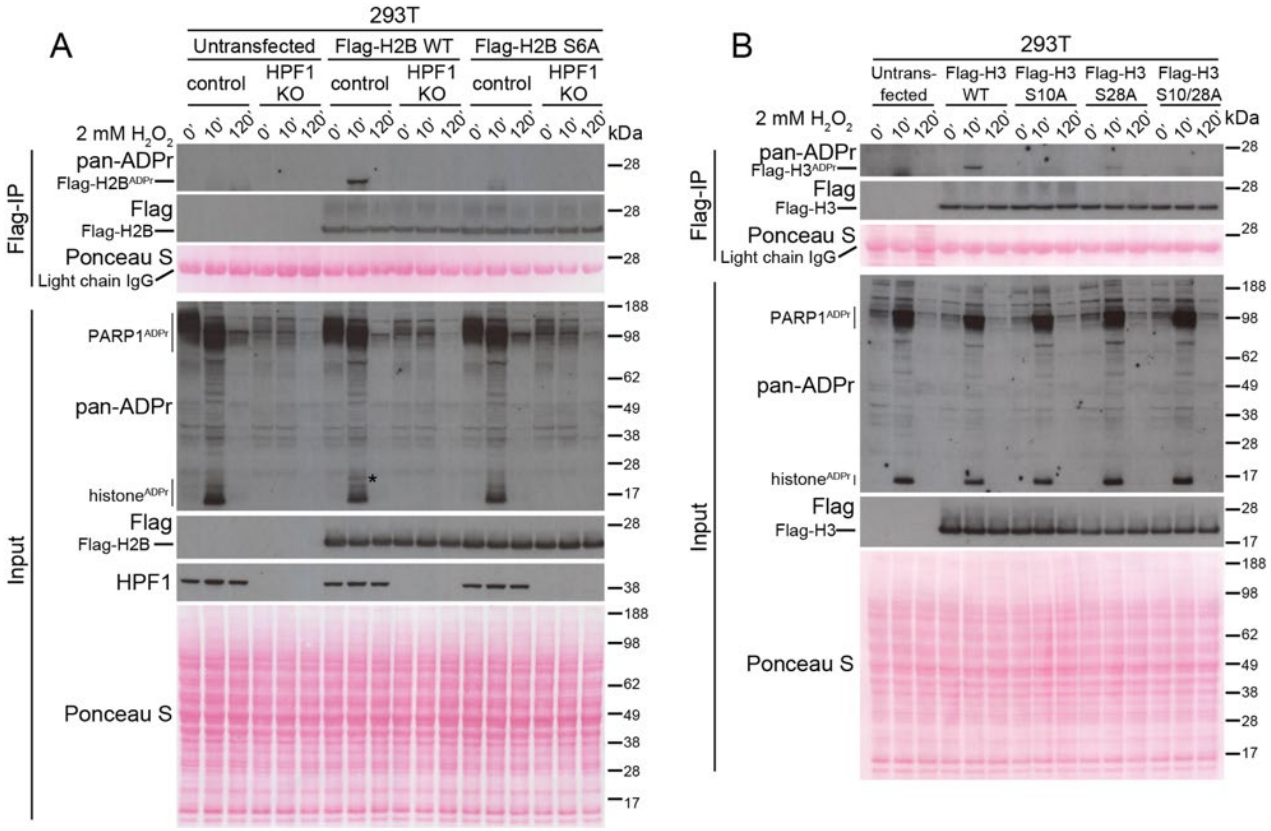


Figure 8. Serines 6 and 10 are the main ADPr sites on histone H2B and H3, respectively.

(A) 293T control and HPF1 KO cells were transfected with Flag-H2B WT or S6A mutant construct, and treated with H_2O_2. The levels of Flag-H2B ADPr were assessed by Flag-immunoprecipitation (Flag-IP) and subsequent Western blotting analysis. An asterisk marks the ADP-ribosylated Flag-H2B detected in control cells. The experiment was performed by Luca Palazzo and myself. Representative Western blots from 2 independent experiments are shown. (B) 293T cells were transfected with Flag-H3 WT, S10A, S28A or S10/28A double mutant construct, and treated with H_2O_2. After Flag-IP, the levels of ADPr were compared by Western blotting. Representative Western blots from 2 independent experiments are shown. The figures were adapted from (Palazzo et al., 2018).

To further corroborate the abundance of serine-ADPr in response to DNA damage, I sought to confirm a number of additional chromatin-associated serine-ADPr substrates. I have selected a set of candidates, including linker histones H1.1, H1.2, H1.3, H1.4 and high-mobility group (HMG) HMGA1, HMGB1 and HMGN1, which are among the most abundant cellular substrates of serine-ADPr (Bonfiglio et al., 2017), for cellular validation of their ADPr type.

H1 and HMG proteins are the most abundant architectural chromatin-binding proteins in human cells, whose interplay is known to regulate chromatin condensation state and the ability of other regulatory factors to access their binding sites on chromatin (Postnikov and Bustin, 2016; Reeves, 2015). In general, H1 histones promote chromatin compaction, while HMG proteins promote chromatin decompaction and formation of distorted DNA structures. Linker H1 histones are a heterogeneous family

with higher sequence variability between species compared to core histones. In total, eleven H1 subtypes have been identified in mammals: five somatic H1 variants (H1.1 to H1.5), the replacement H1 (H1.0), germ cell-specific H1s (H1t, H1T2, HILS1 and H1oo) and H1x (Kalashnikova et al., 2016). In human embryonic stem cells (hESCs), pluripotency factors occupy the H1.5 promoter, to a lower extent the H1.3 promoter and sporadically the H1.1 promoter, which suggests a pivotal role of these subtypes in differentiation and development. H1.0 becomes the predominant H1 variant in differentiated cells, which is accompanied by a decrease in the expression of H1.1–H1.5. The HMG superfamily is composed of HMGA, HMGB and HMGN families, each having distinct protein structure and DNA or chromatin binding motif and being ubiquitously present in all vertebrate cells (Postnikov and Bustin, 2016).

Using the approach described above for H2B and H3, I confirmed that all these candidates are ADP-ribosylated following H_2O_2 treatment in 293T cells (Figure 9). Of note, H1.5 that was not listed as an ADPr substrate in (Bonfiglio et al., 2017; Leidecker et al., 2016) and later in a more recent mass spectrometry study (Larsen et al., 2018) was not modified in the same conditions (Figure 9E). As ADPr of the H1.1, H1.2, H1.3, H1.4, HMGA1, HMGB1 and HMGN1 was completely abolished in HPF1 KO cells (Figure 9), these proteins are predominantly ADP-ribosylated at serine residues under DNA damage conditions. A substantial increase in H1.2 and H1.4 ADPr in 293T cells lacking ARH3 under both basal and DNA damage conditions (Figure S2) further proved that histone H1.2 and H1.4 ADPr largely occurs on serine residues in human cells. Additionally, as reported in (Hendriks et al., 2021), I was able to demonstrate HPF1-dependent, although weaker, ADPr of the replacement histone H1.0. Germ cell-specific H1x was also ADP-ribosylated following H_2O_2 treatment in 293T cells (data not shown), while modification status of other linker H1 histone variants was not assessed during this work.

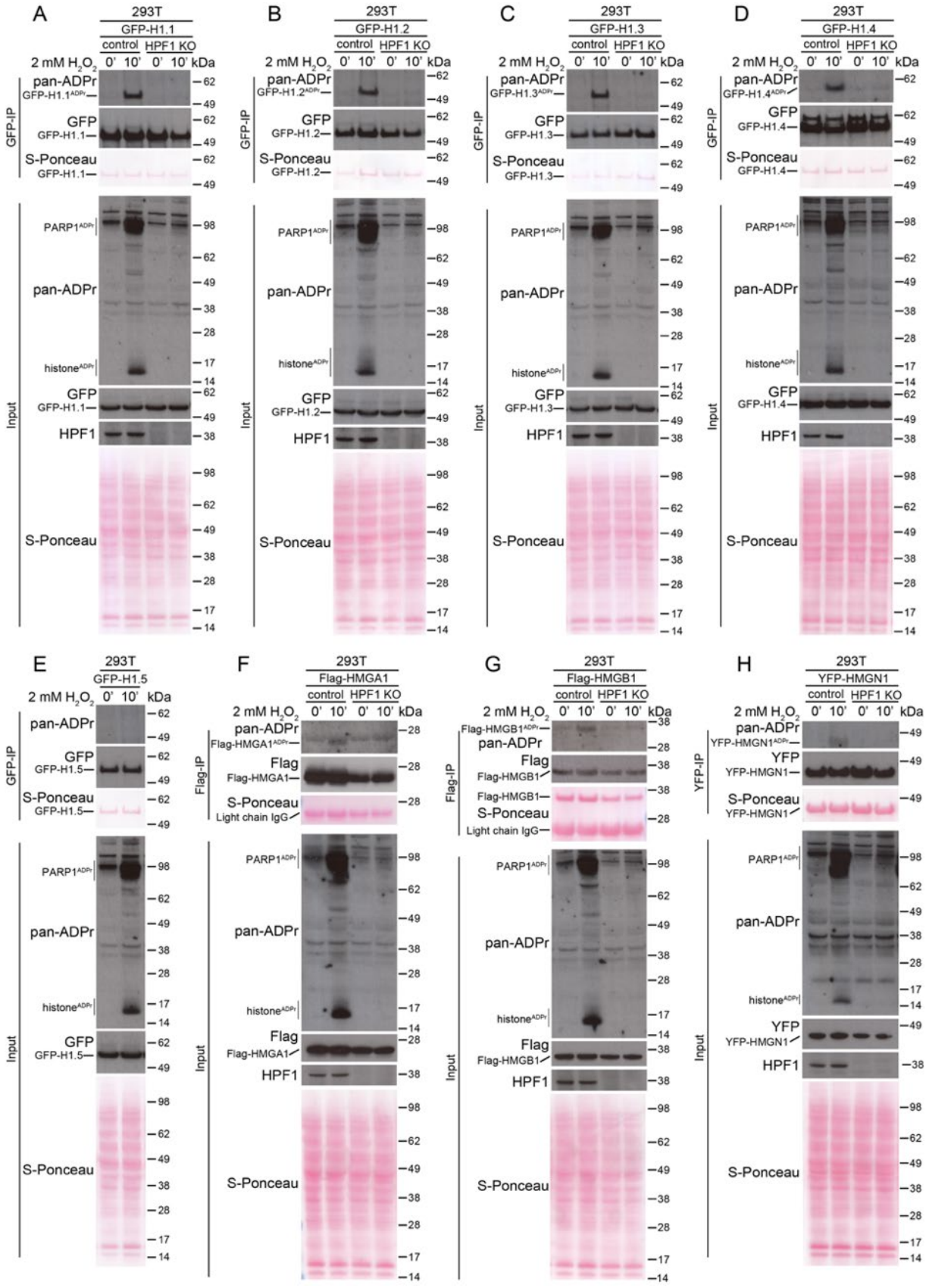


Figure 9. ADPr of high-mobility group and histone H1 proteins is HPF1-dependent.

293T control and HPF1 KO cells were transfected with GFP-H1.1 (A), GFP-H1.2 (B), GFP-H1.3 (C), GFP-H1.4 (D), GFP-H1.5 (E), Flag-HMGA1 (F), Flag-HMGB1 (G) or YFP-HMGN1 (H) construct. Following H_2O_2 treatment and immunoprecipitation (IP), the levels of ADPr were compared by Western

blotting. Representative Western blots from 2 independent experiments are shown. Figures A-E were partially adapted from (Hendriks et al., 2021).

Next, I set out to validate the exact sites of ADPr on a number of the selected candidates taking advantage of mass spectrometry data from (Bonfiglio et al., 2017) and a later study that was published at the time of carrying out these experiments (Larsen et al., 2018). First, I generated mammalian expression constructs of GFP-H1.2 and GFP-H1.4 in which one or all of four main mass spectrometry-predicted sites were substituted with alanine by site-directed mutagenesis. While the WT proteins were efficiently modified upon H_2O_2 treatment in 293T cells, simultaneous mutation of the four main sites eliminated detectable ADPr (Figure 10). This further confirmed that H1.2 and H1.4 are predominantly ADP-ribosylated at serine residues under DNA damage conditions in human cells. Almost complete loss of the modification signal upon H1.2 serine 188 to alanine substitution, suggested that serine 188 is the main site of DNA damage-induced ADPr on histone H1.2, although mutation of serine 36 or 150 also resulted in a noticeable reduction in the modification levels (Figure 10A). Out of the four selected sites on H1.4, mutation of serine 27 led to the most striking decrease in the modification, suggesting that serine 27 is the predominant site of histone H1.4 ADPr in response to DNA damage (Figure 10B).

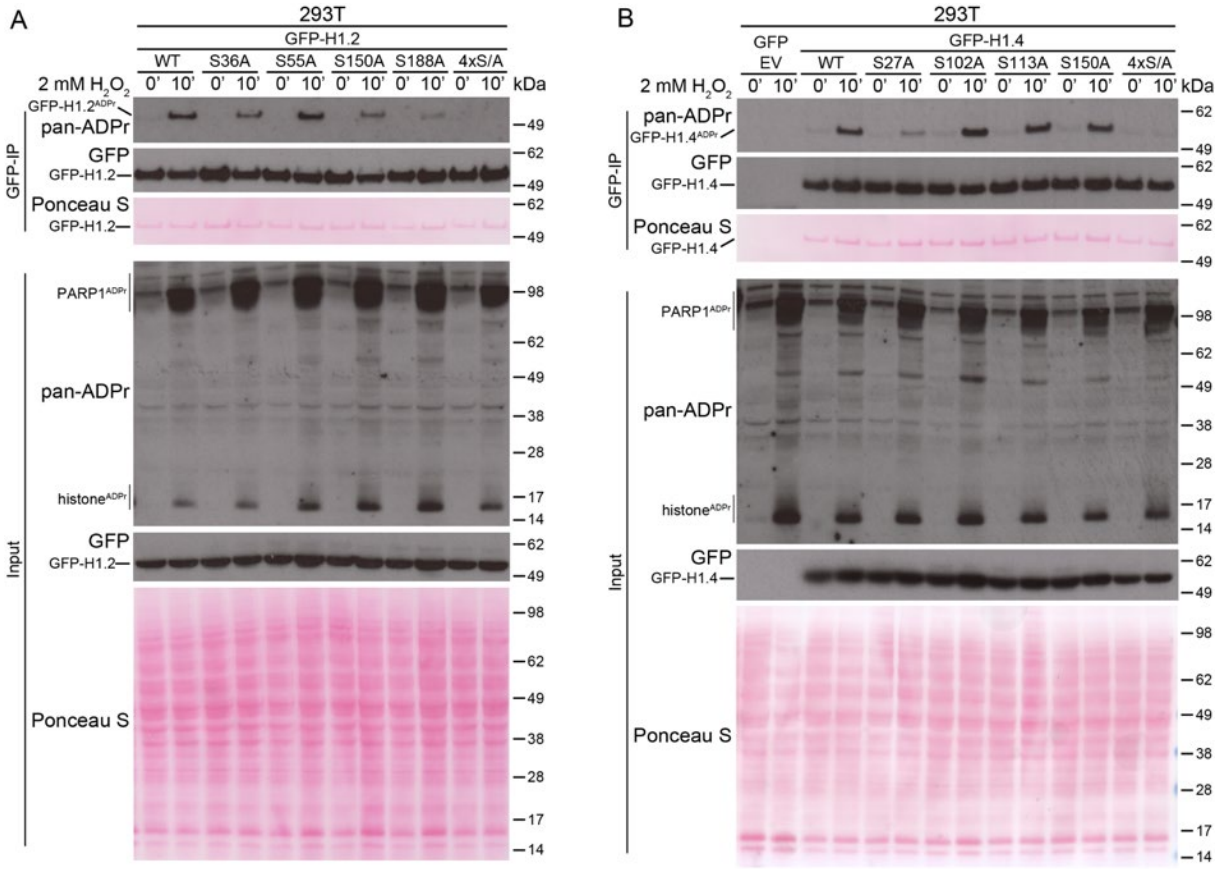


Figure 10. Serines 188 and 27 are the main sites of ADPr on histone H1.2 and H1.4, respectively.

293T cells were transfected with GFP-H1.2 WT, S36A, S55A, S150A, S188A or 4xS/A (A), or GFP-H1.4 WT, S27A, S102A, S113A, S150A or 4xS/A construct (B), and treated with H_2O_2. Following immunoprecipitation (IP), the levels of ADPr were compared by Western blotting. Representative Western blots from 2 independent experiments are shown. Figure A was partially adapted from (Hendriks et al., 2021).

Then, I performed a similar validation of the main HMGA1, HMGB1 and HMGN1 serine-ADPr sites from the available mass spectrometry datasets (Bonfiglio et al., 2017; Larsen et al., 2018). While the WT proteins were efficiently modified upon H_2O_2 treatment in 293T cells, mutagenesis of serine 8, serine 181 or serine 25 resulted in the loss of detectable ADPr on HMGA1, HMGB1 or HMGN1, respectively (Figure 11), therefore identifying the main sites of HMGA1, HMGB1 and HMGN1 DNA damage-induced ADPr.

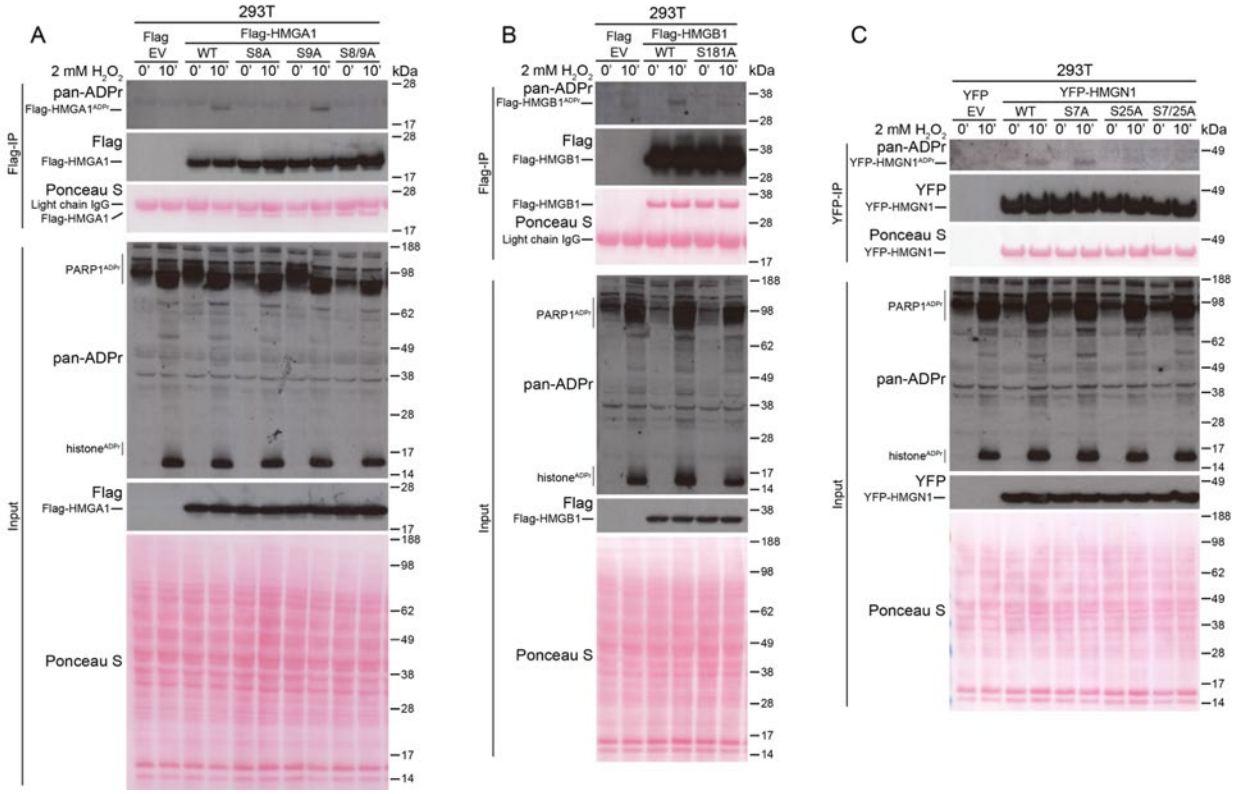


Figure 11. Serines 8, 181 and 25 are the main ADPr sites of HMGA1, HMGB1 and HMGN1, respectively.

293T cells were transfected with Flag-HMGA1 WT, S8A, S9A or S8/9A (A), Flag-HMGB1 WT or S181A (B), or YFP-HMGN1 WT, S7A, S25A or S7/25A (C) and treated with H_2O_2. Following immunoprecipitation (IP), the levels of ADPr were compared by Western blotting. Representative Western blots from 2 independent experiments are shown.

Overall, this section presents a simple approach that can be used for the validation and study of many other candidate ADPr sites in human cells, namely by overexpression of tagged WT and serine to alanine mutant proteins followed by their immunoprecipitation and Western blotting using anti-pan-ADPr reagent.

2.2.3. 'KS' and 'RS' motifs are preferred targets for serine-ADP-ribosylation on histone H3

According to the previously published mass spectrometry studies (Abplanalp et al., 2017; Bilan et al., 2017; Bonfiglio et al., 2017; Leidecker et al., 2016), the sites of serine-ADPr are often preceded by lysine and, less frequently, arginine. This sequence preference was confirmed *in vitro* using H3 peptide by Edward Bartlett in our lab (Bartlett et al., 2018), and so I sought to confirm the importance of the 'KS' consensus in human cells. I prepared the constructs expressing Flag-H3 protein with lysine 9 substituted to alanine (K9A) or arginine (K9R). Whereas K9A mutation led to a dramatic reduction in Flag-H3 ADPr, similar to that for S10A mutant, K9R mutant

was still efficiently ADP-ribosylated, although to a lesser extent than WT Flag-H3 (Figure 12).

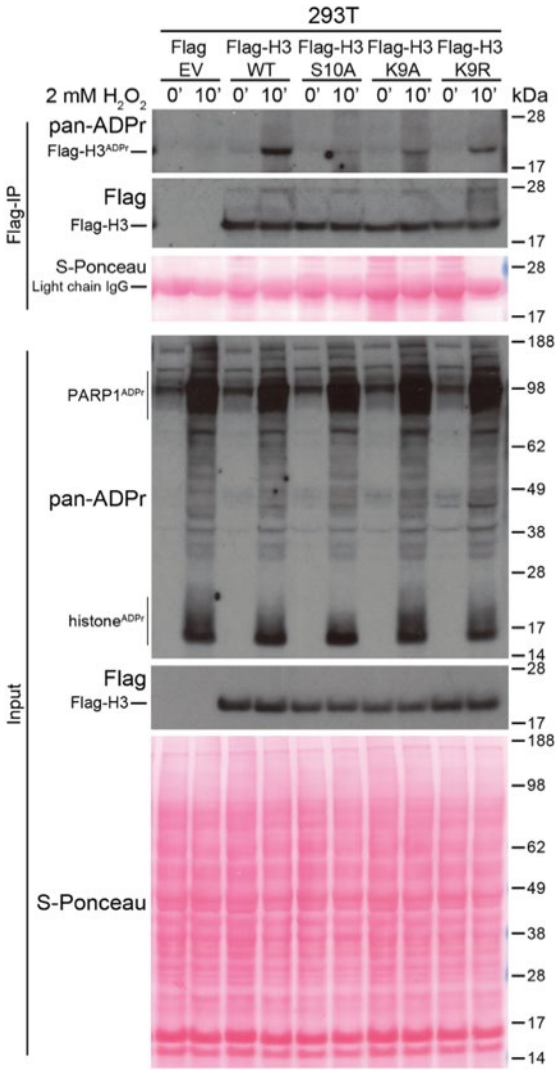


Figure 12. The preceding lysine is important for histone H3 serine 10 ADPr.

293T cells were transfected with Flag empty vector (EV), Flag-H3 WT, S10A, K9A or K9R mutant construct, and treated with H_2O_2. After Flag-H3 immunoprecipitation (Flag-IP), the levels of ADPr were compared by Western blotting. Representative Western blots from 3 independent experiments are shown. The figure was adapted from (Bartlett et al., 2018).

This confirmed that 'KS' and, to a lesser extent 'RS', is the preferred motif for H3 serine-ADPr. Moreover, these data suggested the importance of a positive charge on lysine or arginine that precedes the targeted serine in other substrates bearing the same 'KS' or 'RS' consensus motif.

2.2.4. Crosstalk between DNA damage-induced histone serine-ADP-ribosylation and canonical histone posttranslational modifications

Histone proteins are subject to a large variety of PTMs that directly regulate gene expression and are also involved in DNA damage signalling (Lawrence et al., 2016).

As ADPr modifications are negatively charged and bulky, they are very likely to interfere with other histone PTMs. ADPr of H3 serines 10 and 28 is particularly intriguing, since phosphorylation (P) of these residues is crucial during mitosis (Wang and Higgins, 2013), and acetylation (ac) of the preceding lysine 9 and 27 is important in the regulation of gene expression (Saksouk et al., 2015). The *in vitro* experiments performed by Edward Bartlett in our lab (Bartlett et al., 2018) suggested that ADPr of H3S10 inhibits phosphorylation of H3S10 and acetylation H3K9, and *vice versa*. Similar results were obtained for H3S28ADPr, H3S28P and H3K27ac. These findings were confirmed by mass spectrometry analysis carried out by the Ivan Matic group (Bartlett et al., 2018), which also identified two groups of H3 PTMs that can either coexist or are mutually exclusive with H3 serine-ADPr in human cells (Figure 13A).

To characterise the interplay between H3 serine-ADPr and other PTMs in human cell, I sought to assess the levels of H3S10P, H3K9ac and several other PTMs in the proximity of H3 ADPr sites in 293T cells following DNA damage. While I observed a substantial decrease in H3K9ac and H3S10P levels 2 h after treatment, the levels of H3K9me3, that can coexist with H3S10ADPr according to our mass spectrometry data, remained stable (Figure 13B). At the same time, no noticeable changes in H3K27ac and H3K27me3 levels were detected, that is in agreement with our data that serine 10, but not serine 28, is the main ADPr site on H3 in 293T cells (Figure 8B). The acetylation levels of K36 and K56, located further on H3 N-terminal tail or in the core H3 domain, respectively, also did not show any noticeable changes. However, total acetylation (pan-Kac) of histones was substantially reduced following DNA damage, similar to H3K9ac levels. This suggests that the lysine residues preceding serine-ADPr sites might be the major lysine residues deacetylated in response to DNA damage. In concordance, we also observed DNA damage-induced deacetylation of H2BK5 that precedes the main H2B serine-ADPr site serine 6 in our experimental settings.

Pre-treatment with the PARPi Olaparib completely blocked DNA damage-induced deacetylation of H3K9 and dephosphorylation of H3S10, and prevented total histone and H2BK5 deacetylation (Figure 13B). The levels of cell cycle proteins cyclin A, B1, E1 and p21 were unaffected by Olaparib treatment. This further suggests that histone serine-ADPr, phosphorylation and neighbouring acetylation, in particular H3S10ADPr, H3S10P and H3K9ac, are mutually exclusive marks in DNA damage signalling.

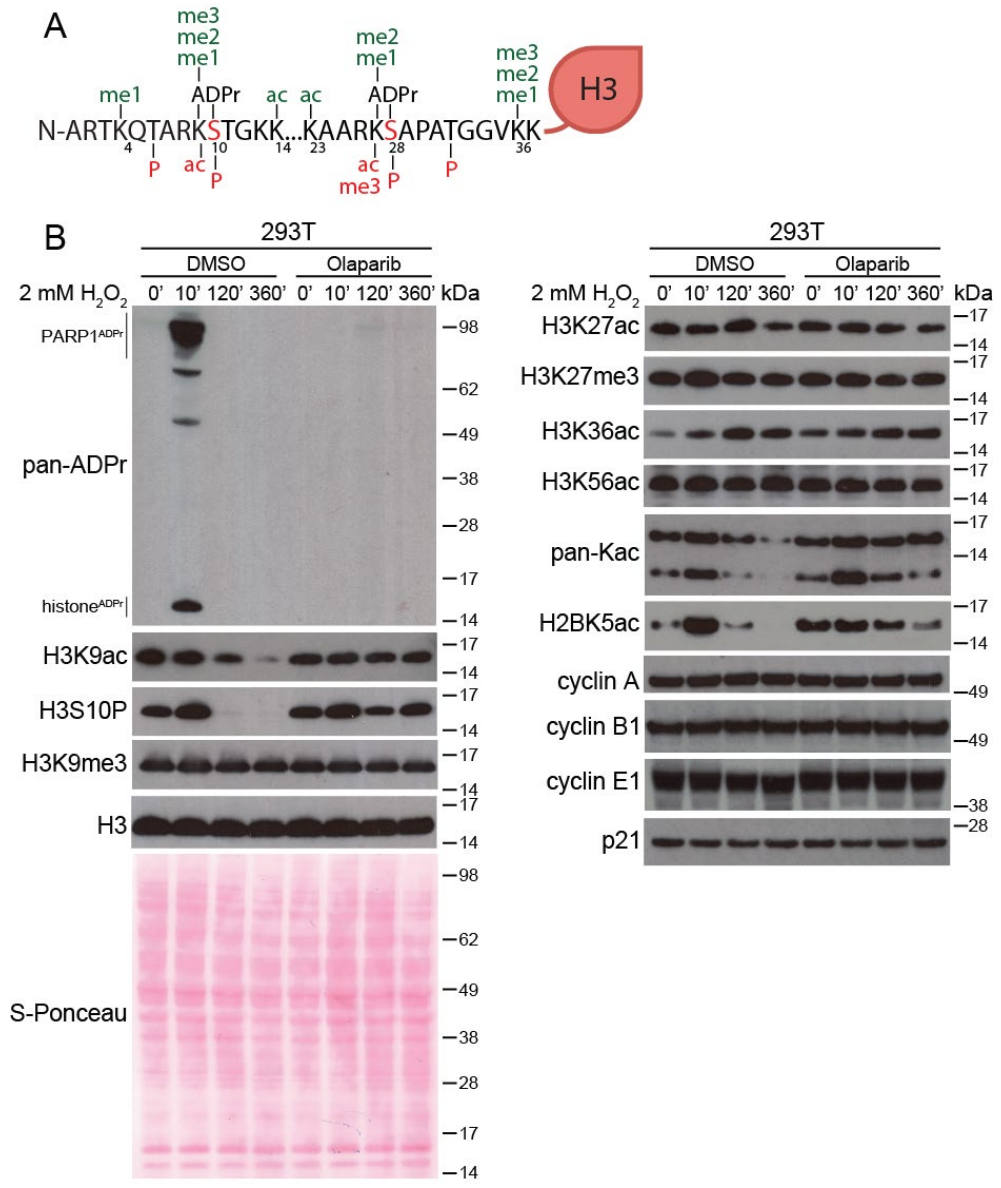


Figure 13. DNA damage-induced histone H3 serine-ADPr interferes with proximal acetylation and phosphorylation, but not methylation.

(A) Schematic summary of canonical H3 marks that can coexist (shown in green) or interfere (in red) with serine-ADPr based on the mass spectrometry analysis of U2OS cell extracts (Bartlett et al., 2018). (B) 293T cells were pre-treated with DMSO or Olaparib, treated with H_2O_2, and the cell lysates were analysed by Western blotting with the indicated antibodies. Representative Western blots from 3 independent experiments are shown. Figure B was partially adapted from (Bartlett et al., 2018).

2.3. Discussion

The results provided in this chapter established serine-ADPr, which is controlled by HPF1 and ARH3, as the major form of cellular ADPr in response to DNA damage (Palazzo et al., 2018). The discovery of serine as the main acceptor of DNA damage-induced ADPr in human cells (Palazzo et al., 2018) was soon substantiated by a large-scale mass spectrometry study, reporting that 3,029 out of 3,450 (88%) H_2O_2-induced ADPr sites in HeLa cells are localized to serine residues (Larsen et al.,

2018). This was followed by several other proteomics studies, with a very recent study providing a broad overview by combining several published datasets (Bilan et al., 2017; Bonfiglio et al., 2017; Buch-Larsen et al., 2020; Hendriks et al., 2019; Larsen et al., 2018), confirming that, among both 9,029 H_2O_2-induced and 643 physiological ADPr sites detected in HeLa cells, ADPr predominantly occurs on serine residues (84% and 62%, respectively) (Buch-Larsen et al., 2020). Finally, another study has validated the dependence of serine-ADP-ribosylome on HPF1 and ARH3, demonstrating up to 1000-fold regulation across the KO U2OS cell lines. (Hendriks et al., 2021). Overall, these studies present a valuable resource for subsequent validations and functional characterisations of ADPr sites in human cells.

Next, the results in this chapter provided initial insights into the cellular crosstalk between serine-ADPr and canonical histone marks (Bartlett et al., 2018). Specifically, I described serine 10 as the main ADPr site of histone H3 (Palazzo et al., 2018), and showed the importance of the preceding positively charged lysine amino acid for its ADPr in human cells (Bartlett et al., 2018). The preference of the lysine-serine motif for serine-ADPr was consistent with the previous and following mass spectrometry studies (Bilan et al., 2017; Bonfiglio et al., 2017; Buch-Larsen et al., 2020, 2021; Hendriks et al., 2019, 2021; Larsen et al., 2018; Leidecker et al., 2016).

Furthermore, we demonstrated that H3 serine 10 ADPr is mutually exclusive with its phosphorylation and acetylation, but not methylation, of the preceding lysine 9 (Bartlett et al., 2018) (Figure 14). These observations were later confirmed by other studies (Hananya et al., 2021; Liszczak et al., 2018). Moreover, significant co-targeting of serine-ADPr and phosphorylation beyond H3 serine 10 site was demonstrated by a subsequent mass spectrometry study, reporting 483 co-targeted sites in HeLa cells (Larsen et al., 2018). Further studies confirmed this observation (Hendriks et al., 2019, 2021), extending the analysis to include neighbouring acetylation and methylation, with the majority of co-modification with acetylation and methylation found to reside on histones, in contrast to co-modification with phosphorylation which predominantly occurred on non-histone proteins (Hendriks et al., 2021). Altogether, these findings provide compelling evidence for the site-specific regulatory interplay between serine-ADPr and other cellular PTMs in human cells.

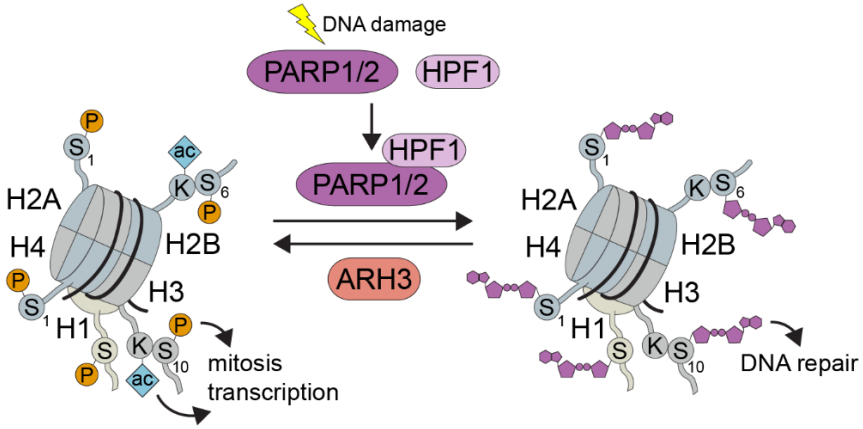


Figure 14. Serine-ADPr as an additional component of the histone code.

Since H3K9ac and H3S10P marks are strongly associated with active transcription and mitosis, respectively (Lawrence et al., 2016), it is only logical that they become undesirable in the event of persistent DNA damage, and thus prompt ADPr of H3S10 would serve as a protection mechanism from their modification. Accordingly, I observed a decrease in general H3K9ac and H3S10P levels after DNA damage (Bartlett et al., 2018), that has previously been reported in several independent studies (Bártová et al., 2011; Meyer et al., 2016; Monaco et al., 2005; Tjeertes et al., 2009). On the other hand, the levels of H3K9me3, which is associated with transcriptional repression (Lawrence et al., 2016), remained stable following H_2O_2 treatment (Bartlett et al., 2018) and other DNA damage stimuli (Tjeertes et al., 2009). However, the observed decrease in histone acetylation and phosphorylation levels was significantly delayed compared to the increase in total ADPr levels. The molecular mechanisms underlying this are unclear and remain to be addressed in the future studies. One possible explanation of this could be the activation of DNA damage checkpoints accompanied by prolonged cell-cycle arrest preventing further cell proliferation, however the levels of several cell cycle proteins assessed in this study remained stable throughout the experiment.

In addition to histone H3, the results included in this chapter validated a number of other serine ADPr substrates, identifying serine 6, serine 188, serine 27, serine 8, serine 181 and serine 25 as the main sites of H2B, H1.2, H1.4, HMGA1, HMGB1 and HMGN1 ADPr, respectively. While a number of recent works have provided initial insights into the role of some of these modifications in human cells (Hananya et al., 2021; Hendriks et al., 2021; Li et al., 2018), further studies are needed before any conclusions can be drawn. Since H1 and HMG proteins are the most abundant chromatin-binding factors in human cells, whose interplay is known to regulate many cellular processes, including DNA replication, transcription, DNA repair and

chromatin dynamics (Postnikov and Bustin, 2016; Reeves, 2015), it will be of great importance to address how serine-ADPr affects their cellular functions. Given that ADPr is a negatively charged and bulky modification, it is possible that DNA damage-induced ADPr of these chromatin-associated factors will interfere with its binding to chromatin, perhaps contributing to the fine-tuning of the chromatin remodelling process, allowing efficient DNA repair. The main serine-ADPr site on HMGN1, serine 25, is a particularly interesting candidate for future studies, since this site is shared by all five members of the HMGN family (Bonfiglio et al., 2017; Larsen et al., 2018) and is located at the interaction interface of HMGNs and nucleosome core proteins (Prymakowska-Bosak et al., 2001). It will be of interest to check whether serine 25 ADPr or mutation affects HMGN1 binding to nucleosomes and its cellular distribution. On the other hand, it is curious why, in contrast to all the other studied linker H1 histone variant, only H1.5 ADPr could not be so far observed in human cell. It is possible that this selectivity could be somehow linked to the recently identified role of H1.5 in the regulation of splice site selection and alternative splicing, a function that has not been demonstrated for the other linker histones (Behrends and Engmann, 2020).

Overall, the crosstalk between serine-ADPr and other cellular PTMs adds another layer of complexity to our understanding of the role of serine-ADPr in human cells and awaits further investigation.

3. Serine-ADP-ribosylation controls cell response to PARP1/2 inhibition

3.1. Introduction

Given the recent discovery of the prevalence of serine-ADPr in human cells (Bilan et al., 2017; Bonfiglio et al., 2017; Buch-Larsen et al., 2020; Hendriks et al., 2019; Larsen et al., 2018; Leidecker et al., 2016), we hypothesized that modulating the levels of this modification might also affect cellular response to PARP1/2 inhibition. Indeed, the abundance of physiological serine-ADPr could already be seen by Western blotting as an increase in total ADPr following the loss of ARH3 (e.g., in Figure 7).

Therefore, in this chapter, we sought to investigate whether globally altering cellular serine-ADPr levels through manipulating HPF1 and ARH3 levels would affect cellular response to PARP1/2 inhibition. Furthermore, we attempted to demonstrate the

physiological importance of specific serine-ADPr sites, focusing on the main sites of PARP1 ADPr, which constitute a major part of total ADPr in human cells.

3.2. Results

3.2.1. HPF1 and ARH3 control serine-ADP-ribosylation levels and determine cellular response to PARP1/2 inhibitors

To assess whether HPF1 and serine-ADPr impact the cellular response to PARP1/2 inhibition, I first tested the sensitivity of U2OS cells lacking HPF1 to several PARPis by performing long-term colony formation assays. To this end, I used the established clinically relevant PARPis: Olaparib, Talazoparib, Veliparib, Niraparib and Rucaparib, which, as discussed in Section 1.2.1.1, differ in their specificity and pharmacological properties. I observed a marked sensitisation of HPF1 KO cells to all the five PARPis (Figures 11A and 11B), suggesting that HPF1 loss is synthetically lethal with PARP1/2 inhibition. This is consistent with the sensitivity of HPF1 KO U2OS cells to Olaparib, which was observed in our lab by Ian Gibbs-Seymour (Gibbs-Seymour et al., 2016). To include additional controls, I assessed HPF1 KO U2OS cell sensitivity to several other compounds, PARP3 inhibitor ME032835, PARP5a/5b inhibitor XAV-93936 and PARGi PDD00017273. Given that the loss of HPF1 did not significantly impact cell sensitivity to these inhibitors (Figures 15B-D), the observed sensitisation effect is specific to PARP1/2 inhibition. Importantly, simultaneous loss of HPF1 and PARP1 largely rescued the sensitivity of HPF1 KO cells to Olaparib (Figure 15E), as was shown previously by Ian Gibbs-Seymour in our lab (Gibbs-Seymour et al., 2016). This supports the dependence of the PARPi-induced toxicity on the physical presence of PARP1 protein, implying that prolonged PARP1 retention on damaged DNA contributes to the synthetic lethality of HPF1 loss and PARP1/2 inhibition.

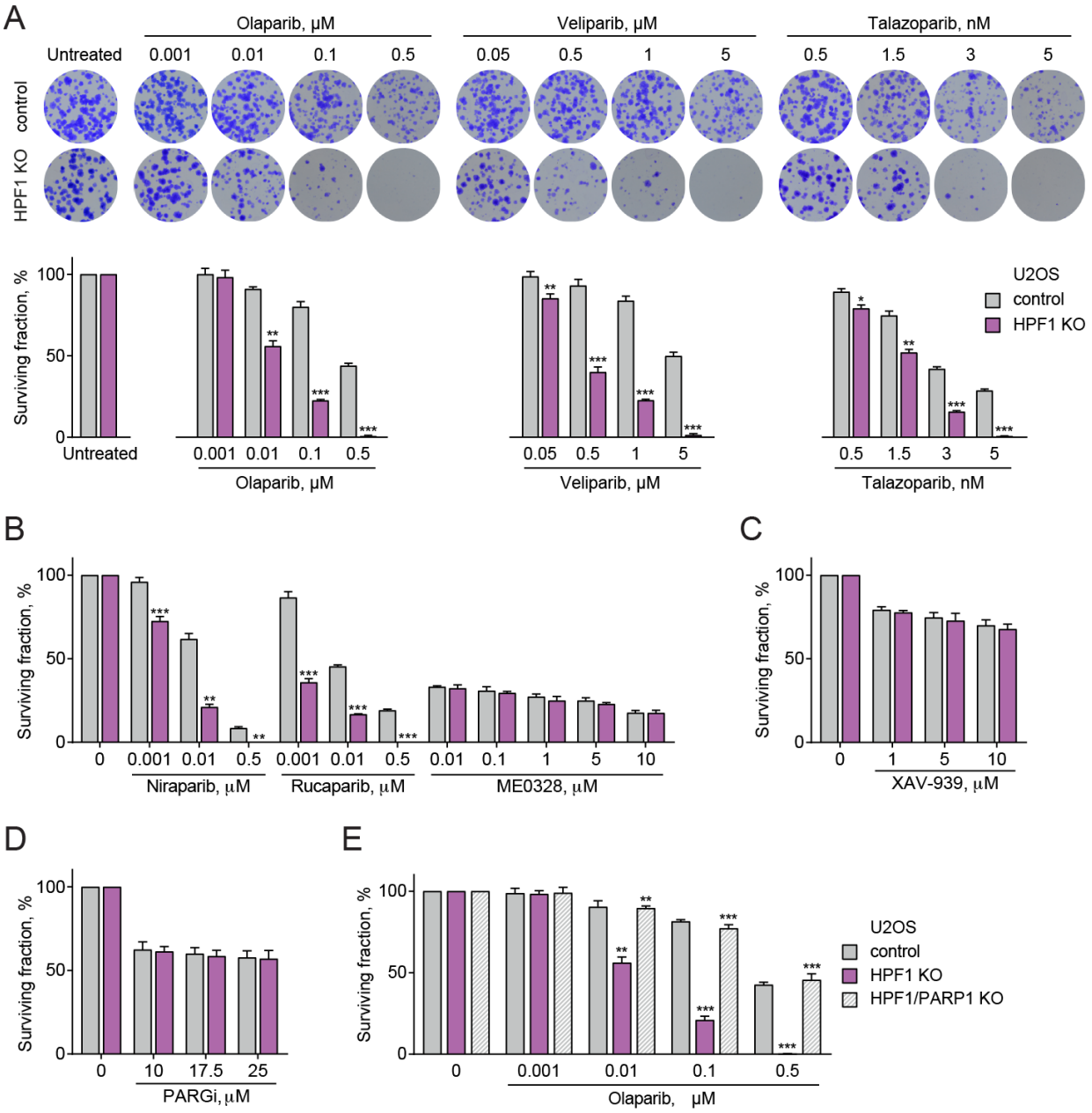


Figure 15. Loss of HPF1 specifically sensitises cells to PARP1/2 inhibitors but not to inhibitors of other factors involved in the regulation of cellular ADPr.

(A) Representative images (top) and quantification (bottom) of colony formation assay with control and HPF1 KO U2OS cells treated with DMSO or as indicated. (A-D) Reduced survival of HPF1 KO cells after treatment with PARP1/2 inhibitors Olaparib, Veliparib, Talazoparib, Niraparib and Rucaparib but not with PARP3 inhibitor ME0328 (B), PARP5a/b inhibitor XAV-939 (C), or PARGi (D) as determined by colony formation assays. The experiments in (B-D) were performed by Josephine Groslambert and myself. (E) Increased sensitivity of HPF1 KO cells to Olaparib treatment is abolished upon concurrent PARP1 KO. Data are shown as mean±SD, n=3, *, $p < 0.05$; **, $p < 0.01$; ***, $p < 0.001$ (two- tailed Student's t-test). The figures were adapted from (Prokhorova et al., 2021b).

Next, I characterised the mechanisms underlying the sensitivity of HPF1-deficient cells to PARP1/2 inhibition. I observed that the loss of HPF1 results in increased DSB formation, as marked by increased levels of γH2AX, upon Olaparib treatment (Figures 16A and S3). Then, I examined the cell cycle distribution by flow cytometry

using double staining with EdU and DAPI (the gating strategy is provided in Figure S4). Olaparib treatment of HPF1 KO cells caused an accumulation of endoreplicating polyploid cells (increased subpopulation of cell with >4N DNA content), decreased cell proliferation (reduced EdU incorporation or S-phase subpopulation) and increased cell death (enriched SubG1 subpopulation of cells with fragmented DNA) (Figures 16B, D). The accumulation of cells with >4N DNA content suggested an eventual failure of the mitotic checkpoint in HPF1 KO cells treated with Olaparib, which eventually exit from mitosis (mitotic slippage) without undergoing cytokinesis rather than being arrested in the subsequent G1 phase. Under the same conditions, I also confirmed an increase in DSB formation by flow cytometry using a different antibody against γH2AX (Figure 16C). These data indicate that the loss of HPF1 potentiates PARPi-induced cytotoxicity, including accumulation of DNA damage. Moreover, simultaneous HPF1 loss and PARP1/2 inhibition interferes with DNA replication, chromatin segregation and cell division. Similar changes have previously been linked with the cytotoxic effects of PARP1/2 inhibition (Michelena et al., 2018; Noël et al., 2006; Schoonen et al., 2017), indicating that the loss of HPF1 aggravates PARPi-induced cytotoxicity.

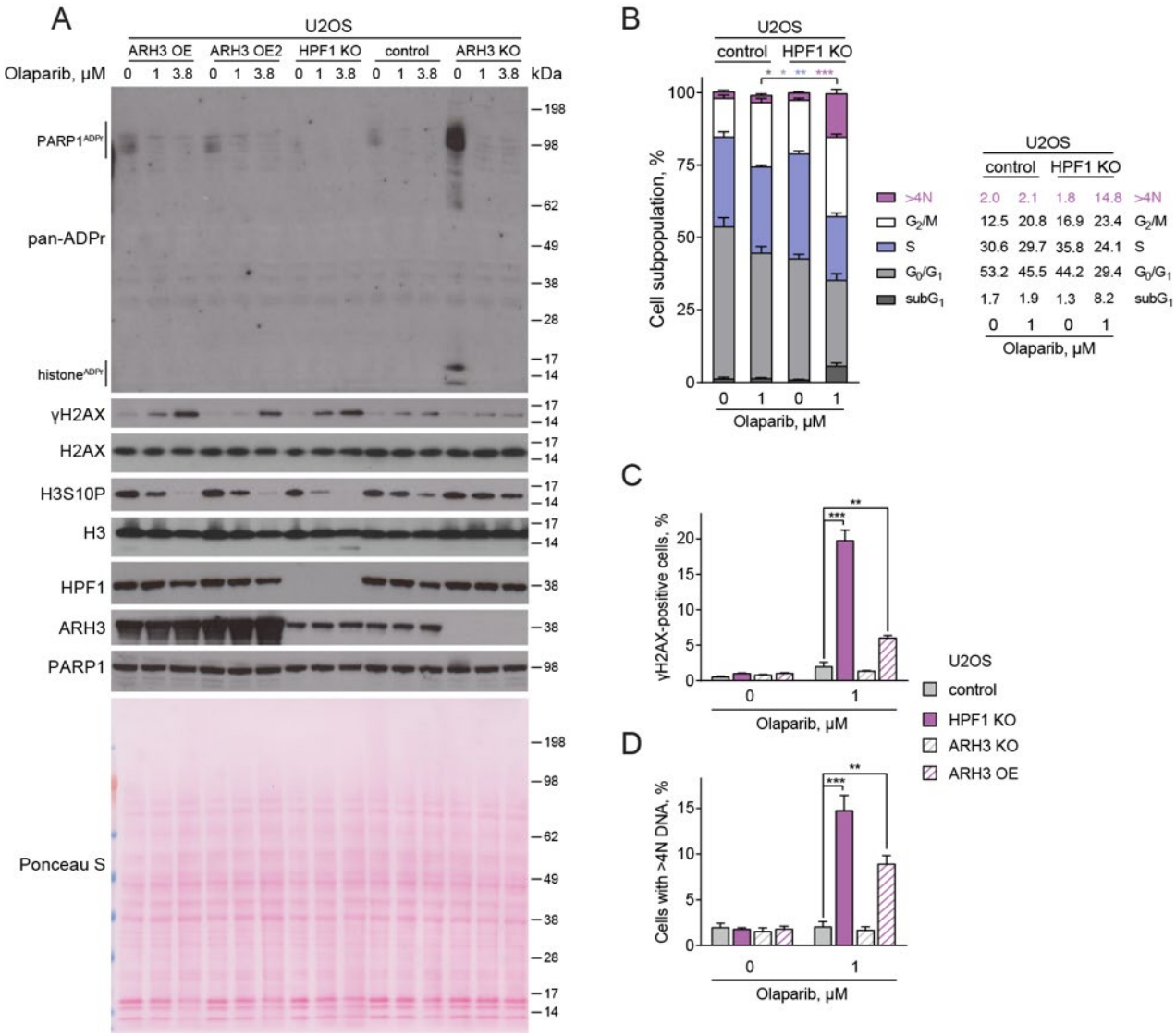


Figure 16. Cytotoxic effects of PARP1/2 inhibition depend on cellular HPF1 and ARH3 protein levels.

(A) ARH3 overexpression (OE), HPF1 KO, control and ARH3 KO U2OS cells were treated with DMSO, 1 or 3.8 μM of Olaparib over the course of 6 days. ADPr, γH2AX and H3S10P levels were analysed by Western blotting. A repeat of the experiment with an additional lower concentration of Olaparib is provided in Figure S3. Representative Western blots from 3 independent experiments are shown. (B) Flow cytometry analysis of EdU- and DAPI-stained control and HPF1 KO U2OS cells following 4-day exposure to Olaparib followed by 1-h EdU pulse. Asterisks in different colours indicate significant difference in corresponding cell subpopulations. Right panel, mean values corresponding to the graph on the left. (C, D) HPF1 and ARH3 protein levels in U2OS cells correlated with the effects of 4-day Olaparib treatment on γH2AX formation (C) and accumulation of cells with >4 N DNA content (D) as observed by flow cytometry. (B-D) Data are shown as mean ± SEM of three (B) or five (C, D) independent experiments. *$p < 0.05$; **$p < 0.01$; ***$p < 0.001$ (two-tailed Student's t-test). Flow cytometry gating strategy for the analyses is shown in Figure S4. The figures were adapted from (Prokhorova et al., 2021b).

Given that PARP1 trapping is a major cause of PARPi-induced cytotoxicity and that PARP1 was previously suggested to be de-trapped from DNA breaks by its own

activity, presumably through electrostatic interference (Ferros and Olivera, 1982; Zahradka and Ebisuzaki, 1982), we additionally assessed the effect of HPF1 loss on PARP1 residence time on damaged DNA. To follow the recruitment of endogenous PARP1 to the sites of DNA damage induced by laser micro-irradiation, we transiently expressed GFP-tagged PARP1 chromobody in control and HPF1 KO U2OS cells. We observed a markedly slower detachment of PARP1 from DNA damage sites both in untreated and Olaparib-treated cells lacking HPF1 (Figure 17). These date are consistent with previous results obtained following YFP-PARP1 overexpression (Gibbs-Seymour et al., 2016) and indicate that HPF1-mediated ADPr facilitates PARP1 release from DNA breaks, which contributes to cellular tolerance to PARP1/2 inhibition.

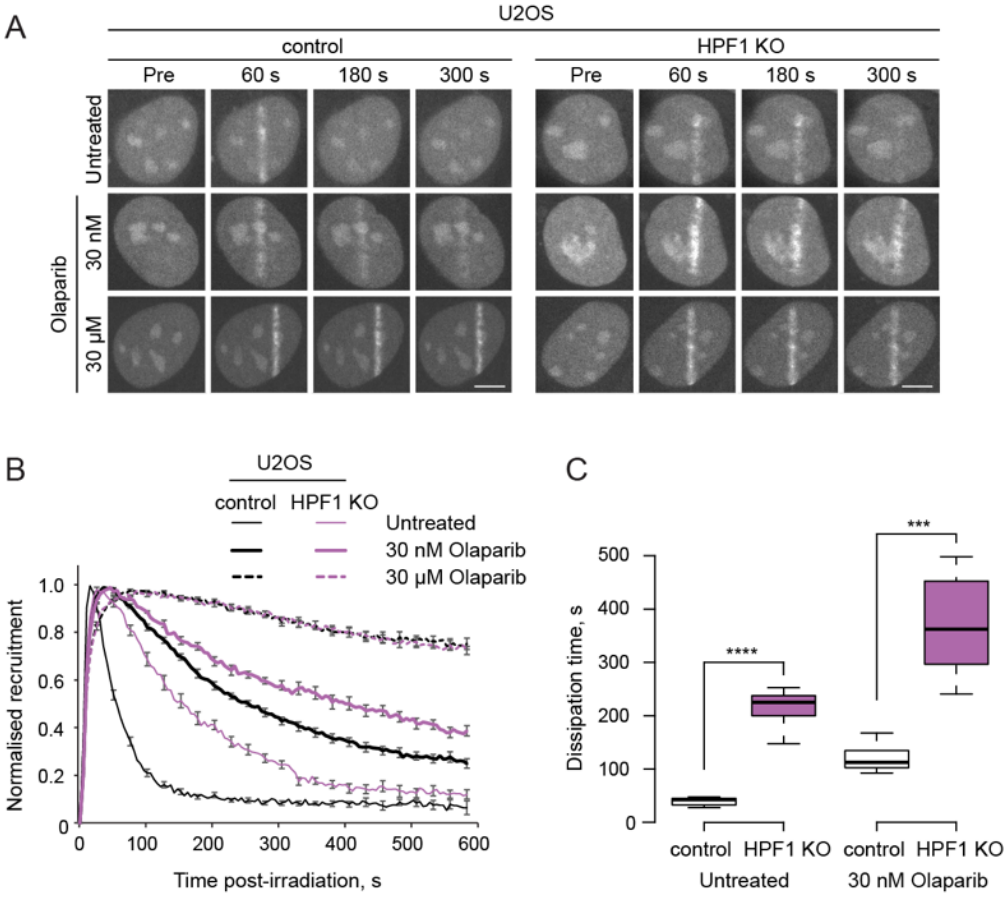


Figure 17. HPF1-mediated serine-ADPr promotes PARP1 release from damaged DNA.

(A) Representative images of endogenous PARP1 accumulation at the sites of DNA damage induced by laser micro-irradiation as detected using GFP-PARP1 chromobody in control and HPF1 KO U2OS cells treated as indicated. Scale bar, 5 µm. (B) Quantification of PARP1 accumulation kinetics in (A). Individual curves were normalised to maximum recruitment. (C) Quantification of dissipation times corresponding to the time required to dissipate 50% of the maximum PARP1 signal in (A) in untreated or 30 nM Olaparib-treated conditions. 30 nM of Olaparib was selected for the quantification as the concentration specifically inhibiting PARP1, and to some extent PARP2, whereas 30 µM of Olaparib is likely to non-specifically inhibit other PARP enzymes in human cells. The box limits correspond to the

25th and 75th percentiles and the bold line indicates the median value. The whiskers extend 1.5 times the interquartile range. Data are shown as mean ± SEM from the analysis of at least 10 nuclei, ***p<0.001, ****p<0.0001 (two-tailed Student's t-test). The experiments were carried out by Rebecca Smith, Siham Zentout and Sébastien Huet, and the figures were adapted from (Prokhorova et al., 2021b).

Since HPF1 deficiency remarkably reduces cellular levels of serine-linked ADPr (Bonfiglio et al., 2017), we hypothesized that increased PARPi sensitivity upon the loss of HPF1 is mainly due to the loss of serine-ADPr. To test this hypothesis, I suppressed serine-ADPr by increasing its hydrolysis, namely by stably overexpressing the serine-specific hydrolase ARH3 in U2OS cells. Strikingly, similarly to HPF1 loss, overexpression of ARH3 resulted in increased sensitivity to PARP1/2 inhibition by Olaparib and Veliparib (Figure 18). Along the same lines, Olaparib treatment of ARH3-overexpressing cells caused a marked increase in γH2AX formation (Figures 16A, S3 and 16C) and in the percentage of cells with >4N DNA content (Figure 16D). The levels of cell proliferation (S-phase subpopulation) and cell death (SubG1 subpopulation) were not significantly changed in response to Olaparib treatment (data not shown). In addition, I detected a substantial decrease in H3S10P levels, a marker of cells undergoing mitosis, in both HPF1-deficient and ARH3-overexpressing cells treated with Olaparib (Figure 16A). This suggests that both cells with HPF1 loss and ARH3 overexpression were unable to enter mitosis and, given the observed accumulation of polyploid cells, continued with DNA replication.

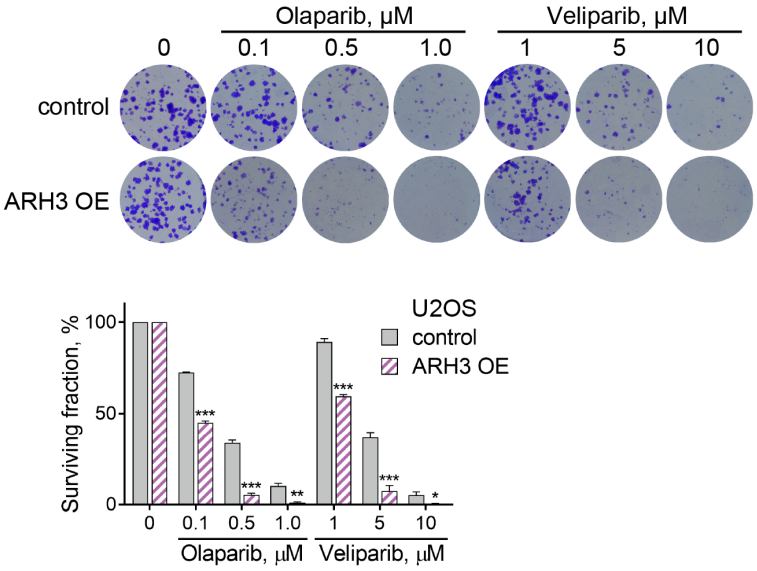


Figure 18. ARH3 overexpression renders cells more sensitive to PARP1/2 inhibition.

Representative images (top) and quantification (bottom) of colony formation assay with control and ARH3 overexpression (OE) U2OS cells treated with DMSO or as indicated. Data are shown as mean±SD, n=3, *p<0.05, **p<0.01, ***p<0.001 (two-tailed Student's t-test). The figure was partially adapted from (Prokhorova et al., 2021b).

Finally, I hypothesised that whereas decreasing cellular levels of serine-ADPr leads to PARPi sensitivity, on the contrary, increasing global levels of serine-ADPr could result in PARPi resistance. Excitingly, the loss of ARH3 in U2OS cells, which leads to accumulation of serine-ADPr (e.g., in Figures 7, 16A and S3), indeed caused a marked resistance to Olaparib (Figure 19) blocking induction of γH2AX (Figures 16A and S3), polyploidy (Figures 16B and 16D) and reduction in the levels of mitotic cells (Figure 16A). The levels of cell proliferation (S-phase subpopulation) were not significantly changed in response to Olaparib treatment, whereas cell death levels (SubG1 subpopulation) were significantly increased although to a lesser extent than in Olaparib-treated HPF1 KO cells (data not shown).

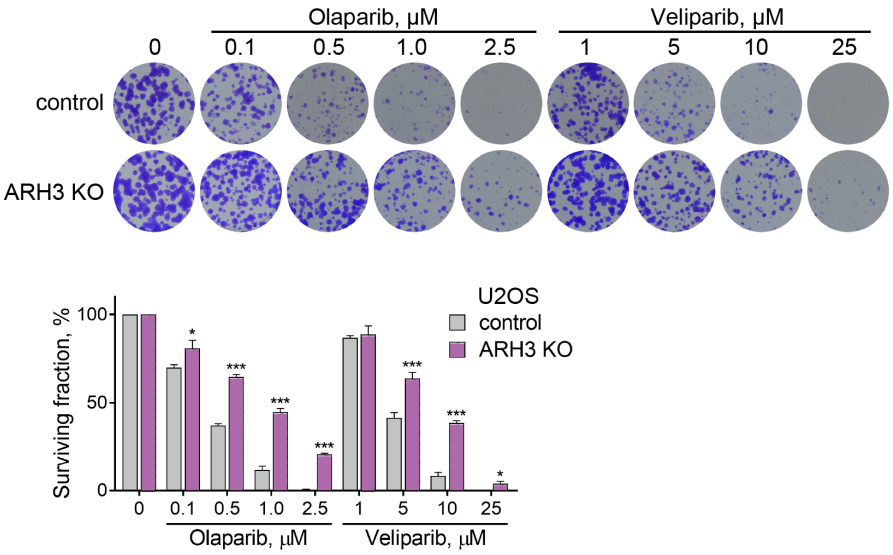


Figure 19. Loss of ARH3 confers resistance to PARP1/2 inhibitor treatment.

Representative images (top) and quantification (bottom) of colony formation assay with control and ARH3 KO U2OS cells treated with DMSO or as indicated. Data are shown as mean±SD, n=3, *p<0.05, ***p<0.001 (two-tailed Student's t-test). The figure was partially adapted from (Prokhorova et al., 2021b).

Collectively, the results presented in this section strongly suggest that the levels of serine-linked ADPr, which are specifically controlled by HPF1 and ARH3, modulate cellular sensitivity and response to PARPis, including the extent of PARP1 retention on damaged DNA and PARPi-induced accumulation of unrepaired DNA damage.

3.2.2. Serines 499, 507 and 519 are the major sites of PARP1 ADP-ribosylation

Whereas manipulation of HPF1 and ARH3 levels likely affects modification levels of at least hundreds of serine-ADPr substrates, we attempted to identify the effects of specific serine-ADPr sites on global ADPr levels and on the cellular response to

PARP1/2 inhibition. We focused on PARP1 itself, whose modification accounts for a major fraction of total ADPr in unstressed conditions and following its induction by different DNA damaging agents, including H_2O_2 and MMS. This can be detected by Western blotting directly or after immunoprecipitation (Figures 7, 16A, S3 and 20).

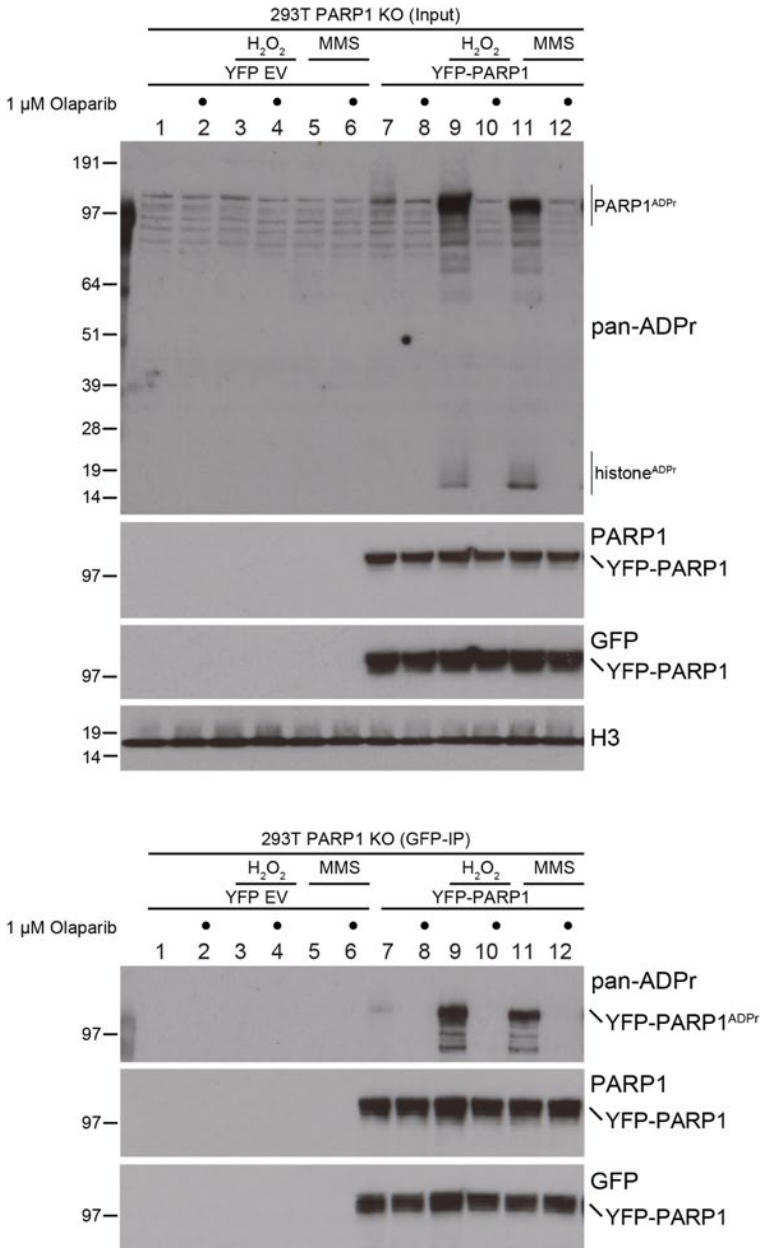


Figure 20. DNA damaging agents H_2O_2 and MMS induce similar patterns of cellular ADPr.

PARP1 KO 293T cells were pre-treated with 1 μM Olaparib for 12 h followed by 10 min 2 mM H_2O_2 treatment or 30 min 0.1% MMS treatment in the presence of DMSO or 1 μM Olaparib. ADPr signals were analysed in GFP-immunoprecipitation (GFP-IP) and input samples by Western blotting. Representative Western blots from 3 independent experiments are shown. The figure was adapted from (Prokhorova et al., 2021b).

A number of PARP1 ADPr sites were detected by mass spectrometry, in particular in its auto-modification domain (Bilan et al., 2017; Bonfiglio et al., 2017; Buch-Larsen et al., 2020; Daniels et al., 2015; Hendriks et al., 2019; Larsen et al., 2018; Li et al.,

2019), which consists of the central BRCT domain and a neighbouring unstructured region (Figure 21). Whereas there are multiple detected or predicted ADPr sites within this PARP1 domain, their cellular functions have not been analysed through mutational studies. We focused on the highlighted three serine (499, 507 and 519) and six glutamate (471, 484, 488, 491, 513 and 514) residues, generating constructs that have three simultaneous serine to alanine or six glutamate to alanine substitutions (Figure 21).

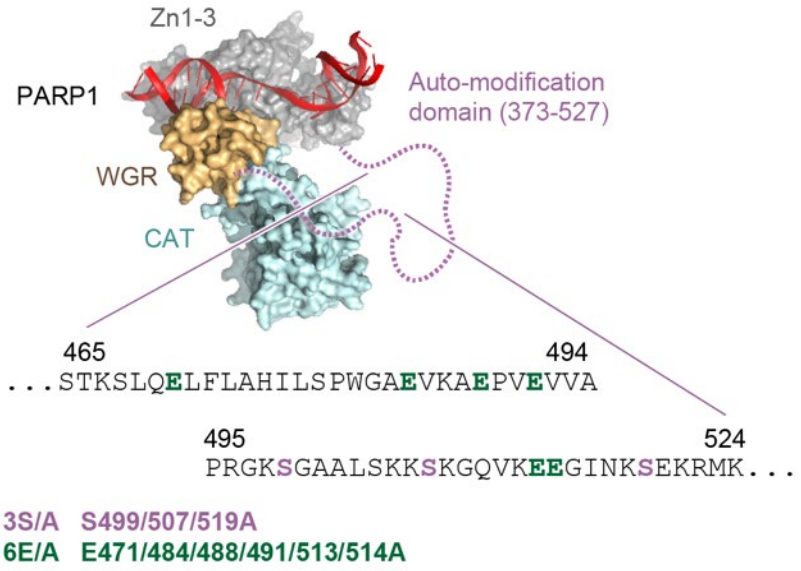


Figure 21. Model of PARP1 bound to a single-strand DNA break including mass spectrometry-identified sites in the auto-modification domain of PARP1.

Surface representation of PARP1 bound to DNA (red ribbon) with a single-strand break. The auto-modification domain fragment missing from the structures is shown schematically and its sequence containing mutated ADPr sites is provided. Alignment of the structures from PDB accessions 4DQY, 2N8A and 2LE0 was performed by Marcin Suskiewicz. The figure was adapted from (Prokhorova et al., 2021b).

Following transient expression of WT, S499/507/519A (3S/A) and E471/484/488/491/513/514A (6E/A) YFP-PARP1 in PARP1 U2OS KO cells, I compared ADPr levels in untreated conditions, after exposure to MMS or overexpression of Flag-HPF1 (Figure 22). YFP-PARP1 WT and 6E/A ADPr signals were relatively similar in all of the three conditions, in particular upon serine-ADPr induction by MMS treatment or Flag-HPF1 overexpression. However, the modification was markedly decreased in the 3S/A mutant in all the conditions, indicating that the most of PARP1 ADPr locates to the three mutated serine residues under both basal and DNA damage conditions, with these three serine sites being predominantly modified in the presence of HPF1.

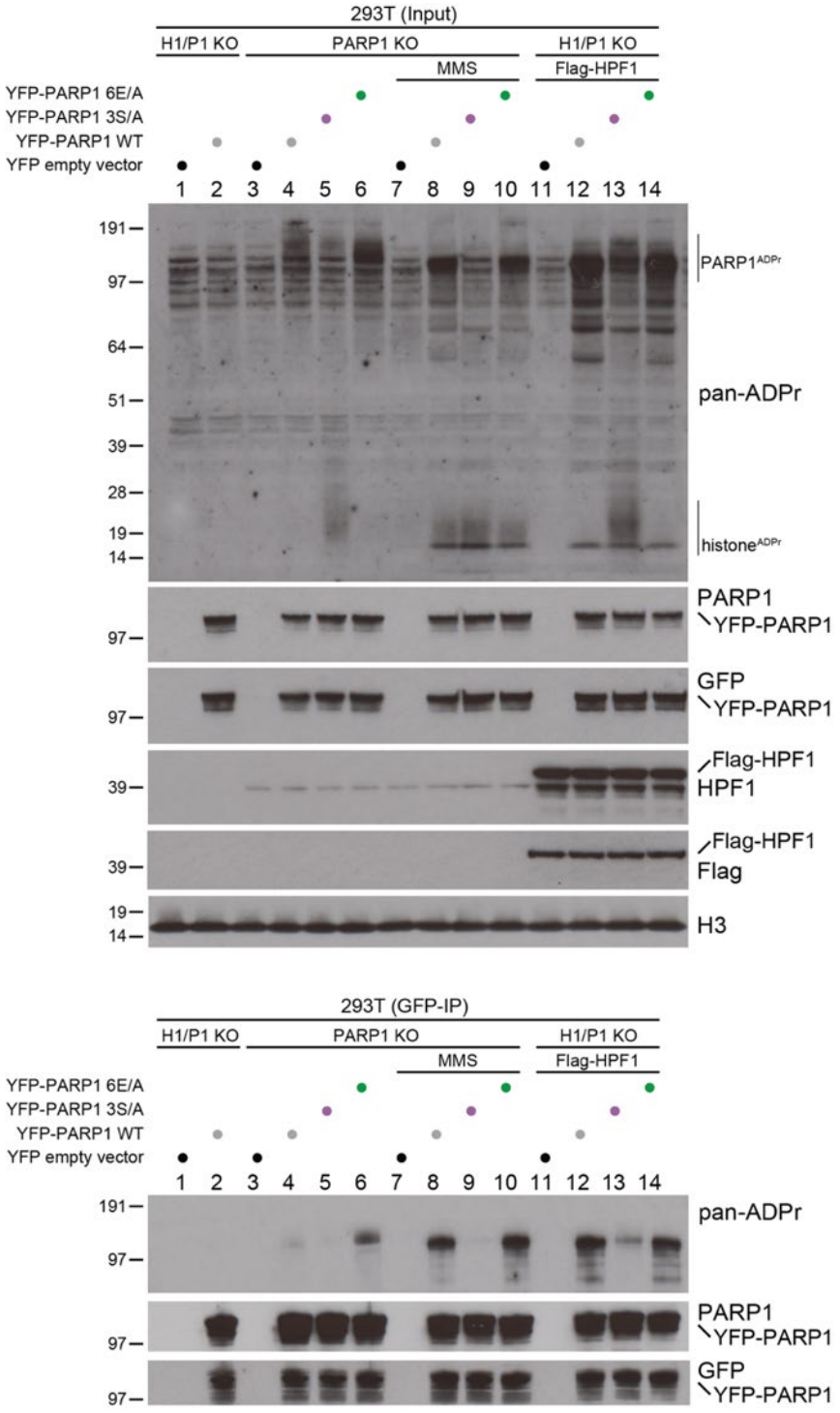


Figure 22. Serines 499, 507 and 519 are the main sites of PARP1 ADPr.

HPF1/PARP1 KO (H1/P1 KO) and PARP1 KO 293T cells were transfected using the indicated constructs and left untreated or treated with 0.1% MMS. Mutation in key PARP1 serine (S499/507/519A, 3S/A), but not glutamate (E471/484/488/491/513/514A, 6E/A), ADPr sites reduced the levels of endogenous and MMS- or Flag-HPF1 overexpression (OE)-induced PARP1 ADPr. GFP-PARP1 immunoprecipitation (GFP-IP) and input samples were analysed by Western blotting for ADPr levels. Representative Western blots from 3 independent experiments are shown. The figure was adapted from (Prokhorova et al., 2021b).

This is in agreement with our previous observations, obtained by Western blotting in Section 2.2.1, that a major fraction of PARP1 ADPr is HPF1-dependent (Palazzo et

al., 2018), which can also be seen in Figure 22 both in HPF1 KO YFP-PARP1 WT-overexpressing cells directly or after immunoprecipitation. All the three YFP-PARP1 variants remained active as demonstrated by their ability to ADP-ribosylate histones, with YFP-PARP1 3S/A overexpression even leading to an increase in histone ADPr, possibly due to more free HPF1 and NAD^+ available after the loss of the main sites of PARP1 ADPr.

3.2.3. Loss of PARP1 ADP-ribosylation at serines 499, 507 and 519 leads to increased sensitivity to PARP1/2 inhibition

Having identified the main sites of PARP1 endogenous and exogenous stress-induced ADPr, serines 499, 507 and 519, we sought to examine their effect on cellular response to PARP1/2 inhibition. We generated PARP1 KO Flp-In T-REx U2OS cells with stable integration of genes encoding YFP, YFP-PARP1 WT or 3S/A under doxycyline-inducible promoters. In agreement with Figure 15E and previous reports (Gibbs-Seymour et al., 2016; Murai et al., 2012), showing that Olaparib sensitivity is dependent on PARP1 presence, PARP1 KO cells complemented with YFP vector or any of the vectors but in the absence of doxycline were resistant to Olaparib (Figures 23A and 23B). Induction of PARP1 WT or 3S/A expression to the levels similar to that of endogenous PARP1 resulted in a marked increase in the sensitivity to Olaparib, which was substantially stronger for PARP1 3S/A mutant compared to PARP1 WT (Figure 23A). Moreover, similarly to the effect of global suppression of serine-ADPr in Section 3.2.1, loss of the main three PARP1 ADPr sites in 3S/A mutant led to an increase in the levels of Olaparib-induced DNA damage (Figure 23C).

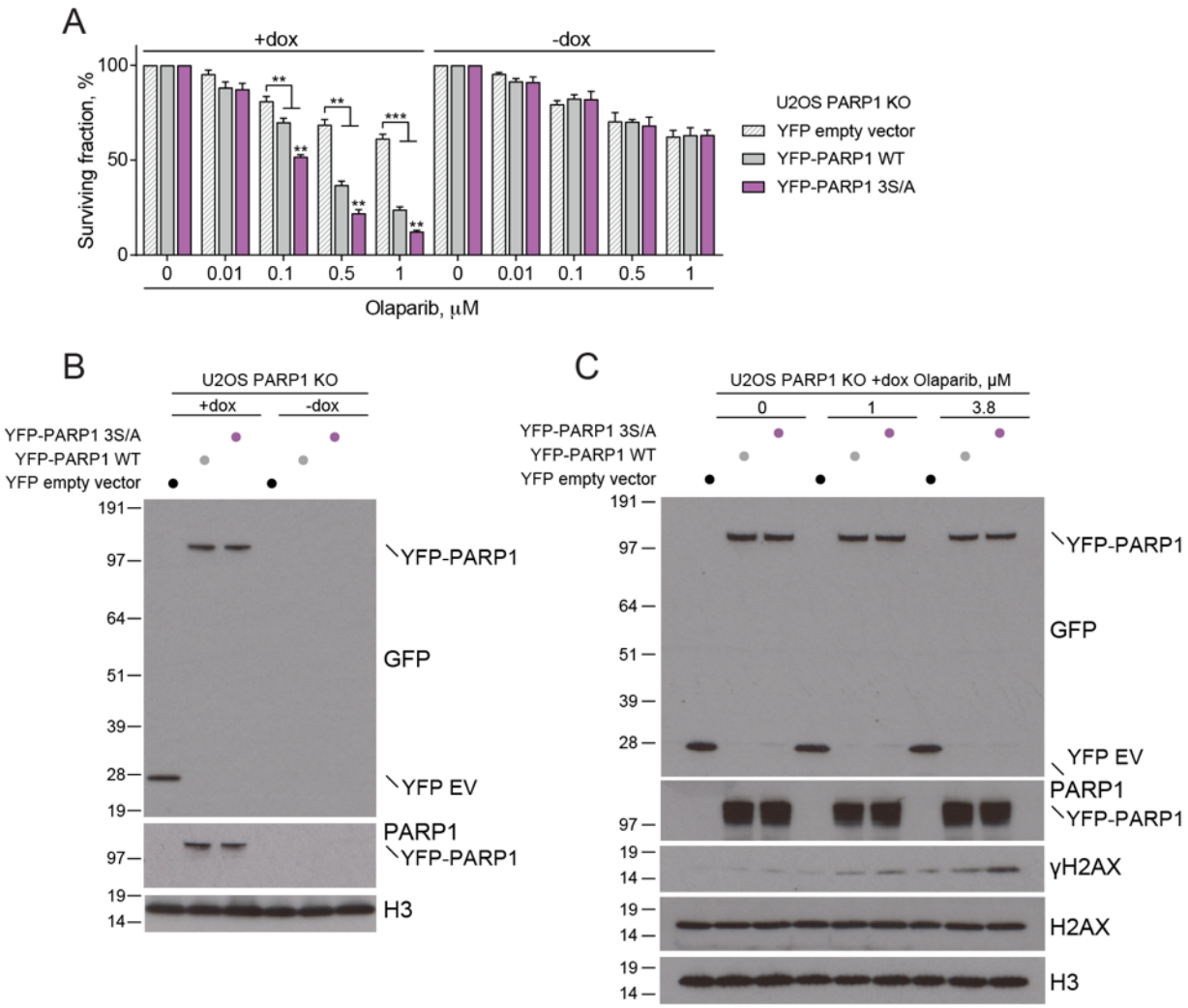


Figure 23. Loss of the main PARP1 ADPr sites serine 499, 507 and 519 leads to increased cell sensitivity to PARP1/2 inhibition and DNA damage accumulation.

(A Quantification of colony formation assay using Flp-In T-Rex PARP1 KO U2OS cells with doxycycline (dox)-inducible expression of YFP empty vector, YFP-PARP1 WT or 3S/A mutant treated with DMSO or as indicated. Data are shown as mean±SD, n=3, **p<0.01, ***p<0.001 (two-tailed Student's t-test). (B) Control comparison of expression of YFP empty vector (EV), YFP-PARP1 WT and 3S/A mutant in (A) by Western blotting. Representative Western blots from 2 independent experiments are shown. (C) Loss of key serine-ADPr sites in PARP1 3S/A mutant leads to increased γH2AX formation following 6-day Olaparib treatment as analysed by Western blotting. Representative Western blots from 2 independent experiments are shown. The figures were adapted from (Prokhorova et al., 2021b).

Furthermore, similarly to the loss of global HPF1-medicated ADPr (Figure 17), the loss of serine 499, 507 and 519, but not glutamate 471, 484, 488, 491, 513 and 514, modification resulted in prolonged GFP-PARP1 accumulation at the sites of DNA damage induced by laser micro-irradiation (Figure 24). This indicates that serine-ADPr, in particular on serines 499, 507 and 519, counteracts PARP1 trapping and

allows for the timely detachment of PARP1 from DNA damage sites in human cells.

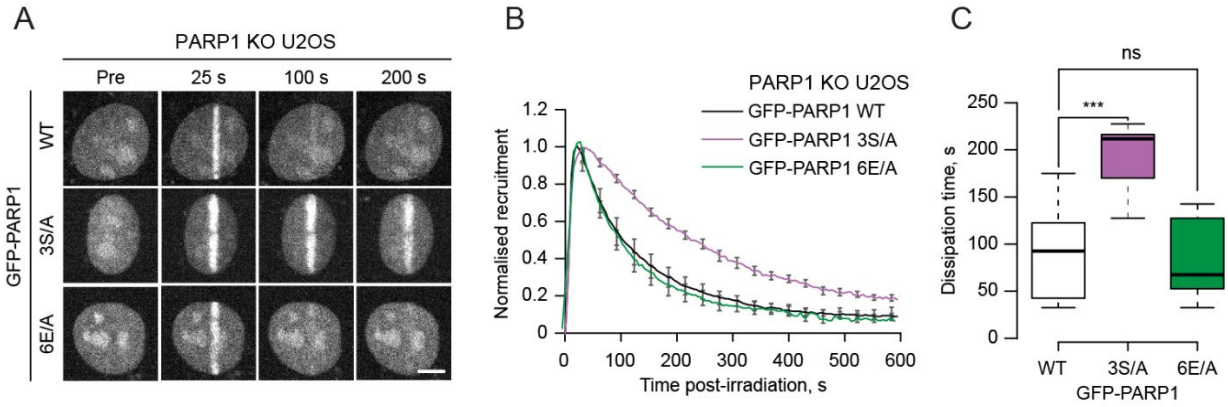


Figure 24. PARP1 ADPr at serines 499, 507 and 519 promotes PARP1 release from damaged DNA.

(A) Representative images and quantifications (B, C) of GFP-PARP1 accumulation at the sites of DNA damage induced by laser micro-irradiation in control and HPF1 KO U2OS cells. Scale bar, 5 μm. (B) GFP-PARP1 accumulation kinetics normalised to maximum recruitment. (C) GFP-PARP1 dissipation times corresponding to the time required to dissipate 50% of the maximum GFP-PARP1 signal. The box limits correspond to the 25th and 75th percentiles and the bold line indicates the median value. The whiskers extend 1.5 times the interquartile range. Data are shown as mean ± SEM from the analysis of at least 10 nuclei, ***p<0.001 (two-tailed Student's t-test). The experiments were carried out by Rebecca Smith, Siham Zentout and Sébastien Huet, and the figures were adapted from (Prokhorova et al., 2021b).

Collectively, the findings in this chapter demonstrate the importance of serine-ADPr for promoting PARP1 release from damaged DNA, and thus counteracting PARP1 trapping and preventing PARPi-induced cytotoxicity, in particular induction of DNA damage and cell death. According to the results presented in this section, a substantial part of that effect could be attributed to three serine-ADPr sites, PARP1 serines 499, 507 and 519, the main sites of PARP1 ADPr in human cells.

3.3. Discussion

Following the recent discovery of serine residues as the main acceptors of both endogenous and stress-induced ADPr in human cells (Bilan et al., 2017; Bonfiglio et al., 2017; Buch-Larsen et al., 2020; Hendriks et al., 2019; Larsen et al., 2018; Leidecker et al., 2016), in this chapter we examined the relationship between cellular serine-ADPr levels and response to PARP1/2 inhibition. To this end, we employed the loss of HPF1 or overexpression of ARH3 to globally decrease serine-ADPr and loss of ARH3 to increase modification levels. We demonstrated a clear negative correlation between the levels of serine-ADPr and PARPi sensitivity (Prokhorova et al., 2021b).

Our findings that the loss of HPF1 renders cells more sensitive to PARP1/2 inhibition (Gibbs-Seymour et al., 2016; Prokhorova et al., 2021b) are in agreement with the results of recent genetic screens carried out using different cell lines and PARPis (Clements et al., 2020; DeWeirdt et al., 2020; Hewitt et al., 2021; Juhász et al., 2020). The increased PARPi sensitivity of HPF1-deficient cells could be explained by the fact that the complex that is formed by HPF1 and PARP1 to catalyse serine-ADPr (Suskiewicz et al., 2020) requires higher PARPi concentrations to be suppressed compared to PARP1 alone. Although future structural studies are needed to provide a mechanistic explanation, in agreement with HPF1 notably stimulating the rate of serine-ADPr reaction (Langelier et al., 2021), the PARP1-HPF1 complex produces substantially higher levels of ADPr than PARP1 in the presence of PARPis, contributing to inhibitor tolerance (Prokhorova et al., 2021b). Given that HPF1 not only directs PARP1 activity towards serine residues, but also limits the length of PAR polymers produced by PARP1, which has recently been explained by an HPF1-mediated switch in PARP1 activity from polymerase to hydrolase (Rudolph et al., 2021), it would also be of interest to assess whether the shorter length of ADPr generated in the presence of HPF1 could also contribute to the increased resistance of PARP1-HPF1 complex to PARPis in human cells.

Consistent with the above, the loss of HPF1 potentiated PARPi-induced cytotoxicity rather than triggered separate events. Most notably, HPF1 deficiency resulted in increased accumulation of DNA damage and prolonged residence of PARP1 at the sites of DNA breaks both in untreated and PARPi-treated cells. Although we observed the sensitivity of HPF1-deficient cells to all the five clinically relevant PARPis tested, including the weakest PARP1 trapper Veliparib, Talazoparib that exhibits the highest trapping efficiency demonstrated the highest cytotoxicity (Murai et al., 2014), with complete killing of HPF1 KO cells achieved with as little as 5 nM, while the concentration of 5 μM was needed for Veliparib. However, the comparison of the effects of Veliparib and Talazoparib on PARP1 residence time on damaged DNA was not performed in this work. Whilst future studies are needed to address the extent to which prolonged PARP1 retention on damaged DNA often referred to as trapping contributes to the synthetic lethality between HPF1 and PARP1/2 inhibition, the genetic dependency on PARP1 for PARPi-induced cytotoxicity in HPF1/PARP1 KO cells additionally suggested that the lethality associated with PARP1/2 inhibition in HPF1 KO cells is dependent on PARP1 trapping.

Similar to HPF1 loss, overexpression of specific serine-ADPr hydrolase ARH3 increased cellular sensitivity to PARP1/2 inhibition and the levels of PARPi-induced DNA damage. On the contrary, cells lacking ARH3 became more resistant to the treatment and DNA damage induction, confirming that PARPi sensitivity is negatively correlated with the levels of serine-ADPr. However, the effects of modulating ARH3 levels on PARP1 residence time on damaged DNA were not assessed in this work and remain to be addressed in the future studies.

Importantly, from a therapeutic perspective, these results also highlight HPF1 and ARH3 as potential biomarkers for predicting PARPi sensitivity in cancers. Indeed, according to cBioPortal (TCGA PanCancer Atlas Studies), HPF1 gene may be lost, for instance in undifferentiated stomach adenocarcinomas (15.4%) and lung squamous cell carcinomas (3.7%), whereas ARH3 gene may be amplified in ovarian epithelial tumours (6.3%).

Next in this chapter, we examined the importance of specific ADPr sites, focusing on the main sites of PARP1, which itself is one of the major ADPr substrates. Through mutational studies we demonstrated that the loss of serines 499, 507 and 519 results in a marked reduction of PARP1 ADPr, whereas the loss of glutamates 471, 484, 488, 491, 513 and 514 does not affect its levels. Moreover, we were able to demonstrate the importance of just these three serine sites on PARP1 in counteracting PARPi cytotoxicity, in particular DNA damage accumulation and prolonged retention of PARP1 at DNA damage sites, with the latter also observed in more recent studies (Hendriks et al., 2021; Smith et al., 2021). Accordingly, already the loss of PARP1 serine 499, 507 and 519 ADPr rendered cells significantly more sensitive to PARP1/2 inhibition. However, its effect on PARPi sensitivity, as well as on PARP1 residence time on damaged DNA, was less striking than that of HPF1 deficiency. Therefore, serine-ADPr targets other than PARP1 could certainly also provide a substantial contribution towards protecting human cell from prolonged PARP1 retention on damaged DNA and other events underlying PARPi-induced toxicity.

Overall, serine-ADPr, including but not limited to ADPr of PARP1 serines 499, 507 and 519, counteracts prolonged PARP1 retention on damaged DNA often referred to as trapping and prevents PARPi-induced DNA damage and cell death (Figure 25). Of note, this confirms the previously suggested role of PARP1 ADPr in its release from DNA breaks (Ferros and Olivera, 1982; Zahradka and Ebisuzaki, 1982), specifically stressing the role of serine ADPr sites, including PARP1 serines 499, 507 and 519, in

de-trapping PARP1. Whilst it is possible that non-serine linked ADPr could to some extent contribute to PARP1 detachment from DNA damage sites, serine-ADPr will persist with higher doses of PARPis since PARP1-HPF1 complex requires higher concentrations of PARPis to block its activity (Prokhorova et al., 2021b).

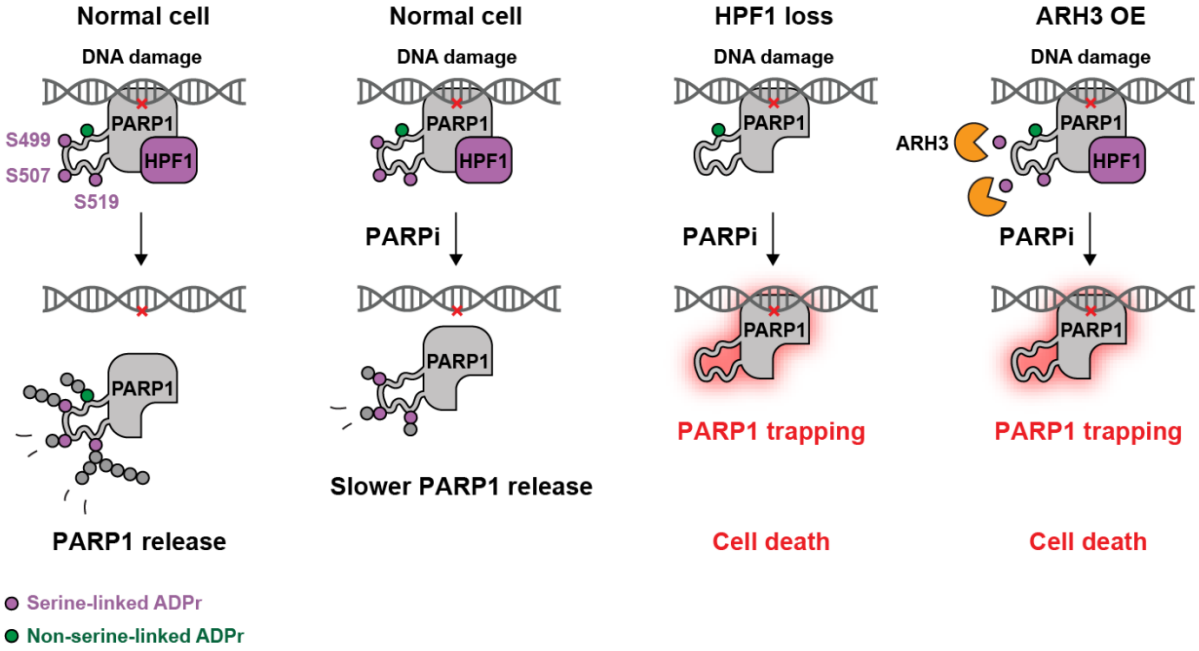


Figure 25. Proposed model of the effect of HPF1 loss and ARH3 overexpression on PARPi response.

In normal cells, following PARP1 activation by DNA damage, PARP1 and HPF1 form a composite enzyme that efficiently ADP-ribosylates serine residues. Serine-ADPr, especially on PARP1 serines 499, 507 and 519, then promotes the detachment of PARP1 from DNA damage sites. Upon treatment with a PARPi, the PARP1-HPF1 complex partially escapes inhibition, and the resultant serine-ADPr promotes the release of PARP1 from damaged DNA, thus sufficiently counteracting PARP1 trapping. This mechanism is compromised in cells with HPF1 deficiency (because of the loss of efficient serine-ADPr synthesis) or ARH3 overexpression (OE, because of higher rates of serine-ADPr hydrolysis). PARPi treatment of these cells results in high levels of PARP1 trapping and eventually leads to cell death.

More generally, our findings underscore the embeddedness of PARP1 within a broader network that includes serine-ADPr factors HPF1 and ARH3, both of which provide a substantial contribution in determining the cellular response to the sources of DNA damage, in particular PARPis (Figure 26).

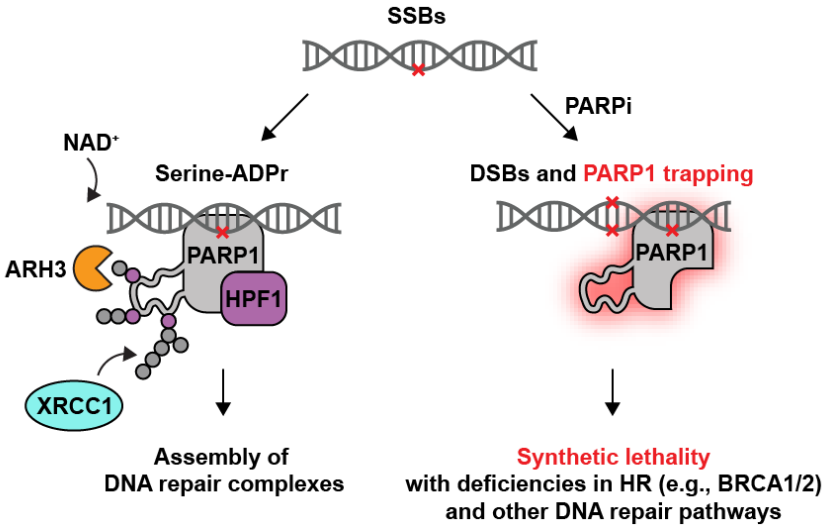


Figure 26. The role of HPF1 and ARH3 in the regulation of PARP1 function.

PARP1 plays a key role in SSB repair. PARP1 detects and binds to SSBs and synthetizes ADPr, most notably serine-ADPr, which levels are additionally controlled in cells by serine-specific regulators, HPF1 and ARH3. A scaffolding protein XRCC1 is recruited to SSBs through direct interaction with PARP1-synsetised PAR, and in turn promotes the recruitment of the enzymes required for SSB repair. Prolonged retention of PARP1 on damaged DNA often referred to as trapping is a major cause of PARPi-induced cytotoxicity, threatening genome integrity and eventually leading to cell death, especially in cells with deficiencies in HR repair genes BRCA1/2 or other DNA repair genes.

However, whether levels of HPF1 and ARH3 directly affect the recruitment of XRCC1 and other ADPr-binding factors involved in the DDR remains to be investigated. Of note, one recent study has already reported XRCC1 and DNA ligase 3 recruitment in an HPF1-dependent manner during alternative Okazaki fragment ligation when DNA ligase 1 is absent (Kumamoto et al., 2021). Moreover, at least almost half of the factors involved in DNA repair are itself substrates of ADPr (Buch-Larsen et al., 2020). With 84% of the 9,029 DNA damage-induced ADPr sites in human cells being on serine residues (Buch-Larsen et al., 2020), it is likely that modulating the levels of specific serine-ADPr regulators, HPF1 and ARH3 (Hendriks et al., 2021) will also affect the function of the modified DNA repair proteins. Future studies will clarify the extent to which HPF1 and ARH3 status affects the recruitment and function of factors involved in the DDR, as well as in other cellular processes.

Altogether, the levels of serine-ADPr and its specific regulators HPF1 and ARH3 predict cancer cell sensitivity to PARP1/2 inhibition, which could be exploited therapeutically. Mechanistically, serine-ADPr, in particular on PARP1 serines 499, 507 and 519, promotes de-trapping of PARP1 and prevents PARPi-induced accumulation of DNA damage, contributing to cellular tolerance to PARP1/2 inhibition.

4. Functional synergy and synthetic lethal interaction between the major ADP-ribosylation 'erasers' ARH3 and PARG

4.1. Introduction

The emerging role of ARH3 hydrolase in the control of cellular levels of mono-ADPr (Abplanalp et al., 2017; Fontana et al., 2017; Hanzlikova et al., 2020) and, at least in certain cellular contexts, poly-ADPr (Danhauser et al., 2018; Ghosh et al., 2018; Mashimo et al., 2013, 2019), as discussed in Section 1.1.2, suggested that both ARH3 and PARG might complement each other in maintaining ADPr homeostasis. However, despite a great interest in PARP1 as a target for cancer therapy and the arising therapeutic potential of PARG inhibition (Chen and Yu, 2019; Lord and Ashworth, 2017; Nagashima et al., 2020; Pillay et al., 2019; Slade, 2020), the relative contribution of ARH3 and PARG to the regulation of cellular ADPr levels has remained unclear.

In this chapter, we addressed the separation of function between ARH3 and PARG under both unstressed and exogenous DNA damage conditions. To this end, we employed several newly developed tools for studying mono-ADPr, including anti-mono-ADPr AbD33204 and anti-histone H3 S10/28-linked MAR antibodies (Bonfiglio et al., 2020). Furthermore, we elaborated on our findings in Section 3.2.1 that the protein levels of ARH3, through modulating the levels of serine-ADPr, affect cellular sensitivity to PARP1/2 inhibition. Finally, we extended our findings to neurodegenerative phenotypes caused by loss-of-function mutations in ARH3.

4.2. Results

4.2.1. Loss of ARH3 activity results in the accumulation of chromatin-associated serine-linked mono-ADP-ribosylation throughout the cell cycle

The loss of ARH3 results in the accumulation of serine-ADPr not only in response to exogenous DNA damage but also in untreated conditions, as was previously shown in Figure 7 and reported in (Fontana et al., 2017; Palazzo et al., 2018). To better characterise the housekeeping role of ARH3 in the reversal of endogenous ADPr, we assessed ADPr levels and localization in control and ARH3 KO U2OS cells at different cell cycle stages. Subcellular fractionation followed by Western blotting using anti-pan-ADP antibodies, anti-mono-ADPr AbD33204 and anti-histone H3

S10/28-linked MAR antibodies showed strong ADPr accumulation in ARH3 KO but not control cells, and the modification was predominantly detected in the chromatin fraction (Figure 27).

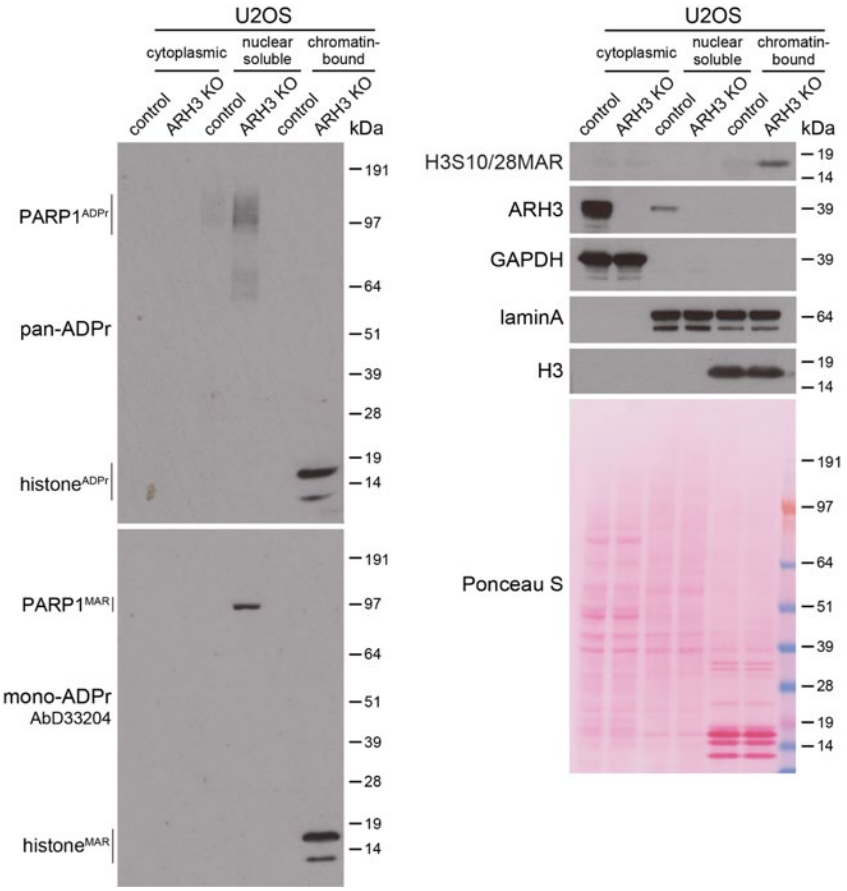


Figure 27. Loss of ARH3 leads to accumulation of chromatin-bound mono-ADPr.

Western Blotting analysis of ADPr signals in control and ARH3 KO U2OS cells subjected to subcellular fractionation. Representative Western blots from 3 independent experiments are shown. The figure was adapted from (Prokhorova et al., 2021a).

Similarly, immunofluorescence analysis using the pan-ADPr reagent or anti-mono-ADPr AbD33204 antibody in cells pre-extracted with detergent before fixation to retain chromatin-associated proteins but remove cytoplasmic and nuclear soluble components, also demonstrated ADPr enrichment in ARH3 KO cells. Strikingly, ADPr persisted not only in all the stages of interphase, but even on condensed chromatin throughout different stages of mitosis (Figure 28).

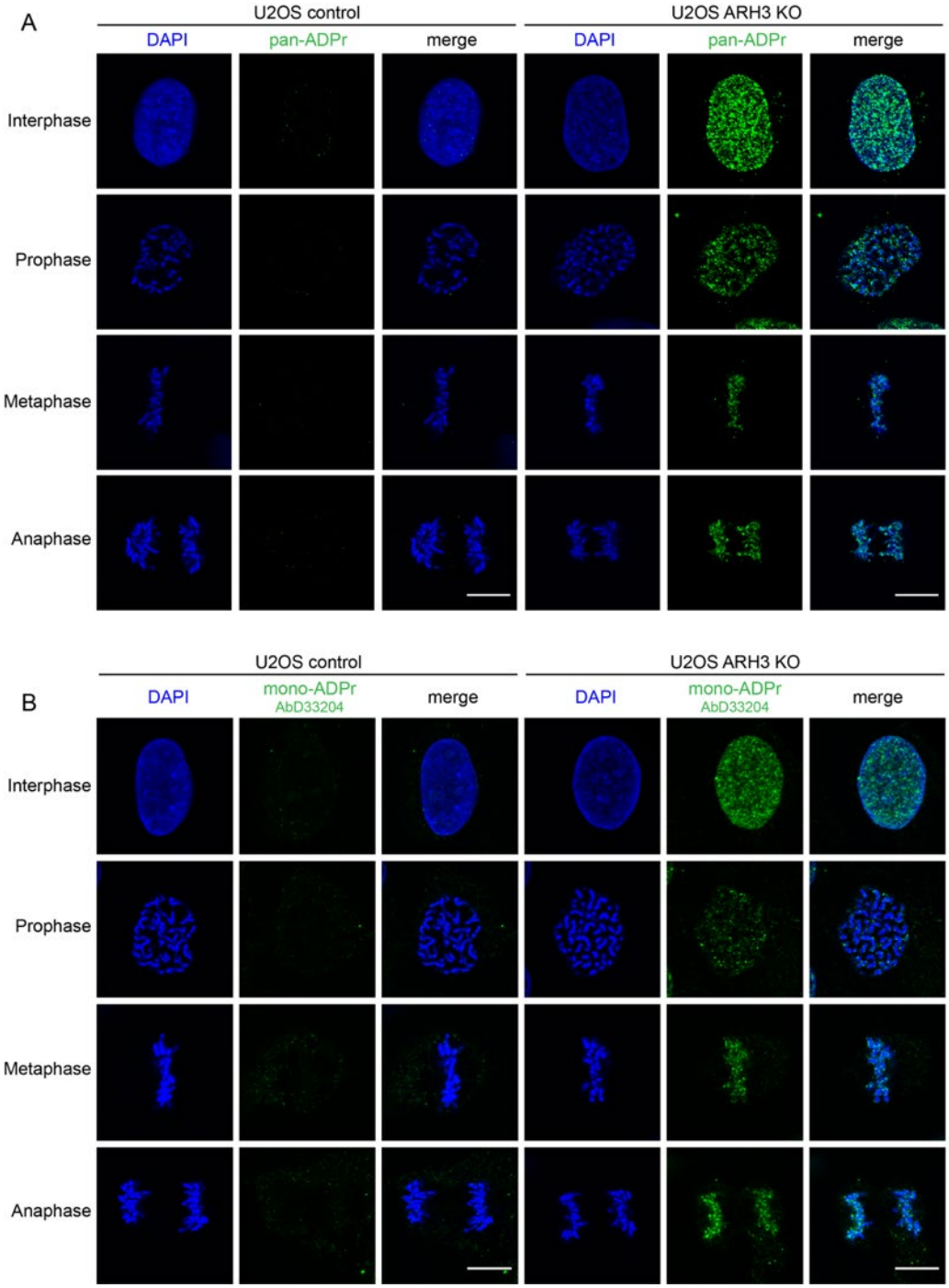


Figure 28. ARH3-deficient cells accumulate chromatin-bound mono-ADPr throughout different stages of the cell cycle.

Immunofluorescence analysis of pan-ADPr (A) and mono-ADPr (B) signals in detergent pre-extracted control and ARH3 KO U2OS cells at different stages of the cell cycle. Scale bars, 10 μm. The experiments were performed by Thomas Agnew and myself. Representative images of at least 300 cells analysed in 3 independent experiments are shown. The figures were adapted from (Prokhorova et al., 2021a).

Surprisingly, the loss of ARH3 resulting in a marked enrichment of mono-ADPr is well tolerated as ARH3 KO cells displayed proliferation rates similar to those in control cells (Figure S5) and normally progressed through multiple cell cycles. This is unexpected given that mono-ADPr is enriched on chromatin, even during mitosis,

and that persistent ADPr may affect canonical histone modifications critical for cell proliferation (Bartlett et al., 2018).

4.2.2. Both ARH3 and PARG are required for timely reversal of endogenous and exogenous stress-induced poly-ADP-ribosylation

Next, I explored ARH3 function under exogenous stress conditions, using a short treatment with H_2O_2 to induce ADPr. Consistent with our previous findings (e.g., Figure 7), ARH3 loss resulted in increased ADPr levels in both untreated and H_2O_2-treated 293T cells as detected using anti-pan-ADPr reagent, with the strongest signals corresponding to PARP1 and histone ADPr (Figure 29A). 2 h after the treatment, H_2O_2-induced ADPr returned to basal levels in control cells but remained elevated in ARH3 KO cells. A short 1-h pre-treatment with the PARPi Olaparib completely blocked the induction of ADPr in control cells, demonstrating its PARP1/2 dependence. Conversely, the elevated levels of PARP1 and histone ADPr in ARH3 KO cells persisted even after 1-h pre-treatment with Olaparib (Figure 29A).

Despite a higher hydrolytic activity of PARG against long PAR chains *in vitro*, ARH3 is also able to hydrolase PAR, although with much lower efficiency (Fontana et al., 2017; Oka et al., 2006). To assess whether these two enzymes cooperate in regulating cellular poly-ADPr levels, I treated control and ARH3 KO cells with PARGi PDD00017273 (James et al., 2016). The treatment led to a dramatic increase in H_2O_2-induced ADPr in control and ARH3-deficient 293T (Figure 29A) and U2OS cells (Figure 29B) as detected using anti-pan-ADPr reagent and anti-poly-ADPr antibody. This indicates that PARG performs the most of poly-ADPr hydrolysis following DNA damage induction. However, H_2O_2-induced ADPr was strongly reduced in PARGi-treated control but not ARH3 KO 293T cells 2 and even 6 h after treatment (Figure 29A). This suggests that, although being slower and less efficient than PARG, ARH3 also contributes to the turnover of DNA damage-induced poly-ADPr in human cells. Of note, simultaneous inhibition of PARG and loss of ARH3 led to a substantially greater persistence of ADPr compared to their individual effects combined, indicating that their roles in the hydrolysis of ADPr are not redundant but rather synergistic.

Importantly, in the absence of exogenous stress, loss of ARH3 resulted only in a very small increase in poly-ADPr (Figure 29B), suggesting that endogenous ADPr in cells lacking ARH3 indeed predominantly consists of mono-ADPr. Conversely, just 1-h

pre-treatment of ARH3-deficient cells with PARGi caused a substantial enrichment of poly-ADPr (Figure 29B).

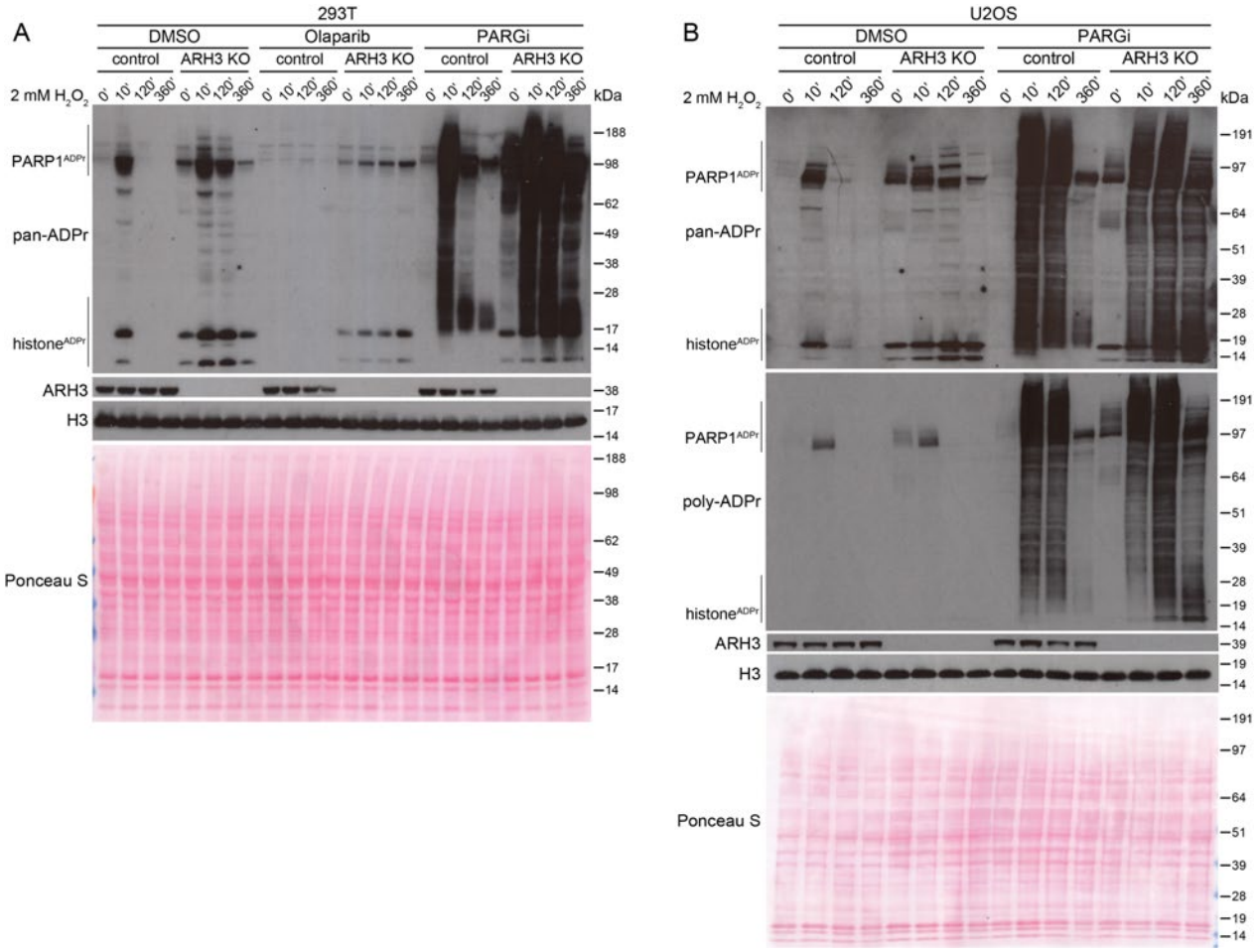


Figure 29. PARG inhibition leads to greater accumulation and persistence of both ADPr in unstressed conditions and ADPr induced by exogenous DNA damage in ARH3-deficient cells.

(A) Control and ARH3 KO 293T cells were pre-treated with DMSO, 10 μM Olaparib or 10 μM PARGi for 1 h followed by H_2O_2 treatment as indicated. ADPr signals were analysed by Western blotting. (B) Control and ARH3 KO U2OS cells were pre-treated with DMSO or 10 μM PARGi for 1 h followed by H_2O_2 treatment in the presence of DMSO or 10 μM PARGi. ADPr signals were analysed by Western blotting. Representative Western blots from 2 independent experiments are shown. The figures were adapted from (Prokhorova et al., 2021a).

Prolonged treatment resulted in further accumulation of ADPr, in particular poly-ADPr, as observed by Western blotting (Figures 30A-C) and immunofluorescence following pre-extraction with detergent prior to fixation to retain only chromatin-bound proteins (Figure 31). Conversely, only a small enrichment of poly-ADPr was detected in control cells even after prolonged PARGi treatment, indicating that both PARG and ARH3 play a key role in the maintenance of endogenous levels of poly-ADPr.

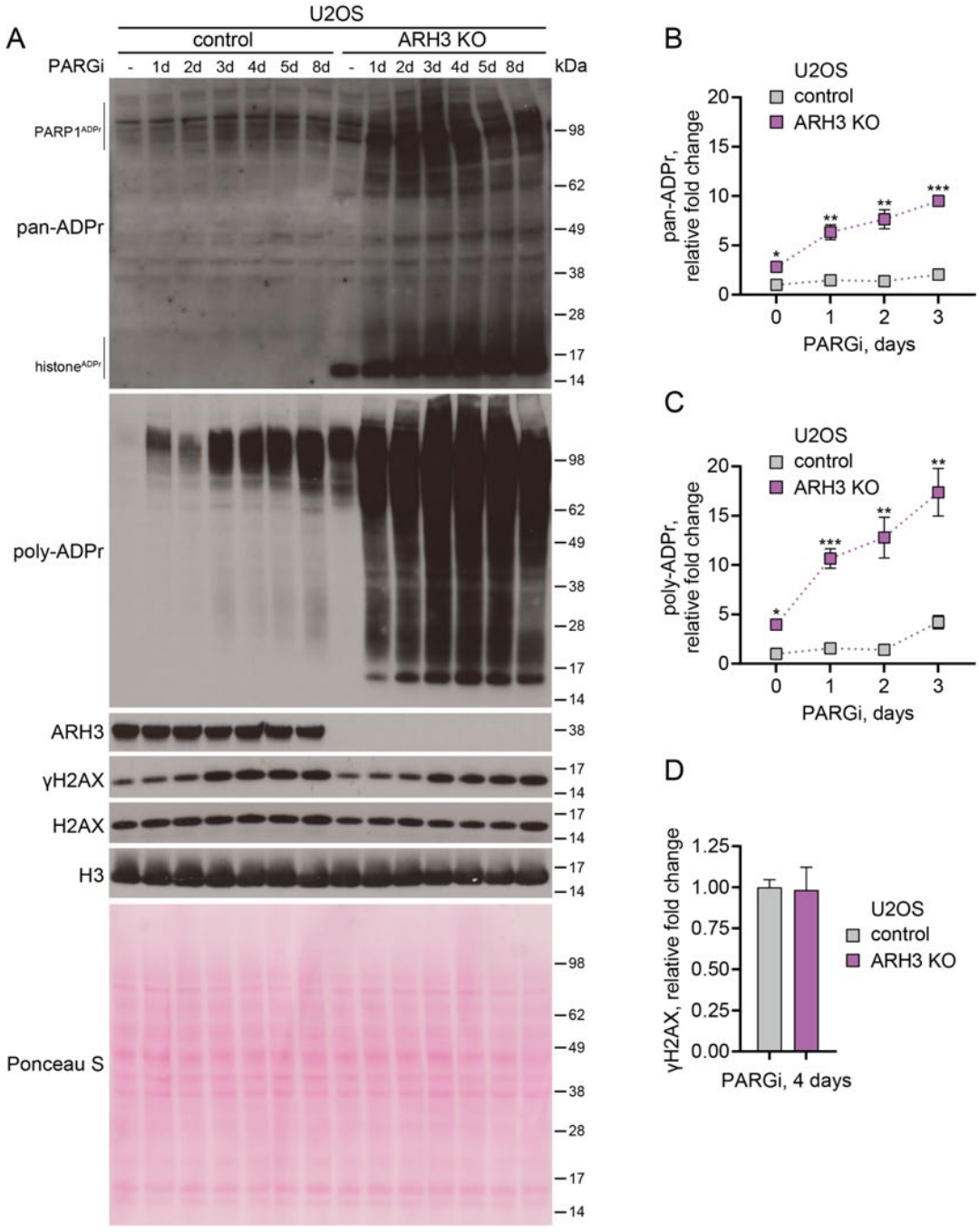


Figure 30. Excessive accumulation of ADPr upon simultaneous PARG inhibition and ARH3 deficiency does not lead to increased γH2AX formation.

(A) Control and ARH3 KO U2OS cells were treated with DMSO for 8 days or with 25 μM PARGi as indicated. ADPr and γH2AX levels were analysed by Western blotting. Representative Western blots from 3 independent experiments are shown. (B, C) Densitometry analysis of pan-ADPr (B) or poly-ADPr (C) to histone H3 ratios detected by Western blotting as in (A). Data represent fold change relative to DMSO-treated control cells and are shown as mean±SEM, n=3, *p<0.05, **p<0.01, ***p<0.001 (two-tailed Student's t-test). (D) Densitometry analysis of γH2AX to H2AX ratios after 4 days of treatment with 25 μM PARGi detected by Western blotting as in (A). The quantifications in (B-D) were performed by Thomas Agnew and myself. The figures were adapted from (Prokhorova et al., 2021a).

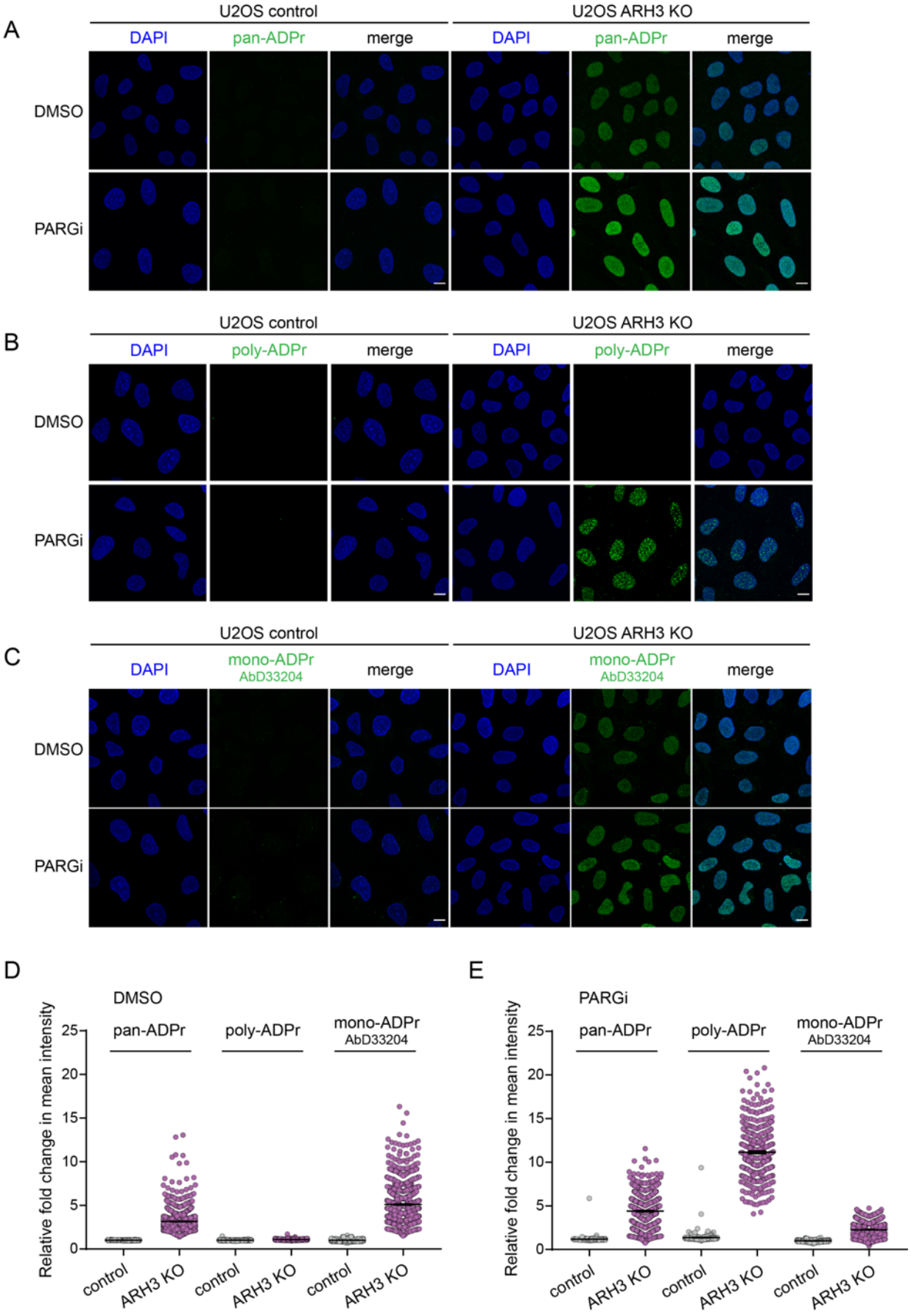


Figure 31. PARG inhibition leads to excessive accumulation of poly-ADPr in ARH3-deficient cells.

(A-C) Immunofluorescence analysis of the levels of pan-ADPr (A), poly-ADPr (B) or mono-ADPr (C) in cells treated with DMSO or 25 μM PARGi for 6 days and pre-extracted with a detergent prior to

fixation. Scale bars, 10 μm. (D, E) Quantification of (A-C) for 6-day DMSO (D) or 25 μM PARGi treatment (E). Data are provided as fold change in mean intensity per nucleus relative to control cells treated with DMSO. Data are shown as mean±SEM, more than 300 cells were analysed per each condition. The experiments and quantifications were performed by Thomas Agnew and myself. The figures were adapted from (Prokhorova et al., 2021a).

To rule out possible side-effects of PARG inhibition, I performed siRNA-mediated PARG knockdown and observed a similar enrichment of ADPr specifically in ARH3 KO but not control U2OS cells (Figure 32A). Moreover, I obtained similar results following ARH3 deletion and PARG inhibition in HeLa cells (Figure 32B), confirming the universality of our observations.

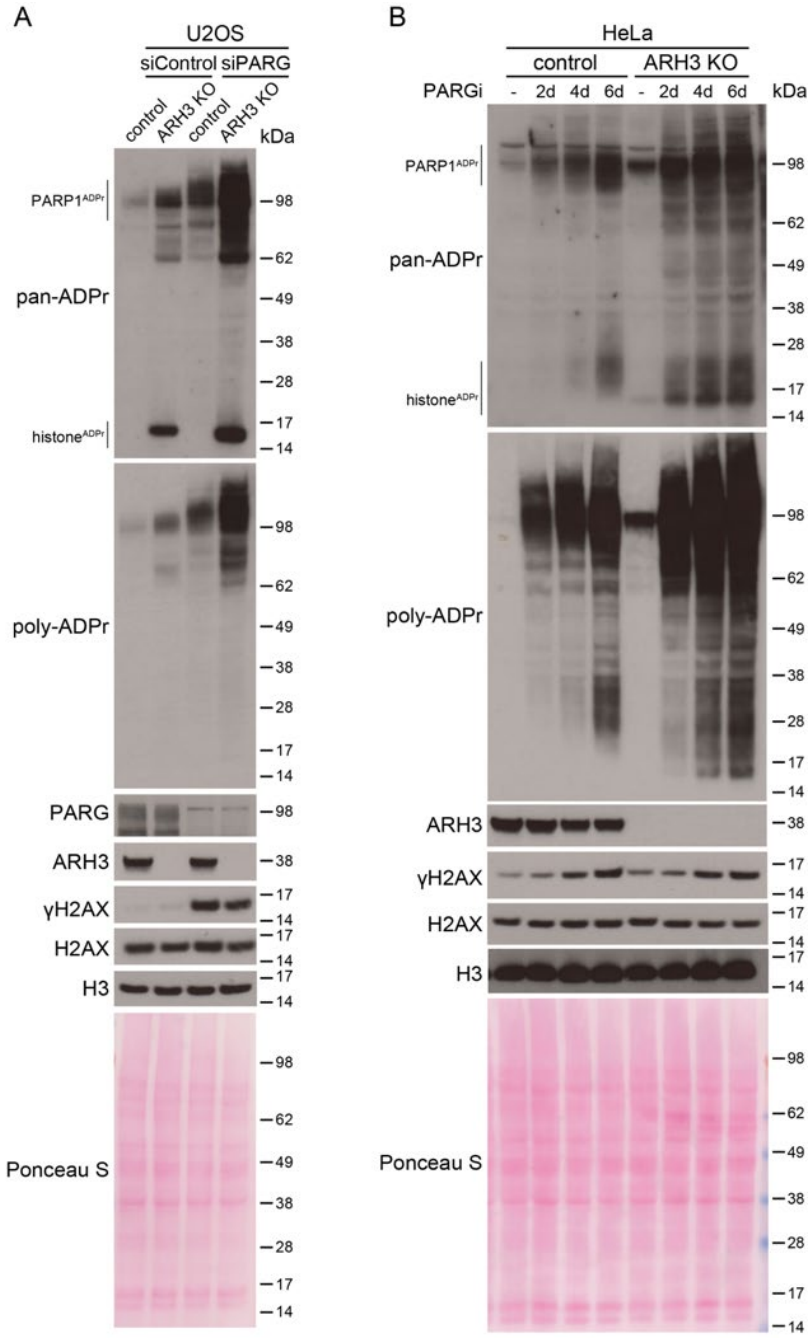


Figure 32. Excessive accumulation of ADPr is observed both upon PARG inhibition and siRNA-mediated PARG knockdown, and is a widespread phenomenon.

(A) Western blotting analysis of ADPr and γH2AX levels in control and ARH3 KO U2OS cells 72 h after PARG siRNA transfection. (B) Control and ARH3 KO HeLa cells were treated with DMSO for 6 days or with 25 μM PARGi for the indicated number of days. ADPr and γH2AX levels were analysed by Western blotting. Representative Western blots from 2 independent experiments are shown. The figures were adapted from (Prokhorova et al., 2021a).

Overall, the above data clearly demonstrated that ARH3 contributes to the hydrolysis of both endogenous and stress-induced poly-ADPr. However, enrichment of mono-ADPr, but not poly-ADPr, in untreated ARH3 KO cells (Figures 31B-D) and remarkable hydrolytic activity of ARH3 against serine-linked MAR *in vitro* (Figure 33A) indicate that ARH3 is critical for the removal of initial MAR rather than the products of its extension. Conversely, PARG cannot reverse initial serine-linked MAR, although some increase in mono-ADPr in ARH3 KO cells following PARGi treatment could be observed possibly because PARG is able to remove some other types of mono-ADPr in human cells or due to unspecific binding of the anti-mono-ADPr antibody used to poly-ADPr (Figure 31B and 31E). On the other hand, PARG is the main enzyme that hydrolyses poly-ADPr, which mainly consists of PARP1 modification when exogenous stresses are absent and ARH3 is present (Figures 26A and 28). ARH3 also contributes to the reversal of at least basal PARP1 modification, presumably short PAR that can be detected by anti-pan-ADPr reagent but not anti-poly-ADPr antibody. Notable increase in endogenous poly-ADPr following dual suppression of ARH3 and PARG implies that ARH3 is crucial for preventing accumulation of not only stress-induced, but also basal poly-ADPr. The fact that the effect of simultaneous ARH3 and PARG suppression on endogenous levels of ADPr is markedly greater than the sum of the individual effects, again highlights synergy rather than redundancy or additivity between the two hydrolases.

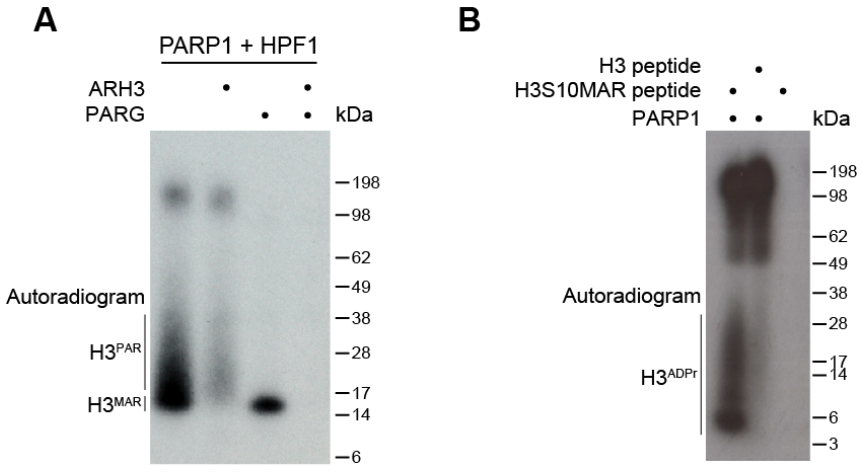


Figure 33. Distinct regulation of the initiation and elongation stages in the ADPr reaction *in vitro*.

(A) Radioactive ADPr assay of histone H3 and subsequent hydrolysis by ARH3 and PARG enzymes alone or combined. Performed by Marcin Suskiewicz. (B) Radioactive ADPr assay carried out using unmodified H3 peptide or H3 peptide with S10-linked MAR (H3S10MAR). Performed by Kang Zhu. Representative Autoradiograms from 3 independent experiments are shown. The figures were adapted from (Prokhorova et al., 2021a).

Indeed, both ARH3 and PARG hydrolases contribute to the maintenance of low levels of cellular poly-ADPr (Figures 30A and 32), and combined ARH3 and PARG activity is required for the complete reversal of serine-linked PAR *in vitro* (Figure 33A). However, ARH3 controls poly-ADPr levels largely indirectly, by removing initial serine-ADPr attachments serving as 'primers' for subsequent elongation to PAR. In the absence of ARH3 and in the presence of PARG, these initial attachments persist as serine-linked MAR and only when PARG activity is supressed they become stably extended by PARP1/2 to PAR.

Furthermore, the above data suggest the existence of two distinct steps in the ADPr reaction, namely initiation and elongation, with the reverse steps predominantly performed by ARH3 and PARG, respectively. Given that the initiation of serine-ADPr by PARP1 requires HPF1 to complete its active site (Suskiewicz et al., 2020), and that ADPr elongation, in particular on PARP1 itself, can proceed on its own in a processive reaction mode and is notably faster than the initiation (Mendoza-Alvarez and Alvarez-Gonzalez, 1993, 1999; Naegeli et al., 1989), we suggested that whilst the initiation of serine-ADPr is catalysed by PARP1-HPF1, PARP1 alone is sufficient to perform the elongation. In agreement, while PARP1 alone did not modify histone H3 peptide *in vitro*, it robustly poly-ADP-ribosylated the same peptide when it was 'primed' with an initial serine-linked MAR prior to the reaction (Figure 33B). This supports the existence of separate initiation and elongation stages in the ADPr reaction with distinct regulation of its forward and reverse steps.

4.2.3. ARH3 loss sensitises cancer cells to PARG inhibition and renders cells more resistant to PARP1/2 inhibitors

Suppression of PARG activity was previously found to result in the accumulation of a DSB marker, γH2AX (Chen and Yu, 2019; Pillay et al., 2019; Ray Chaudhuri et al., 2015). Consistent with this, inhibition or siRNA-mediated knockdown of PARG led to elevated γH2AX levels in control and ARH3 KO U2OS and HeLa cells (Figures 30A,

30D and 32). Surprisingly, ARH3 loss alone or in combination with PARG suppression did not increase γH2AX levels.

Despite there being no additive effect of PARG and ARH3 suppression on γH2AX formation, we hypothesized that persistent accumulation of chromatin ADPr would be toxic to the cell. Indeed, I observed that ARH3 loss led to a marked sensitisation of U2OS (Figures 34A and 34B) and HeLa cells (Figure 34D) to PARGi by performing long-term colony formation assays. To assess whether this is due to the accumulation of PARP1/2-dependent ADPr, I attempted to rescue this phenotype by PARP1/2 inhibition. Indeed, the addition of PARPis Olaparib or Veliparib suppressed the toxicity of PARG inhibition in both ARH3 KO U2OS (Figures 34A and 34C) and HeLa cells (Figure 34E).

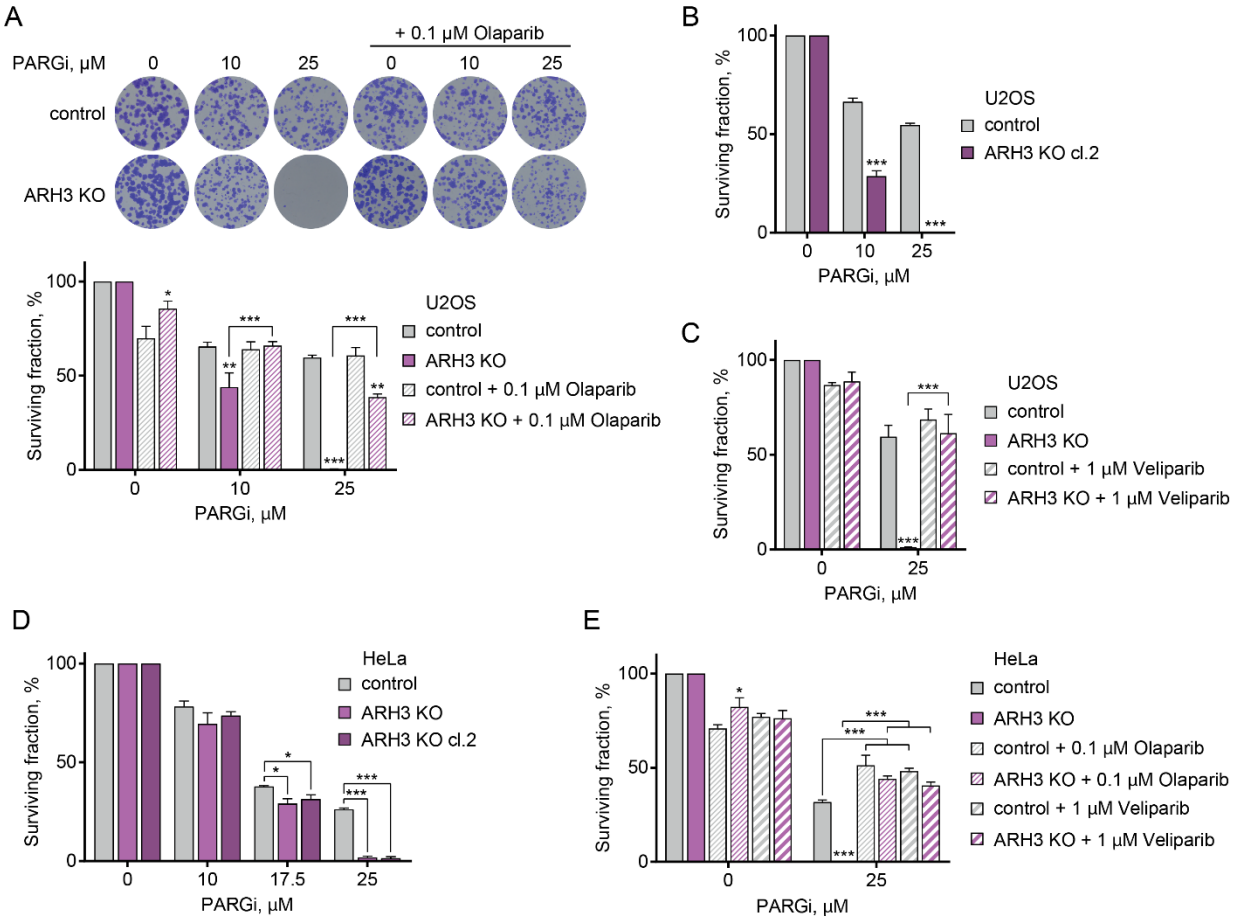


Figure 34. ARH3 deficiency is synthetically lethal with PARG inhibition in a PARP1/2-dependent manner.

(A-C) Representative images (A, top) and quantification (A, bottom, B, C) of colony formation assay using control and ARH3 KO U2OS cells treated with DMSO or as indicated. (D, E) Quantification of colony formation assay using control and ARH3 KO HeLa cells treated with DMSO or as indicated. Data are shown as mean±SD, n=3, *p<0.05, **p<0.01, ***p<0.001 (two-tailed Student's t-test). The figures were adapted from (Prokhorova et al., 2021a).

Then, to confirm that the observed sensitivity of ARH3-deficient cells to PARG inhibition is specifically due to the loss of ARH3 enzymatic activity, we genetically complemented ARH3 KO U2OS cells with either ARH3 WT or D77/78N, a catalytically-inactive mutant that completely lacks the ability to hydrolyse ADPr (Fontana et al., 2017; Oka et al., 2006). Complementation with ARH3 WT, but not D77/78N, rescued ARH3 KO U2OS sensitivity to PARGi (Figure 35A) and restored the reversal of PARGi- and H_2O_2-induced ADPr (Figures 35B and S6).

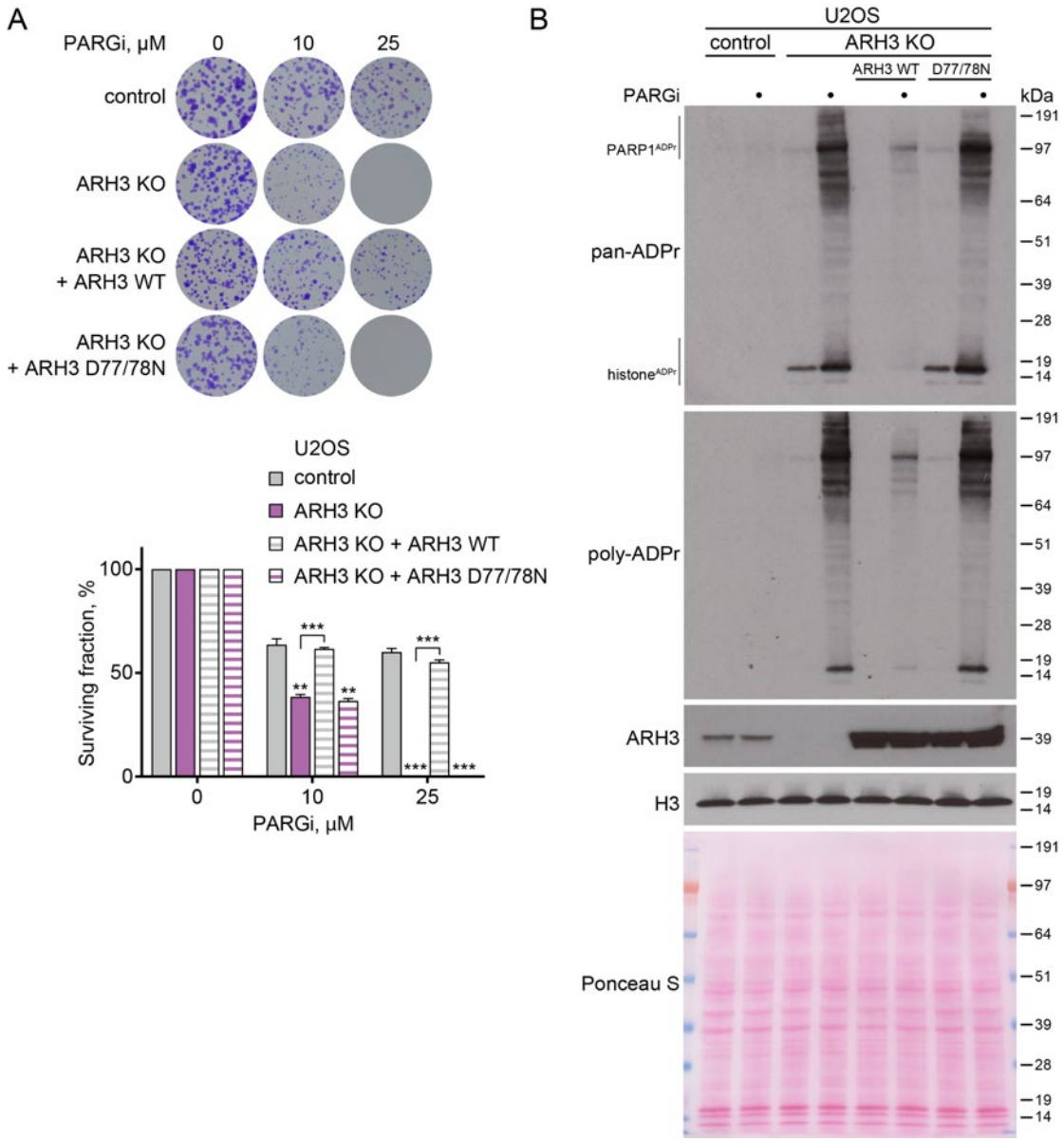


Figure 35. Complementation with ARH3 WT, but not catalytically inactive D77/78N mutant, rescues PARGi sensitivity and ADPr reversal in ARH3-deficient cells.

(A) Representative images (top) and quantification (bottom) of colony formation assay using control and ARH3 KO U2OS cells complemented with ARH3 WT or D77/78N catalytically inactive mutant and treated with DMSO or PARGi. Data are shown as mean±SD, n=3, **p<0.01, ***p<0.001 (two-tailed Student's t-test). (B) Cells from (A) were treated with 25 μM PARGi for 4 days. ADPr signals were analysed by Western blotting. The experiment in (B) was performed by Josephine Groslambert and

myself. Representative Western blots from 2 independent experiments are shown. The figures were adapted from (Prokhorova et al., 2021a).

Altogether, these findings reveal a synthetic lethal interaction between ARH3 and PARG hydrolases which is caused by extreme accumulation and persistence of endogenous poly-ADPr. Furthermore, these results show that whilst chromatin-bound mono-ADPr is well tolerated throughout multiple cell cycles, accumulation of poly-ADPr is highly toxic to the cell.

Next, I sought to examine whether persistently increased poly-ADPr in cells with ARH3 and PARG suppression would affect cell proliferation and cell cycle progression as assessed by EdU and DAPI staining using flow cytometry (representative scatterplots are shown in Figure S7). Interestingly, PARG inhibition or ARH3 deficiency alone caused an enrichment of S-phase subpopulations in both U2OS (Figures 36A, 36B and S8A) and HeLa cells (Figures 36C and 36D). Whilst this was not further explored in this work, it is possible that elevated levels of ADPr could slow down the rates of DNA replication, resulting in more cells undergoing S-phase for a longer period of time. PARG inhibition in ARH3 KO cells significantly reduced the number of S-phase cells and induced a marked accumulation of subG1 subpopulation of cells with fragmented DNA (Figures 36A and 36C), which was completely rescued by the PARPi Olaparib (Figures 36A and 36B). Moreover, a longer 24-h EdU pulse-labelling showed a further decrease in DNA synthesis and cell proliferation in ARH3 KO U2OS cells treated with PARGi which was again rescued by Olaparib (Figure S8B).

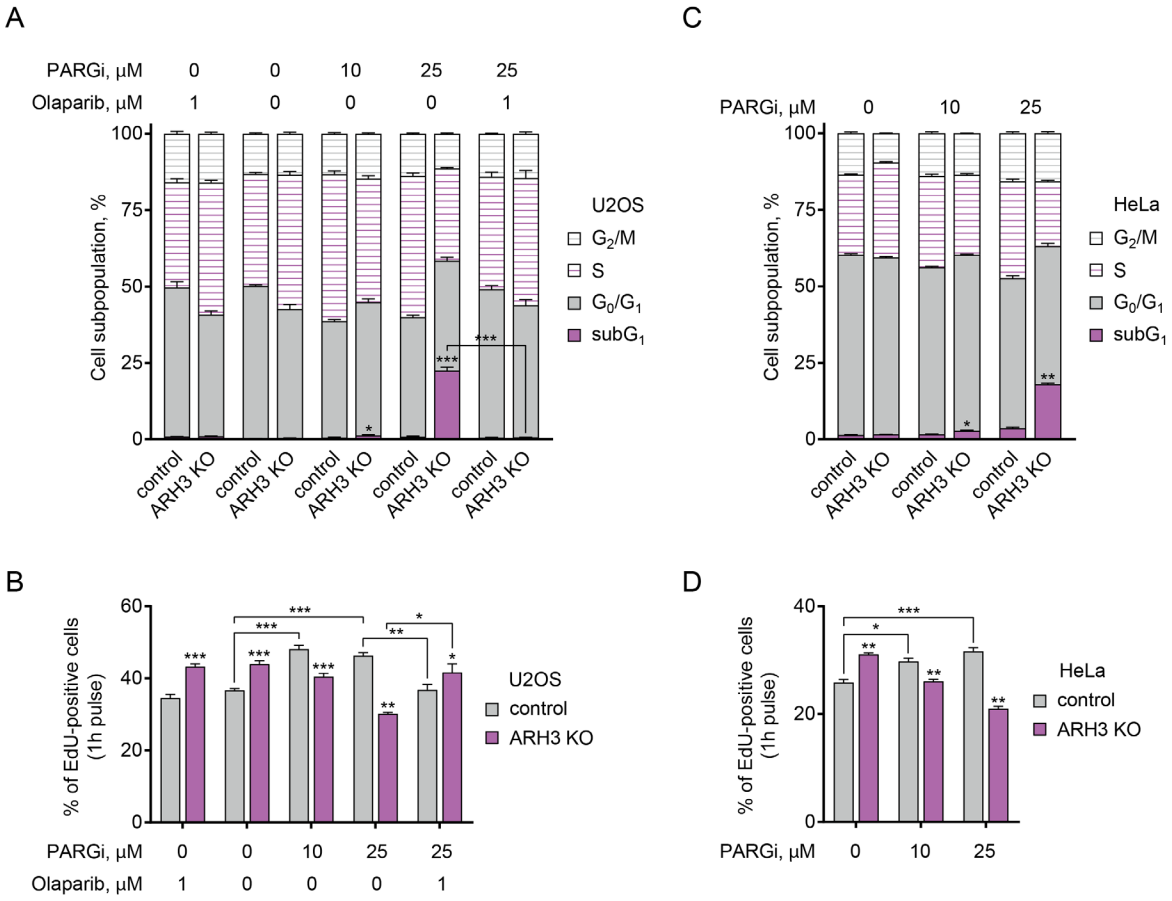


Figure 36. PARG inhibition disrupts cell cycle progression in ARH3-deficient cells in a PARP1/2-dependent manner.

(A, C) Flow cytometry analysis of EdU- and DAPI-stained control and ARH3 KO U2OS (A) or HeLa (C) cells after 6-day exposure to DMSO or indicated treatment and 1-h EdU pulse. (B, D) Cell proliferation and DNA synthesis after exposure to DMSO or indicated treatment of control and ARH3 KO U2OS (B) or HeLa (D) cells for 6 days and 1-h EdU pulse. Data are shown as mean±SEM, n=4 (A, B), n=3 (C, D), *p<0.05, **p<0.01, ***p<0.001 (two-tailed Student's t-test). Flow cytometry gating strategy for the analyses is shown in Figure S7. The figures were adapted from (Prokhorova et al., 2021a).

Altogether, while loss of either PARG or ARH3 activity alone resulted in the accumulation of cells undergoing S-phase, exposure of ARH3-deficient cells to PARGi notably reduced DNA synthesis and cell proliferation. A quantitively greater and qualitatively different outcome of the simultaneous ARH3 and PARG suppression compared to their individual inactivation again confirms that their functions are synergistic. This is consistent with the model suggested in Section 4.2.2 where ARH3 and PARG each predominantly perform one of the two steps needed for the prevention of persistent accumulation of poly-ADPr, namely reversal of initial serine-ADPr attachments by ARH3 and hydrolysis of their subsequent elongation products by PARG.

In agreement with Section 3.2.1, describing loss of ARH3 as a potential mechanism of PARPi resistance, I also detected a significant decrease in cell proliferation in

Olaparib-treated control compared to ARH3 KO U2OS cells in the above flow cytometry experiments (Figure 36B). Moreover, a modest but statistically significant reduction in survival of control compared to ARH3 KO U2OS and HeLa cells with low Olaparib concentration in both U2OS (Figure 34A) and HeLa cells (Figure 34E) could be observed. To further explore the effect of ARH3 loss on cell sensitivity to PARP1/2 inhibition, I examined this in the context of BRCA1/2 deficiency, in which PARPis show particularly promising clinical results. Whereas, as expected, siRNA-mediated knockdown of BRCA1 or BRCA2 led to a dramatic sensitisation of U2OS cells to Olaparib, ARH3 KO cells showed a substantial resistance to Olaparib compared to control cells (Figures 37A and S9A). Moreover, ARH3 loss resulted in increased PARPi resistance in triple-negative breast cancer (TNBC) SUM149PT (BRCA1-mutant, BRCA2-WT) and SUM159PT (BRCA1/2-WT) cells (Figures 37B, 37C and S9B). Similar to U2OS cells, BRCA1 or BRCA2 siRNA-mediated knockdown sensitised SUM159PT cells to PARP1/2 inhibition by Olaparib, and ARH3 KO cells were significantly more resistant to Olaparib than control cells (Figures 37D and S9C).

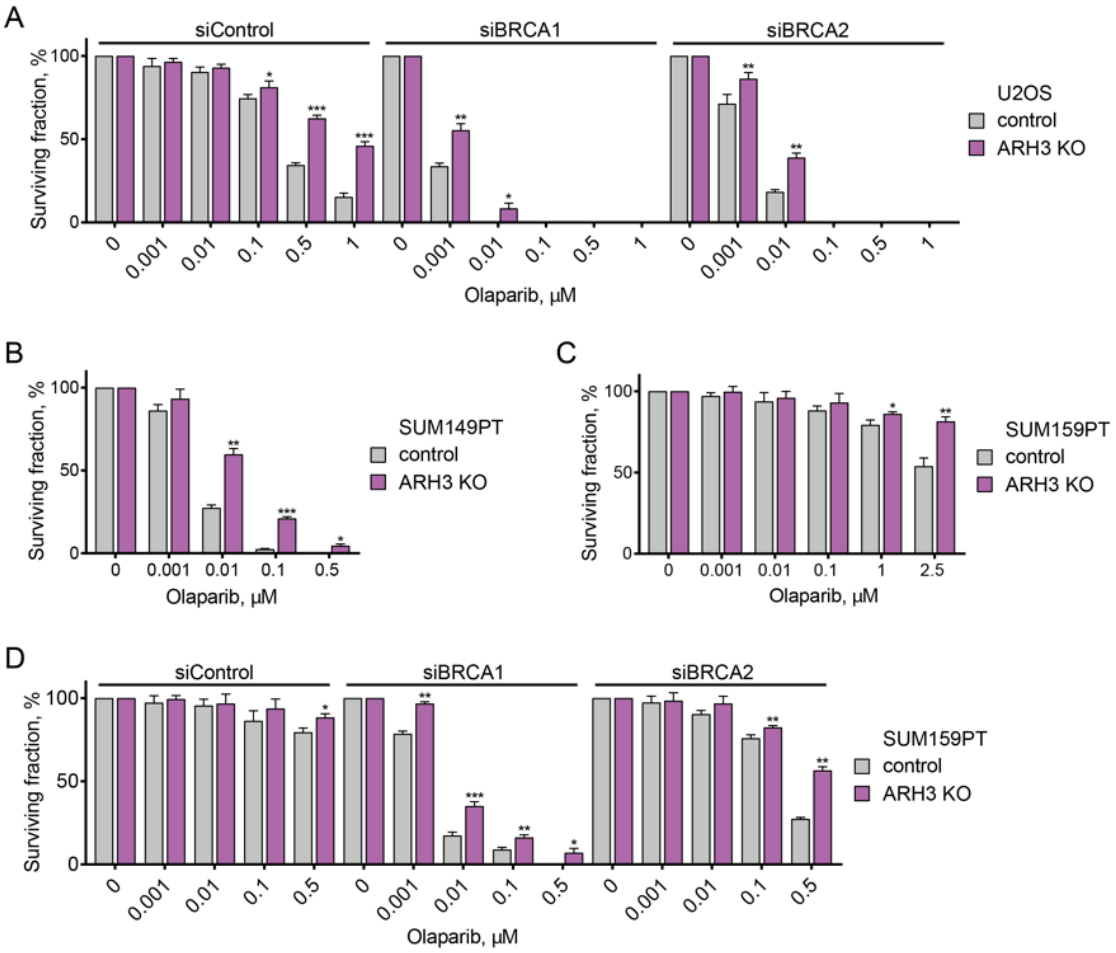


Figure 37. ARH3 loss renders cancer cells resistant to PARP1/2 inhibition.

(A, D) Quantification of colony formation assay using control and ARH3 KO U2OS (A) or SUM159PT (D) cells transfected with BRCA1 or BRCA2 siRNA and treated with DMSO or Olaparib. (B, C) Quantification of colony formation assay using control and ARH3 KO SUM149PT (B) or SUM159PT (C) cells treated with DMSO or Olaparib. Data are shown as mean±SD, n=3, *p<0.05, ***p<0.001 (two-tailed Student's t-test). The figures were adapted from (Prokhorova et al., 2021a).

Altogether, these results confirm that, in addition to rendering cells sensitive to PARG inhibition, ARH3 loss confers resistance to PARP1/2 inhibition in different types of cells, including BRCA1/2-deficient cancers.

4.2.4. Accumulation and persistence of chromatin-bound poly-ADP-ribosylation affects histone modification and transcription profiles

To further examine the mechanism underlying the toxicity of excessive poly-ADPr, we examined whether its accumulation is accompanied by NAD^+ depletion. Despite PARP1 being a major cellular consumer of NAD^+ (Cohen, 2020), there were no statistically significant changes in NAD^+ levels in cells with dual ARH3 and PARG suppression (Figure S10), arguing against its depletion being a major cause of poly-ADPr toxicity in our experimental system.

Next, given the pronounced accumulation of histone ADPr following PARG inhibition in ARH3 KO cells, I assessed whether neighbouring histone PTMs, in particular acetylation, may be affected. Histone H3S10, which was validated in Section 2.2.2, is one of the main sites of cellular serine-ADPr, and was shown to be mutually exclusive with acetylation of H3K9 (H3K9ac) by our and other groups (Bartlett et al., 2018; Larsen et al., 2018; Liszczak et al., 2018). In agreement with this, prolonged PARG inhibition led to a marked reduction in H3K9ac in ARH3-deficient but not control U2OS (Figure 38 and S11) and 293T cells (Figure 39B). Importantly, the observed decrease in H3K9ac levels was rescued by Olaparib, confirming the mutually exclusive relationship between histone ADPr and neighbouring acetylation. On the other hand, H3K9me3, H3S10P and total H3 levels remained stable in all the conditions (Figures 38 and 39B).

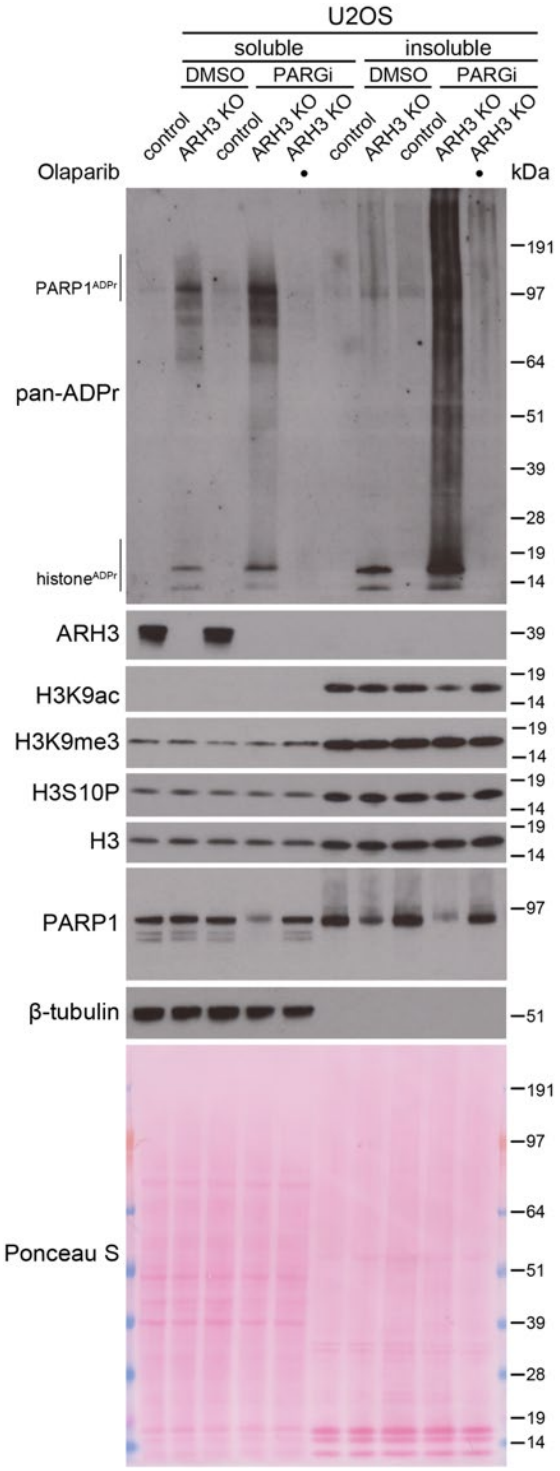


Figure 38. Excessive ADPr in PARGi-treated ARH3-deficient cells interferes with histone acetylation.

Control and ARH3 KO U2OS cells were treated with DMSO or 25 μM PARGi for 6 days. ADPr, H3K9ac, H3K9me3, H3S10P modification and protein levels were analysed by Western blotting. Representative Western blots from 3 independent experiments are shown. The figure was adapted from (Prokhorova et al., 2021a).

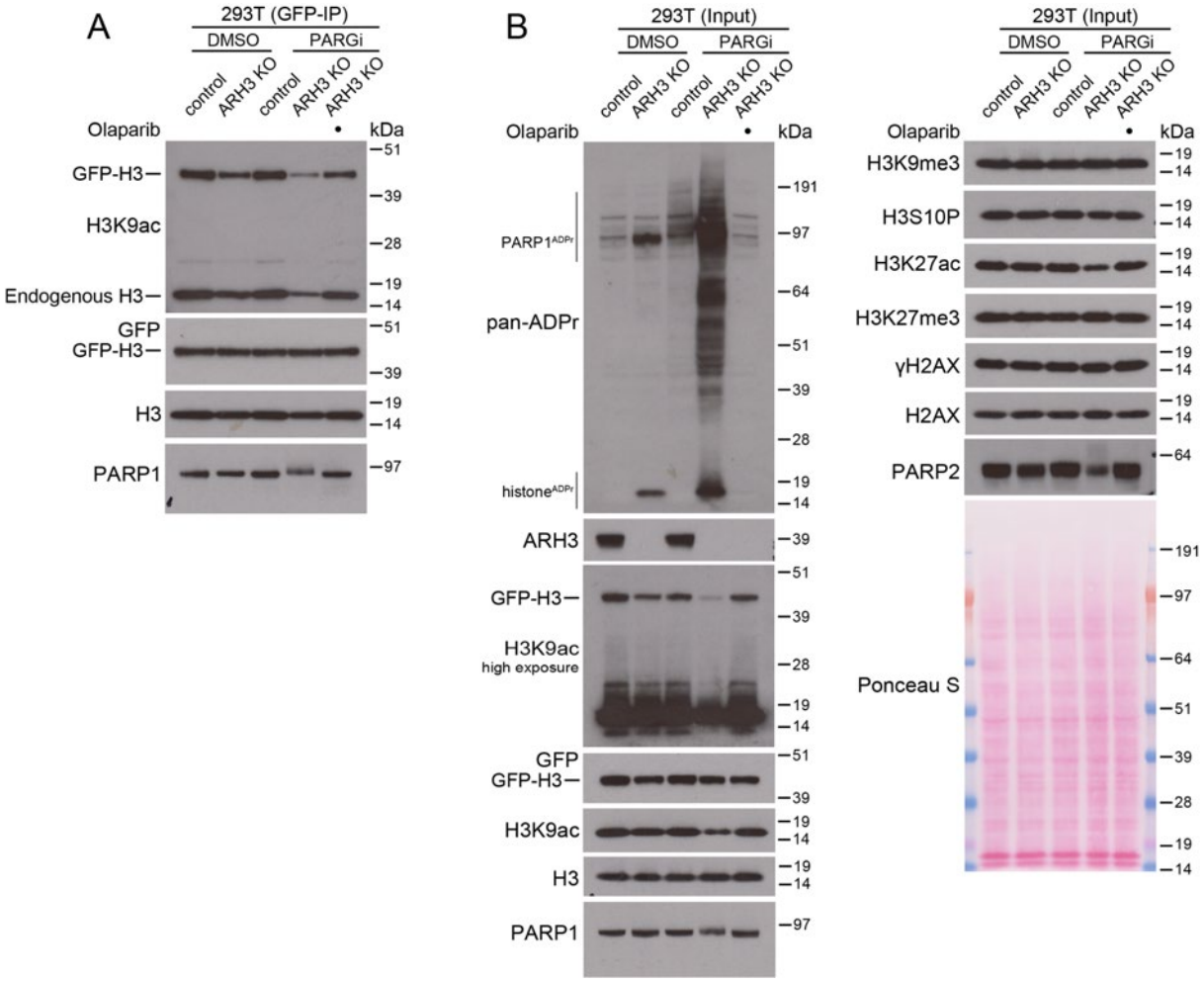


Figure 39. Accumulation of histone H3 ADPr interferes with neighbouring acetylation marks even in the absence of exogenous DNA damage.

Control and ARH3 KO 293T cells were treated with DMSO, 5 μM PARGi or 5 μM PARGi and 0.5 μM Olaparib for 4 days and transfected with GFP-H3 in the presence of inhibitors for 24 h. GFP-H3 immunoprecipitation (GFP-IP, A) and input samples (B) were analysed by Western blotting for ADPr, H3 modification, γH2AX, PARP1 and PARP2 levels. Representative Western blots from 3 independent experiments are shown. The figures were adapted from (Prokhorova et al., 2021a).

Furthermore, to specifically monitor H3 modification in newly incorporated nucleosomes, I performed transient 24-h overexpression of GFP-H3 in control and ARH3 KO 293T cells, demonstrating that in this system ARH3 KO alone already leads to a substantial decrease in GFP-H3 K9ac levels (Figures 39A and 40). Importantly, this effect was also observed on endogenous histone H3 co-immunoprecipitated with the nucleosomes that incorporated GFP-H3 and was reversed upon treatment with the PARPi Olaparib or Veliparib (Figure 40).

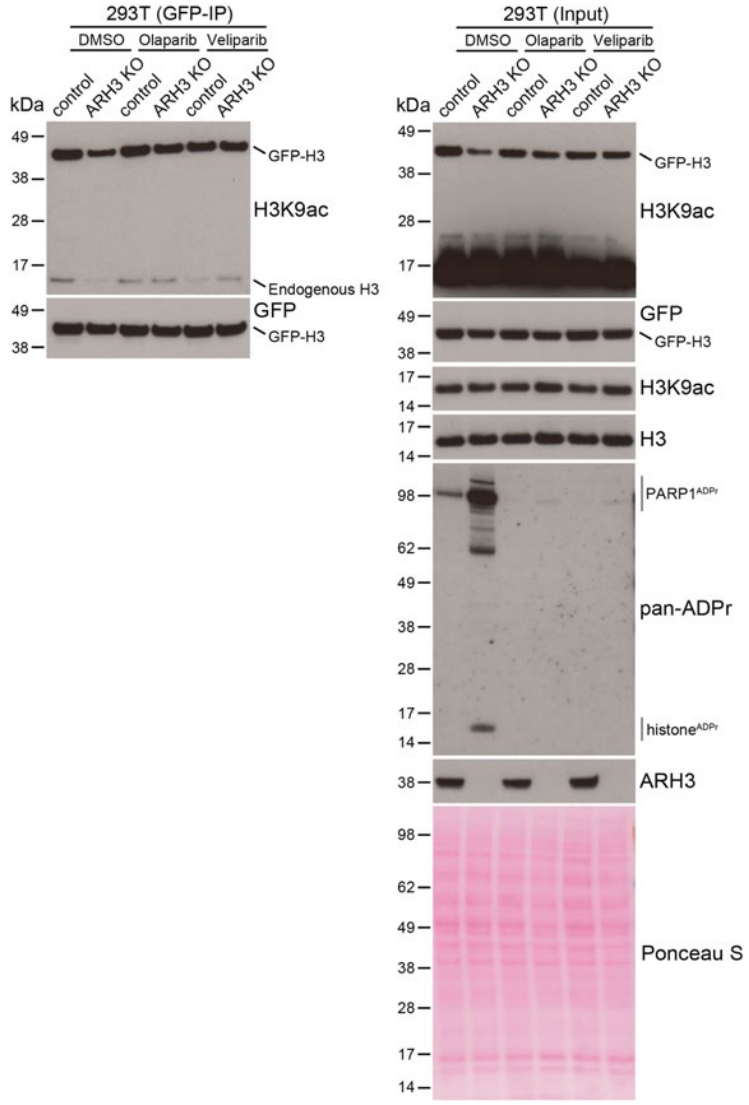


Figure 40. ARH3 loss leads to reduced histone H3 lysine 9 acetylation in newly incorporated nucleosomes.

Control and ARH3 KO 293T cells were treated with DMSO, 0.5 μM Olaparib or 5 μM Veliparib for 3 days and transfected with GFP-H3 in the presence of inhibitors for 24 h. GFP-H3 immunoprecipitation (GFP-IP) and input samples were analysed by Western blotting for ADPr and H3K9ac levels. Representative Western blots from 2 independent experiments are shown. The figure was adapted from (Hanzlikova et al., 2020).

Exposure to PARGi resulted in a further decrease in K9ac of GFP-tagged H3 and associated endogenous H3 (Figure 39A). Additionally, I observed a decrease in endogenous H3K27ac, but not in H3K27me3 levels, in this scenario (Figure 39B).

Given strong association of H3K9ac and H3K27ac marks with actively transcribed regions (Lawrence et al., 2016) and a recent report that fibroblasts from ARH3-deficient patients acquire alterations in gene expression (Hanzlikova et al., 2020), our results suggest that extreme poly-ADPr caused by simultaneous suppression of ARH3 and PARG could affect cellular transcription. Of note, the reduction in H3K9ac and H3K27ac levels occurred even prior to an increase in γH2AX formation in 293T

cells (Figure 39B), further indicating that dysregulation of chromatin modification rather than induction of DNA damage contributes to the toxicity of excessive poly-ADPr in cells with dual ARH3 and PARG suppression.

Moreover, I detected a profound decrease in protein levels of PARP1 and PARP2 by Western blotting in this condition (Figures 38, 39B and 41). To exclude that this could be an artefact of excessive ADPr on PARP1 and PARP2 preventing protein recognition by the corresponding antibodies used or diluting the antibody signal across the lane due to the changes in protein mobility, enzymatic treatments of ARH3 KO U2OS cell extracts collected post 6-day 25 μM PARGi treatment by adding recombinant human ARH3 and/or PARG proteins were performed. Whereas the treatment with ARH3 alone or in combination with PARG removed all ADPr, and treatment with PARG alone erased all ADPr except the protein-linked MAR as was detected by anti-pan-ADPr reagent, the signals detected by anti-PARP1 and -PARP2 antibodies remained unchanged (data not shown). In accordance, proteomics analysis performed in control and ARH3 KO U2OS cells revealed a significant about 2-fold decrease in PARP1 and PARP2 levels in response to 4-day treatment with 25 μM PARGi in ARH3 KO cells (from personal communications with Michael Nielsen group). This decrease in protein levels of PARP1 and PARP2 by itself could contribute to transcriptional alterations (Kim et al., 2020a; Páhi et al., 2020).

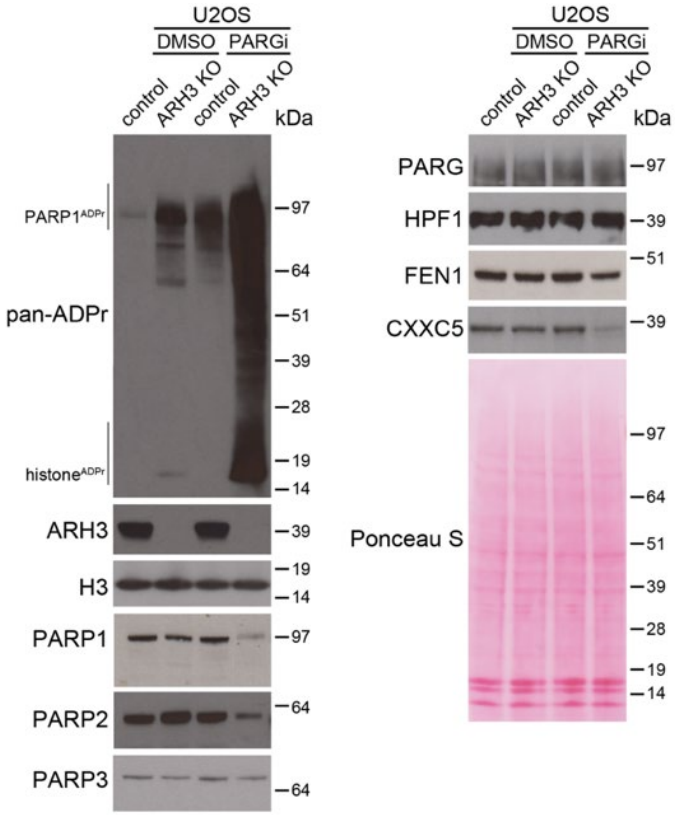


Figure 41. Excessive ADPr in PARGi-treated ARH3-deficient cells leads to a decrease in PARP1 and PARP2 protein levels.

Control and ARH3 KO U2OS cells were treated with DMSO or 25 μM PARGi for 4 days. ADPr and protein levels were analysed by Western blotting. Representative Western blots from 3 independent experiments are shown. The figure was adapted from (Prokhorova et al., 2021a).

To address this, we performed RNA-sequencing (sample reproducibility is shown in Figure S12) and differential gene expression analysis. We observed significant changes in the transcriptome of ARH3 KO U2OS cells following PARGi treatment with 748 upregulated and 827 downregulated protein-coding, and 403 upregulated and 438 downregulated non-protein-coding genes (Figures 42A). In comparison, only 147 protein-coding genes were found to be differentially expressed in ARH3-deficient patient fibroblasts (Hanzlikova et al., 2020). Although we did not detect significant changes in expression PARP1/2 mRNA, indicating post-transcriptional reduction of their protein levels, we observed a decrease in FEN1 and CXXC5 expression both on mRNA and protein levels (Figure 41). To identify the pathways, which alterations could contribute to the toxicity of PARG inhibition in ARH3-deficient cells, we employed commonly used Gene Set Enrichment Analysis (GSEA) (Mootha et al., 2003; Subramanian et al., 2005). We highlighted 13 cellular pathways that were significantly affected by PARG inhibition in ARH3 KO cells (Figure 42B), including downregulated lagging strand synthesis and DNA strand elongation pathways, in which FEN1 is a central player.

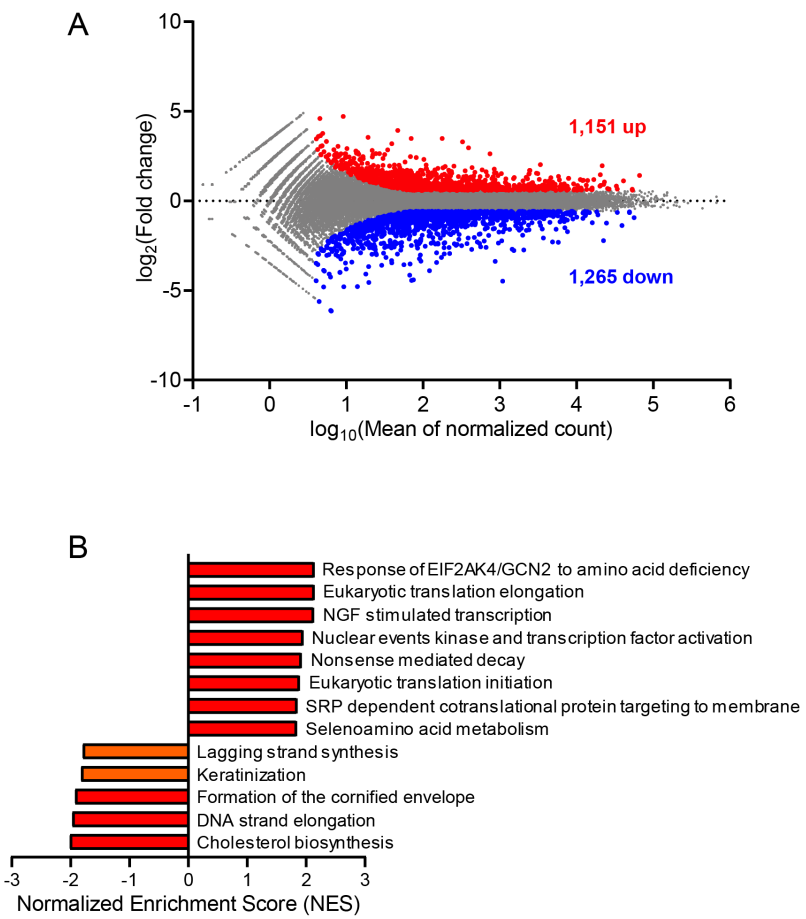


Figure 42. PARG inhibition results in dysregulation of transcription in ARH3-deficient cells.

(A) MA plot demonstrating differentially expressed genes (upregulated genes are shown in red, downregulated genes are shown in blue) in ARH3 KO U2OS cells treated with 25 μM PARGi for 4 days against ARH3 KO U2OS cells treated with DMSO. n=3, adjusted $p<0.05$, absolute fold change>1.5. (B) Significantly upregulated and downregulated pathways identified by gene set enrichment analysis (GSEA) in ARH3 KO U2OS cells treated with 25 μM PARGi for 4 days against ARH3 KO U2OS cells treated with DMSO. n=3, $q<0.05$ (in red), $q<0.1$ (in orange). Data analysis was performed by Michael Tellier. The figures were adapted from (Prokhorova et al., 2021a).

To elaborate on the function of the observed post-transcriptional reduction in PARP1 levels following PARG inhibition in ARH3 KO cells, I examined the effect of PARP1 overexpression on cell survival. In agreement with our findings that PARP1/2 inhibition rescues the sensitivity of ARH3-deficient cells to PARG inhibition by preventing ADPr, PARP1 overexpression further exacerbated PARGi-induced toxicity and ADPr accumulation (Figure 43). Notably, whereas I detected a considerable decrease in protein levels of PARP1/2 that can catalyse poly-ADPr, I did not detect changes in protein levels of PARP3 (Figure 41) which is only able to perform mono-ADPr (Azarm and Smith, 2020).

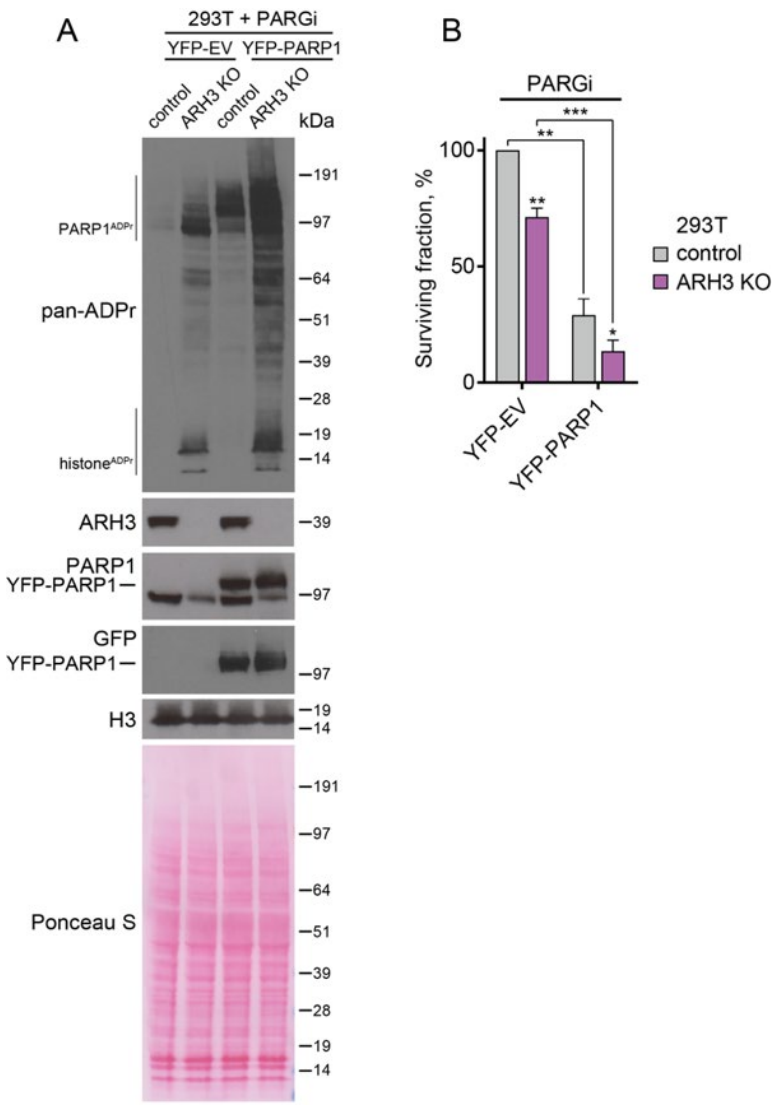


Figure 43. Overexpression of PARP1 further exacerbated PARGi-induced toxicity and ADPr accumulation.

Control and ARH3 KO 293T cells were transfected with YFP empty vector (EV) or PARP1-YFP and treated with 5 μM PARGi for 3 days. Western blot analysis of ADPr and PARP1 levels (A) and quantification of cell survival by cell count (B) and are shown. (A) Representative Western blots from 2 independent experiments are shown. Data in (B) represent mean±SEM, n=4, *p<0.05, **p<0.01, ***p<0.001 (two-tailed Student's t-test). The figures were adapted from (Prokhorova et al., 2021a).

Overall, the observed post-transcriptional downregulation of PARP1/2 in cells lacking both ARH3 and PARG function could be an adaptive consequence rather than the cause of the synthetic lethality phenotype, and may serve as a survival mechanism to escape the toxicity of excessive poly-ADPr and develop tolerance to PARG and/or ARH3 inhibition.

In summary, excessive poly-ADPr upon simultaneous suppression of ARH3 and PARG resulted in dysregulation of histone acetylation and transcription profiles, which likely contributes to its toxicity. The effects of the combined loss of ARH3 and PARG activity were many-fold greater and qualitatively different than of their

individual suppression not only in the case of dysregulation of histone modification and gene expression profiles, but also post-transcriptional PARP1/2 downregulation. This again confirms the synergy rather than redundancy or additivity between ARH3 and PARG and underlines the importance of the two-step model of the ADPr reaction proposed in Section 4.2.2 in the maintenance of cellular homeostasis.

4.2.5. Loss of ARH3 function sensitises primary patient fibroblasts to the induction of poly-ADP-ribosylation

Several patients have recently been reported to harbour pathogenic mutations in ARH3 causing progressive neurodegeneration (Danhauser et al., 2018; Ghosh et al., 2018; Mashimo et al., 2019). Danique Beijer et al. identified a new pathogenic missense mutation in ARH3 NM_017825: c.77G>T (p.Cys26Phe) (C26F) and obtained primary fibroblasts from a patient homozygous for the C26F mutation and from an unaffected healthy individual (Beijer et al., 2021). The patient was born to consanguineous parents after an uneventful pregnancy and at term delivery, and already at the age of 15 months, she presented with febrile seizures. By the age of 6 years, she developed normal but delayed speech, showed moderate intellectual disability, growth retardation, moderate scoliosis, and pes cavus. From the age of 10 years, the patient developed moderate atrophy of intrinsic hand muscles and mild atrophy of the distal lower limbs, with a clearly more pronounced weakness in the upper than in the lower limbs. At the age of 13 years, the brain magnetic resonance imaging (MRI) was normal, whereas the electroencephalogram (EEG) showed sporadic epileptiform activity in frontocentral localization, without clinical seizures. The electromyography (EMG) showed a pronounced axonal motor polyneuropathy, with normal sensory parameters. The motor regression was temporarily ameliorated by the treatment with gammaglobulins, but at the age of 16 years, the patient passed away because of respiratory failure (Beijer et al., 2021).

Using the obtained ARH3 C26F mutant patient-derived primary human fibroblasts, we observed that C26F mutation caused a substantial reduction in ARH3 protein levels (Figure S13) which is indicative of a loss-of-function allele. As shown in the Figure 2, the residue C26 is located in the core of a conserved helical bundle in the structure of ARH3. Positioning of this residue within the structure suggests that an increase in Van der Waals volume upon the C26F mutation is incompatible with correct protein folding. When recombinant production of C26F ARH3 protein in *E.coli.* as previously described in (Fontana et al., 2017) was attempted, robust overexpression in whole cell lysate, but complete insolubility of the protein was

observed (Beijer et al., 2021). This confirms that the C26F mutation is destabilizing and causes misfolding of ARH3, explaining highly reduced levels of ARH3 protein in C26F cell lysates (Figure S13).

Similar to ARH3 KO cells, I observed endogenous chromatin ADPr enrichment throughout all stages of the cell cycle (Figure 44), as well as elevated basal and PARGi-induced total ADPr, in ARH3 C26F mutant compared to control primary patient fibroblasts (Figures 44, 45A and 45B). Moreover, I demonstrated that ARH3 C26F mutation sensitised cells to PARGi treatment (Figure 45C), and resulted in a reduction in PARP1 and H3K9ac, but not H3K9me3 and H3S10P, levels following PARG inhibition (Figure 45A). Importantly, all of the observed phenotypes were rescued by the PARPi Olaparib.

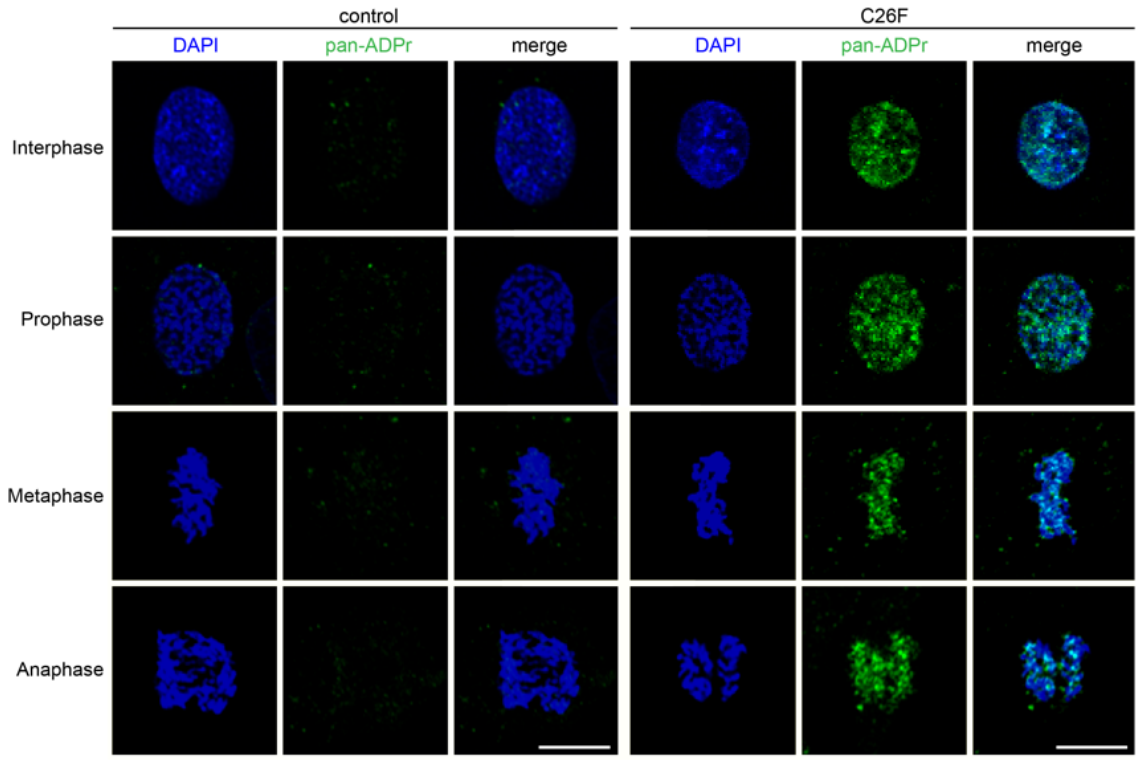


Figure 44. Loss of ARH3 function in patient-derived primary human fibroblasts leads to the accumulation of endogenous chromatin ADPr throughout the cell cycle.

Immunofluorescence analysis of the levels of pan-ADPr in detergent pre-extracted control and ARH3 C26F mutant patient-derived primary human fibroblasts at different stages of the cell cycle. Scale bars, 10 μm. Representative images of at least 200 cells analysed in 2 independent experiments are shown. The figure was adapted from (Prokhorova et al., 2021a).

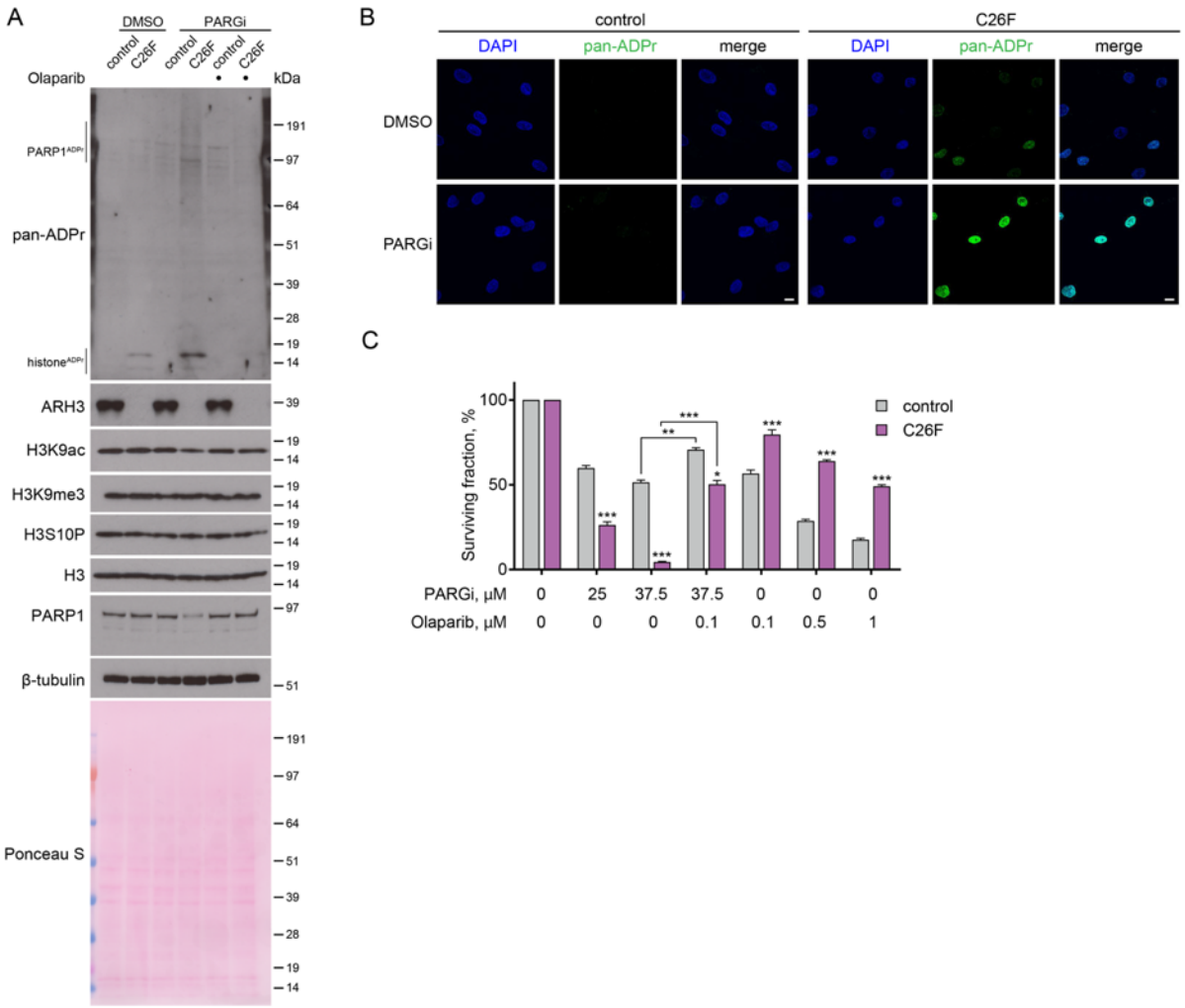


Figure 45. Loss of ARH3 activity in patient-derived primary human fibroblasts leads to the accumulation of ADPr, PARGi sensitivity and PARPi resistance.

(A) Control and C26F mutant patient-derived primary human fibroblasts were treated with DMSO, 25 μM PARGi or 25 μM PARGi and 1 μM Olaparib for 10 days. ADPr, H3 modification and PARP1 levels were analysed by Western blotting. Representative Western blots from 2 independent experiments are shown. (B) Immunofluorescence analysis of the levels of pan-ADPr in cells treated with DMSO or 25 μM PARGi for 4 days and pre-extracted with a detergent prior to fixation. Scale bars, 10 μm. (C) Quantification of crystal violet assay using cells treated with DMSO or as indicated. Data are shown as mean±SD, n=3, *p<0.05, **p<0.01, ***p<0.001 (two-tailed Student's t-test. The figures were adapted from (Prokhorova et al., 2021a).

Then, I genetically complemented C26F cells with either ARH3 WT or catalytically inactive D77/78N mutant and observed the rescue of the phenotypes only upon complementation with ARH3 WT (Figure 46).

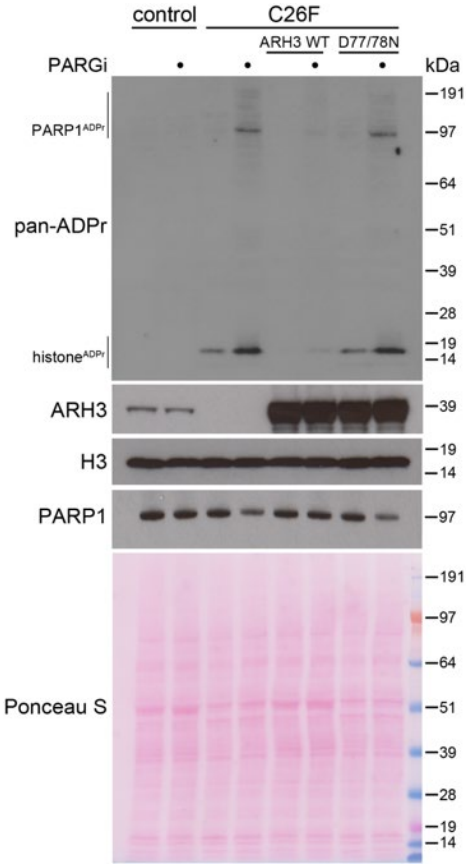


Figure 46. Complementation with ARH3 WT, but not catalytically inactive D77/78N mutant, rescues the phenotype of ARH3-deficient patient-derived primary human fibroblasts.

Control and ARH3 C26F mutant patient-derived primary human fibroblasts complemented with ARH3 WT or catalytically inactive ARH3 D77/78N were treated with 25 μM PARGi for 4 days. ADPr and PARP1 signals were analysed by Western blotting. Representative Western blots from 2 independent experiments are shown. The figure was adapted from (Prokhorova et al., 2021a).

Of note, similar to ARH3 loss in U2OS and other cell lines, the C26F mutation rendered cells more resistant to PARPi treatment (Figure 45C). This suggests that PARPi administration might be a safe therapeutic measure for the prevention of stress-induced accumulation of toxic poly-ADPr in patients with ARH3 deficiency.

To support the relevance of the above findings to cell types more related to neurodegeneration, I assessed the effect of ARH3 deficiency on PARGi and PARPi sensitivity in glioblastoma U251 cells. As expected, ARH3 loss rendered cells more sensitive to PARG inhibition and resistant to PARP1/2 inhibition by Olaparib (Figures 47A and 47B). Again, following PARGi treatment, I detected an increase in ADPr and a reduction in PARP1 levels in ARH3-deficient compared to control cells (Figure 47C).

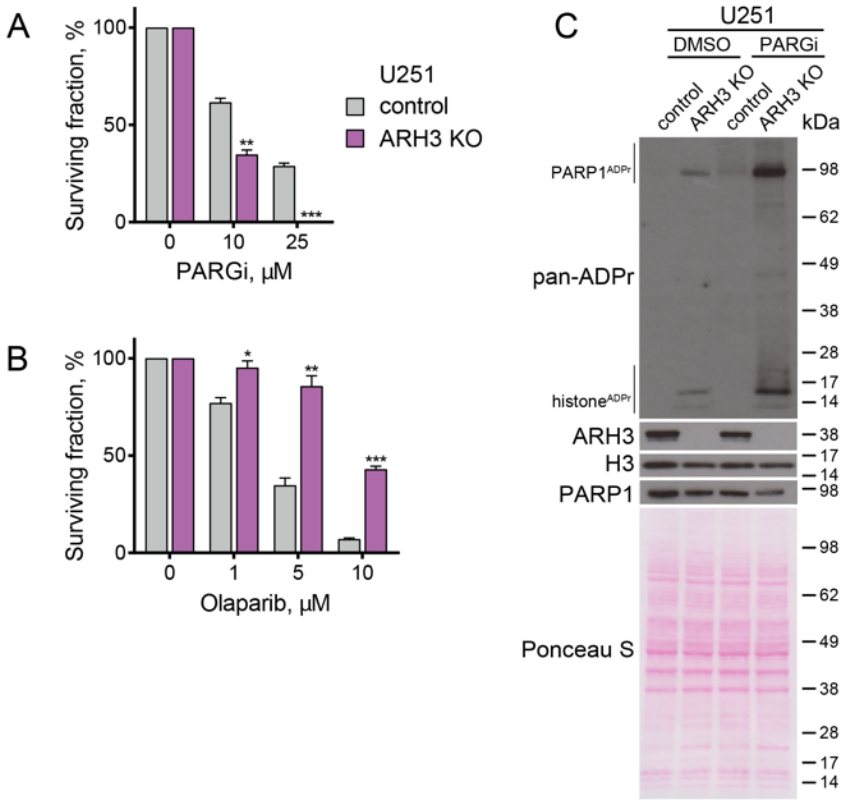


Figure 47. ARH3 deficiency leads to the accumulation ADPr, PARGi sensitivity and PARPi resistance in glioblastoma cells.

(A, B) Quantification of colony formation assay using control and ARH3 KO U251 cells treated with DMSO, PARGi (A) or PARPi (B). Data are shown as mean±SD, n=3, *p<0.05, **p<0.01, ***p<0.001 (two-tailed Student's t-test). (C) Western blotting analysis of ADPr and PARP1 levels in control and ARH3 KO U251 cells after 4-day treatment with DMSO or 25 μM PARGi. Representative Western blots from 2 independent experiments are shown. The figures were adapted from (Prokhorova et al., 2021a).

Collectively, these data confirm that the loss of ARH3 function leads to the enrichment of endogenous chromatin ADPr, which is not toxic in itself but 'primes' the cells for subsequent accumulation of detrimental poly-ADPr, eventually causing PARP1/2-dependent cell death. Notably, our findings demonstrate that ARH3 deficiency not only sensitises cells to PARG inhibition, but also confers resistance to PARP1/2 inhibition. This could be exploited in the treatment of patients with loss-of-function mutations in ARH3 by allowing safer use of higher doses of PARPis in ameliorating neurodegeneration progression.

4.3. Discussion

In this chapter, we described a distinct separation of function between ARH3 and PARG hydrolases in maintaining cellular ADPr levels and revealed a striking synergetic effect and synthetic lethality of their combined deficiency (Prokhorova et al., 2021a). To this end, we generated ARH3-deficient cells and used PARGi

PDD00017273 (James et al., 2016) to allow for the detection of endogenous ADPr which is normally transient and kept at a low level (Figure 48A).

Using ARH3-deficient cells, we demonstrated that serine-linked MAR is constantly generated at all stages of the cell cycle and is largely chromatin-associated (Figure 48B). In agreement with this, a multitude of chromatin and chromatin-binding proteins have been identified as serine-ADPr substrates in recent mass spectrometry studies (Bonfiglio et al., 2017; Buch-Larsen et al., 2020; Hendriks et al., 2019, 2021; Larsen et al., 2018). Surprisingly, this accumulation of chromatin serine-mono-ADPr is well tolerated by the cell, suggesting a potential application of ARH3 suppression as a tool for functional studies of serine-ADPr substrates and specific modification sites under undamaged conditions.

Together with other recent findings, these data confirm that ARH3 is the main hydrolase of endogenous serine-mono-ADPr (Abplanalp et al., 2017; Bonfiglio et al., 2020; Fontana et al., 2017; Hanzlikova et al., 2020; Hendriks et al., 2021; Palazzo et al., 2018), while PARG efficiently removes long PAR chains (Figure 48A-C), that, in unstressed conditions, are largely composed of PARP1 poly-ADPr but could also arise from DNA replication-associated events, e.g., unligated Okazaki fragments (Hanzlikova et al., 2018). Notably, whereas the enrichment of mono-ADPr in ARH3-deficient cells is well tolerated by the cell, combined ARH3 and PARG suppression results in the accumulation and persistence of poly-ADPr which is highly toxic and leads to distinct (patho)physiological effects (Figure 48D). These effects include dysregulation of histone modification, gene expression, DNA synthesis and cell proliferation, and eventually cause PARP1/2-dependent cell death. Therefore, the data in this chapter discriminate between the physiological effects of mono- and poly-ADPr and reveals that the observed toxicity of excessive poly-ADPr serves as a mechanistic basis for the discovered synthetic lethality between ARH3 and PARG in cancer cells (Prokhorova et al., 2021a).

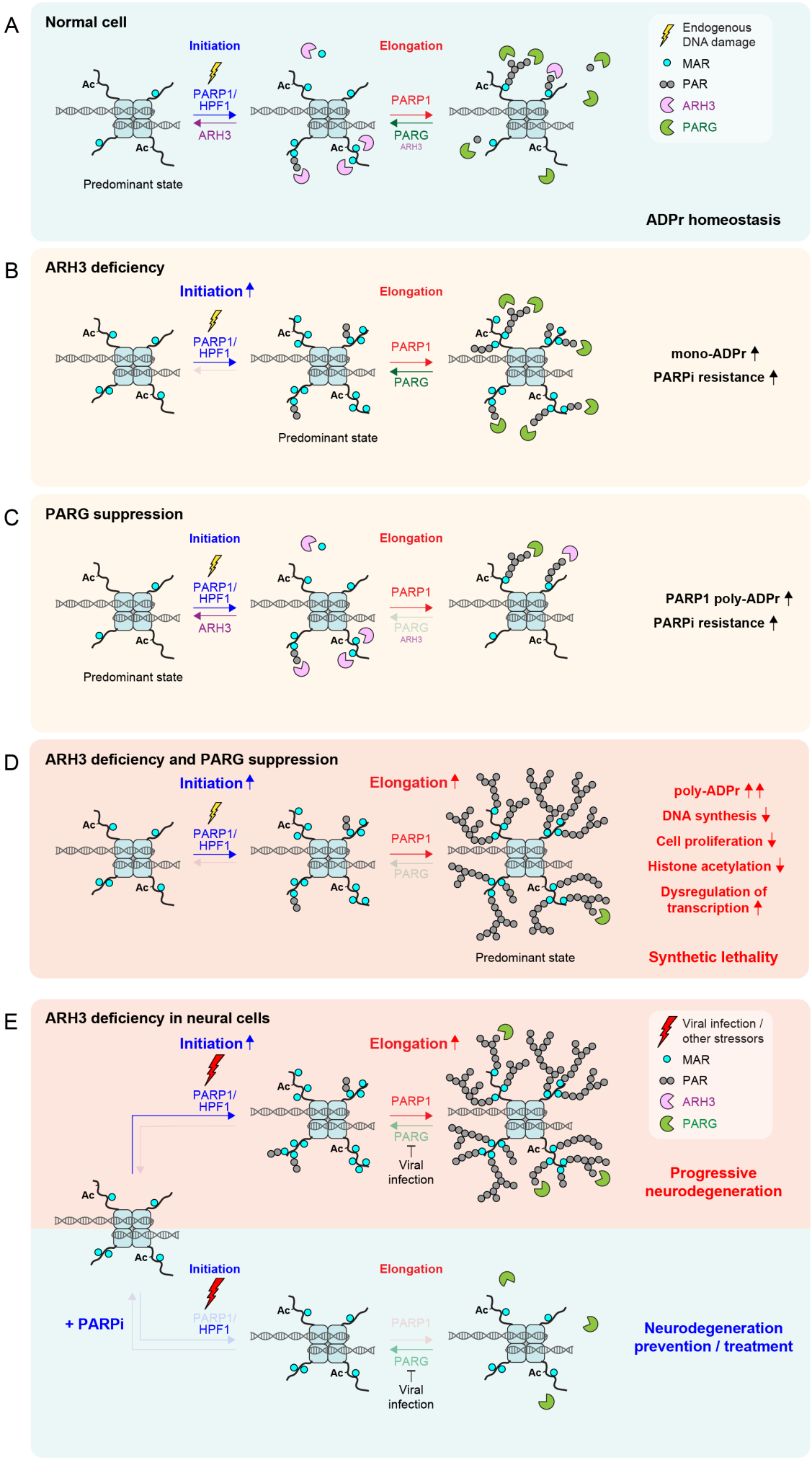

A
Normal cell
Initiation
Elongation
PARP1/
HPF1
ARH3
PARP1
PARG
ARH3
Ac
Predominant state
Endogenous
DNA damage
MAR
PAR
ARH3
PARG
ADPr homeostasis
B
ARH3 deficiency
Initiation
Elongation
Predominant state
mono-ADPr
PARPi resistance
C
PARG suppression
Initiation
Elongation
Predominant state
PARP1 poly-ADPr
PARPi resistance
D
ARH3 deficiency and PARG suppression
Initiation
Elongation
Predominant state
poly-ADPr
DNA synthesis
Cell proliferation
Histone acetylation
Dysregulation of
transcription
Synthetic lethality
E
ARH3 deficiency in neural cells
Initiation
Elongation
Viral
infection
Viral infection /
other stressors
MAR
PAR
ARH3
PARG
Progressive
neurodegeneration
+ PARPi
Neurodegeneration
prevention / treatment

Figure 48. Proposed model of two-step ADPr reaction and stress-induced pathogenesis in neurodegeneration patients with ARH3 deficiency.

(A) The first step of the ADPr reaction, initiation, requires PARP1 activation, e.g. by endogenous DNA damage, and formation of a joint active site with its partner protein HPF1. The second step of the ADPr reaction, elongation, can be catalysed by PARP1 alone. ARH3 and PARG hydrolases are responsible for the reversal of initiation and elongation steps, respectively. (B) ARH3 deficiency leads to the accumulation of serine-linked MAR and short PAR initiation sites, which elongation cannot be efficiently performed due to the presence of PARG activity. (C) The initiation sites necessary for the subsequent elongation are removed if ARH3 activity is present, and PARG suppression results only in a slight accumulation of elongation products, mainly comprised of PARP1 poly-ADPr but not chromatin-bound poly-ADPr. (D) Simultaneous ARH3 deficiency and PARG suppression leads to both initiation and elongation steps proceeding without its reversal. The initiation sites are accumulated and uncontrollably extended to long PAR chains, which is toxic to the cell and eventually causes PARP1/2-dependent cell death. (E) ARH3-deficient neural cells accumulate serine-linked MAR and short PAR initiation sites, and are in a 'primed' state for robust elongation in response to additional stressors, e.g., viral infection, that could lead to PARG downregulation, promoting pathogenic accumulation of poly-ADPr and therefore neurodegeneration (top). PARPi treatment could alleviate stress-induced neurodegeneration in ARH3-deficient neural cells through preventing the generation of both initiation and elongation products (bottom). The figure was adapted from (Prokhorova et al., 2021a).

From a fundamental point of view, these findings also allow us to suggest the existence of two distinct steps in cellular ADPr reaction, namely initiation and elongation (Figure 48A), similarly to some other PTMs, in particular ubiquitination. Although in the case of the ADPr reaction both steps involve PARP1, initiation of ADPr at serine sites requires PARP1 activation, e.g. by DNA damage, and a partner protein HPF1 (Suskiewicz et al., 2020), and is reversed by ARH3 (Fontana et al., 2017). Then, PARP1-mediated elongation of the initiation sites, particularly on PARP1 itself, can be performed on its own and is remarkably faster than the initiation, suggesting a processive mode of the modification (Mendoza-Alvarez and Alvarez-Gonzalez, 1993, 1999; Naegeli et al., 1989), but PARG efficiently counteracts this activity in human cells. Therefore, ARH3 deficiency alone mainly leads to the enrichment of initial serine-mono- and likely oligo-ADPr of at least up to three ADPr units (Rudolph et al., 2021), but long PAR chains do not accumulate due to the activity of PARG (Figure 48B). On the contrary, PARG inhibition alone results in the persistence of elongation products only, which to some extent increases PARP1 modification but largely does not affect global ADPr, since ARH3 cleaves the initial 'primers' essential for the subsequent elongation by PARP1 (Figure 48C). Simultaneous ARH3 deficiency and PARG suppression unleashes both initiation and elongation of ADPr, leading to unrestrained accumulation and persistence of extreme levels of poly-ADPr (Figure 48D). Collectively, we suggest that initiation and

elongation of ADPr are distinct events both in their synthesis and reversal (Prokhorova et al., 2021a). This evolutionary separation of function between ARH3 and PARG in vertebrates therefore creates two defence stages providing a secure protection against the accumulation of toxic poly-ADPr beyond a critical threshold.

Whereas vertebrates have evolved multiple PAR-binding factors that play a critical role in genome surveillance, chromatin organization, gene expression, protein degradation and other cellular processes (Ahel et al., 2009; Chou et al., 2010; Luijsterburg et al., 2016; Mehrotra et al., 2011; Teloni and Altmeyer, 2016), the role of endogenous ADPr is poorly understood. In Section 2.2.4, we provided the first insights into the crosstalk between histone serine-ADPr and canonical marks under exogenous DNA damage conditions, including that histone ADPr is mutually exclusive with neighbouring acetylation but not methylation (Bartlett et al., 2018). In this chapter, we extend these findings to unstressed conditions, showing that chromatin mono-ADPr and short poly-ADPr could affect histone acetylation, but not methylation, in certain scenarios, e.g., on newly incorporated nucleosomes (Hanzlikova et al., 2020).

Whilst it was suggested that unligated Okazaki fragments arising during replication could be the main cause of endogenous chromatin ADPr (Hanzlikova et al., 2020), these modifications could also have a previously undescribed housekeeping role similar to canonical histone marks. Indeed, with 9,117 ADPr sites on proteins involved in various cellular pathways, 82% of which are at serine residues (Buch-Larsen et al., 2020), it is likely that already the effects of ARH3 loss alone will be pleiotropic, and will be exacerbated following additional PARG suppression, as shown in this chapter for histone acetylation and a number of other cellular pathways. Accordingly, future work will undoubtedly identify additional molecular mechanisms involved in the reported in this thesis toxicity of the simultaneous suppression of ARH3 and PARG, although the assessment of a number of other potentially contributing mechanisms in this work did not reveal their involvement in our experimental models.

For instance, in contrast to the effect of PARG inhibition alone, we did not observe an increase in γH2AX levels following ARH3 loss alone or in combination with PARG suppression, which could be indicative of there being no additive effect of PARG and ARH3 suppression on DSB formation. However, a more direct assessment of DNA break formation, e.g., using the comet assay, was not performed in this work and could be employed in the future studies to provide more clarity on the involvement of

ARH3 and PARG in DNA repair. Interestingly, the measurement of the formation and repair of DNA breaks induced by oxidative stress agent H_2O_2, alkylating agent MMS, or DNA Topoisomerase I inhibitor camptothecin using alkaline comet assay in (Hanzlikova et al., 2020) demonstrated similar rates of SSB induction and repair in both control and ARH3 KO U2OS cells, suggesting that ARH3 could be indeed dispensable for at least SSB repair in human cells.

Moreover, despite PARP1 being a major cellular consumer of NAD^+, which excessive activation leads to ATP depletion (Cohen, 2020), we were not able to observe a statistically significant effect of ARH3 loss and/or PARG inhibition on cellular NAD^+ levels in this work or a noticeable effect of ARH3 loss of cellular ATP levels (data not shown). Similarly, no difference in NAD^+ levels or their depletion in response to exogenous DNA damage was detected in ARH3 KO U2OS cells in (Hanzlikova et al., 2020).

Furthermore, despite excessive PARP1 activation being known to result in the release of PAR chains with subsequent induction of parthanatos, a PARP1-dependent mode of regulated necrotic cell death, we could not confirm its induction in our experimental models (data not shown), not being able to observe the main reported biochemical steps of this mode of cell death, namely the release of apoptosis inducible factor (AIF) from the mitochondria and its translocation to the nucleus together with nuclease migration inhibitory factor (MIF) that then induces large-scale DNA fragmentation (Prokhorova et al., 2020). Yet, there have also been several reports of AIF-independent PARP1-mediated regulated necrotic cell death, suggesting that AIF nuclear translocation might be dispensable and dependent on a cellular context (Prokhorova et al., 2020). The assessment of the markers of the induction of other modes of regulated cell death such as apoptosis, cellular senescence and autophagy in this work also did not reveal their involvement in the toxicity of the simultaneous loss of ARH3 and PARG function (data not shown).

PARG inhibition, in particular in combination with genotoxic agents or radiotherapy, has recently emerged as a promising approach in cancer treatment (Slade, 2020). Whereas PARGi PDD00017273 is unsuitable for clinical studies because of poor bioavailability (Gravells et al., 2017; James et al., 2016), PARGis with improved potency and properties, that were recently developed by IDEAYA Biosciences (https://media.ideayabio.com/2022-01-10-IDEAYA-Biosciences-Announces-Corporate-and-Portfolio-Update-for-J-P-Morgan-40th-Annual-Healthcare-Conference) and (Chen and Yu, 2019; Houl et al., 2019), could prove good candidates for clinical

application. Notably, the synthetic lethality between PARG and ARH3 may also be exploited as a therapeutic strategy in cancers with ARH3 or PARG downregulation. Therefore, developing clinically relevant ARH3 inhibitors, building up on previous structural and biochemical studies (Drown et al., 2018; Liu et al., 2020; Rack et al., 2018), would be highly beneficial as an independent approach or in combination with PARG inhibition. Of note, downregulation of PARG has been reported as a mechanism of PARPi resistance caused by the resultant increase in poly-ADPr (Gogola et al., 2018; Gomez et al., 2020), and PARG has been identified as a top PARPi resistance gene in cancer cells (DeWeirdt et al., 2020; Gogola et al., 2018; Juhász et al., 2020). According to our data, ARH3 inhibitors could be applied to target these PARPi-resistant cancers with PARG downregulation. Elaborating on our initial results in Section 3.2.1, we also demonstrate the loss of ARH3 could be another mechanism through which different cancer types, including BRCA1/2-deficient cancers, could acquire resistance to PARPis. Overall, our findings highlight the potential of ARH3 both as a drug target and as a predictive biomarker for cancer cell sensitivity to PARP and PARG inhibition.

Finally, the findings in the last section of this chapter provide additional insights into the progression of neurodegeneration in ARH3-deficient patients (Danhauser et al., 2018; Ghosh et al., 2018; Mashimo et al., 2019). In general, defective reversal of ADPr by PARG and TARG1 hydrolases was already reported as the cause of neurodegenerative phenotypes (Hanai et al., 2004; Sharifi et al., 2013). Our data suggest that ARH3-deficient neural cells have increased levels of basal serine-mono- and possibly oligo-ADPr, in particular on chromatin, that persist throughout the cell cycle but are normally not toxic. When neural cells lacking ARH3 function encounter additional stressors, e.g. viral infection or environmental stressors (Ghosh et al., 2018; Grady et al., 2012), they may accumulate extreme levels of poly-ADPr that shortly overwhelm cell tolerance (Figure 48E, top) and eventually lead to PARP1/2-dependent cell death. Notably, infection by herpesviruses was shown to induce poly-ADPr by specifically downregulating PARG (Grady et al., 2012), in this way mimicking PARG inhibition, providing a plausible mechanistic rationale for the deterioration in patients with ARH3 deficiency. Therefore, we suggest that constitutive mono-ADPr efficiently ‘primes’ cells lacking ARH3 function for stress-induced poly-ADPr rather than being toxic in itself. Additionally, in agreement with several recent reports (Danhauser et al., 2018; Ghosh et al., 2018; Mashimo et al., 2019), our findings imply that the stress-induced neural cell death in ARH3-deficient patients could be prevented by PARPi administration (Figure 48E, bottom). Our

findings that the loss of ARH3 function confers resistance to PARP1/2 inhibition suggest that reduced PARPi toxicity would allow safe therapeutic use of PARPis in ARH3-deficient patients with minimised side effects.

In summary, in this chapter, we distinguish between the separate initiation and elongation steps in the ADPr reaction, revealing a synergy between ARH3 and PARG hydrolases and clarifying the molecular basis of ADPr reversal. We discriminate between the effects of cellular mono- and poly-ADPr, demonstrating that while the former is constantly generated on chromatin throughout the cell cycle and is non-toxic, the accumulation of the latter bears distinct pathogenic consequences. Moreover, we identify the synthetic lethal interaction between ARH3 and PARG, which is caused by excessive poly-ADPr, and underscore ARH3 as a promising drug target and a biomarker for cancer cell sensitivity to PARP and PARG inhibition. Furthermore, we extend the role of ARH3 beyond cancer to restraining the detrimental accumulation of poly-ADPr in neural cells, and highlight the therapeutic potential of PARPis in alleviating the progression of neurodegeneration in patients with ARH3 deficiency.

5. General Discussion

Although the first notion of ADPr is going back as far as 1963 (Chambon et al., 1963), until recently it was unknown what protein residues are mainly targeted by this modification. The discovery of serine-ADPr in 2016 (Leidecker et al., 2016) and the subsequent characterisation of the basic molecular mechanisms behind this modification, as described in Sections 1.1.1, 1.1.2 and 1.1.3 (Figure 49), has fuelled rapid progress in the field, stimulating an ever increasing number of studies addressing the regulation and function of serine-ADPr in human cells.

With the realisation that serine residues are the primary cellular targets of DNA damage-induced ADPr (Section 2.2.1 and (Palazzo et al., 2018)), a number of follow-up mass-spectrometry studies, including (Buch-Larsen et al., 2020) comprising 9,029 ADPr sites, 84% of which are on serine residues, have provided a valuable resource for the subsequent characterisation of ADPr sites in human cells. Crosstalk between these serine-ADPr sites and other cellular PTMs adds an additional layer of complexity to cellular regulation. However, except for initial findings on its interplay with other histone PTMs (Sections 2.2.4, 4.2.4, (Bartlett et al., 2018; Hananya et al., 2021; Hanzlikova et al., 2020; Hendriks et al., 2021; Liszczak et al., 2018; Prokhorova et al., 2021a) and Figure 49), it is waiting for further investigation.

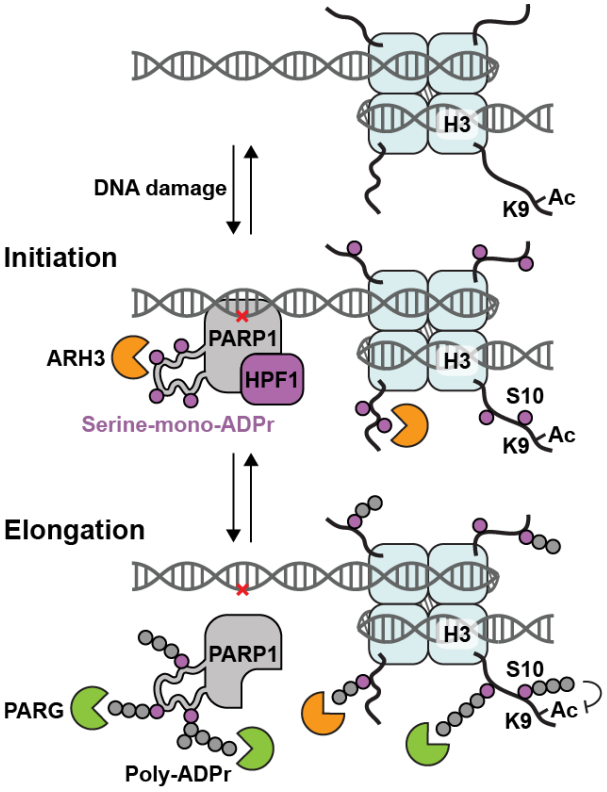


Figure 49. Serine-ADPr reaction and its crosstalk with neighbouring acetylation modifications in human cells.

In response to PARP1 activation by DNA damage or other stimuli, the composite PARP1-HPF1 enzyme performs the initiation step of the reaction, specifically modifying serine residues on PARP1 itself, histones and other substrates. The initial serine-linked MAR (shown in purple) and short PAR are then extended by PARP1 to poly-ADPr (shown in grey) during the elongation step. These modifications then promote recruitment and function of DDR factors, but, at the same time, they are quickly reversed by hydrolases to allow for efficient DNA repair. PARG is the hydrolase that removes most of poly-ADPr (reversal of the elongation step), and ARH3 efficiently removes serine-linked mono- and short poly-ADPr (reversal of the initiation step). While enrichment of serine-linked MAR is normally well tolerated by the cell, accumulation of poly-ADPr is highly toxic and interferes with neighbouring acetylation marks, as in this example between histone H3 serine 10 ADPr and lysine 9 acetylation, a crucial active transcription mark.

Given the predominance of serine-ADPr not only in DNA damage signalling, but also in physiological conditions (Buch-Larsen et al., 2020), it would not be surprising if modulating the levels of specific serine-ADPr regulators HPF1 and ARH3 also affects cell response to PARP1/2 inhibition. Indeed, a recent study comparing the outcomes of genetic deletion of HPF1 and ARH3 in human cells has demonstrated up to 1,000-fold regulation of serine-ADP-ribosylome by HPF1 and ARH3 (Hendriks et al., 2021). Accordingly, here we revealed a strong negative correlation between the levels of serine-ADPr and cellular sensitivity to PARP1/2 inhibition (Sections 3.2.1, 4.2.3, 4.2.5, (Prokhorova et al., 2021b, 2021a) and Figure 50), elaborating on the initially observed synthetically lethal interaction between PARP1/2 inhibition and HPF1

deficiency (Gibbs-Seymour et al., 2016). Thus, similar to the loss of HPF1, which is required for the initiation of serine-ADPr, overexpression of ARH3, that specifically reverses serine-ADPr initiation (Figures 48A and 49), also rendered cells more sensitive to PARPis, potentiating the prolonged PARP1 retention on damaged DNA often referred to as trapping, accumulation of DNA damage and other effects of PARPi-induced cytotoxicity. This suggests the existence of a minimum threshold of ADPr that is needed for the maintenance of cell viability, in particular for sufficient DNA repair (Figure 50).

Excitingly, in addition to demonstrating the effects of manipulating global levels of serine-ADPr on the cellular response to PARP1/2 inhibition, we observed that already loss of only three serine-ADPr sites on PARP1 (serines 499, 507 and 519) markedly reduces both PARP1 ADPr and cellular tolerance to PARPis without impeding PARP1 ability to catalyse ADPr (Sections 3.2.2, 3.2.3 and (Prokhorova et al., 2021b)). Moreover, our findings provide novel insights into the cellular regulation of one of the major causes of PARPi cytotoxicity, prolonged PARP1 retention on damaged DNA or trapping. In agreement with the previously suggested role of ADPr synthesis in PARP1 detachment from DNA damage sites, presumably due to electrostatic interference (Ferros and Olivera, 1982; Zahradka and Ebisuzaki, 1982), our data specifically underscore the role of serine-ADPr, especially on PARP1 serines 499, 507 and 519, in de-trapping PARP1 from DNA damage sites (Figure 25).

While HPF1 deficiency or ARH3 overexpression sensitised cells to PARP1/2 inhibition, on the contrary, loss of ARH3 rendered cells more resistant to PARPis. Importantly, we were able to validate these results in different cellular models, including BRCA1/2-deficient TNBC cells (Section 4.2.3), in which PARPis provide particular clinical benefits. This suggests that, similarly to suppression of the main poly-ADPr hydrolase PARG (Gogola et al., 2018; Gomez et al., 2020), downregulation of ARH3 could represent an additional mechanism of innate and acquired PARPi resistance in cancers. In both scenarios, the resistance is caused by the resultant increase in cellular ADPr levels.

Strikingly, we observed that while loss of ARH3 or PARG activity alone is well tolerated by the cell, simultaneous suppression of the two hydrolases is synthetically lethal due to the extreme accumulation and persistence of poly-ADPr, which has distinct pathophysiological effects (Sections 4.2.3, 4.2.4, (Prokhorova et al., 2021a) and Figure 50). This allowed us to discriminate between the effects of cellular mono-

and poly-ADPr, demonstrating that while the former is constantly generated on chromatin throughout the cell cycle and is non-toxic, the accumulation of the latter strongly negatively charged and bulky polymers bears distinct pathogenic consequences. Whilst future work is required to provide a mechanistic explanation for this distinction, one possible mechanism could be the that whilst MAR has no effect on liquid-liquid phase separation (McGurk et al., 2018), excessive accumulation of PAR could result in its disruption in cells. With the increasing PAR length, more PAR-binding proteins would be locally enriched, leading to the condensation of proteins and possibly formation of cellular compartments, e.g., stress granules (Leung, 2020), disrupting the normal function of the sequestered factors.

Mechanistically, the remarkably greater effect of the simultaneous loss of ARH3 and PARG hydrolases, could be explained by their synergistic roles in the reversal of ADPr (Section 4.2.2). This is consistent with the proposed model of two-step serine-ADPr reaction, in which HPF1 notably stimulates the rate of serine-ADPr initiation by PARP1 compared to ADPr elongation, which can be performed by PARP1 alone, and ARH3 efficiently removes the initial serine-linked MAR and short PAR, whereas PARG reverses the products of their elongation (Figures 48A and 49).

Importantly, the discovered mechanism of synthetic lethality between ARH3 and PARG provides an alternative therapeutic opportunity to overcome PARPi resistance, especially in cancers with ARH3 or PARG suppression, by harnessing the toxicity of going above a maximum threshold of ADPr (Figure 50). This highlights the potential of ARH3 as a drug target, in particular in cancers with PARG downregulation, and underlines the need for ARH3 inhibitor development. On the other hand, PARGis, which are currently in preclinical and initial clinical development, could prove particularly effective against cancers with downregulation of ARH3.

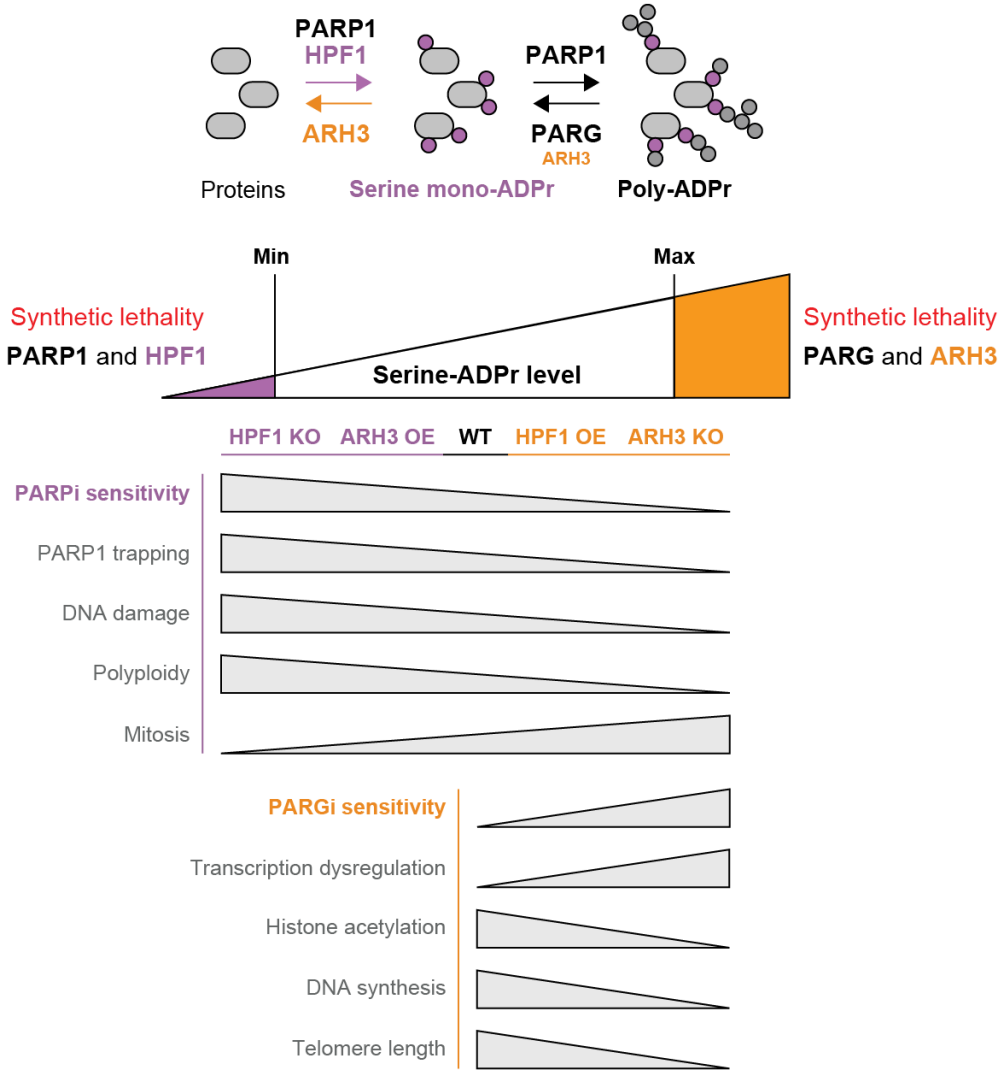


Figure 50. Proposed model of the relationship between serine-ADPr levels controlled by HPF1 and ARH3 and cellular response to PARP1/2 and PARG inhibition.

Schematic representation of serine-ADPr synthesis and removal (top). Summary of the proposed impact of HPF1 and ARH3 loss or overexpression (OE) on serine-ADPr levels and cellular response to PARP1/2 and PARG inhibition (bottom). The effects of ARH3 OE on PARP1 trapping and the effects of HPF1 OE remain to be experimentally validated. The effect of PARG inhibition on telomere length in ARH3 KO cells was described in (Prokhorova et al., 2021a).

Whilst some initial efforts to develop ARH3 inhibitors have identified a small molecule compound AI26 binding to the catalytic pocket of ARH3 with a good affinity (Liu et al., 2020), further work is required for the development of this potential lead compound or identification and development of better candidate molecules. Similarly, future studies are needed to address whether PARP1-HPF1 complex rather than PARP1 alone could be a better target in cancer therapy. Whilst currently developed clinically relevant PARPis are not predicted to make a direct interaction with HPF1, the close proximity of several HPF1 residues to the active site of PARP1 suggests that inhibitors developed to bind to the composite PARP1-HPF1 active site could have improved specificity and potency.

Collectively, these findings highlight the potential of HPF1 and ARH3 as novel predictive biomarkers of PARPi and, at least in the case of ARH3, PARGi sensitivity in cancers. Although future studies are needed to assess HPF1 and ARH3 protein expression and whether this is correlated with PARPi and, if clinically approved, PARGi sensitivity in patient samples, some preliminary data already suggested that HPF1 and ARH3 expression can vary in certain types of tumours. For instance, according to cBioPortal (TCGA PanCancer Atlas Studies), HPF1 gene is lost in 15.4% of undifferentiated stomach adenocarcinomas and 3.7% of lung squamous cell carcinomas, whereas ARH3 gene is amplified in 6.3% of ovarian epithelial tumours and deleted in 3.2% of miscellaneous neuroepithelial tumours.

While toxicity of insufficient ADPr is used to induce cell death in cancer therapy, reducing excessive ADPr toxicity is important in preventing and alleviating progression of neurodegenerative and other non-oncological diseases. Given that several loss-of-function ARH3 mutations have been linked to progressive neurodegeneration in patients (Beijer et al., 2021; Danhauser et al., 2018; Ghosh et al., 2018; Mashimo et al., 2019), we attempted to extend our findings beyond cancer to neurodegenerative phenotypes. Indeed, our data suggest that ARH3, efficiently reversing the initiation step of the serine-ADPr reaction, prevents stress-induced elongation of initiation products, and in this way protects neural cells from pathogenic accumulation of poly-ADPr (Section 4.2.5, Figure 48E and (Prokhorova et al., 2021a). In agreement with previous reports (Danhauser et al., 2018; Ghosh et al., 2018; Mashimo et al., 2019), our findings that ARH3 loss confers resistance to PARP1/2 inhibition highlight administration of PARPis, in particular with reduced or no trapping activity if developed for clinical applications (Kim et al., 2021), as a promising strategy for ameliorating neurodegeneration in ARH3-deficient patients.

Altogether, this study provides novel insights into the abundance, regulation and role of serine-ADPr in human cells, including a number of therapeutic implications in cancer and neurodegeneration. From a more general point of view, these data allow us to suggest the existence of minimum and maximum thresholds for ADPr (Figure 50), crossing of which would be detrimental to cellular homeostasis.

6. Conclusions and Future Directions

Overall, this thesis provides novel insights into the role of serine-ADPr in human cells, building up on the recent discoveries of HPF1, a PARP1/2-interacting protein required for switching its specificity towards serines (Bonfiglio et al., 2017; Gibbs-

Seymour et al., 2016), and ARH3, a specific hydrolase of serine-ADPr (Fontana et al., 2017). Despite rapid progress in the new field of serine-ADPr, many questions yet remain to be answered. Whilst we show that the loss of HPF1 potentiates PARPi-induced toxicity, leading to prolonged residence of PARP1 at the sites of DNA breaks often referred to as PARP1 trapping, it remains to be addressed how modulating the levels of ARH3 expression would affect PARP1 residence time at damaged DNA in untreated and PARPi-treated cells. Given the findings that long-term PARG suppression prevents PARPi-induced accumulation of PARP1 at the sites of DNA breaks (Gogola et al., 2018), it could be anticipated that suppression of ARH3 would have a similar effect, whereas, on the contrary, overexpression of ARH3 would potentiate PARP1 trapping (Figure 50). In order to provide the full picture of the regulation of PARP1 trapping and de-trapping by serine-specific factors HPF1 and ARH3 in human cells, it would also be important to assess the effects of HPF1 overexpression on PARP1 residence time at DNA damage sites, as well as in general on cellular sensitivity to PARPis and PARGis.

Then, whilst this work describes three main sites of PARP1 ADPr, namely serine 499, 507 and 519, and their role in counteracting PARPi-induced toxicity, including prolonged retention of PARP1 at the sites of DNA damage, it would be of interest to extend this analysis to other PARP1 mutations, e.g., E988K and E988Q, which notably reduce PARP1 elongation activity, or mutations that have been clinically identified in PARPi-resistant tumours.

Furthermore, whilst the loss of HPF1 was previously shown to render cells more sensitive to an alkylating agent MMS (Gibbs-Seymour et al., 2016), it remains to be assessed whether modulating ARH3 levels or losing PARP1 serine 499, 507 and 519 ADPr would also affect its sensitivity. Similarly, given the involvement of PARP1 in the repair of various types of DNA damage, it would be important to extend this assessment to different types of DNA damage, clarifying whether PARP1 serine-ADPr activity is ubiquitously needed for its role in DNA repair.

Future work will undoubtedly provide more clarification into the observed in this work distinction between the effects of serine-linked mono- and poly-ADPr accumulation in human cells. For instance, it would be of interest to investigate the molecular mechanisms by which excessive serine-linked poly- but not mono-ADPr of PARP1/2 triggers the described here post-transcriptional reduction in PARP1/2 proteins levels, which presumably helps the cells to partially escape the toxicity of excessive poly-

ADPr in the scenario of its suppressed reversal upon the loss of ARH3 and PARG hydrolase activity.

As PARP1 inhibition, and likely specifically inhibition of its HPF1-dependent function, holds a great promise in cancer therapy, designing more specific PARPis targeting the composite catalytic site formed between HPF1 and PARP1 presents a promising future direction towards improving the efficacy of current PARPi-based therapies and reducing the side effects associated with their primary pharmacology. Further elucidation of the embeddedness of PARP1 in a broader ADPr network including HPF1, other PARPs, ARH3, PARG and other ADPr hydrolases, as well as its involvement in other cellular pathways, will further improve our understanding of PARP1 function in human cells, forming a novel basis for the development of future therapeutic strategies.

7. Materials and Methods

7.1. Cell culture

Human U2OS osteosarcoma (ATCC HTB-96), cervix adenocarcinoma HeLa (ATCC CCL-2), embryonic kidney (HEK) 293T (ATCC CRL-3216) cells were acquired from ATCC and grown in DMEM (Sigma) supplemented with 10% FBS (Gibco) and penicillin-streptomycin (100 U/mL, Gibco). Human triple-negative breast cancer SUM149PT (CVCL_3422) and SUM159PT (CVCL_5423) were a gift from Ian Gibbs-Seymour (University of Oxford) and were cultured in Ham's F-12 (Gibco) supplemented with 5% FBS (Gibco), HEPES (10 mM, Gibco), Insulin (5 µg/mL, Sigma) and Hydrocortisone (5 µg/mL, Sigma). Human glioblastoma U251 cells (CVCL_0021) were a gift from Omer Dushek (University of Oxford) and were cultured in DMEM (Sigma) supplemented with 10% FBS (Gibco) and penicillin-streptomycin (100 U/mL, Gibco). All cell lines were cultured at 37°C with 5% CO_2.

To induce DNA damage, cells were incubated with 2 mM H_2O_2 (Sigma) in DPBS with calcium and magnesium (Gibco) for the indicated times, or treated with 2 mM MMS (Sigma) in DMEM for 1 h and left to recover in fresh media for the indicated times. For PARP or PARG inhibition, cells were pre-treated with 10 µM Olaparib (Cayman Chemical) or 10 µM PARGi PDD00017273 (Sigma) for 1 h, and Olaparib or PARGi PDD00017273 was added to the DPBS solution in the case of subsequent DNA damage induction.

Human U2OS Flp-In T-REx osteosarcoma cells were a gift from Daniel Durocher (Lunenfeld-Tanenbaum Research Institute) and were grown in DMEM (Sigma) supplemented with 10% FBS (Sigma), 50 µg/mL Zeocin (Invitrogen) and 4 µg/mL Blasticidin (InvivoGen). To resemble endogenous PARP1 protein expression levels, U2OS Flp-In T-REx PARP1 KO cells with inducible expression of YFP empty vector or YFP-PARP1 WT were treated with 0.1 µg/mL doxycycline, YFP-PARP1 3S/A expression was induced with 0.5 µg/mL doxycycline. The media was replenished every 3 days to maintain expression levels in long-term assays.

The patient-derived primary human fibroblasts were obtained from a cartilage biopsy from a patient carrying a homozygous C26F ARH3 mutation and were provided by Jonathan Baets (University of Antwerp). A control skin-derived fibroblast line was obtained from a healthy individual. Fibroblast cultures were maintained in DMEM (Sigma) supplemented with 15% FBS (Gibco), 1% L-Glutamine (Sigma) and penicillin-streptomycin (100 U/mL, Gibco) at 37°C with 5% CO_2.

7.2. Generation of cell lines

For the generation of CRISPR/Cas9 KO cell lines, a pair of sgRNA was designed to introduce a deletion into the gene of interest. U2OS ARH3 KO, HPF1 KO and PARP1 KO, 293T HPF1 KO, PARP1 KO and HPF1/PARP1 KO were generated previously (Fontana et al., 2017; Gibbs-Seymour et al., 2016).

The protocol for generating ARH3 KO 293T, HeLa, SUM149PT, SUM159PT and U251 cell lines was used previously for U2OS cells (Fontana et al., 2017). sgRNA 210 (GCGCTGCTCGGGGACTGCGT) and sgRNA 212 (GGGCGAGACGTCTATAAGGC) were used to remove part of ARH3 exon 1 and part of the downstream intron, including the splice donor site. sgRNAs were cloned into epX459(1.1), which Joey Riepsaame (Genome Engineering Oxford) generated by subcloning enhanced Cas9 (eSpCas9) v1.1 into plasmid pX459. ARH3 KO SUM149PT and U251 cells were generated by Thomas Agnew and James Holder, respectively. The protocol for generation of HeLa HPF1 KO and PARP1 KO U2OS Flp-In T-REx cells was previously described for U2OS and 293T cells (Gibbs-Seymour et al., 2016). sgRNA 1 (CAGCAGAATTCCCCGATCCG) and sgRNA 2 (TCGGCGGTGGCGGGAAGCGC) targeting HPF1 exon 1, or sgRNA 2.1 (CCACCTCAACGTCAGGGTG) and sgRNA 2.2 (TGGGTTCTCTGAGCTTCGT) targeting PARP1 exon 2 were cloned into the PX462 vector. PARP1 KO U2OS Flp-In T-REx cells were produced by Florian Zobel. Cells were transfected with control sgRNA or co-transfected with sgRNA pair (1:1 ratio) using TransIT-LT1 Transfection

Reagent (Mirus Bio), Polyfect (Qiagen) or Lipofectamine 3000 Transfection Reagent (Invitrogen), following the manufacturer's instructions. 24 h after transfection, the cells were selected with Puromycin (InvivoGen) for 36 h and seeded at low densities on 96-well plates (0.4 cells/well) or 15-cm dishes. Single colonies were propagated, and individual clones were screened by Western blotting. Colonies expressing Flag-tagged Cas9 protein were discarded.

Generation of U2OS cells with constitutive ARH3 overexpression and complementation of U2OS ARH3 KO cells with ARH3 WT or catalytically inactive D77/78N mutant were carried out by Thomas Agnew. Cells were plated in 6-cm dishes and transiently transfected with pDEST12.2-ARH3 WT or D77/78N using TransIT-LT1 Transfection Reagent (Mirus Bio) according to the manufacturer's protocol. After 24 h, the cells were transferred into 15-cm dishes and allowed to grow for 48 h in complete DMEM. After 48 h, the media was replaced with complete DMEM supplemented with 1 mg/mL G-148 solution (Sigma) for 10 days to select for resistant cells integrated with the pDEST12.2 ARH3 constructs. Once G-148 resistance single cell colonies had formed, individual clones were transferred to individual dishes. Individual cell colonies were propagated and screened for successful integration by PCR. ARH3 expression levels were analysed by Western blotting on positive colonies.

Generation of U2OS Flp-In T-REx PARP1 KO cells with inducible expression of YFP empty vector, YFP-PARP1 WT or 3S/A was performed by Florian Zobel. Cells were plated in 6-well plates and co-transfected with YFP empty vector or plasmids encoding YFP-PARP1 WT or 3S/A and the Flp recombinase plasmid pOG44 (1:9 ratio) using TransIT-LT1 Transfection Reagent (Mirus Bio) according to the manufacturer's instructions. 24 h after transfection, cells were transferred into 15-cm dishes. 24 h later, the media was supplemented with 4 µg/mL Blasticidin (InvivoGen) and 200 µg/mL Hygromycin B Gold (InvivoGen). The media in the dishes was subsequently changed every 2-3 days for two weeks to select for resistant colonies. Individual clones were propagated and screened following 24 h incubation with 1 µg/mL doxycycline (Sigma) by fluorescence microscopy and Western blotting.

For the complementation of ARH3 C26F mutant patient-derived primary human fibroblasts, mammalian expression lentiviral ARH3 untagged pLX304 (Addgene #25890) constructs were generated using LR Clonase II enzyme mix (Invitrogen). To prepare lentivirus particles, pLX304-ARH3 WT or pLX304-ARH3 D77/78N were co-transfected with packaging plasmids pCMV-VSV-G and pCMV-dR8.2 dvpr (Addgene

plasmids #8485 and #8455) using Polyfect (Qiagen) following the manufacturer's instructions into 293T cells. Lentiviral supernatants were collected 36 h after transfection, filtered and used for infection of ARH3 C26F mutant patient-derived primary human fibroblasts in the presence of 2 µg/mL of polybrene (Sigma). After 48 h, the media was replaced with complete DMEM supplemented with 3 µg/mL Blasticidin (InvivoGen) for 7 days to select for resistant cells integrated with pLX304 ARH3 constructs. ARH3 expression levels were analysed by Western blotting.

7.3. Western blotting

The cells were lysed with Triton-X100 lysis buffer (50 mM Tris-HCl pH 8.0, 100 mM NaCl, 1% Triton X-100) supplemented with 2.5 mM $MgCl_2$, protease and phosphatase inhibitors (Roche), PARG inhibitor PDD00017273 (Bio-Techne or Sigma, 1 µM), PARP1/2 inhibitor Olaparib (Cayman Chemical, 1 µM, with the exception of 293T cells, for which 2 µM was used) and Benzonase (Sigma) for 30 min at 4°C, centrifuged at 14,000 rpm for 15 min, and the supernatants were collected. Protein concentrations were analysed by Bradford Protein Assay (Bio-Rad). Proteins were boiled in 1x NuPAGE LDS sample buffer (Invitrogen) with 2-Mercaptoethanol (Sigma) or TCEP (Sigma), resolved on NuPAGE Novex 4-12% Bis-Tris gels (Invitrogen), and transferred onto nitrocellulose membranes (Bio-Rad) using Trans-Blot Turbo Transfer System (Bio-Rad). The membranes were blocked in PBS with 0.1% Tween 20 and 5% non-fat dried milk for 1 h at room temperature, and incubated overnight with primary antibodies (1:1,000, unless stated otherwise) at 4°C, followed by 1-h incubation with peroxidase-conjugated secondary antibodies (Dako) at room temperature. Anti-poly-ADPr rabbit antibody (4336-BPC-100) was purchased from Trevigen. Rabbit anti-pan-ADPr (MABE1016; 1:1,500), anti-mono-ADPr (MABE1076), anti-histone H3 (07–690, 1:5,000), anti-histone H3K56ac (04-11350), and mouse anti-PARG (MABS61, 1:500), anti-PARP2 (MABE18, 1:500), anti-GAPDH (MAB374, 1:3,000), anti-cyclin B1 (05-373), anti-BRCA1 (OP92, 1:500) and anti-BRCA2 (OP95, 1:500) antibodies were from Millipore. Rabbit anti-ARH3/ADPRHL2 (HPA027104, 1:2,000) antibody was from Atlas Antibodies. Rabbit anti-PARP1 (ab32138), anti-H3S10P (ab5176), anti-H3K9me3 (ab8898), anti-H3K27ac (ab4729), anti-γH2AX (ab2893), anti-GFP (ab290, 1:10,000), anti-β-tubulin (ab6046; 1:5,000), anti-laminA (ab26300), anti-FEN1 (ab17994), and mouse anti-H3K27me3 (ab6002) and anti-Hsp70 (ab2787) antibodies were purchased from Abcam. Rabbit anti-H3K9ac (9649), anti-H3K27ac (8173), anti-H3K36ac (27683), anti-H2BK5ac (2574), anti-pan-Kac (9441), anti-H2AX (7631), anti-CXXC5 (84546),

and mouse anti-cyclin E1 (4129) antibodies were from Cell Signaling. Mouse anti-GFP (sc-9996, 1:10,000) antibody and rabbit anti-cyclin A (sc-751) and anti-p21 (sc-397) antibodies were from Santa Cruz Biotechnology. Rabbit anti-PARP3 (11289-1-AP) antibody was from Proteintech. Rabbit anti-mono-ADPr (AbD33204, 1:500) and human anti-H3S10/28MAR (AbD33644, 1:500) antibodies were described in (Bonfiglio et al., 2020). Custom-made rabbit HPF1 antibody was described in (Gibbs-Seymour et al., 2016). Custom-made rabbit anti-H3K27me3 antibody was a gift from Rob Klose (University of Oxford). Anti-Flag HRP-conjugated (A8592; 1:5,000) mouse antibody was from Sigma-Aldrich. Blots were developed using ECL (Invitrogen) and analysed by exposing to films.

7.4. Plasmids and site-directed mutagenesis

Full-length human histone H2B and H3.1 cDNAs were cloned into pDONR221 vector (Thermo Fisher Scientific) using Gateway BP Clonase II Enzyme mix (Invitrogen). pDONR221 constructs expressing HMGA1, HMGB1 and HMGN1 were obtained from the DNASU Plasmid Repository. Using Gateway LR Clonase II (Invitrogen), H2B, H3.1, HMGA1 and HMGB1 were sub-cloned into a destination vector expressing proteins with the C-terminal 3xFlag tag, and HMGN1 into a destination vector expressing an N-terminally YFP-tagged protein. Plasmids expressing human histone H1.1, H1.2, H1.3, H1.4, H1.5 with C-terminal eGFP tag were a kind gift from Sébastien Huet (Université de Rennes 1). ARH3 cDNA was cloned from an ARH3 expression construct, that was a gift from Paul Hergenrother (University of Illinois), into the pDONR221 vector (Invitrogen). ARH3 catalytic mutant D77/78N was made using QuikChange Lightning Site-Directed Mutagenesis Kit (Agilent). Mammalian expression ARH3 untagged pDEST12.2 (Invitrogen) constructs were generated using LR Clonase II enzyme mix (Invitrogen). Vectors for mammalian expression of full-length human HPF1 and PARP1 with N-terminal Flag or YFP tags were previously described (Gibbs-Seymour et al., 2016).

Point mutations were produced using QuikChange Lightning site-directed mutagenesis kit (Agilent) following the manufacturer’s instructions.

7.5. siRNA transfection

siRNA transfection was performed using Lipofectamine RNAiMAX (Invitrogen) and 20 nM siRNA for the indicated time according to the manufacturer’s instructions. Silencer Select Negative Control No. 1 and 2 siRNAs, siPARG (s16159) and

siBRCA1 (s458) were from Ambion (Invitrogen). siBRCA2 (D-003462-04, GAAGAAUGCAGGUUUAAUA) was purchased from Dharmacon.

7.6. Plasmid transfection and protein immunoprecipitation

Flag- or GFP-immunoprecipitation followed by Western blotting was used to analyse the modification status of the precipitated proteins and their mutant versions. Wild-type proteins and their mutants were expressed in 293T cells. The cells were plated, cultured overnight and transfected using Polyfect (Qiagen) with a plasmid expressing the protein of interest for 24 h. The cell lysates were obtained the same as for Western blotting. Protein concentrations were normalized, then the cell lysates were incubated with anti-Flag M2 agarose-conjugated mouse antibody (Sigma) or GFP-Trap_MA magnetic agarose beads (ChromoTek) for 1-2 h whilst rotating at 4°C. The beads were washed several times with Triton-X100 lysis buffer and eluted with 2x NuPAGE LDS sample buffer (Invitrogen) with 2-Mercaptoethanol (Sigma) or TCEP (Invitrogen). The samples were then analysed by Western Blotting.

To obtain Figures S4C and S4D, control and ARH3 KO 293T cells were plated in 10-cm dishes with DMSO, 5 μM PDD00017273 or 5 μM PDD00017273 and 0.5 μM Olaparib. After 4 days, the cells were transfected with a plasmid expressing H3.1-GFP in the presence of inhibitors for 24 h using Polyfect (Qiagen) following the manufacturer's instructions. The cells were washed with PBS and lysed as described above. Protein concentrations were normalized, and the cell lysates were incubated with GFP-Trap MA magnetic agarose beads (ChromoTek) for 2 h while rotating at 4 °C. The beads were washed five times with Triton X-100 lysis buffer and eluted with 2x NuPAGE LDS sample buffer (Invitrogen) with TCEP (Sigma). The samples were then analysed by Western blotting. For Figures S4E and S4F, control and ARH3 KO 293T cells were plated and transfected 24 h later with a plasmid expressing YFP empty vector or YFP-PARP1 and treated with 5 μM PARGi for 3 days. Then, the cells were trypsinized and counted using MOXI Z Automated Cell Counter, lysed with Triton-X100 lysis buffer and analysed by Western blotting.

7.7. Immunofluorescence and confocal microscopy

Cells were seeded on glass coverslips and grown in the indicated conditions. Cells were washed with PBS and, when indicated, pre-extracted with 0.2% Triton X-100/PBS supplemented with 1 μM Olaparib and 1 μM PARGi PDD00017273 for 5 min and washed with PBS. Then, the cells were fixed with 4% paraformaldehyde (PFA, Sigma) for 15 min supplemented with 1 μM Olaparib and 1 μM PARGi

PDD00017273, washed with PBS, permeabilized with 0.2% Triton X-100/PBS for 10 min and blocked with 10% FBS (Gibco) for 30 min. Incubation with primary rabbit antibodies (anti-pan-ADPr, MABE1016, 1:500; anti-poly-ADPr, ALX-210-890A-0100, 1:500; anti-mono-ADPr AbD33204 (Bonfiglio et al., 2020)) was performed for 2 h at room temperature followed by washing and 1-h incubation with Alexa Fluor 488-conjugated goat anti-rabbit secondary antibody (Molecular Probes/Thermo Fisher Scientific, A11034, 1:500). Coverslips were washed with PBS and counterstained with 0.1 µg/mL DAPI (4,6-diamidino-2-phenylindole, Sigma) in PBS for 10 min. After washing with PBS, coverslips were mounted onto glass slides with Mowiol 4-88 (Sigma). Images were acquired on Olympus Fluoview FV1200 confocal microscope using 40x/1.3, 60x/1.40 and 100x/1.40 Oil UPlanSApo objectives under non-saturating conditions. Image quantification was performed using CellProfiler (McQuin et al., 2018).

7.8. Live-cell imaging following laser micro-irradiation

The experiments in Figures 33 and 39 were performed by Rebecca Smith, Siham Zentout and Sébastien Huet (Université de Rennes 1). Cells were seeded in 8-well imaging chambers and transfected with TagGFP2-PARP1 chromobody (Chromotek) (Figure 22), or GFP-PARP1 WT or mutant (Figure 33) with X-tremeGene HP (Roche) for 48 h prior to imaging. Cells were sensitised with 0.15 µg/mL Hoechst 33342 for 1 h at 37 °C. Immediately before imaging, the medium was replaced with CO_2-independent phenol red-free Leibovitz's L15 medium (Life Technologies) with 20% FBS (Gibco) and, where indicated, Olaparib was added for 30 min prior to imaging. Live-cell imaging of cells maintained at 37 °C with a heating chamber was performed on Nikon Ti-E inverted microscope equipped with a spinning-disk scan head CSU-X1 from Yokogawa at a rotation speed of 5,000 rpm, a Plan APO 60x/1.4N.A. oil-immersion objective lens and a sCMOS ORCA Flash 4.0 camera. Laser micro-irradiation and local photoactivation at 405 nm were performed along a 16 µm line through the nucleus using a single-point scanning head (iLas2 from Roper Scientific) coupled to the epifluorescence backboard of the microscope. To ensure reproducibility, laser power at 405 nm was set to 125 µW at the sample level. Cells were maintained at 37 °C with a heating chamber. Protein recruitment was quantified using custom-made MATLAB (MathWorks) routines available in a GitHub repository at https://github.com/sehuet/Recruitment-break.

7.9. Flow cytometry

Cells were seeded in 6-well plates, treated and incubated with 10 mM EdU for 1 or 24 h at the end of treatment. Cells were harvested by trypsinization and labelled using the Click-iT Plus EdU Alexa Fluor 647 Flow Cytometry Assay Kit (Invitrogen) according to the manufacturer's instructions. For the analysis of DNA damage levels, cells were then stained, while protected from light, with γH2AX primary antibody (Cell Signaling, 9718S, 1:200) in 1% BSA in PBS for 1 h at room temperature, washed once and incubated for 30 min with Alexa Fluor 488-conjugated goat anti-rabbit secondary antibody (Molecular Probes/Thermo Fisher, A11034, 1:500) in 1% BSA in PBS. For DAPI staining, cell pellets were resuspended in 1 mg/mL DAPI solution in PBS and incubated, protected from light, for 10 min. Cells were washed in PBS and analysed immediately after staining on Cytoflex LX (Beckman Coulter) or Cytek DxP8 (Becton Dickinson). Post-acquisition analysis was performed in FlowJo software (BD Biosciences).

7.10. Cell proliferation assays

Cells were plated at low densities in 6-well plates (700 cells/well for U2OS and SUM159PT cells, 800 cells/well for HeLa cells, 900 cells/well for SUM149PT, U251 and U2OS Flp-In T-Rex cells) and grown in the indicated conditions for 11 days. Cells were fixed and stained with 0.5% crystal violet in 25% methanol for 30 min, washed and air-dried. For patient-derived primary human fibroblasts crystal violet assays, 1,400 cells/well were plated in 6-well plates in the indicated conditions. Media containing DMSO or fresh inhibitors was replaced every 4 days and cells were processed after 18 days as described above. Quantification was performed using ImageJ/Fiji software. The surviving fraction at each dose was calculated after normalisation to the plating efficiency of untreated samples. Each experiment was performed in triplicates. For quantification of cell proliferation in Figure S5, U2OS control and ARH3 KO cells were plated in 6-well plates, and were trypsinized and counted after 24 h, 48 h, 72 h, 96 h and 120 h using MOXI Z Automated Cell Counter.

7.11. *In vitro* ADP-ribosylation assays

The experiments to obtain Figure 27A were carried out by Marcin Suskiewicz. 2 µg of histone H3 (1-21) peptide or H3 (1-21) S10MAR peptide, a gift from Ivan Matic (Max Planck Institute for Biology of Ageing), was incubated with 1 µM recombinant human PARP1 protein in reaction buffer (50 mM Tris-HCl, pH 8.0, 100 mM NaCl, 2 mM

$MgCl_2$, activated DNA and 50 μM NAD^+ spiked with ^{32}P-NAD^+ from Perkin Elmer) at 37 °C for 30 min. The experiments to obtain Figure 27B were performed by Kang Zhu. 5 uM H3/H4 tetramer was incubated at room temperature for 20 min with recombinant human 100 nM PARP1 and 2 uM HPF1 proteins, 200 μM NAD^+ and 500 nM DNA duplex (5′-ATCAGATAGCATCTGTGCGGCCGCTTAGGG-3′ and 5′-CCCTAAGCGGCCGCACAGATGCTATCTGAT-3′, Sigma) in the reaction buffer containing Mg^{2+} required by ARH3 (50 mM Tris, pH 7.5, 50 mM NaCl, and 2 mM $MgCl_2$). Cold NAD^+ was spiked with a small amount of ^{32}P-NAD^+. Under the reaction conditions, only H3 appears to be modified. The ADP-ribosylation reactions were stopped by addition of 2 μM Olaparib. ADP-ribose hydrolysis was started by adding recombinant human 1 μM ARH3 and/or PARG proteins and allowed to proceed at room temperature for 50 min. All concentrations are final, after mixing. Reactions were stopped by addition of 4x NuPAGE LDS sample buffer (Invitrogen) and incubation at 95 °C for 5 min. Samples were then analysed by SDS-PAGE, including Instant Blue staining (Sigma), washing with water and gel drying, followed by autoradiography.

7.12. RNA-sequencing data generation and analysis

Control and ARH3 KO U2OS cells were treated with DMSO or 25 μM PARGi for 4 days. RNA extraction was carried out by Thomas Agnew. RNA was extracted using Direct-zol RNA MiniPrep Plus kit (Zymo Research) according to the manufacturer's instructions. PolyA library preparation and RNA sequencing was performed by the Oxford Genomics Centre at the Wellcome Centre for Human Genetics. Briefly, RNA was quantified using RiboGreen (Invitrogen) on the FLUOstar OPTIMA plate reader (BMG Labtech) and the size profile and integrity analysed on the 2200 or 4200 TapeStation (Agilent, RNA ScreenTape). Input material was normalised to 100 ng prior to library preparation. Polyadenylated transcript enrichment and strand specific library preparation was completed using NEBNext Ultra II Directional RNA library prep kit following manufacturer's instructions. Libraries were amplified on a Tetrad (Bio-Rad) using in-house unique dual indexing primers based on (Lamble et al., 2013). Individual libraries were normalised using Qubit, and the size profile was analysed on the 2200 or 4200 TapeStation. Individual libraries were normalized and pooled together accordingly. The pooled library was diluted to ~10 nM for storage. The 10 nM library was denatured and further diluted prior to loading on the sequencer. Paired end sequencing was performed using a NovaSeq 6000 S4 Reagent Kit v1.5 (300 cycles).

Data analysis was carried out by Michael Tellier. Adapters were trimmed with Cutadapt version 1.18 (Martin, 2011) in paired-end mode with the following parameters: -q 15, 10 --minimum-length 10 -A AGATCGGAAGAGCGTCGTGTAGGGAAAGAGTGT -a AGATCGGAAGAGCACACGTCTGAACTCCAGTCA. Trimmed reads were first mapped to the ribosomal repeats to remove all the reads mapping to rDNA genes with STAR version 2.7.3a (Dobin et al., 2013) and the parameters: --runThreadN 16 --readFilesCommand gunzip -c –k --outReadsUnmapped Fastx --limitBAMsortRAM 20000000000 --outSAMtype BAM SortedByCoordinate. The unmapped reads were mapped to the human hg38 reference genome with STAR and the parameters --runThreadN 16 --readFilesCommand gunzip -c –k --limitBAMsortRAM 20000000000 --outSAMtype BAM SortedByCoordinate. SAMtools version 1.9 (Li et al., 2009) was used to retain only properly mapped reads and produced strand-specific bam files. FPKM-normalized bigwig files were created with deepTools version 3.4.2 (Ramírez et al., 2016) bamCoverage tool with the parameters -bs 10 -p max --normalizeUsing RPKM. For differential expression analysis, the aligned reads were aggregated on the Gencode V31 annotation with HTseq-count version 0.11.3 (Anders et al., 2015) and the list of differentially expressed genes obtained with DESeq2 version 3.12 (Love et al., 2014), keeping only the genes with a fold change < -1.5 or > 1.5 and an adjusted p-value of 0.05. The values for the correlation heatmap were obtained with deepTools multiBigwigSummary with the parameters bins and –bs 10000 followed by plotCorrelation --outFileCorMatrix and the parameters --corMethod pearson --skipZeros –removeOutliers. The list of normalized read counts for each gene across each sample was obtained with DESeq2. Reactome pathways enrichment from the MSigDB database (c2.cp.reactome.v7.2.symbols.gmt) were performed using GSEA version 4.1.0 (Mootha et al., 2003; Subramanian et al., 2005) with the following parameters: number of permutations: 1000; permutation type: gene_set; enrichment statistic: weighted; metric for ranking genes: Signal2Noise. The generated RNA-sequencing data are available in the Gene Expression Omnibus repository, https://www.ncbi.nlm.nih.gov/geo (accession GEO: GSE167060).

7.13. Quantification and statistical analysis

Prism 7 (GraphPad) was used for statistical analysis, where *p<0.05, **p<0.01, ***p<0.001, ****p<0.0001. Details of statistical analyses are described in the figure legends.

References

Abplanalp, J., Leutert, M., Frugier, E., Nowak, K., Feurer, R., Kato, J., Kistemaker, H.V.A., Filippov, D. V., Moss, J., Caflisch, A., et al. (2017). Proteomic analyses identify ARH3 as a serine mono-ADP-ribosylhydrolase. Nat. Commun. *8*, 2055.

Ahel, D., Horejsí, Z., Wiechens, N., Polo, S.E., Garcia-Wilson, E., Ahel, I., Flynn, H., Skehel, M., West, S.C., Jackson, S.P., et al. (2009). Poly(ADP-ribose)-dependent regulation of DNA repair by the chromatin remodeling enzyme ALC1. Science *325*, 1240–1243.

Ahel, I., Ahel, D., Matsusaka, T., Clark, A.J., Pines, J., Boulton, S.J., and West, S.C. (2008). Poly(ADP-ribose)-binding zinc finger motifs in DNA repair/checkpoint proteins. Nature.

Ahmadian, M.R., Stege, P., Scheffzek, K., and Wittinghofer, A. (1997). Confirmation of the arginine-finger hypothesis for the GAP-stimulated GTP-hydrolysis reaction of Ras. Nat. Struct. Biol. 1997 49 *4*, 686–689.

Amé, J.-C., Rolli, V., Schreiber, V., Niedergang, C., Apiou, F., Decker, P., Muller, S., Höger, T., Murcia, J.M., and de Murcia, G. (1999). PARP-2, A Novel Mammalian DNA Damage-dependent Poly(ADP-ribose) Polymerase. J. Biol. Chem. *274*, 17860–17868.

Anders, S., Pyl, P.T., and Huber, W. (2015). HTSeq--a Python framework to work with high-throughput sequencing data. Bioinformatics *31*, 166–169.

Andronikou, C., and Rottenberg, S. (2021). Studying PAR-Dependent Chromatin Remodeling to Tackle PARPi Resistance. Trends Mol. Med. *27*, 630–642.

Azarm, K., and Smith, S. (2020). Nuclear PARPs and genome integrity. Genes Dev. *34*, 285–301.

Bacic, L., Gaullier, G., Sabantsev, A., Lehmann, L.C., Brackmann, K., Dimakou, D., Halic, M., Hewitt, G., Boulton, S.J., and Deindl, S. (2021). Structure and dynamics of the chromatin remodeler alc1 bound to a parylated nucleosome. Elife *10*.

Balasubramaniam, S., Beaver, J.A., Horton, S., Fernandes, L.L., Tang, S., Horne, H.N., Liu, J., Liu, C., Schrieber, S.J., Yu, J., et al. (2017). FDA approval summary: Rucaparib for the treatment of patients with deleterious BRCA mutation–associated advanced ovarian cancer. Clin. Cancer Res. *23*, 7165–7170.

Barkauskaite, E., Brassington, A., Tan, E.S., Warwicker, J., Dunstan, M.S., Banos, B., Lafite, P., Ahel, M., Mitchison, T.J., Ahel, I., et al. (2013). Visualization of poly(ADP-ribose) bound to PARG reveals inherent balance between exo- and endo-glycohydrolase activities. Nat. Commun. *4*, 2164.

Barkauskaite, E., Jankevicius, G., and Ahel, I. (2015). Structures and Mechanisms of Enzymes Employed in the Synthesis and Degradation of PARP-Dependent Protein ADP-Ribosylation. Mol. Cell *58*, 935–946.

Bartlett, E., Bonfiglio, J.J., Prokhorova, E., Colby, T., Zobel, F., Ahel, I., and Matic, I. (2018). Interplay of Histone Marks with Serine ADP-Ribosylation. Cell Rep. *24*, 3488-3502.e5.

Bártová, E., Šustáčková, G., Stixová, L., Kozubek, S., Legartová, S., and Foltánková, V. (2011). Recruitment of Oct4 protein to UV-damaged chromatin in embryonic stem cells. PLoS One *6*.

Baxter, J.S., Zatreanu, D., Pettitt, S.J., and Lord, C.J. (2022). Resistance to DNA repair inhibitors in

cancer . Mol. Oncol.

Behrends, M., and Engmann, O. (2020). Linker histone H1.5 is an underestimated factor in differentiation and carcinogenesis. Environ. Epigenetics *6*.

Beijer, D., Agnew, T., Rack, J.G.M., Prokhorova, E., Deconinck, T., Ceulemans, B., Peric, S., Rasic, V.M., Jonghe, P. De, Ahel, I., et al. (2021). Biallelic ADPRHL2 mutations in complex neuropathy affect ADP ribosylation and DNA damage response. Life Sci. Alliance *4*, e202101057.

Bilan, V., Leutert, M., Nanni, P., Panse, C., and Hottiger, M.O. (2017). Combining Higher-Energy Collision Dissociation and Electron-Transfer/Higher-Energy Collision Dissociation Fragmentation in a Product-Dependent Manner Confidently Assigns Proteomewide ADP-Ribose Acceptor Sites. Anal. Chem. *89*, 1523–1530.

Bilokapic, S., Suskiewicz, M.J., Ahel, I., and Halic, M. (2020). Bridging of DNA breaks activates PARP2–HPF1 to modify chromatin. Nature *585*, 609–613.

Blessing, C., Mandemaker, I.K., Gonzalez-Leal, C., Preisser, J., Schomburg, A., and Ladurner, A.G. (2020). The Oncogenic Helicase ALC1 Regulates PARP Inhibitor Potency by Trapping PARP2 at DNA Breaks. Mol. Cell *80*, 862-875.e6.

Bonfiglio, J.J., Fontana, P., Zhang, Q., Colby, T., Gibbs-Seymour, I., Atanassov, I., Bartlett, E., Zaja, R., Ahel, I., and Matic, I. (2017). Serine ADP-Ribosylation Depends on HPF1. Mol. Cell *65*, 932-940.e6.

Bonfiglio, J.J., Leidecker, O., Dauben, H., Longarini, E.J., Colby, T., San Segundo-Acosta, P., Perez, K.A., and Matic, I. (2020). An HPF1/PARP1-Based Chemical Biology Strategy for Exploring ADP-Ribosylation. Cell *183*, 1086-1102.e23.

Bouwman, P., Aly, A., Escandell, J.M., Pieterse, M., Bartkova, J., Van Der Gulden, H., Hiddingh, S., Thanasoula, M., Kulkarni, A., Yang, Q., et al. (2010). 53BP1 loss rescues BRCA1 deficiency and is associated with triple-negative and BRCA-mutated breast cancers. Nat. Struct. Mol. Biol. *17*, 688–695.

Bryant, H.E., Schultz, N., Thomas, H.D., Parker, K.M., Flower, D., Lopez, E., Kyle, S., Meuth, M., Curtin, N.J., and Helleday, T. (2005). Specific killing of BRCA2-deficient tumours with inhibitors of poly(ADP-ribose) polymerase. Nature *434*, 913–917.

Buch-Larsen, S.C., Hendriks, I.A., Lodge, J.M., Rykær, M., Furtwängler, B., Shishkova, E., Westphall, M.S., Coon, J.J., and Nielsen, M.L. (2020). Mapping Physiological ADP-Ribosylation Using Activated Ion Electron Transfer Dissociation. Cell Rep. *32*, 108176.

Buch-Larsen, S.C., Rebak, A.K.L.F.S., Hendriks, I.A., and Nielsen, M.L. (2021). Temporal and Site-Specific ADP-Ribosylation Dynamics upon Different Genotoxic Stresses. Cells 2021, Vol. 10, Page 2927 *10*, 2927.

Caldecott, K.W. (2014). Protein ADP-ribosylation and the cellular response to DNA strand breaks. DNA Repair (Amst). *19*, 108–113.

Callen, E., Di Virgilio, M., Kruhlak, M.J., Nieto-Soler, M., Wong, N., Chen, H.T., Faryabi, R.B., Polato, F., Santos, M., Starnes, L.M., et al. (2013). 53BP1 mediates productive and mutagenic DNA repair through distinct phosphoprotein interactions. Cell *153*, 1266–1280.

Challa, S., Stokes, M.S., and Kraus, W.L. (2021). MARTs and MARylation in the Cytosol: Biological Functions, Mechanisms of Action, and Therapeutic Potential. Cells 2021, Vol. 10, Page 313 *10*, 313.

Chambon, P., Weill, J.D., and Mandel, P. (1963). Nicotinamide mononucleotide activation of new DNA-dependent polyadenylic acid synthesizing nuclear enzyme. Biochem. Biophys. Res. Commun. *11*, 39–43.

Chapman, J.R., Barral, P., Vannier, J.B., Borel, V., Steger, M., Tomas-Loba, A., Sartori, A.A., Adams, I.R., Batista, F.D., and Boulton, S.J. (2013). RIF1 Is Essential for 53BP1-Dependent Nonhomologous End Joining and Suppression of DNA Double-Strand Break Resection. Mol. Cell *49*, 858–871.

Chaudhuri, A.R., Callen, E., Ding, X., Gogola, E., Duarte, A.A., Lee, J.E., Wong, N., Lafarga, V., Calvo, J.A., Panzarino, N.J., et al. (2016). Replication fork stability confers chemoresistance in BRCA-deficient cells. Nature *535*, 382–387.

Chen, S.H., and Yu, X. (2019). Targeting dePARylation selectively suppresses DNA repair–defective and PARP inhibitor–resistant malignancies. Sci. Adv. *5*, eaav4340.

Chen, Q., Kassab, M.A., Dantzer, F., and Yu, X. (2018). PARP2 mediates branched poly ADP-ribosylation in response to DNA damage. Nat. Commun. *9*, 3233.

Chou, D.M., Adamson, B., Dephoure, N.E., Tan, X., Nottke, A.C., Hurov, K.E., Gygi, S.P., Colaiacovo, M.P., and Elledge, S.J. (2010). A chromatin localization screen reveals poly (ADP ribose)-regulated recruitment of the repressive polycomb and NuRD complexes to sites of DNA damage. Proc. Natl. Acad. Sci. *107*, 18475–18480.

Christie, E.L., Pattnaik, S., Beach, J., Copeland, A., Rashoo, N., Fereday, S., Hendley, J., Alsop, K., Brady, S.L., Lamb, G., et al. (2019). Multiple ABCB1 transcriptional fusions in drug resistant high-grade serous ovarian and breast cancer. Nat. Commun. *10*, 1295.

Clark, J.B., Ferris, G.M., and Pinder, S. (1971). Inhibition of nuclear NAD nucleosidase and poly ADP-ribose polymerase activity from rat liver by nicotinamide and 5'-methyl nicotinamide. Biochim. Biophys. Acta *238*, 82–85.

Clements, K.E., Schleicher, E.M., Thakar, T., Hale, A., Dhoonmoon, A., Tolman, N.J., Sharma, A., Liang, X., Imamura Kawasawa, Y., Nicolae, C.M., et al. (2020). Identification of regulators of poly-ADP-ribose polymerase inhibitor response through complementary CRISPR knockout and activation screens. Nat. Commun. *11*, 6118.

Cohen, M.S. (2020). Interplay between compartmentalized NAD + synthesis and consumption: a focus on the PARP family. Genes Dev. *34*, 254–262.

Cortes, U., Tong, W.-M., Coyle, D.L., Meyer-Ficca, M.L., Meyer, R.G., Petrilli, V., Herceg, Z., Jacobson, E.L., Jacobson, M.K., and Wang, Z.-Q. (2004). Depletion of the 110-Kilodalton Isoform of Poly(ADP-Ribose) Glycohydrolase Increases Sensitivity to Genotoxic and Endotoxic Stress in Mice. Mol. Cell. Biol. *24*, 7163–7178.

Crawford, K., Bonfiglio, J.J., Mikoč, A., Matic, I., and Ahel, I. (2018). Specificity of reversible ADP-ribosylation and regulation of cellular processes. Crit. Rev. Biochem. Mol. Biol. *53*, 64–82.

Curtin, N.J., and Szabo, C. (2020). Poly(ADP-ribose) polymerase inhibition: past, present and future. Nat. Rev. Drug Discov. 2020 1910 *19*, 711–736.

Danhauser, K., Alhaddad, B., Makowski, C., Piekutowska-Abramczuk, D., Syrbe, S., Gomez-Ospina, N., Manning, M.A., Kostera-Pruszczyk, A., Krahn-Peper, C., Berutti, R., et al. (2018). Bi-allelic ADPRHL2 Mutations Cause Neurodegeneration with Developmental Delay, Ataxia, and Axonal Neuropathy. Am. J. Hum. Genet. *103*, 817–825.

Daniels, C.M., Ong, S.E., and Leung, A.K.L. (2015). The Promise of Proteomics for the Study of ADP-Ribosylation. Mol. Cell *58*, 911–924.

DeWeirdt, P.C., Sangree, A.K., Hanna, R.E., Sanson, K.R., Hegde, M., Strand, C., Persky, N.S., and Doench, J.G. (2020). Genetic screens in isogenic mammalian cell lines without single cell cloning. Nat. Commun. *11*, 752.

Dobin, A., Davis, C.A., Schlesinger, F., Drenkow, J., Zaleski, C., Jha, S., Batut, P., Chaisson, M., and Gingeras, T.R. (2013). STAR: ultrafast universal RNA-seq aligner. Bioinformatics *29*, 15–21.

Drown, B.S., Shirai, T., Rack, J.G.M., Ahel, I., and Hergenrother, P.J. (2018). Monitoring Poly(ADP-ribosyl)glycohydrolase Activity with a Continuous Fluorescent Substrate. Cell Chem. Biol. *25*, 1562-1570.e19.

Edwards, S.L., Brough, R., Lord, C.J., Natrajan, R., Vatcheva, R., Levine, D.A., Boyd, J., Reis-Filho, J.S., and Ashworth, A. (2008). Resistance to therapy caused by intragenic deletion in BRCA2. Nature *451*, 1111–1115.

Endicott, J.A., Noble, M.E.M., and Johnson, L.N. (2012). The structural basis for control of eukaryotic protein kinases. Annu. Rev. Biochem. *81*, 587–613.

Fahrer, J., Kranaster, R., Altmeyer, M., Marx, A., and Bürkle, A. (2007). Quantitative analysis of the binding affinity of poly(ADP-ribose) to specific binding proteins as a function of chain length. Nucleic Acids Res. *35*, e143–e143.

Falchook, G.S., Patel, M.R., Yap, T.A., McEachern, K., Kuplast-Barr, K., Utley, L., Cleary, L., Manyak, E., Bozon, V., Parasuraman, S., et al. (2021). A first-in-human phase 1 study of a novel PARP7 inhibitor RBN-2397 in patients with advanced solid tumors. J. Clin. Oncol. *39*, 3000–3000.

Farmer, H., McCabe, N., Lord, C.J., Tutt, A.N.J., Johnson, D.A., Richardson, T.B., Santarosa, M., Dillon, K.J., Hickson, I., Knights, C., et al. (2005). Targeting the DNA repair defect in BRCA mutant cells as a therapeutic strategy. Nature *434*, 917–921.

Farreś, J., Martín-Caballero, J., Martínez, C., Lozano, J.J., Llacuna, L., Ampurdanés, C., Ruiz-Herguido, C., Dantzer, F., Schreiber, V., Villunger, A., et al. (2013). Parp-2 is required to maintain hematopoiesis following sublethal γ-irradiation in mice. Blood *122*, 44–54.

Ferros, A.M., and Olivera, B.M. (1982). Poly(ADP-ribosylation) in vitro. Reaction parameters and enzyme mechanism. J. Biol. Chem. *257*, 7808–7813.

Fontana, P., Bonfiglio, J.J., Palazzo, L., Bartlett, E., Matic, I., and Ahel, I. (2017). Serine ADP-ribosylation reversal by the hydrolase ARH3. Elife *6*, e28533.

Fugger, K., Hewitt, G., West, S.C., and Boulton, S.J. (2021). Tackling PARP inhibitor resistance. Trends in Cancer *7*, 1102–1118.

Gaullier, G., Roberts, G., Muthurajan, U.M., Bowerman, S., Rudolph, J., Mahadevan, J., Jha, A., Rae,

P.S., and Luger, K. (2020). Bridging of nucleosome-proximal DNA double-strand breaks by PARP2 enhances its interaction with HPF1. PLoS One *15*.

Ghosh, S.G., Becker, K., Huang, H., Dixon-Salazar, T., Chai, G., Salpietro, V., Al-Gazali, L., Waisfisz, Q., Wang, H., Vaux, K.K., et al. (2018). Biallelic Mutations in ADPRHL2, Encoding ADP-Ribosylhydrolase 3, Lead to a Degenerative Pediatric Stress-Induced Epileptic Ataxia Syndrome. Am. J. Hum. Genet. *103*, 431–439.

Gibbs-Seymour, I., Fontana, P., Rack, J.G.M., and Ahel, I. (2016). HPF1/C4orf27 Is a PARP-1-Interacting Protein that Regulates PARP-1 ADP-Ribosylation Activity. Mol. Cell *62*, 432–442.

Gibson, B.A., Zhang, Y., Jiang, H., Hussey, K.M., Shrimp, J.H., Lin, H., Schwede, F., Yu, Y., and Kraus, W.L. (2016). Chemical genetic discovery of PARP targets reveals a role for PARP-1 in transcription elongation. Science (80-.). *353*, 45–50.

Gibson, B.A., Conrad, L.B., Huang, D., and Kraus, W.L. (2017). Generation and Characterization of Recombinant Antibody-like ADP-Ribose Binding Proteins. Biochemistry *56*, 6305–6316.

Gill, D.M., Pappenheimer, A.M., Brown, R., and Kurnick, J.T. (1969). Studies on the mode of action of diphtheria toxin. VII. Toxin-stimulated hydrolysis of nicotinamide adenine dinucleotide in mammalian cell extracts. J. Exp. Med. *129*, 1–21.

Gogola, E., Duarte, A.A., de Ruiter, J.R., Wiegant, W.W., Schmid, J.A., de Bruijn, R., James, D.I., Guerrero Llobet, S., Vis, D.J., Annunziato, S., et al. (2018). Selective Loss of PARG Restores PARylation and Counteracts PARP Inhibitor-Mediated Synthetic Lethality. Cancer Cell *33*, 1078-1093.e12.

Gomez, M.K., Illuzzi, G., Colomer, C., Churchman, M., Hollis, R.L., O'connor, M.J., Gourley, C., Leo, E., and Melton, D.W. (2020). Identifying and overcoming mechanisms of PARP inhibitor resistance in homologous recombination repair-deficient and repair-proficient high grade serous ovarian cancer cells. Cancers (Basel). *12*, 11–14.

Grady, S.L., Hwang, J., Vastag, L., Rabinowitz, J.D., and Shenk, T. (2012). Herpes Simplex Virus 1 Infection Activates Poly(ADP-Ribose) Polymerase and Triggers the Degradation of Poly(ADP-Ribose) Glycohydrolase. J. Virol. *86*, 8259–8268.

Gravells, P., Grant, E., Smith, K.M., James, D.I., and Bryant, H.E. (2017). Specific killing of DNA damage-response deficient cells with inhibitors of poly(ADP-ribose) glycohydrolase. DNA Repair (Amst). *52*, 81–91.

Groslambert, J., Prokhorova, E., and Ahel, I. (2021). ADP-ribosylation of DNA and RNA. DNA Repair (Amst). *105*.

Guillemette, S., Serra, R.W., Peng, M., Hayes, J.A., Konstantinopoulos, P.A., Green, M.R., Green, M.R., and Cantor, S.B. (2015). Resistance to therapy in BRCA2 mutant cells due to loss of the nucleosome remodeling factor CHD4. Genes Dev. *29*, 489–494.

Gupte, R., Liu, Z., and Kraus, W.L. (2017). PARPs and ADP-ribosylation: recent advances linking molecular functions to biological outcomes. Genes Dev. *31*, 101–126.

Haikarainen, T., Maksimainen, M.M., Obaji, E., and Lehtiö, L. (2018). Development of an Inhibitor Screening Assay for Mono-ADP-Ribosyl Hydrolyzing Macrodomains Using AlphaScreen Technology.

SLAS Discov. Adv. Sci. Drug Discov. *23*, 255–263.

Hanai, S., Kanai, M., Ohashi, S., Okamoto, K., Yamada, M., Takahashi, H., and Miwa, M. (2004). Loss of poly(ADP-ribose) glycohydrolase causes progressive neurodegeneration in Drosophila melanogaster. Proc. Natl. Acad. Sci. *101*, 82–86.

Hananya, N., Daley, S.K., Bagert, J.D., and Muir, T.W. (2021). Synthesis of ADP-Ribosylated Histones Reveals Site-Specific Impacts on Chromatin Structure and Function. J. Am. Chem. Soc. *143*, 10847–10852.

Hanzlikova, H., Kalasova, I., Demin, A.A., Pennicott, L.E., Cihlarova, Z., and Caldecott, K.W. (2018). The Importance of Poly(ADP-Ribose) Polymerase as a Sensor of Unligated Okazaki Fragments during DNA Replication. Mol. Cell *71*, 319-331.e3.

Hanzlikova, H., Prokhorova, E., Krejcikova, K., Cihlarova, Z., Kalasova, I., Kubovciak, J., Sachova, J., Hailstone, R., Brazina, J., Ghosh, S., et al. (2020). Pathogenic ARH3 mutations result in ADP-ribose chromatin scars during DNA strand break repair. Nat. Commun. *11*, 3391.

Hartwell, L.H., Szankasi, P., Roberts, C.J., Murray, A.W., and Friend, S.H. (1997). Integrating genetic approaches into the discovery of anticancer drugs. Science (80-.).

Hein, M.Y., Hubner, N.C., Poser, I., Cox, J., Nagaraj, N., Toyoda, Y., Gak, I.A., Weisswange, I., Mansfeld, J., Buchholz, F., et al. (2015). A Human Interactome in Three Quantitative Dimensions Organized by Stoichiometries and Abundances. Cell *163*, 712–723.

Hendriks, I.A., Larsen, S.C., and Nielsen, M.L. (2019). An Advanced Strategy for Comprehensive Profiling of ADP-ribosylation Sites Using Mass Spectrometry-based Proteomics. Mol. Cell. Proteomics *18*, 1010–1026.

Hendriks, I.A., Buch-Larsen, S.C., Prokhorova, E., Elsborg, J.D., Rebak, A.K.L.F.S., Zhu, K., Ahel, D., Lukas, C., Ahel, I., and Nielsen, M.L. (2021). The regulatory landscape of the human HPF1- and ARH3-dependent ADP-ribosylome. Nat. Commun. *12*, 1–16.

Hewitt, G., Borel, V., Segura-Bayona, S., Takaki, T., Ruis, P., Bellelli, R., Lehmann, L.C., Sommerova, L., Vancevska, A., Tomas-Loba, A., et al. (2021). Defective ALC1 nucleosome remodeling confers PARPi sensitization and synthetic lethality with HRD. Mol. Cell *81*, 767-783.e11.

Honjo, T., Nishizuka, Y., Hayaishi, O., and Kato, I. (1968). Diphtheria Toxin-dependent Adenosine Diphosphate Ribosylation of Aminoacyl Transferase II and Inhibition of Protein Synthesis. J. Biol. Chem. *243*, 3553–3555.

Hopkins, T.A., Shi, Y., Rodriguez, L.E., Solomon, L.R., Donawho, C.K., Di Giammarino, E.L., Panchal, S.C., Wilsbacher, J.L., Gao, W., Olson, A.M., et al. (2015). Mechanistic dissection of PARP1 trapping and the impact on in vivo tolerability and efficacy of PARP inhibitors. Mol. Cancer Res. *13*, 1465–1477.

Houl, J.H., Ye, Z., Brosey, C.A., Balapiti-Modarage, L.P.F., Namjoshi, S., Bacolla, A., Laverty, D., Walker, B.L., Pourfarjam, Y., Warden, L.S., et al. (2019). Selective small molecule PARG inhibitor causes replication fork stalling and cancer cell death. Nat. Commun. *10*, 5654.

Hoy, S.M. (2018). Talazoparib: First Global Approval. Drugs *78*, 1939–1946.

https://media.ideayabio.com/2022-01-10-IDEAYA-Biosciences-Announces-Corporate-and-Portfolio-Update-for-J-P-Morgan-40th-Annual-Healthcare-Conference IDEAYA Biosciences Announces Corporate and Portfolio Update for J.P. Morgan 40th Annual Healthcare Conference - Jan 10, 2022.

Huang, D., Camacho, C. V, Setlem, R., Ryu, K.W., Parameswaran, B., Gupta, R.K., and Kraus, W.L. (2020). Functional Interplay between Histone H2B ADP-Ribosylation and Phosphorylation Controls Adipogenesis. Mol. Cell *79*, 934-949.e14.

Ison, G., Howie, L.J., Amiri-Kordestani, L., Zhang, L., Tang, S., Sridhara, R., Pierre, V., Charlab, R., Ramamoorthy, A., Song, P., et al. (2018). FDA approval summary: Niraparib for the maintenance treatment of patients with recurrent ovarian cancer in response to platinum-based chemotherapy. Clin. Cancer Res. *24*, 4066–4071.

James, D.I., Smith, K.M., Jordan, A.M., Fairweather, E.E., Griffiths, L.A., Hamilton, N.S., Hitchin, J.R., Hutton, C.P., Jones, S., Kelly, P., et al. (2016). First-in-class chemical probes against poly(ADP-ribose) glycohydrolase (PARG) inhibit DNA repair with differential pharmacology to olaparib. ACS Chem. Biol. *11*, 3179–3190.

Jaspers, J.E., Kersbergen, A., Boon, U., Sol, W., Van Deemter, L., Zander, S.A., Drost, R., Wientjens, E., Ji, J., Aly, A., et al. (2013). Loss of 53BP1 causes PARP inhibitor resistance in BRCA1-mutated mouse mammary tumors. Cancer Discov. *3*, 68–81.

Johannes, J.W., Balazs, A., Barratt, D., Bista, M., Chuba, M.D., Cosulich, S., Critchlow, S.E., Degorce, S.L., Di Fruscia, P., Edmondson, S.D., et al. (2021). Discovery of 5-{4-[(7-Ethyl-6-oxo-5,6-dihydro-1,5-naphthyridin-3-yl)methyl]piperazin-1-yl}- N -methylpyridine-2-carboxamide (AZD5305): A PARP1–DNA Trapper with High Selectivity for PARP1 over PARP2 and Other PARPs. J. Med. Chem. *64*, 14498–14512.

Juhász, S., Smith, R., Schauer, T., Spekhardt, D., Mamar, H., Zentout, S., Chapuis, C., Huet, S., and Timinszky, G. (2020). The chromatin remodeler ALC1 underlies resistance to PARP inhibitor treatment. Sci. Adv. *6*, 8626–8644.

Kalashnikova, A.A., Rogge, R.A., and Hansen, J.C. (2016). Linker histone H1 and protein-protein interactions. Biochim. Biophys. Acta *1859*, 455.

Kawamitsu, H., Hoshino, H. o., Okada, H., Miwa, M., Sugimura, T., and Momoi, H. (1984). Monoclonal Antibodies to Poly(adenosine diphosphate ribose) Recognize Different Structures. Biochemistry *23*, 3771–3777.

Kim, C., Chen, C., and Yu, Y. (2021). Avoid the trap: Targeting PARP1 beyond human malignancy. Cell Chem. Biol. *28*, 456–462.

Kim, D.S., Challa, S., Jones, A., and Kraus, W.L. (2020a). PARPs and ADP-ribosylation in RNA biology: From RNA expression and processing to protein translation and proteostasis. Genes Dev. *34*, 302–320.

Kim, G., Ison, G., McKee, A.E., Zhang, H., Tang, S., Gwise, T., Sridhara, R., Lee, E., Tzou, A., Philip, R., et al. (2015). FDA approval summary: Olaparib monotherapy in patients with deleterious germline BRCA-mutated advanced ovarian cancer treated with three or more lines of chemotherapy. Clin. Cancer Res. *21*, 4257–4261.

Kim, J.J., Lee, S.Y., Choi, J.H., Woo, H.G., Xhemalce, B., and Miller, K.M. (2020b). PCAF-Mediated Histone Acetylation Promotes Replication Fork Degradation by MRE11 and EXO1 in BRCA-Deficient Cells. Mol. Cell *80*, 327-344.e8.

Kinosada, H., Okada-Iwasaki, R., Kunieda, K., Suzuki-Imaizumi, M., Takahashi, Y., Miyagi, H., Suzuki, M., Motosawa, K., Watanabe, M., Mie, M., et al. (2021). The dual pocket binding novel tankyrase inhibitor K-476 enhances the efficacy of immune checkpoint inhibitor by attracting CD8+ T cells to tumors. Am. J. Cancer Res. *11*, 264.

Kliza, K.W., Liu, Q., Roosenboom, L.W.M., Jansen, P.W.T.C., Filippov, D. V., and Vermeulen, M. (2021). Reading ADP-ribosylation signaling using chemical biology and interaction proteomics. Mol. Cell *81*, 4552-4567.e8.

Koh, D.W., Lawler, A.M., Poitras, M.F., Sasaki, M., Wattler, S., Nehls, M.C., Stöger, T., Poirier, G.G., Dawson, V.L., and Dawson, T.M. (2004). Failure to degrade poly(ADP-ribose) causes increased sensitivity to cytotoxicity and early embryonic lethality. Proc. Natl. Acad. Sci. U. S. A. *101*, 17699–17704.

Krastev, D.B., Li, S., Sun, Y., Wicks, A.J., Hoslett, G., Weekes, D., Badder, L.M., Knight, E.G., Marlow, R., Pardo, M.C., et al. (2022). The ubiquitin-dependent ATPase p97 removes cytotoxic trapped PARP1 from chromatin. Nat. Cell Biol. *24*, 62–73.

Kumamoto, S., Nishiyama, A., Chiba, Y., Miyashita, R., Konishi, C., Azuma, Y., and Nakanishi, M. (2021). HPF1-dependent PARP activation promotes LIG3-XRCC1-mediated backup pathway of Okazaki fragment ligation. Nucleic Acids Res. *49*, 5003–5016.

LaFargue, C.J., Dal Molin, G.Z., Sood, A.K., and Coleman, R.L. (2019). Exploring and comparing adverse events between PARP inhibitors. Lancet Oncol. *20*, e15–e28.

Lamble, S., Batty, E., Attar, M., Buck, D., Bowden, R., Lunter, G., Crook, D., El-Fahmawi, B., and Piazza, P. (2013). Improved workflows for high throughput library preparation using the transposome-based nextera system. BMC Biotechnol. *13*, 104.

Langelier, M.F., Billur, R., Sverzhinsky, A., Black, B.E., and Pascal, J.M. (2021). HPF1 dynamically controls the PARP1/2 balance between initiating and elongating ADP-ribose modifications. Nat. Commun. 2021 121 *12*, 1–14.

Larsen, S.C., Hendriks, I.A., Lyon, D., Jensen, L.J., and Nielsen, M.L. (2018). Systems-wide Analysis of Serine ADP-Ribosylation Reveals Widespread Occurrence and Site-Specific Overlap with Phosphorylation. Cell Rep. *24*, 2493-2505.e4.

Lawrence, M., Daujat, S., and Schneider, R. (2016). Lateral Thinking: How Histone Modifications Regulate Gene Expression. Trends Genet. *32*, 42–56.

Leidecker, O., Bonfiglio, J.J., Colby, T., Zhang, Q., Atanassov, I., Zaja, R., Palazzo, L., Stockum, A., Ahel, I., and Matic, I. (2016). Serine is a new target residue for endogenous ADP-ribosylation on histones. Nat. Chem. Biol. *12*, 998–1000.

Leung, A.K.L. (2020). Poly(ADP-ribose): A Dynamic Trigger for Biomolecular Condensate Formation. Trends Cell Biol. *30*, 370.

Li, H., Handsaker, B., Wysoker, A., Fennell, T., Ruan, J., Homer, N., Marth, G., Abecasis, G., and

Durbin, R. (2009). The Sequence Alignment/Map format and SAMtools. Bioinformatics *25*, 2078–2079.

Li, P., Zhen, Y., and Yu, Y. (2019). Site-specific analysis of the Asp- and Glu-ADP-ribosylated proteome by quantitative mass spectrometry. In Methods in Enzymology, (Methods Enzymol), pp. 301–321.

Li, Z., Li, Y., Tang, M., Peng, B., Lu, X., Yang, Q., Zhu, Q., Hou, T., Li, M., Liu, C., et al. (2018). Destabilization of linker histone H1.2 is essential for ATM activation and DNA damage repair. Cell Res. *28*, 756–770.

Lin, W., Amé, J.-C., Aboul-Ela, N., Jacobson, E.L., and Jacobson, M.K. (1997). Isolation and Characterization of the cDNA Encoding Bovine Poly(ADP-ribose) Glycohydrolase. J. Biol. Chem. *272*, 11895–11901.

Liszczak, G., Diehl, K.L., Dann, G.P., and Muir, T.W. (2018). Acetylation blocks DNA damage–induced chromatin ADP-ribosylation. Nat. Chem. Biol. *14*, 837–840.

Liu, C., Vyas, A., Kassab, M.A., Singh, A.K., and Yu, X. (2017). The role of poly ADP-ribosylation in the first wave of DNA damage response. Nucleic Acids Res. *45*, 8129–8141.

Liu, X., Xie, R., Yu, L.L., Chen, S.H., Yang, X., Singh, A.K., Li, H., Wu, C., and Yu, X. (2020). Al26 inhibits the ADP-ribosylhydrolase ARH3 and suppresses DNA damage repair. J. Biol. Chem. *295*, 13838–13849.

Lord, C.J., and Ashworth, A. (2017). PARP inhibitors: Synthetic lethality in the clinic. Science (80-.). *355*, 1152–1158.

Love, M.I., Huber, W., and Anders, S. (2014). Moderated estimation of fold change and dispersion for RNA-seq data with DESeq2. Genome Biol. *15*, 550.

Luijsterburg, M.S., de Krijger, I., Wiegant, W.W., Shah, R.G., Smeenk, G., de Groot, A.J.L., Pines, A., Vertegaal, A.C.O., Jacobs, J.J.L., Shah, G.M., et al. (2016). PARP1 Links CHD2-Mediated Chromatin Expansion and H3.3 Deposition to DNA Repair by Non-homologous End-Joining. Mol. Cell *61*, 547–562.

Martello, R., Leutert, M., Jungmichel, S., Bilan, V., Larsen, S.C., Young, C., Hottiger, M.O., and Nielsen, M.L. (2016). Proteome-wide identification of the endogenous ADP-ribosylome of mammalian cells and tissue. Nat. Commun. *7*.

Martin, M. (2011). Cutadapt removes adapter sequences from high-throughput sequencing reads. EMBnet.Journal *17*, 10.

Mashimo, M., Kato, J., and Moss, J. (2013). ADP-ribosyl-acceptor hydrolase 3 regulates poly (ADP-ribose) degradation and cell death during oxidative stress. Proc. Natl. Acad. Sci. U. S. A. *110*, 18964–18969.

Mashimo, M., Bu, X., Aoyama, K., Kato, J., Ishiwata-Endo, H., Stevens, L.A., Kasamatsu, A., Wolfe, L.A., Toro, C., Adams, D., et al. (2019). PARP1 inhibition alleviates injury in ARH3-deficient mice and human cells. JCI Insight *4*.

McGurk, L., Gomes, E., Guo, L., Mojsilovic-Petrovic, J., Tran, V., Kalb, R.G., Shorter, J., and Bonini,

N.M. (2018). Poly(ADP-Ribose) Prevents Pathological Phase Separation of TDP-43 by Promoting Liquid Demixing and Stress Granule Localization. Mol. Cell *71*, 703-717.e9.

McQuin, C., Goodman, A., Chernyshev, V., Kamentsky, L., Cimini, B.A., Karhohs, K.W., Doan, M., Ding, L., Rafelski, S.M., Thirstrup, D., et al. (2018). CellProfiler 3.0: Next-generation image processing for biology. PLOS Biol. *16*, e2005970.

Mehrotra, P.V., Ahel, D., Ryan, D.P., Weston, R., Wiechens, N., Kraehenbuehl, R., Owen-Hughes, T., and Ahel, I. (2011). DNA Repair Factor APLF Is a Histone Chaperone. Mol. Cell *41*, 46–55.

Mendoza-Alvarez, H., and Alvarez-Gonzalez, R. (1993). Poly(ADP-ribose) polymerase is a catalytic dimer and the automodification reaction is intermolecular. J. Biol. Chem. *268*, 22575–22580.

Mendoza-Alvarez, H., and Alvarez-Gonzalez, R. (1999). Biochemical characterization of mono(ADP-ribosyl)ated poly(ADP-ribose) polymerase. Biochemistry *38*, 3948–3953.

Ménissier de Murcia, J., Ricoul, M., Tartier, L., Niedergang, C., Huber, A., Dantzer, F., Schreiber, V., Amé, J.C., Dierich, A., LeMeur, M., et al. (2003). Functional interaction between PARP-1 and PARP-2 in chromosome stability and embryonic development in mouse. EMBO J. *22*, 2255–2263.

Meyer, B., Fabbrizi, M.R., Raj, S., Zobel, C.L., Hallahan, D.E., and Sharma, G.G. (2016). Histone H3 Lysine 9 Acetylation Obstructs ATM Activation and Promotes Ionizing Radiation Sensitivity in Normal Stem Cells. Stem Cell Reports *7*, 1013–1022.

Michelena, J., Lezaja, A., Teloni, F., Schmid, T., Imhof, R., and Altmeyer, M. (2018). Analysis of PARP inhibitor toxicity by multidimensional fluorescence microscopy reveals mechanisms of sensitivity and resistance. Nat. Commun. *9*, 1–16.

Min, W.K., Cortes, U., Herceg, Z., Tong, W.M., and Wang, Z.Q. (2010). Deletion of the nuclear isoform of poly(ADP-ribose) glycohydrolase (PARG) reveals its function in DNA repair, genomic stability and tumorigenesis. Carcinogenesis *31*, 2058–2065.

Mohapatra, J., Tashiro, K., Beckner, R.L., Sierra, J., Kilgore, J.A., Williams, N.S., and Liszczak, G. (2021). Serine ADP-ribosylation marks nucleosomes for ALC1-dependent chromatin remodeling. Elife *10*.

Monaco, L., Kolthur-Seetharam, U., Loury, R., Murcia, J.M., de Murcia, G., and Sassone-Corsi, P. (2005). Inhibition of Aurora-B kinase activity by poly(ADP-ribosyl)ation in response to DNA damage. Proc. Natl. Acad. Sci. U. S. A. *102*, 14244–14248.

Mootha, V.K., Lindgren, C.M., Eriksson, K.-F., Subramanian, A., Sihag, S., Lehar, J., Puigserver, P., Carlsson, E., Ridderstråle, M., Laurila, E., et al. (2003). PGC-1α-responsive genes involved in oxidative phosphorylation are coordinately downregulated in human diabetes. Nat. Genet. *34*, 267–273.

Moynahan, M.E., Chiu, J.W., Koller, B.H., and Jasint, M. (1999). Brca1 controls homology-directed DNA repair. Mol. Cell *4*, 511–518.

Moynahan, M.E., Pierce, A.J., and Jasin, M. (2001). BRCA2 is required for homology-directed repair of chromosomal breaks. Mol. Cell *7*, 263–272.

Mullard, A. (2021). Targeted protein degraders crowd into the clinic. Nat. Rev. Drug Discov. *20*, 247–

250.

Murai, J., Huang, S.Y.N., Das, B.B., Renaud, A., Zhang, Y., Doroshow, J.H., Ji, J., Takeda, S., and Pommier, Y. (2012). Trapping of PARP1 and PARP2 by clinical PARP inhibitors. Cancer Res. *72*, 5588–5599.

Murai, J., Huang, S.Y.N., Renaud, A., Zhang, Y., Ji, J., Takeda, S., Morris, J., Teicher, B., Doroshow, J.H., and Pommier, Y. (2014). Stereospecific PARP trapping by BMN 673 and comparison with olaparib and rucaparib. Mol. Cancer Ther. *13*, 433–443.

Murai, J., Feng, Y., Yu, G.K., Ru, Y., Tang, S.W., Shen, Y., and Pommier, Y. (2016). Resistance to PARP inhibitors by SLFN11 inactivation can be overcome by ATR inhibition. Oncotarget *7*, 76534–76550.

Naegeli, H., Loetscher, P., and Althaus, F.R. (1989). Poly ADP-ribosylation of proteins. Processivity of a post-translational modification. J. Biol. Chem. *264*, 14382–14385.

Nagashima, H., Lee, C.K., Tateishi, K., Higuchi, F., Subramanian, M., Rafferty, S., Melamed, L., Miller, J.J., Wakimoto, H., and Cahill, D.P. (2020). Poly(ADP-ribose) glycohydrolase inhibition sequesters NAD+ to potentiate the metabolic lethality of alkylating chemotherapy in IDH-mutant tumor cells. Cancer Discov. *10*, 1673–1689.

Noël, G., Godon, C., Fernet, M., Giocanti, N., Mégnin-Chanet, F., and Favaudon, V. (2006). Radiosensitization by the poly(ADP-ribose) polymerase inhibitor 4-amino-1,8-naphthalimide is specific of the S phase of the cell cycle and involves arrest of DNA synthesis. Mol. Cancer Ther. *5*, 564–574.

Noordermeer, S.M., Adam, S., Setiaputra, D., Barazas, M., Pettitt, S.J., Ling, A.K., Olivieri, M., Álvarez-Quilón, A., Moatti, N., Zimmermann, M., et al. (2018). The shieldin complex mediates 53BP1-dependent DNA repair. Nature *560*, 117–121.

Nowak, K., Rosenthal, F., Karlberg, T., Bütepage, M., Thorsell, A.G., Dreier, B., Grossmann, J., Sobek, J., Imhof, R., Lüscher, B., et al. (2020). Engineering Af1521 improves ADP-ribose binding and identification of ADP-ribosylated proteins. Nat. Commun. *11, 5199*.

Oka, S., Kato, J., and Moss, J. (2006). Identification and characterization of a mammalian 39-kDa poly(ADP-ribose) glycohydrolase. J. Biol. Chem. *281*, 705–713.

Páhi, Z.G., Borsos, B.N., Pantazi, V., Ujfaludi, Z., and Pankotai, T. (2020). PARylation During Transcription: Insights into the Fine-Tuning Mechanism and Regulation. Cancers (Basel). *12*, 183.

Palazzo, L., Thomas, B., Jemth, A.-S., Colby, T., Leidecker, O., Feijs, K., Zaja, R., Loseva, O., Puigvert, J.C., Matic, I., et al. (2015). Processing of Protein ADP-ribosylation by Nudix Hydrolases. Biochem. J. 293–301.

Palazzo, L., Daniels, C.M., Nettleship, J.E., Rahman, N., McPherson, R.L., Ong, S.E., Kato, K., Nureki, O., Leung, A.K.L., and Ahel, I. (2016). ENPP1 processes protein ADP-ribosylation in vitro. FEBS J. 3371–3388.

Palazzo, L., Leidecker, O., Prokhorova, E., Dauben, H., Matic, I., and Ahel, I. (2018). Serine is the major residue for ADP-ribosylation upon DNA damage. Elife *7*, e34334.

Pettitt, S.J., Krastev, D.B., Brandsma, I., Dréan, A., Song, F., Aleksandrov, R., Harrell, M.I., Menon,

M., Brough, R., Campbell, J., et al. (2018). Genome-wide and high-density CRISPR-Cas9 screens identify point mutations in PARP1 causing PARP inhibitor resistance. Nat. Commun. *9*, 1849.

Pilié, P.G., Gay, C.M., Byers, L.A., O'Connor, M.J., and Yap, T.A. (2019). PARP inhibitors: Extending benefit beyond BRCA-mutant cancers. Clin. Cancer Res. *25*, 3759–3771.

Pillay, N., Tighe, A., Nelson, L., Littler, S., Coulson-Gilmer, C., Bah, N., Golder, A., Bakker, B., Spierings, D.C.J., James, D.I., et al. (2019). DNA Replication Vulnerabilities Render Ovarian Cancer Cells Sensitive to Poly(ADP-Ribose) Glycohydrolase Inhibitors. Cancer Cell *35*, 519-533.e8.

Pleschke, J.M., Kleczkowska, H.E., Strohm, M., and Althaus, F.R. (2000). Poly(ADP-ribose) binds to specific domains in DNA damage checkpoint proteins. J. Biol. Chem. *275*, 40974–40980.

Plummer, R., Dua, D., Cresti, N., Drew, Y., Stephens, P., Foegh, M., Knudsen, S., Sachdev, P., Mistry, B.M., Dixit, V., et al. (2020). First-in-human study of the PARP/tankyrase inhibitor E7449 in patients with advanced solid tumours and evaluation of a novel drug-response predictor. Br. J. Cancer 2020 1234 *123*, 525–533.

Pommier, Y., O'Connor, M.J., and de Bono, J. (2016). Laying a trap to kill cancer cells: PARP inhibitors and their mechanisms of action. Sci. Transl. Med. *8*.

Posavec Marjanović, M., Crawford, K., and Ahel, I. (2017). PARP, transcription and chromatin modeling. Semin. Cell Dev. Biol. *63*, 102–113.

Postnikov, Y. V., and Bustin, M. (2016). Functional interplay between histone H1 and HMG proteins in chromatin. Biochim. Biophys. Acta - Gene Regul. Mech. *1859*, 462–467.

Prados-Carvajal, R., Irving, E., Lukashchuk, N., and Forment, J. V. (2022). Preventing and overcoming resistance to parp inhibitors: A focus on the clinical landscape. Cancers (Basel). *14*, 44.

Prokhorova, E., Agnew, T., Wondisford, A.R., Tellier, M., Kaminski, N., Beijer, D., Holder, J., Groslambert, J., Suskiewicz, M.J., Zhu, K., et al. (2021a). Unrestrained poly-ADP-ribosylation provides insights into chromatin regulation and human disease. Mol. Cell *81*, 2640-2655.e8.

Prokhorova, E., Zobel, F., Smith, R., Zentout, S., Gibbs-Seymour, I., Schützenhofer, K., Peters, A., Groslambert, J., Zorzini, V., Agnew, T., et al. (2021b). Serine-linked PARP1 auto-modification controls PARP inhibitor response. Nat. Commun. 2021 121 *12*, 1–12.

Prokhorova, E.A., Egorshina, A.Y., Zhivotovsky, B., and Kopeina, G.S. (2020). The DNA-damage response and nuclear events as regulators of nonapoptotic forms of cell death. Oncogene *39*, 1–16.

Prymakowska-Bosak, M., Misteli, T., Herrera, J.E., Shirakawa, H., Birger, Y., Garfield, S., and Bustin, M. (2001). Mitotic phosphorylation prevents the binding of HMGN proteins to chromatin. Mol Cell Biol *21*, 5169–5178.

Rack, J.G.M., Ariza, A., Drown, B.S., Henfrey, C., Bartlett, E., Shirai, T., Hergenrother, P.J., and Ahel, I. (2018). (ADP-ribosyl)hydrolases: Structural Basis for Differential Substrate Recognition and Inhibition. Cell Chem. Biol. *25*, 1533-1546.e12.

Rack, J.G.M., Palazzo, L., and Ahel, I. (2020). (ADP-ribosyl)hydrolases: structure, function, and biology. Genes Dev. *34*, 263–284.

Ramírez, F., Ryan, D.P., Grüning, B., Bhardwaj, V., Kilpert, F., Richter, A.S., Heyne, S., Dündar, F.,

and Manke, T. (2016). deepTools2: a next generation web server for deep-sequencing data analysis. Nucleic Acids Res. *44*, W160–W165.

Ray Chaudhuri, A., Ahuja, A.K., Herrador, R., and Lopes, M. (2015). Poly(ADP-Ribosyl) Glycohydrolase Prevents the Accumulation of Unusual Replication Structures during Unperturbed S Phase. Mol. Cell. Biol. *35*, 856–865.

Reeves, R. (2015). High mobility group (HMG) proteins: Modulators of chromatin structure and DNA repair in mammalian cells. DNA Repair (Amst). *36*, 122–136.

Rondinelli, B., Gogola, E., Yücel, H., Duarte, A.A., Van De Ven, M., Van Der Sluijs, R., Konstantinopoulos, P.A., Jonkers, J., Ceccaldi, R., Rottenberg, S., et al. (2017). EZH2 promotes degradation of stalled replication forks by recruiting MUS81 through histone H3 trimethylation. Nat. Cell Biol. *19*, 1371–1378.

Ronson, G.E., Piberger, A.L., Higgs, M.R., Olsen, A.L., Stewart, G.S., McHugh, P.J., Petermann, E., and Lakin, N.D. (2018). PARP1 and PARP2 stabilise replication forks at base excision repair intermediates through Fbh1-dependent Rad51 regulation. Nat. Commun. 2018 91 *9*, 1–12.

Rottenberg, S., Jaspers, J.E., Kersbergen, A., Van Der Burg, E., Nygren, A.O.H., Zander, S.A.L., Derksen, P.W.B., De Bruin, M., Zevenhoven, J., Lau, A., et al. (2008). High sensitivity of BRCA1-deficient mammary tumors to the PARP inhibitor AZD2281 alone and in combination with platinum drugs. Proc. Natl. Acad. Sci. U. S. A. *105*, 17079–17084.

Rudolph, J., Roberts, G., Muthurajan, U.M., and Luger, K. (2021). HPF1 and nucleosomes mediate a dramatic switch in activity of PARP1 from polymerase to hydrolase. Elife *10*.

Sakai, W., Swisher, E.M., Jacquemont, C., Chandramohan, K.V., Couch, F.J., Langdon, S.P., Wurz, K., Higgins, J., Villegas, E., and Taniguchi, T. (2009). Functional restoration of BRCA2 protein by secondary BRCA2 mutations in BRCA2-mutated ovarian carcinoma. Cancer Res. *69*, 6381–6386.

Saksouk, N., Simboeck, E., and Déjardin, J. (2015). Constitutive heterochromatin formation and transcription in mammals. Epigenetics Chromatin *8*, 3.

Schoonen, P.M., Talens, F., Stok, C., Gogola, E., Heijink, A.M., Bouwman, P., Foijer, F., Tarsounas, M., Blatter, S., Jonkers, J., et al. (2017). Progression through mitosis promotes PARP inhibitor-induced cytotoxicity in homologous recombination-deficient cancer cells. Nat. Commun. *8*, 1–13.

Sharifi, R., Morra, R., Appel, C.D., Tallis, M., Chioza, B., Jankevicius, G., Simpson, M.A., Matic, I., Ozkan, E., Golia, B., et al. (2013). Deficiency of terminal ADP-ribose protein glycohydrolase TARG1/C6orf130 in neurodegenerative disease. EMBO J *32*, 1225–1237.

Singh, H.R., Nardozza, A.P., Möller, I.R., Knobloch, G., Kistemaker, H.A.V., Hassler, M., Harrer, N., Blessing, C., Eustermann, S., Kotthoff, C., et al. (2017). A Poly-ADP-Ribose Trigger Releases the Auto-Inhibition of a Chromatin Remodeling Oncogene. Mol. Cell *68*, 860-871.e7.

Slade, D. (2020). PARP and PARG inhibitors in cancer treatment. Genes Dev. *34*, 360–394.

Slade, D., Dunstan, M.S., Barkauskaite, E., Weston, R., Lafite, P., Dixon, N., Ahel, M., Leys, D., and Ahel, I. (2011). The structure and catalytic mechanism of a poly(ADP-ribose) glycohydrolase. Nature *477*, 616–620.

Smith, R., Zentout, S., Chapuis, C., Timinszky, G., and Huet, S. (2021). HPF1-dependent histone ADP-ribosylation triggers chromatin relaxation to promote the recruitment of repair factors at sites of DNA damage. BioRxiv 2021.08.27.457930.

Subramanian, A., Tamayo, P., Mootha, V.K., Mukherjee, S., Ebert, B.L., Gillette, M.A., Paulovich, A., Pomeroy, S.L., Golub, T.R., Lander, E.S., et al. (2005). Gene set enrichment analysis: A knowledge-based approach for interpreting genome-wide expression profiles. Proc. Natl. Acad. Sci. *102*, 15545–15550.

Sun, F.-H., Zhao, P., Zhang, N., Kong, L.-L., Wong, C.C.L., and Yun, C.-H. (2021). HPF1 remodels the active site of PARP1 to enable the serine ADP-ribosylation of histones. Nat. Commun. *12*, 1028.

Suskiewicz, M.J., Zobel, F., Ogden, T.E.H., Fontana, P., Ariza, A., Yang, J.-C., Zhu, K., Bracken, L., Hawthorne, W.J., Ahel, D., et al. (2020). HPF1 completes the PARP active site for DNA damage-induced ADP-ribosylation. Nature *579*, 598–602.

Szántó, M., Brunyánszki, A., Kiss, B., Nagy, L., Gergely, P., Virág, L., and Bai, P. (2012). Poly(ADP-ribose) polymerase-2: emerging transcriptional roles of a DNA-repair protein. Cell. Mol. Life Sci. *69*, 4079–4092.

Teloni, F., and Altmeyer, M. (2016). Readers of poly(ADP-ribose): designed to be fit for purpose. Nucleic Acids Res. *44*, 993–1006.

Thorsell, A.G., Ekblad, T., Karlberg, T., Löw, M., Pinto, A.F., Trésaugues, L., Moche, M., Cohen, M.S., and Schüler, H. (2017). Structural Basis for Potency and Promiscuity in Poly(ADP-ribose) Polymerase (PARP) and Tankyrase Inhibitors. J. Med. Chem. *60*, 1262–1271.

Tjeertes, J. V., Miller, K.M., and Jackson, S.P. (2009). Screen for DNA-damage-responsive histone modifications identifies H3K9Ac and H3K56Ac in human cells. EMBO J. *28*, 1878–1889.

Verma, P., Zhou, Y., Cao, Z., Deraska, P. V., Deb, M., Arai, E., Li, W., Shao, Y., Puentes, L., Li, Y., et al. (2021). ALC1 links chromatin accessibility to PARP inhibitor response in homologous recombination-deficient cells. Nat. Cell Biol. *23*, 160–171.

Vyas, S., Matic, I., Uchima, L., Rood, J., Zaja, R., Hay, R.T., Ahel, I., and Chang, P. (2014). Family-wide analysis of poly(ADP-ribose) polymerase activity. Nat. Commun. *5*, 4426.

Wang, F., and Higgins, J.M.G. (2013). Histone modications and mitosis: Countermarks, landmarks, and bookmarks. Trends Cell Biol. *23*, 175–184.

Wang, M., Weiss, M., Simonovic, M., Haertinger, G., Schrimpf, S.P., Hengartner, M.O., and Von Mering, C. (2012a). PaxDb, a database of protein abundance averages across all three domains of life. Mol. Cell. Proteomics *11*, 492–500.

Wang, Z., Michaud, G.A., Cheng, Z., Zhang, Y., Hinds, T.R., Fan, E., Cong, F., and Xu, W. (2012b). Recognition of the iso-ADP-ribose moiety in poly(ADP-ribose) by WWE domains suggests a general mechanism for poly (ADP-ribosyl)ation-dependent ubiquitination. Genes Dev.

Wright, R.H.G., Lioutas, A., Dily, F. Le, Soronellas, D., Pohl, A., Bonet, J., Nacht, A.S., Samino, S., Font-Mateu, J., Vicent, G.P., et al. (2016). ADP-ribose-derived nuclear ATP synthesis by NUDIX5 is required for chromatin remodeling. Science *352*, 1221–1225.

Xie, S., Mortusewicz, O., Ma, H.T., Herr, P., Poon, R.R.Y., Helleday, T., and Qian, C. (2015). Timeless Interacts with PARP-1 to Promote Homologous Recombination Repair. Mol. Cell *60*, 163–176.

Xu, G., Ross Chapman, J., Brandsma, I., Yuan, J., Mistrik, M., Bouwman, P., Bartkova, J., Gogola, E., Warmerdam, D., Barazas, M., et al. (2015). REV7 counteracts DNA double-strand break resection and affects PARP inhibition. Nature *521*, 541–544.

Yang, C.S., Jividen, K., Spencer, A., Dworak, N., Ni, L., Oostdyk, L.T., Chatterjee, M., Kuśmider, B., Reon, B., Parlak, M., et al. (2017). Ubiquitin Modification by the E3 Ligase/ADP-Ribosyltransferase Dtx3L/Parp9. Mol. Cell *66*, 503-516.e5.

Young, L.M., Marzio, A., Perez-Duran, P., Reid, D.A., Meredith, D.N., Roberti, D., Star, A., Rothenberg, E., Ueberheide, B., and Pagano, M. (2015). TIMELESS Forms a Complex with PARP1 Distinct from Its Complex with TIPIN and Plays a Role in the DNA Damage Response. Cell Rep. *13*, 451–459.

Zahradka, P., and Ebisuzaki, K. (1982). A shuttle mechanism for DNA-protein interactions. The regulation of poly(ADP-ribose) polymerase. Eur. J. Biochem. *127*, 579–585.

Zandarashvili, L., Langelier, M.F., Velagapudi, U.K., Hancock, M.A., Steffen, J.D., Billur, R., Hannan, Z.M., Wicks, A.J., Krastev, D.B., Pettitt, S.J., et al. (2020). Structural basis for allosteric PARP-1 retention on DNA breaks. Science *368*.

Zhang, F., Chen, Y., Li, M., and Yu, X. (2014). The oligonucleotide/oligosaccharide-binding fold motif is a poly(ADP-ribose)-binding domain that mediates DNA damage response. Proc. Natl. Acad. Sci. U. S. A.

Zhang, F., Shi, J., Bian, C., and Yu, X. (2015). Poly(ADP-ribose) mediates the BRCA2-dependent early DNA damage response. Cell Rep. *13*, 678.

Appendix

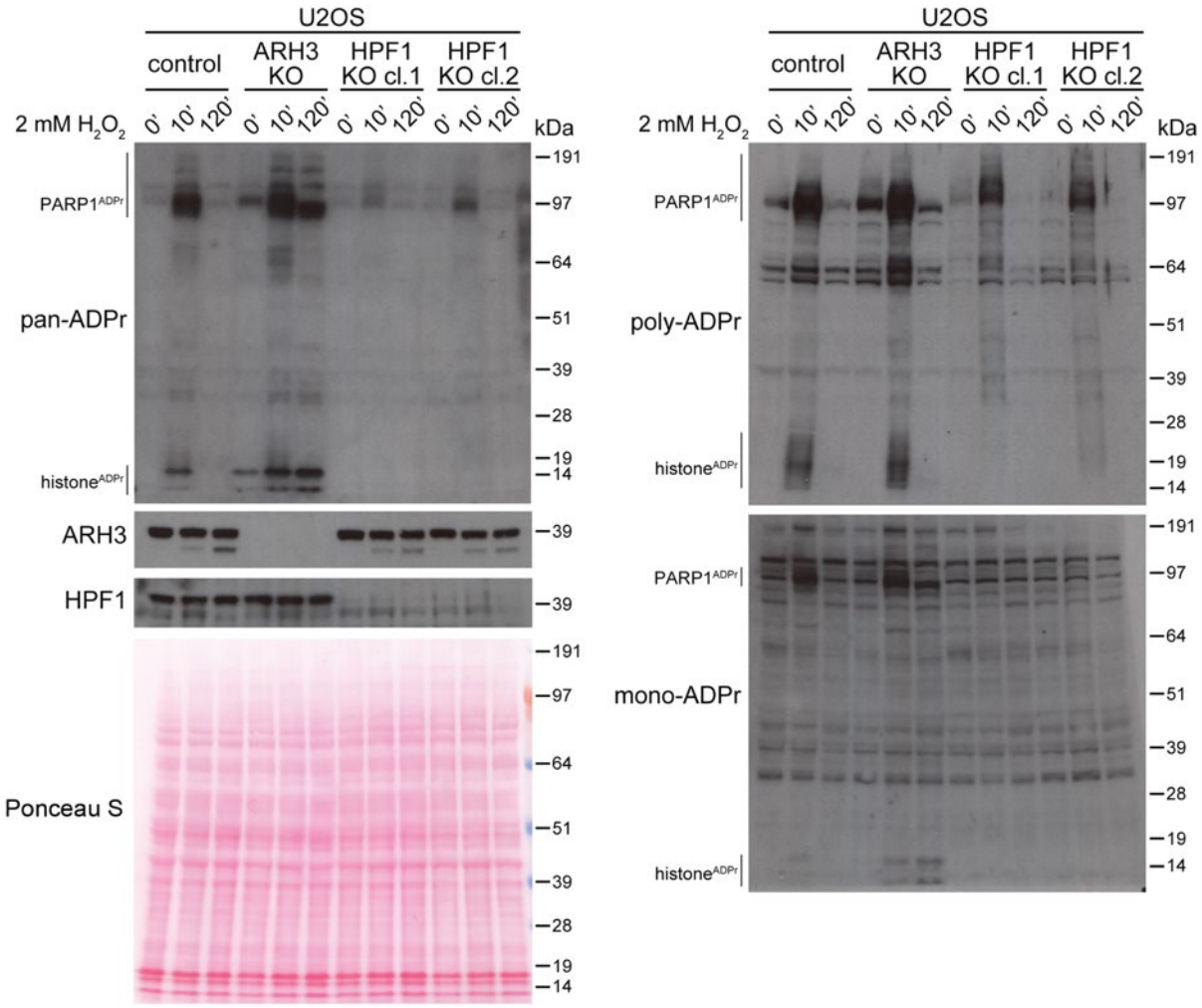


Figure S1. Total DNA damage-induced ADPr is dependent on HPF1. Related to Figure 7.

The levels of ADPr in control, ARH3 KO and two independent HPF1 KO U2OS cell lines treated with H_2O_2 were compared by Western blotting. Representative Western blots from 2 independent experiments are shown. The figure was adapted from (Palazzo et al., 2018).

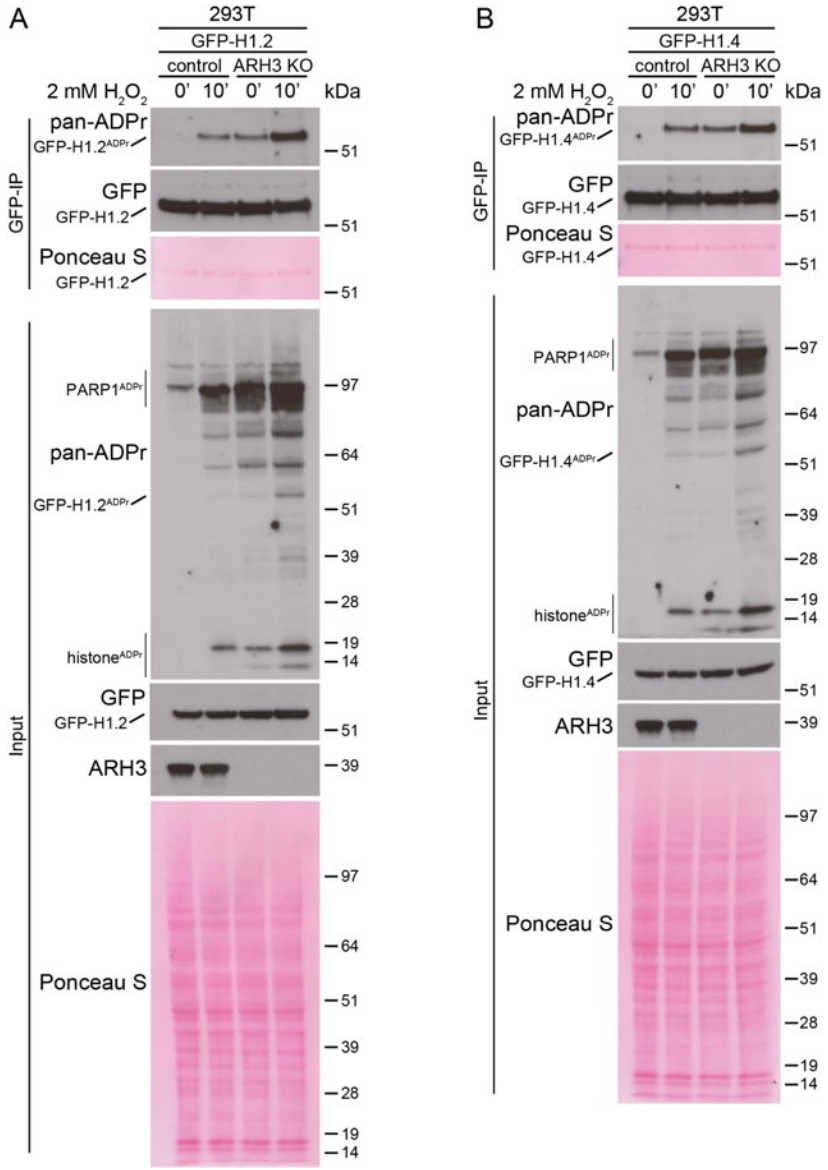


Figure S2. Reversal of H1.2 and H1.4 ADPr is ARH3-dependent. Related to Figure 9.

Control and ARH3 KO 293T cells were transfected with GFP-H1.2 (A) or GFP-H1.4 (B). Following H_2O_2 treatment and GFP-immunoprecipitation (GFP-IP), the levels of ADPr were compared by Western blotting. Representative Western blots from 2 independent experiments are shown. The figures were partially adapted from (Hendriks et al., 2021).

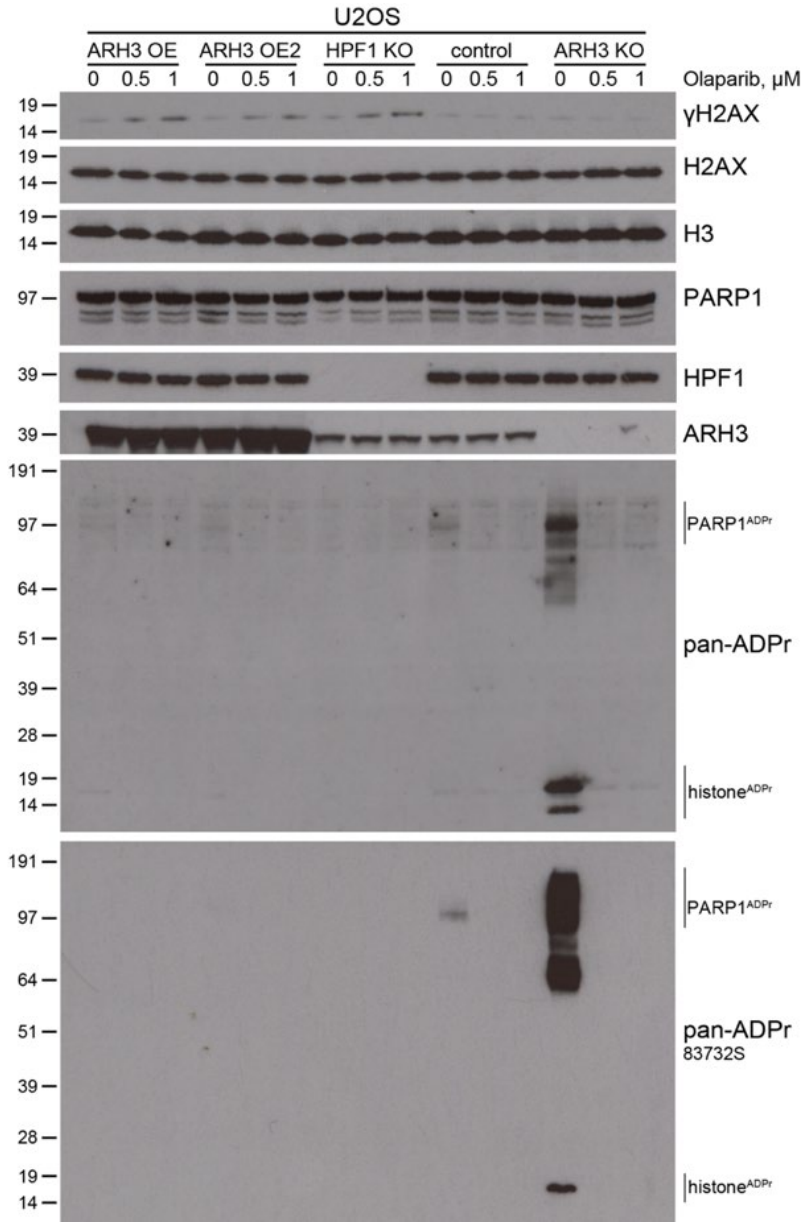


Figure S3. Olaparib-induced γH2AX formation depends on cellular HPF1 and ARH3 protein levels. Related to Figure 16.

A repeat of 6-day Olaparib treatment in Figure A performed with an additional lower inhibitor concentration. ADPr and γH2AX levels were analysed by Western blotting. Representative Western blots from 2 independent experiments are shown. The figure was partially adapted from (Prokhorova et al., 2021b).

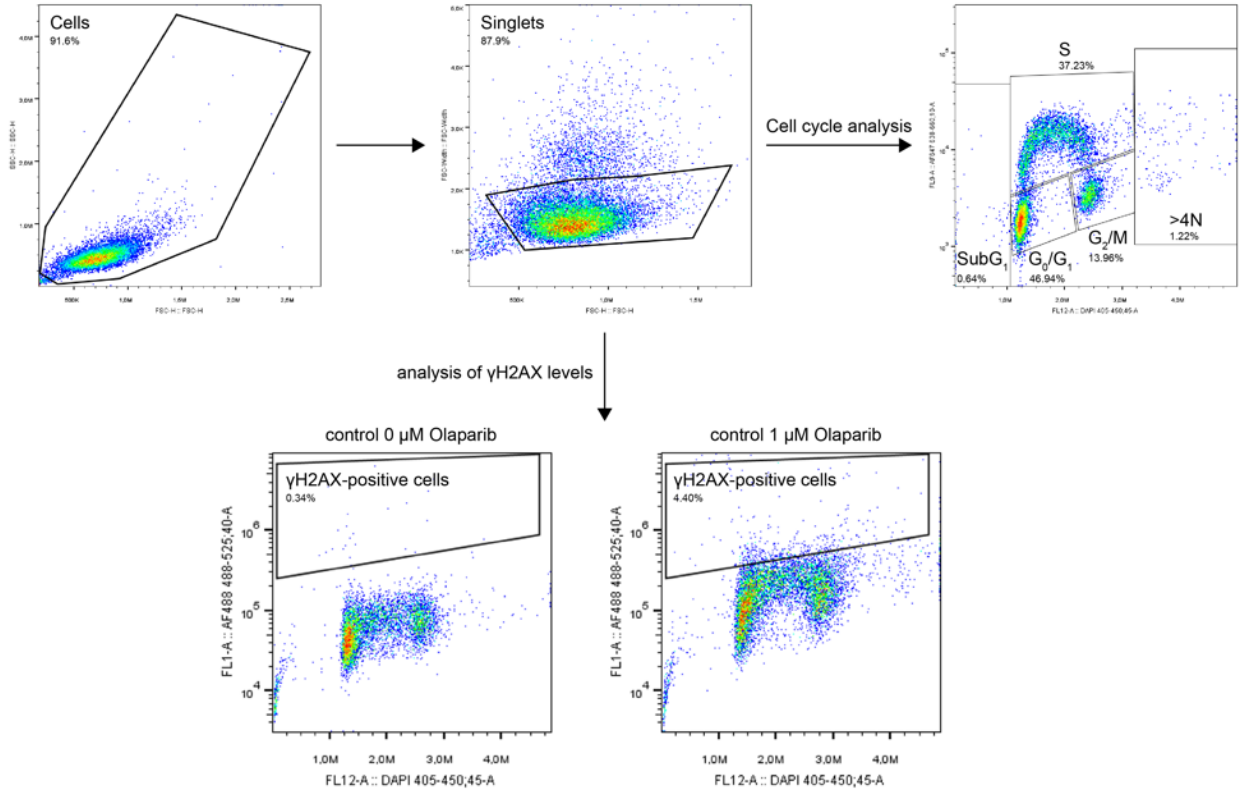


Figure S4. Flow cytometry gating strategy for analysis of Olaparib-induced changes in cell cycle distribution and γH2AX formation. Related to Figure 16.

The figure was adapted from (Prokhorova et al., 2021b).

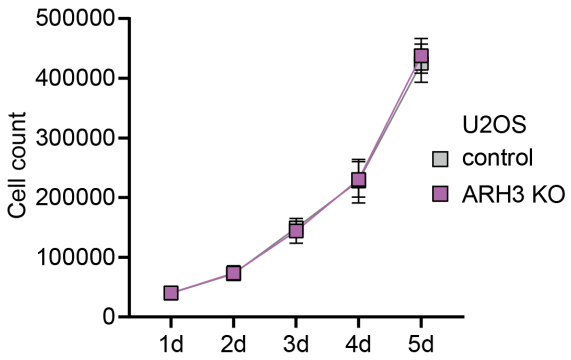


Figure S5. Comparison of control and ARH3 KO cell proliferation rates. Related to Section 4.2.1.

Quantification of control and ARH3 KO U2OS cell proliferation by cell count every 24 h. Data are shown as mean±SD, n=3. The figure was adapted from (Prokhorova et al., 2021a).

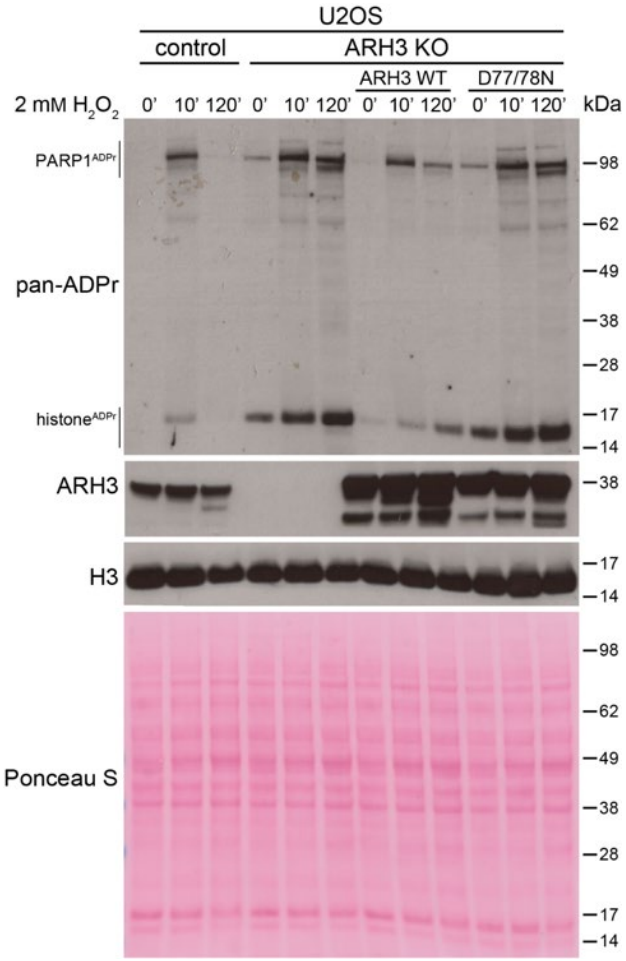


Figure S6. Complementation with ARH3 WT, but not catalytically inactive D77/78N mutant, rescues the reversal of DNA damage-induced ADPr. Related to Figure 35.

Control and ARH3 KO U2OS cells complemented with ARH3 WT or catalytically inactive ARH3 D77/78N were treated with H_2O_2 for the indicated times. ADPr signals were analysed by Western blotting. Representative Western blots from 2 independent experiments are shown. The figure was adapted from (Prokhorova et al., 2021a).

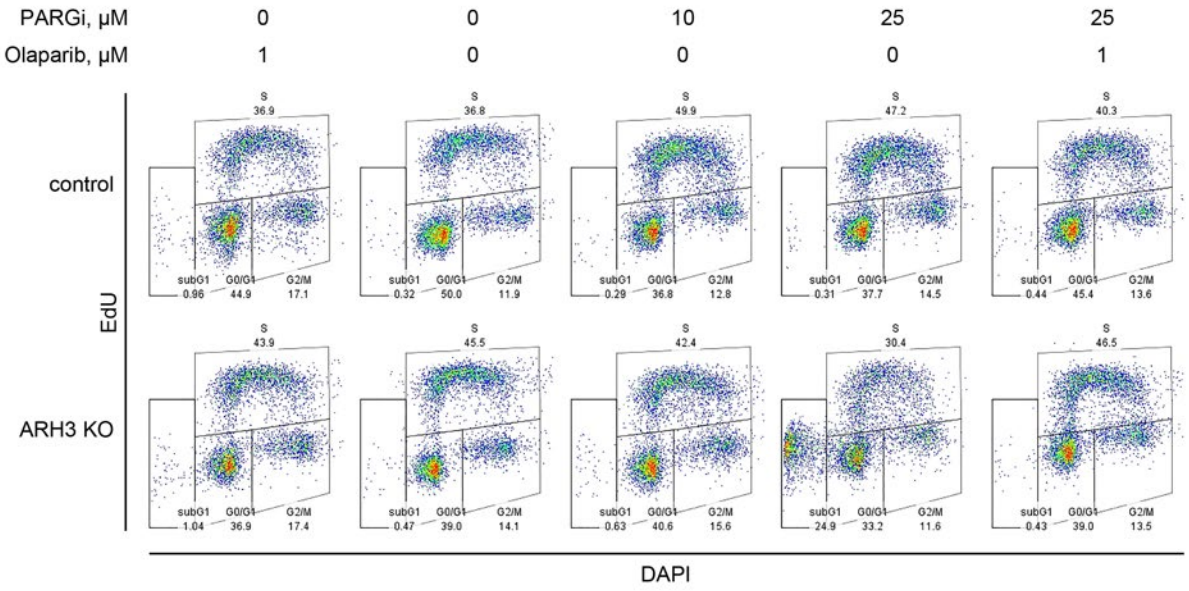


Figure S7. Representative scatterplots of cell cycle analysis by flow cytometry of EdU- and DAPI-stained cells. Related to Figure 36.

Control and ARH3 KO U2OS cells were treated with DMSO or as indicated for 6 days and then subjected to 1-h EdU pulse. The figure was adapted from (Prokhorova et al., 2021a).

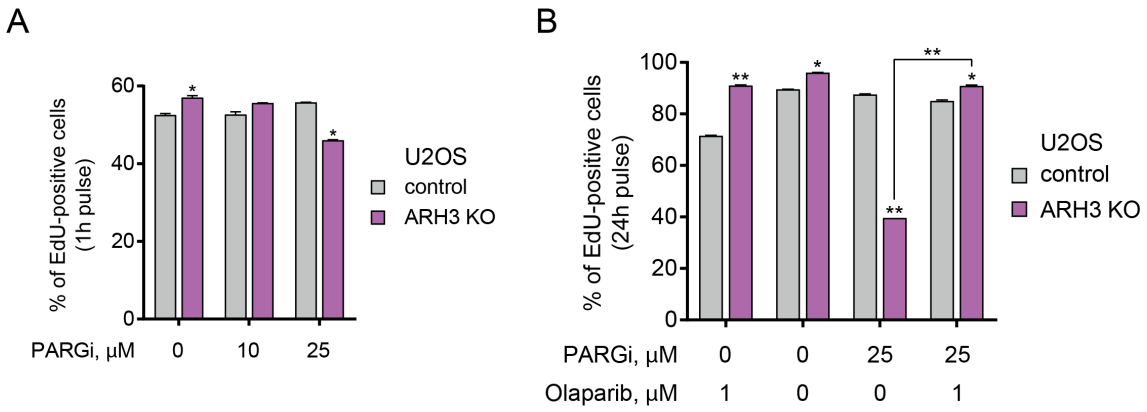


Figure S8. Long-term PARG inhibition perturbs cell proliferation in ARH3 KO cells. Related to Figure 36.

(A) Cell proliferation and DNA synthesis in control and ARH3 KO U2OS cells after exposure to DMSO or PARGi for 2 days and 1-h EdU pulse. (B) Cell proliferation and DNA synthesis after exposure to DMSO or indicated treatment for 6 days and or 24-h EdU pulse. Data are shown as mean±SEM, n=3 (A), n=2 (B), *p<0.05, **p<0.01, ***p<0.001 (two-tailed Student's t-test). The figures were adapted from (Prokhorova et al., 2021a).

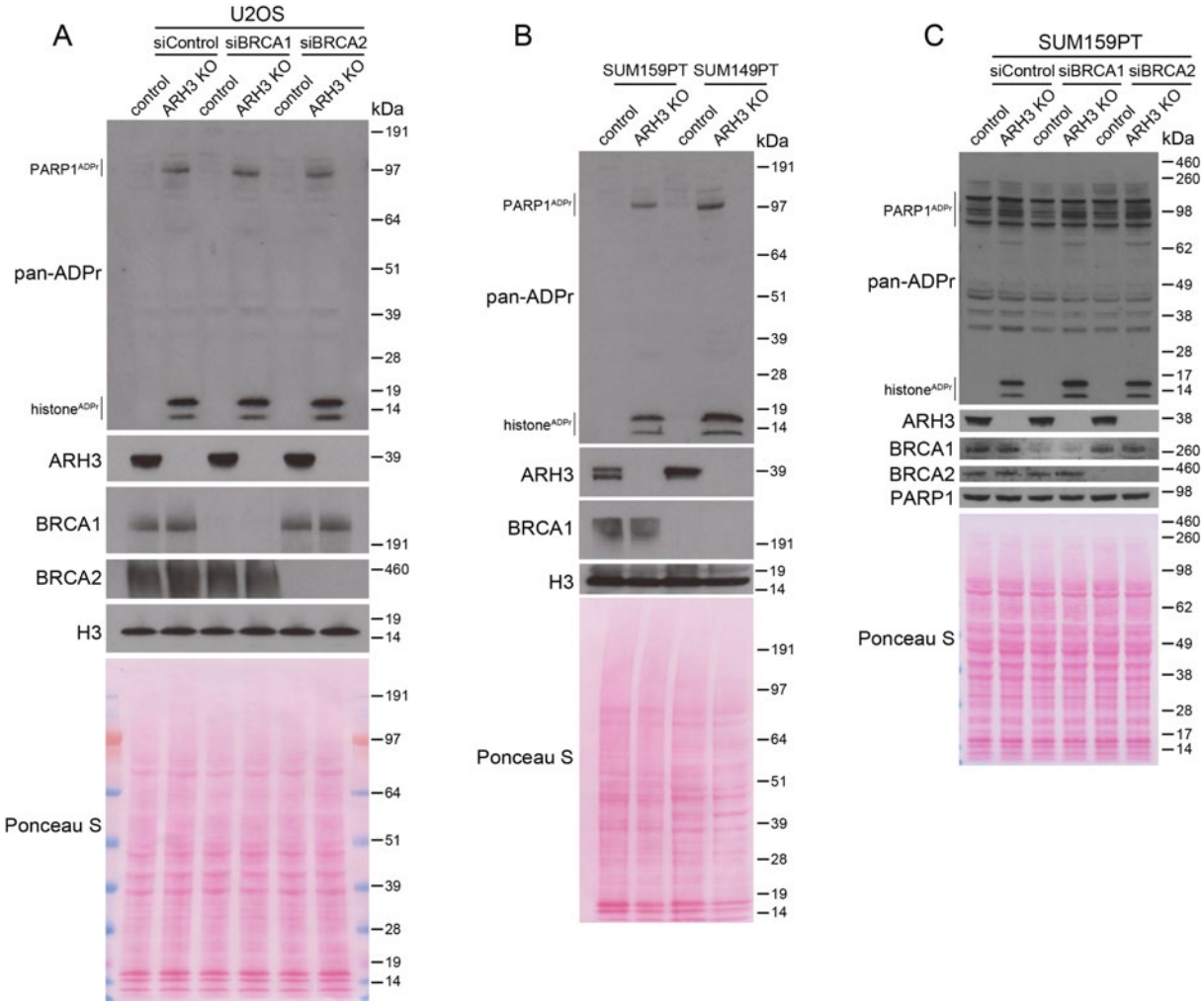


Figure S9. Assessment of ADPr and BRCA1/2 protein levels upon BRCA1/2 knockdown, and in BRCA1 WT and BRCA1 mutant TNBC cells. Related to Figure 37.

(A, C) Western blotting analysis of ADPr signals in control and ARH3 KO U2OS (A) or SUM159PT (C) cells 72 h after BRCA1 or BRCA2 siRNA transfection. The experiment in (C) was performed by Thomas Agnew. (B) Western blotting analysis of ADPr signals in control and ARH3 KO SUM159PT and SUM149PT cells. Representative Western blots from 2 independent experiments are shown. The figures were adapted from (Prokhorova et al., 2021a).

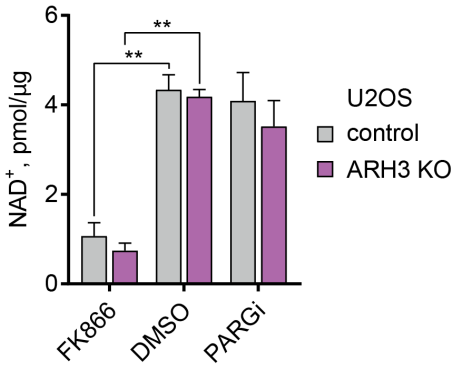


Figure S10. PARG inhibition does not lead to a significant reduction of NAD⁺ levels in ARH3-deficient cells. Related to Section 4.2.4.

NAD^+ quantification assay in control and ARH3 KO U2OS cells treated with DMSO or 25 μM PARGi for 4 days. The 1-day treatment with 10 nM FK866, a highly specific inhibitor of nicotinamide phosphoribosyltransferase (NAMPT), an essential enzyme in the biosynthesis of NAD^+, was used as a negative control to confirm the sensitivity of the NAD^+ quantification assay. Data are shown as mean ± SD, n = 2; **p < 0.01 (two-tailed Student's t test). The experiment was performed by Thomas Agnew and the figure was adapted from (Prokhorova et al., 2021a).

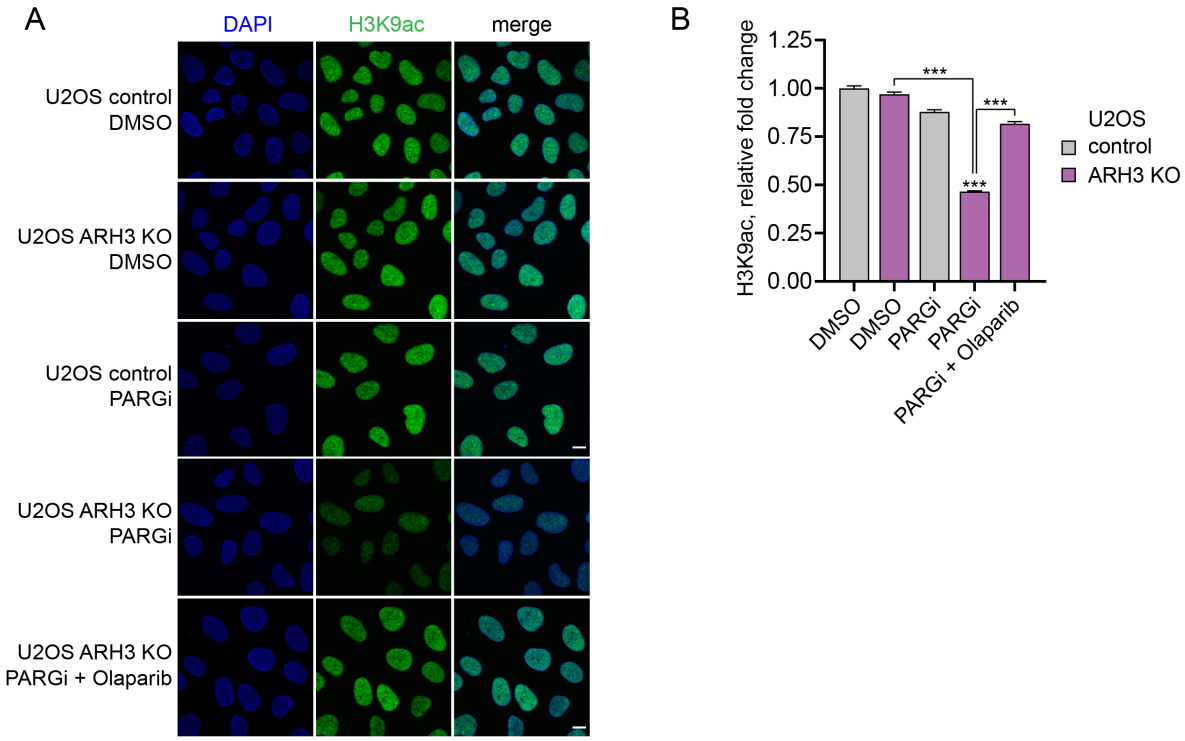


Figure S11. Long-term PARG inhibition leads to a decrease in H3K9ac levels in ARH3-deficient cells. Related to Figure 40.

(A) Control and ARH3 KO U2OS cells were treated with DMSO, 25 μM PARGi or 25 μM PARGi and 1 μM Olaparib for 6 days. H3K9ac levels were compared by immunofluorescence. Scale bars, 10 μm. (B) Quantification of immunofluorescence in (A). Data represent fold change relative to DMSO-treated control cells±SEM, at least 500 cells were analysed per condition, ***p<0.001 (one-way ANOVA followed by Tukey post-test). The experiments and quantifications were performed by Thomas Agnew. The figure was adapted from (Prokhorova et al., 2021a).

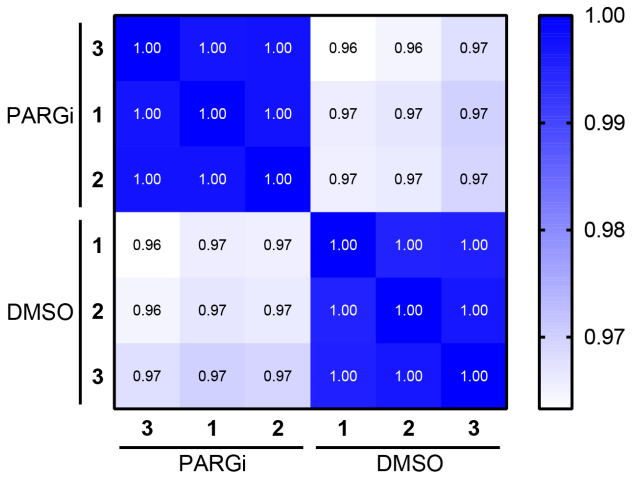


Figure S12. Heat map of Pearson's correlation coefficients used to measure reproducibility of sample preparation and RNA-sequencing results. Related to Figure 42.

Heat map of Pearson's correlation coefficients between three independent replicates of ARH3 KO U2OS cells treated with DMSO or 25 μM PARGi for 4 days. The coefficients were calculated by Michael Tellier. The figure was adapted from (Prokhorova et al., 2021a).

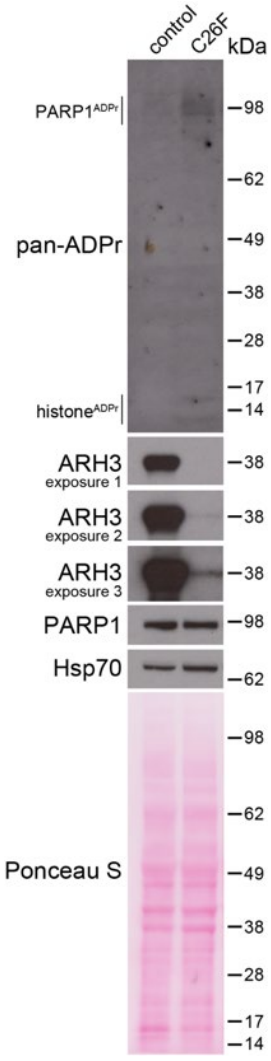


Figure S13. C26F mutation causes a substantial reduction in ARH3 protein levels. Related to Section 4.2.5.

Western blotting analysis of ADPr and ARH3 levels in control and ARH3 C26F mutant patient-derived primary human fibroblasts. Representative Western blots from 3 independent experiments are shown. The figure was adapted from (Prokhorova et al., 2021a).